THE ROLE OF RTNLB3 IN ENDOPLASMIC RETICULUM STRUCTURE AND CYTOKINESIS *IN PLANTA*

P. M. KIVINIEMI

PhD

2017

I dedicate this thesis to the friendship and memory

of Kimberly Taylor and Daniel Small.

Acknowledgements

First and foremost, I would like to express my appreciation and thanks to my supervisors Chris Hawes and Anne Osterrieder. Their unwavering encouragement, guidance, support, knowledge and patience has been invaluable during the course of this project and I will be eternally grateful for the role they have played in my process of completing this research. I could not have wished for two more wonderful people to act as my advisors throughout this work. I would also like to thank Imogen Sparkes for her supervision and insight during the early stages of this study.

I am very thankful for the help of Anne Kearns in helping maintain my cell lines and all the other assistance she has provided in preparing stocks for the growth of my plants. Derek Goto for his repeated attempts to send me BY-2 cells from a highly mitotic line all the way from Japan until some cells survived the transit, from which I could establish a culture here in Oxford. I have greatly appreciated the chats and all the guidance from fellow PhD students and researchers in the department over the years; in particular Verena Kriechbaumer and Frances Tolmie for sharing their knowledge and helping with the confocal microscopy based parts of this work. I'd also like to thank Louise Hughes for teaching me the advanced image processing techniques I've used in this study and Jake Richardson for his assistance with my use of the TEM imaging facilities, in addition to being generally helpful whenever I've needed assistance regarding things in the lab. I'd also like to acknowledge Oxford Brookes University for granting me the Nigel Groome studentship that enabled me to embark on this work and provided funding towards the endeavour.

I'd also like to express my thanks and eternal gratitude to my mother Tuire and her partner Simon for their consistent faith in me and support. I'm also enormously grateful for the support my father Ari has provided in helping me through this work.

There are so many friends to whom I am incredibly grateful for being in my life and who have each played a part in supporting me, keeping my spirits up, generally been there for me and helped ensure I make it through my PhD. I really could not have done it without you. Special mention goes out to Hannah, Joe, Alex, Becca, Karina, Ryan, Sally, Rory, Amy, Jon & Matt.

Contents:

Abstract----------1

List of tables, figures & movie files----------2

Abbreviations----------6

1. Introduction----------9

1.1 The endoplasmic reticulum (ER)----------9

1.1.1 Functions of the ER----------9

1.1.2 Structural and functional ER Domains----------10

1.1.3 ER dynamics and shape----------13

1.2 Mechanisms shaping ER membranes----------15

1.2.1 Influence of the cytoskeleton----------15

1.2.2 ER cisternae----------15

1.2.3 ER tubule dynamics and membrane fusion machinery----------17

1.2.4 ER tubule junctions----------19

1.2.5 Plasma membrane-ER anchor points----------19

1.3 Curving ER membranes----------20

1.3.1 Introduction to the reticulon protein family----------20

1.3.2 Reticulon proteins in vertebrate cells----------25

1.3.3 Reticulon proteins & ER membrane conformation in yeast -------27

1.3.4 Reticulon proteins & the nucleus----------29

1.3.5 Reticulon proteins in plant cells----------30

1.4 The endoplasmic reticulum, mitosis & cytokinesis i*n planta*----------35

1.5 Plasmodesmata----------37

1.5.1 Introduction to plasmodesmata----------37

1.5.2 Plasmodesmatal structure----------38

1.5.3 Plasmodesmatal transport----------41

1.5.4 Plasmodesmata conclusions----------45

1.6 Research Aims of the thesis----------45

1.6.1 Investigate function, localisation & dynamics of RTNLB3 protein in plant cells----------45

1.6.2 Employ high-resolution 3D microscopy techniques to investigate plant ER structure----------45

1.6.3 Elucidate the role of RTNLB3 in cell plate formation----------45

2. Materials & Methods----------46

2.1 DNA constructs used for transformations----------46

2.2 Bacteria----------47

2.2.1 Bacterial culture medium----------47

2.2.2 Antibiotics used for selection of bacteria and constructs----------47

2.2.3 Transformation of competent *Escherichia coli* and DNA extraction----------48

2.2.4 *Agrobacterium tumifaciens* strains----------48

2.2.5 Preparation of competent *Agrobacterium tumifaciens* cells--------49

2.2.6 Transformation of *Agrobacterium tumifaciens* cells----------50

2.3 Bright-Yellow 2 *Nicotiana tabacum* cell culture and modification----------50

2.3.1 Source of BY-2 cell line----------50

2.3.2 Culture of *N. tabacum* BY-2 suspension cells----------50

2.3.3 Establishment of BY-2 suspension culture from calli----------51

2.3.4 Transient transformation of *N. tabacum* BY-2 cells----------51

2.3.5 Stable transformation of wild-type *N. tabacum* BY-2 cells--------53

2.3.6 Synchronisation of *N. tabacum* BY-2 cell cultures----------54

2.4 *Arabidopsis thaliana* plant growth and transformation----------55

2.4.1 MS plates for *Arabidopsis thaliana* plant culture----------55

2.4.2 Sterilisation of *Arabidopsis thaliana* seeds and plating onto MS plates----------55

2.4.3 Growth of *Arabidopsis thaliana* seedlings up to seven days-------56

2.4.4 Growth of *Arabidopsis thaliana* from seedlings to whole plants in soil for seed harvesting----------56

2.4.5 Transformation of *Arabidopsis thaliana* wild-type Columbia plants----------56

2.4.6 Generation of stable *Arabidopsis thaliana* lines----------57

2.5 Electron microscopy preparation----------57

2.5.1 Standard fixation of BY-2 cells----------57

2.5.2 Standard fixation of *Arabidopsis thaliana* roots----------58

2.5.3 Zinc iodide osmium textroxide fixation----------59

2.5.4 Dehydration of fixed samples in ethanol series----------59

2.5.5 Infiltration of fixed samples in SPURR's resin----------60

2.5.6 Sectioning of resin embedded samples----------60

2.5.7 Staining of samples prior to TEM imaging----------60

3. Characterisation of full length and truncated RTLNB3 phenotypes in *Nicotiana tabacum* Bright Yellow 2 (BY-2) mono-culture cells----------62

3.1 Introduction----------62

3.2 Materials & methods----------64

3.2.1 Mitotic index count of synchronisation efficiency with DRAQ5 staining----------64

3.2.2 Screening for expression of liquid BY-2 cultures----------65

3.2.3 Preliminary analysis of ER luminal diameter from thin section transmission electron micrographs----------65

3.3 Results----------66

3.3.1 Development of a rapid transient over expression system of fluorescent protein fusions in BY-2 cells----------66

3.3.2 RTNLB3 labels the ER in interphase BY-2 cells, exhibiting constriction of ER lumen in comparison to wild-type and is specifically recruited at a high concentration to the cell plate during telophase--------66

3.3.3 Generation of stable BY-2 lines expressing RTNLB3-YFP and truncation 2 of RTNLB3-YFP----------68

3.3.4 Establishment of timescale, synchronisation efficiency and optimal protocol for the synchronisation of a BY-2 suspension cell culture--------69

3.3.5 Preliminary analysis of ER luminal diameter from thin section transmission electron micrographs of interphase *N. tabacum* BY-2 cells-71

3.3.6 Transmission electron microscopy of the ER & RTNLB3 during cell plate formation----------73

3.3.7 Transmission electron microscopy employing zinc iodide osmium textroxide fixation to stain the ER membranes----------74

3.4 Discussion----------94

3.4.1 Development of a rapid transient over-expression system of fluorescent protein fusions in BY-2 cells----------94

3.4.2 RTNLB3 labels the ER in interphase BY-2 cells, exhibiting constriction of the ER lumen in comparison to wild-type and is specifically recruited at a high concentration to the cell plate during telophase--------95

3.4.3 Truncation 2 of RTNLB3-YFP is poorly tolerated and high levels of over-expression are lethal to BY-2 cells----------98

3.4.4 Establishment of timescale, synchronisation efficiency and optimal protocol for the synchronisation of a BY-2 suspension cell culture------100

3.4.5 Preliminary analysis of ER luminal diameter from thin section transmission electron micrographs of interphase *N. tabacum* BY-2 cells----------101

3.4.6 Transmission electron microscopy of the ER & RTNLB3 during cell plate formation----------102

3.4.7 Transmission electron microscopy employing zinc iodide osmium textroxide fixation to stain ER membranes in BY-2 cells----------103

4. Generation and confocal microscopy analysis of stable *Arabidopsis thaliana* plants over-expressing RTNLB3 constructs----------106

4.1 Introduction----------106

4.2 Materials & methods----------108

4.2.1 Treatment of leaves with Brefeldin A and Rhodamine hexyl B staining----------108

4.2.2 Confocal microscopy imaging of *Arabidopsis thaliana* plants---108

4.2.3 Screening of *Arabidopsis thaliana* plants using a fluorescence stereomicroscope----------108

4.2.4 Dexamethasone induction of an inducible truncated RTNLB3-YFP construct----------109

4.2.5 Analine blue staining of leaves for callose----------109

4.3 Results----------109

4.3.1 Confocal microscopy analysis of stable over-expression of full-length and truncated RTNLB3-YFP in seven day old *Arabidopsis thaliana* leaf cotyledonary cells----------109

4.3.2 Confocal microscopy analysis of stable over-expression of full-length RTNLB3-YFP in seven day old *Arabidopsis thaliana* roots------111

4.3.3 Confocal microscopy analysis of stable over-expression of induced truncated RTNLB3-YFP in seven day old *Arabidopsis thaliana* roots--112

4.3.4 Localisation of full length & truncated RTNLB3-YFP in *Arabidopsis thaliana* leaf cotyledonary cells treated with Brefeldin A and stained with hexyl-rhodamine B----------113

4.3.5 Staining for callose with analine blue hints at co-localisation of RTNLB3-YFP at plasmodesmata in *Arabidopsis thaliana* leaf epidermal cells----------114

4.4. Discussion----------128

4.4.1 Confocal microscopy analysis of stable over-expression of full-length and truncated RTNLB3-YFP in seven day old *Arabidopsis thaliana* leaf cotyledonary cells----------128

4.4.2 Confocal microscopy analysis of stable over-expression of full-length and inducible truncated RTNLB3-YFP in seven day old *Arabidopsis thaliana* roots----------130

4.4.3 Localisation of full length & truncated RTNLB3-YFP in *Arabidopsis thaliana* leaf cotyledonary cells treated with Brefeldin A and stained with hexyl-rhodamine B----------133

4.4.4 Staining for callose with analine blue hints at co-localisation of RTNLB3-YFP at plasmodesmata in *Arabidopsis thaliana* leaf epidermal cells----------134

5. Transmission electron microscopy analysis of ZIO stained *Arabidopsis thaliana* root tip cells----------136

5.1 Introduction----------136

5.2 Materials & methods----------138

5.2.1 Transmission electron microscopy and tomographic imaging------138

5.2.2 Processing of tomographic datasets----------138

5.3 Results----------139

5.3.1 Thin section transmission electron microscopy of ZIO stained *Arabidopsis thaliana* root tip cells----------139

5.3.2 Thick section transmission electron microscopy of ZIO stained *Arabidopsis thaliana* root tip cells----------141

5.3.3 Transmission electron tomography of ZIO stained *Arabidopsis thaliana* root tip cells----------143

5.4 Discussion----------170

5.4.1 Thin section transmission electron microscopy of ZIO stained *Arabidopsis thaliana* root tip cells----------170

5.4.2 Thick section transmission electron microscopy of ZIO stained *Arabidopsis thaliana* root tip cells----------172

5.4.3 Transmission electron tomography of ZIO stained *Arabidopsis thaliana* root tip cells----------176

6. SBFSEM, 3D reconstruction and analysis of ZIO stained *Arabidopsis thaliana* root tip cells----------179

6.1 Introduction----------179

6.2 Materials & methods----------181

6.2.1 SBFSEM data collection----------181

6.2.2 SBFSEM data processing----------182

6.3 Results----------182

6.3.1 SBFSEM, 3D reconstruction and analysis of wild-type ZIO stained *Arabidopsis thaliana* root tip cells----------182

6.3.2 SBFSEM, 3D reconstruction and analysis of induced truncation 2 of RTNLB3-YFP over-expressing, ZIO stained *Arabidopsis thaliana* root tip cells----------186

6.3.3 SBFSEM, 3D reconstruction and analysis of RTNLB3-YFP over-expressing, ZIO stained *Arabidopsis thaliana* root tip cells----------189

6.4 Discussion----------206

7. Final discussion and conclusion----------215

7.1 Overview of research undertaken----------215

7.2 The truncated RTNLB3 mutant construct in BY-2 *N. tabacum* cells-----215

7.3 Use of the *Arabidopsis thaliana* whole plant system----------216

7.4 Conclusions regarding RTNLB3, truncated RTNLB3 and the cell cycle from light microscopy----------216

7.5 Lethal Arabidopsis thaliana phenotype of truncated RTNLB3-YFP construct----------217

7.6 Over-expression using the 35S promoter as opposed to native----------218

7.7 Conclusions, considerations, and suggestions for future work----------219

8. References----------225

Appendix: Disc

Abstract:

Reticulons are a large family of ER membrane shaping proteins that are ubiquitous to eukaryotic cells. Plants possess the highest number of different reticulon proteins, which contain a conserved reticulon homology domain that has been associated with their ER curvature inducing properties. Individual reticulon family members are suspected to play other roles in cell function, although most remain unknown. RTNLB3 is a reticulon that has been identified in a plasmodesmatal proteomic screen and could play a role in constricting the ER membrane into the highly curved rod of the desmotubule, forming the core of these structures within plant cell walls. The role of the ER in cytokinesis and the importance of the regulation of ER structure during this process has not been previously investigated in detail. This study demonstrates that RTNLB3 becomes highly concentrated at the cell plate during its formation and that over-expression of a non-functional truncated form of the protein interferes with cell wall formation. Over-expression of truncated RTNLB3 results in an increased proportion of cisternal ER within the ER network. Stable over-expression of the construct proved lethal to BY-2 cell lines and *Arabidopsis thaliana* plants. Analysis of meristematic root tip cells of Arabidopsis plants stably transformed with an inducible truncated RTNLB3 construct, and subsequent induction prior to analysis, resulted in disruption to cell plate formation. RTNLB3 therefore may play a direct role in the formation of the cell plate; the loss of regulation of ER membrane curvature within the network prevents successful completion of cytokinesis; or a combination of these factors. The lethal phenotypes observed within this study, and the abnormal ultrastructure of cells identified as a result of over-expression of a mutant form of RTNLB3, demonstrate the importance of this ER shaping protein and ER structure in the process of plant cytokinesis.

List of tables, figures & movie files:

Chapter 1

Figure 1.3.1A – Phylogenetic analysis showing relationships within the *A. thaliana* reticulon family including alternate splice isoforms.

Figure 1.3.1B – Expression maps of At1g64090 RTNLB3 A. thaliana gene from eFP Browser.

Figure 1.3.5 – Topology of RTNLB3 and its truncations within a lipid bilayer and ER tubule.

Chapter 2

Table 2.2.1 - LB culture media

Table 2.2.2 - YEB culture media

Table 2.2.3 - Selection antibiotics

Chapter 3

Table 3.3.1 - Cell counts and mitotic index at a range of time points following aphidicolin wash from a BY-2 tobacco suspension culture stably over-expressing RTNLB3-YFP.

Figure 3.3.1 - Transient over-expression of fluorescent constructs in *N. tabacum* BY-2 cells following 4 days incubation.

Figure 3.3.2 - Confocal micrographs of *N. tabacum* BY-2 cells in interphase, stably over-expressing RTNLB3-YFP constructs and transiently over-expressing GFP-HDEL.

Figure 3.3.3 - Confocal micrographs of *N. tabacum* BY-2 suspension cells undergoing cell plate formation in telophase.

Figure 3.3.4 - Confocal micrographs of *N. tabacum* BY-2 cells overexpressing truncated RTNLB3-YFP.

Figure 3.3.5 - Synchronised BY-2 cell culture stably over-expressing RTNLB3-YFP and chromosomes stained with DRAQ5.

Figure 3.3.6 – 80 nm thin section transmission electron micrographs of interphase *N. tabacum* BY-2 suspension culture cells showing endoplasmic reticulum morphology.

Figure 3.3.7 - Diameter of cross sections of ER in wild type & RTNLB3 overexpressing BY-2 suspension cells.

Figure 3.3.8 - Transmission electron micrographs of *N. tabacum* BY-2 suspension culture cells showing the developing edges of a cell plate.

Figure 3.3.9 - Transmission electron micrographs of *N. tabacum* BY-2 suspension culture cells showing maturing regions of cell plates with ER in contact with new cell wall material.

Figure 3.3.10 - Thin section transmission electron micrographs of zinc iodide osmium textroxide fixed wild-type *N. tabacum* BY-2 suspension culture cells.

Chapter 4

Figure 4.3.1 - Confocal micrographs of the expression phenotypes for stable over-expression of full length RTNLB3-YFP and induced truncation 2 of RTNLB3-YFP in seven day old *Arabidopsis thaliana* cotyledonary leaves.

Figure 4.3.2 - Confocal micrographs of seven day old *Arabidopsis thaliana* plants, stably transformed with an inducible truncated RTNLB3-YFP construct, following 20 hours incubation with DMSO and Silwett-77 solution in the absence of dexamethasone, stained with hexyl-rhodamine B.

Figure 4.3.3 - Confocal micrographs of the over-expression phenotype for stable over-expression of full length RTNLB3-YFP in seven day old *Arabidopsis thaliana* root tips.

Figure 4.3.4 - Confocal micrographs of the expression phenotype of induced truncated RTNLB3-YFP in seven day old *Arabidopsis thaliana* root tips.

Figure 4.3.5 - Confocal micrographs of seven day old *Arabidopsis thaliana* cotyledonary leaves over-expressing RTNLB3-YFP constructs, following Brefeldin A treatment and hexyl-rhodamine B staining.

Figure 4.3.6 - Analine blue staining in 7 day old *Arabidopsis thaliana* plants stably over-expressing RTNLB3-YFP.

Chapter 5

Figure 5.3.1 – Transmission electron micrographs of 80 nm sections of ZIO stained wild-type and control (treated with DMSO and Silwett-77™) *Arabidopsis thaliana* root tip cells at low magnification.

Figure 5.3.2 – Transmission electron micrographs of 80 nm sections of ZIO stained wild-type *Arabidopsis thaliana* root tip cells showing cross walls and ER at high magnification.

Figure 5.3.3 – Transmission electron micrographs of 80 nm sections of ZIO stained *Arabidopsis thaliana* root tip cells of plants following 20 hours induction of truncation 2 of RTNLB3-YFP over-expression.

Figure 5.3.4 – Transmission electron micrographs of 200 nm sections of ZIO stained wild-type *Arabidopsis thaliana* root tip cells showing an overview of cells.

Figure 5.3.5 – Transmission electron micrographs of 200 nm sections of ZIO stained wild-type *Arabidopsis thaliana* root tip cells with sections cut perpendicular to the orientation the cross walls visible.

Figure 5.3.6 - Transmission electron micrographs of 200 nm sections of ZIO stained wild-type *Arabidopsis thaliana* root tip cells showing sections through cross walls and ER.

Figure 5.3.7 – Transmission electron micrographs of 200 nm sections of ZIO stained wild-type *Arabidopsis thaliana* root tip cells treated with DMSO and Silwett-77™.

Figure 5.3.8 – Transmission electron micrographs of 200 nm sections of ZIO stained *Arabidopsis thaliana* root tip cells of plants following 20 hours induction of truncation 2 of RTNLB3-YFP over-expression.

Figure 5.3.9 – Transmission electron micrographs of 200 nm sections of ZIO stained *Arabidopsis thaliana* root tip cells of plants following 20 hours induction of truncation 2 of RTNLB3-YFP over-expression showing association of nuclear envelopes with cell walls.

Figure 5.3.10 – Transmission electron micrographs of 200 nm sections of ZIO stained *Arabidopsis thaliana* root tip cells of plants following 20 hours induction of truncation 2 of RTNLB3-YFP over-expression showing cells with abnormal formations of cross walls.

Figure 5.3.11 - Tomographic data of a cell plate undergoing development in a wild-type *Arabidopsis thaliana* root tip meristematic cell.

Figure 5.3.12: Tomographic data of a cell plate undergoing development in an *Arabidopsis thaliana* root tip meristematic cell over-expressing RTNLB3-YFP.

Chapter 6

Figure 6.3.1 - SBFSEM data and images of 3D reconstructions from the datasets, showing cross walls and ER in interphase wild-type *Arabidopsis thaliana* root tip cells.

Figure 6.3.2 - SBFSEM data and images of 3D reconstructions from the datasets, showing cross walls, nuclear envelopes and ER in interphase wild-type *Arabidopsis thaliana* root tip cells.

Figure 6.3.3 - SBFSEM data and images of 3D reconstructions from the datasets, showing ER and cell plate material in a wild-type *Arabidopsis thaliana* root tip cell undergoing division.

Figure 6.3.4 - SBFSEM data and images of 3D reconstructions from the datasets, showing ER and cell plate material in wild-type *Arabidopsis thaliana* root tip cells undergoing division.

Figure 6.3.5 - SBFSEM data and images of 3D reconstructions from the datasets, showing cross walls, developing cell plates and ER in control DMSO and Silwett[77] treated *Arabidopsis thaliana* root tip cells.

Figure 6.3.6 - SBFSEM data and images of the 3D reconstruction of a mutant cell in an *Arabidopsis thaliana* root tip induced to over-express truncation 2 of RTNLB3-YFP.

Figure 6.3.7 - SBFSEM data and images of 3D reconstructions from the datasets, showing cross walls, developing cell plates and ER in *Arabidopsis thaliana* root tip cells induced to over-express truncation 2 of RTNLB3-YFP.

Figure 6.3.8 - SBFSEM data and images of 3D reconstructions from the datasets, showing cross walls, developing cell plates and ER in *Arabidopsis thaliana* root tip cells over-expressing full length RTNLB3-YFP.

Appendix Disc:

WTCrossWall1.mpg

WTCrossWall2.mpg

WTDiagonalCrossWall1.mpg

WTNECrosswall.mpg

WTPlate1.mpg

Abbreviations:

3D-SIM - Three-dimensional structured illumination microscopy

ATP - Adenosine triphosphate

BFA – Brefeldin A

BMV - Brome mosaic virus

BY-2 – Bright yellow two

CLSM – Confocal laser scanning microscope

CNX – Calnexin

DiOC6 – 3, 3'- Dihexyloxacarbocyanine idodide

DMSO – Dimethyl sulfoxide

DRAQ5 - 1,5-bis{[2-(di-methylamino) ethyl]amino}-4, 8-dihydroxyanthracene-9,10-dione

DW – Distilled water

EM – Electron microscopy

ER – Endoplasmic reticulum

FRAP - Fluorescence recovery after photobleaching

FRET-FLIM - Fluorescence resonance energy transfer - fluorescence lifetime imaging microscopy

GFP – Green fluorescent protein

GTP - Guanosine-5'-triphosphate

LB – Luna-Bertani

NE – Nuclear envelope

NSP – Neuroendocrine specific protein

NPC – Nuclear pore complex

NUP - Plant nucleoporin

PD – Plasmodesmata

RFP – Red fluorescent protein

RHD3 – Root hair defective 3

RNA - ribonucleic acid

RT – Room Temperature

RTN – Reticulon

RTNLB3 – Plant reticulon 3

RHD – Reticulon homology domain

SBF – Serial block face

ssTEM – Serial section transmission electron microscopy

SEM – Scanning electron microscopy

SYTA - Synaptotagmin

TEM – Transmission electron microscopy

TMD – Transmembrane domain

UP – Ultra-pure

VAP27 - Vesicle-associated membrane protein-associated protein 27

WT – Wild-type

YEB – Yeast Extract Broth

YFP – Yellow fluorescent protein

ZIO – Zinc iodide osmium tetroxide

1. Introduction

1.1 The endoplasmic reticulum (ER)

The endoplasmic reticulum (ER) is a large organelle ubiquitous to all eukaryotic cells. Its functions are fundamental to cellular growth, development and maintenance. The organelle was first described by Emilio Veratti in 1902 (Veratti, 1961; Margreth, 2002), however its structural complexities could not be investigated until the introduction of the electron microscope as a tool for biological analysis in the 1950's (Palade & Porter, 1954; Palade, 1955; Porter & Palade, 1957). Since then, a range of techniques including confocal fluorescence and electron microscopy have revealed further details of the structure of the ER.

1.1.1 Functions of the ER

The ER provides the site at which ribosomes are docked to receive mRNA to translate into the proteins, which the cell requires for its survival (Alberts *et al.* 2014). It is also the beginning of the secretory pathway into which the newly synthesised proteins enter. During transport through the ER the proteins are post translationally folded by ER chaperone proteins and folding enzymes, and either progress through the pathway to the Golgi apparatus for trafficking to the required cellular location, are incorporated into the ER membrane, or are targeted for degradation due to defects in folding by the ER quality control system (Vitale & Denecke, 1999; Ma & Hendershot, 2004; Matheson *et al.* 2006; Araki & Nagata, 2012; Brandizzi *et al.* 2003).

The ER membrane serves as a scaffold to which various signalling proteins bind, such as membrane tethered transcription factors that are involved in cellular growth and stress response (Chen *et al.* 2008). The induction of ER stress has been shown to result in autophagic ER membrane turnover (Bernales *et al.* 2006; Liu *et al.* 2012). This multifunctional membrane network is also responsible for lipid biosynthesis (Wallis & Browse, 2010) including the biogenesis of oil bodies and peroxisomes (Huang, 1996; Galili, 2004; Heiland & Erdmann, 2005; Herman, 2008), and the regulation of cellular calcium homeostasis (Hong *et al.* 1999).

In plants the ER additionally houses hormonal receptors with plant-specific roles, such as the regulation of growth, controlled by cellular auxin levels (Chen *et al.* 2002; Friml & Jones, 2010). It is essential for lipid synthesis with chloroplasts in photosynthetic organisms (Benning, 2009) and recent evidence suggests that lytic vacuoles in plants can develop via a pathway independent of the Golgi apparatus, where the ER serves as a membrane source in meristematic cells (Viotti *et al.* 2013). During growth and defence response against pathogens the ER also functions as a compartment for protein storage in many plant tissues (Yamada *et al.* 2011; Ibl & Stoger, 2012).

1.1.2 Structural and functional ER domains

The ER consists of a continuous lipid bilayer that encloses the ER luminal space. This membrane bounded network provides an oxidising intracellular environment in the otherwise reducing conditions maintained in the cytosol (Sparkes *et al.* 2009a). During interphase, beginning at the outer membrane of the nuclear envelope (NE), the same continuous membrane extends to the plasma membrane, through the cell cytoplasm, in an intricate network of tubules and sheets (Goyal & Blackstone, 2013). Therefore the ER has distinct domains with differing structure; the outer NE, tubular ER and cisternal ER (English *et al.* 2009; Sparkes *et al.* 2009a; Goyal & Blackstone, 2013). The membrane contact sites between the ER and other organelles have also been described as structurally and functionally distinct domains, which include associations with mitochondria, Golgi, endosomes, peroxisomes and the plasma membrane (English & Voeltz, 2013a).

In yeast and plants cells the ER, excluding the NE, is often referred to as “cortical ER”, as the majority of the network resides towards the cell periphery near the plasma membrane, whereas in mammalian cells the network is more evenly distributed throughout the cell (Ward & Brandizzi, 2004; Nakano, 2004). As the different structures of ER are all formed of the same membrane, factors must be present that create and maintain structural and functional differences within these distinct regions, however the mechanisms through which the ER is shaped and remodelled has until recent years remained largely unknown.

Cisternal ER is composed of adjacent membrane sheets possessing highly curved edges to form the cisternae, whereas tubular ER consists of narrow tubules that branch and fuse to form an interconnected meshwork (Shibata *et al.* 2006; Sparkes *et al.* 2009a; Westrate *et al.* 2015). The diameter of both the cisternal lumen and tubules has been documented to be approximately 50 nm in mammalian cells and 30 nm in yeast (Bernales *et al.* 2006; Shibata *et al.* 2010; West *et al.* 2011). ER cisternae are often found stacked one on top of another, with recent analysis of mammalian cells having revealed that such stacks are connected via twisted membranes surfaces with helical edges distinct from ER tubules (Terasaki *et al.* 2013). The structure allows for ER sheets to be tightly packed and connected in close proximity. Overall, despite spanning the entire cell from the nuclear envelope to the plasma membrane, the structure of the ER network allows the organelle to extend throughout the cell with space for the traffic of other organelles and cargo around its surface (Friedman & Voeltz, 2011). The cytoskeleton and the ER are highly interdependent and the ER is also implicated the transport of cellular cargo (Stefano *et al.* 2014).

As cisternal ER is flat except for the cisternal rims and tubules exhibit a high degree of curvature throughout, tubules possess a higher surface to volume ratio than sheets and the two structurally distinct domains have been linked to function. ER cisternae have been shown to be the primary sites for protein synthesis, entry into the secretory pathway, post translational modification and folding (Voeltz *et al.* 2002; Shibata *et al.* 2006; Westrate *et al.* 2015). Less is known about the function of ER tubules, however it has been suggested that they could be the primary regions of the ER where signalling between other organelles occurs and where lipid synthesis, delivery and droplet formation take place (Park & Blackstone, 2010; Westrate *et al.* 2015).

In addition to the nuclear, tubular and cisternal ER domains, Staehelin (1997) identified 16 types of morphologically distinct ER membrane domains and described their structural and functional properties. As several of the domains are transient or labile, the work used ultra rapid freezing techniques in combination with electron microscopy to visualise these structures. The domains identified in his study were: the lamin receptor domain; the nuclear pores; the nuclear envelope-ER gates, the microtubule nucleation domains; the protein and oil body-forming domains; the vacuole-forming ER; the actin-binding, the

plasma membrane-anchoring and the vacuole and mitochondrion-attachment domains; the lipid recycling ER cisternae and the plasmodesmata (Staehelin, 1997).

The cisternal and tubular ER morphologies are commonly known as rough and smooth ER respectively, due to the high density of ribosomes housed on the surface of cisternal sheets and their relative absence on the exterior of tubules (Voeltz *et al.* 2002; Shibata *et al.* 2006; Park & Blackstone, 2010). However, it has in recent years become apparent that the terms rough and smooth ER in reference to cisternal and tubular ER do not always hold true. It has been shown in yeast cells that cisternal ER that opposes the plasma membrane in close proximity lacks ribosomes on its surface, which is hypothesised to be due to the tight tethering of the ER at plasma membrane contact sites, resulting in them being excluded from the ER surface (West *et al.* 2011).

Proteins synthesised on ribosomes docked on the ER enter the lumen and are transported to the Golgi if destined for other organelles or for secretion, or are retained for incorporation within either the ER or Golgi membranes. Proteins that are to remain in the cytosol or are destined to be incorporated into mitochondrial, chloroplast, peroxisome or nuclear membranes, are synthesized on ribosomes that are free in the cytosol (Cooper, 2000).

Proteins that are to be translocated to the secretory pathway are targeted to the ER by hydrophobic amino acid targeting sequences, signals located at the amino terminus of the polypeptide chain. The signal sequences are then cleaved from the proteins during their transfer into the lumen of the ER (Cooper, 2000).

The ratio of the ER in tubular and cisternal form varies between cell types and has been linked to cellular function. For example, in pancreatic cells that have a high protein production and secretion capacity the ER network is primarily comprised of stacked ER sheets studded with ribosomes (Shibata *et al.* 2006). A recent study of mammalian cells has indicated that, in addition to ribosomes, the machinery required for protein translocation may be enriched on ER cisternae in comparison to tubules (Friedman & Voeltz, 2011). This enrichment appears to correlate with cisternal ER heavily studded with ribosomes, which is involved in protein production; however whether or not this is the case is yet to be ascertained. In contrast to cells with roles in protein secretion, epithelial and neuronal cells that secrete relatively little protein have primarily tubular

networks with few ribosomes (Terasaki *et al.* 2013; Baumann & Walz, 2001), as do liver hepatocytes in which the ER houses metabolic and detoxifying enzymes (Park & Blackstone, 2010).

The NE is comprised of two ER membrane bilayers, known as the inner and outer nuclear membranes. The shape of the NE is maintained through an assortment of proteins, such as those linking the inner and outer NE membranes, proteins bound to the inner membrane, chromatin and lamin inside the nucleus, and connections with the cytoskeleton (Westrate *et al.* 2015). During cell differentiation and division the ER undergoes dramatic structural rearrangements in its architecture. When metazoan cells undergo mitosis, the tubular peripheral ER transforms into sheets and the nuclear envelope disassembles (Lu *et al.* 2009; Wang *et al.* 2016). The nuclear envelope is also disassembled during cell division in plants, however the rearrangement of the cortical ER throughout this process has not been thoroughly documented. Although in recent years some light has been shed on the factors involved in the generation, maintenance and remodelling of the ER network during interphase, how structural changes occur during the cell cycle remain poorly understood. The process requires regulatory factors to ensure that disassembly occurs at the correct time and that reassembly in daughter cells results in a morphologically correct nuclear envelope and peripheral ER; however the intricacies of the molecular mechanisms of this process are yet to be elucidated.

1.1.3 ER dynamics and shape

Alongside the complex segregation of structure within the ER, the network as a whole is not static and undergoes constant movement. In addition to this movement, the network also remodels and the ratio between tubular and cisternal membrane forms is in constant flux. In metazoan cells the ER network is associated with the microtubule cytoskeleton, whereas in plant cells it is linked to both microtubules and actin filaments (Griffing *et al.* 2016; Borgese *et al.* 2006), and only the actin cytoskeleton in fungal cells (Borgese *et al.* 2006). In plants the movement associated with links to the actin cytoskeleton has been shown to be associated with myosin motor proteins (Sparkes *et al.* 2009b). Similar to the model for actin and myosin association of the tubular ER in plant cells, proposed by

Sparkes *et al.* (2009b), ER tubules in animal cells can grow either along static microtubules with the aid of myosin motors or by attachment via other proteins to extending microtubules (Borgese *et al.* 2006). The role of the cytoskeleton in ER structure will be discussed further in section 1.2.1.

Although the majority of the ER is highly dynamic exhibiting constant movement and remodelling, approximately 5 % has been shown to persist in association with the plasma membrane, including some punctate areas that maintain their localisation (Sparkes *et al.* 2009b). These points act as anchor/contact sites between the plasma membrane and ER, around which the rest of the network remodels (discussed further in section 1.2.5). As well as playing a structural role the sites are essential for communication between the ER and plasma membrane, with the connections facilitating the transport of lipids and calcium ions (Wang *et al.* 2014). The ER is also in close association with, or makes transient contact with, other organelles in the cell such as Golgi bodies, mitochondria, peroxisomes, lipid droplets and endosomes (Phillips & Voeltz, 2016).

The ER surface exhibits a further level of movement independent of network remodelling. When the actin cytoskeleton is disrupted in plants, protein movement continues to occur in the ER membrane, as demonstrated by photoactivation of photoactivatable GFP fused to an ER transmembrane protein that radially diffused from the activation spot (Runions *et al.* 2006).

The shape of organelles is determined by the membranes by which they are bounded, a characteristic that has been conserved throughout evolution between the kingdoms. Although plants and animals carry a somewhat different complement of organelles, the morphology of those which are shared is remarkably similar. This indicates either a necessity to maintain these shapes for the optimum function of each organelle, evolutionarily conserved factors involved that are responsible for producing these structures, or both.

Functions of the ER have been studied in-depth in a range of organisms since the organelles discovery, but the mechanisms which underlie the formation and maintenance of the organelles varied structure had until recently remained unclear. The range of morphologies within the ER membrane requires numerous molecular mechanisms to

explain the formation, maintenance and remodelling of this architecturally complex organelle. Factors now implicated in shaping ER domains include cytoskeletal interactions, homotypic fusion machinery, membrane associated and integral proteins. As the ER is associated with other organelles, including the plasma membrane via abundant and widely distributed contact sites, these may also influence ER architecture (English & Voeltz, 2013a; Stefano *et al*. 2014).

1.2 Mechanisms shaping ER membranes

1.2.1 Influence of the cytoskeleton

In mammalian cells the ER is associated with the microtubules of the cytoskeleton, which are involved in the reorganisation and generation of ER tubules. These processes are mediated by pulling on the membrane network by microtubule associated motor proteins (Waterman-Storer & Salmon, 1998). In contrast, in plants and yeast it is the actin cytoskeleton that is primarily associated with the ER. Similarly to the role microtubule motor proteins have been shown to play in ER structure, actomyosins have been documented to be involved in shaping and remodelling of the network in *Saccharomyces cerevisiae* and a range of plant species (Estrada *et al.* 2003; Quader *et al.* 1989; Liebe & Menzel, 1995; Sparkes *et al.* 2009b). Despite the cytoskeleton acting extrinsically to orchestrate ER architecture, as the ER network shape persists following depolymerisation of the cytoskeleton (Terasaki *et al.* 1986; Prinz *et al.* 2000), other factors are involved that create and maintain the organelle's integral structure of varied morphologies.

1.2.2 ER cisternae

ER cisternae tend to be localised closer to the NE whereas tubules predominate in the periphery (English & Voeltz, 2013a). ER cisternae require mechanisms for the maintenance of the low-curvature sheet membranes, to bring two opposed flat membranes together so that they are stacked with a consistent luminal space, and to curve the edges that connect the opposing sheet membranes.

Although ER cisternae can be created by depleting cells of ER tubulating proteins or through the over-expression of non-functional mutants (Voeltz *et al*. 2006; Anderson and Hetzer, 2008; Sparkes *et al*. 2010; Shibata *et al*. 2010; West *et al*. 2011), sheet formation can also be induced by other factors that have been shown to generate and stabilise ER cisternae. One mechanism identified as a contributing factor to low-curvature sheet regions is the involvement of large protein complexes bound to the membrane surface. Ribosomes and polyribosomes, in association with translocation complexes, likely aid the stabilisation of ER sheet surfaces as indicated by experiments in mammalian and yeast cells (Rolls *et al*, 2002; Shibata *et al*. 2006; Puhka *et al.* 2007; Benyamini *et al.* 2009; Shibata *et al.* 2010). Kinectin proteins and p180, which are integral membrane proteins enriched in ER sheets, are also thought to contribute to stabilising sheet structure by maintaining the flatness of low curvature regions (Zhang & Hu, 2016).

A 63-kDa non-glycosylated ER integral membrane protein known as Climp63 (previously termed p63), which preferentially localises to ER sheets as opposed to tubules, has also been identified as a regulator of cisternal structure (Schweizer *et al*. 1993; Schweizer *et al.* 1995; Klopfenstein *et al*. 2001). Experiments by Shibata *et al.* (2010) in mammalian cells have demonstrated that Climp63 over-expression leads to the formation of ER cisternae. They also showed that when the protein is depleted, although ER cisternae remain intact, size of the luminal space between opposing membrane sheets is reduced by ~20 nm. Electron microscopic analysis has shown that ER cisternae in mammalian cells, which possess endogenous Climp63, maintain a luminal space of ~50 nm, whereas in yeast which lack this protein luminal spacing is ~30 nm (Bernales *et al.* 2006; Shibata *et al*. 2010). It is thought that Climp63 may regulate luminal spacing in cisternae via a homo-oligomerising luminal coiled-coil domain, which is also responsible for regulating its preferential localisation to cisternal ER sheets (Westrate *et al*. 2015). Climp63 also possesses a cytoplasmic microtubule binding domain; whether or not this association is involved in ER architecture or dynamics and what role it may play is yet to be elucidated (English & Voeltz, 2013a).

1.2.3 ER tubule dynamics and membrane fusion machinery

Due to the consistent remodelling of the ER forming new membrane connections within it, homotypic membrane fusion events are constantly occurring (Hawes *et al.* 2015). In metazoan ER networks this fusion is mediated by a family of proteins known as atlastins (ATLs); part of the dynamin family, these are membrane-bound proteins which have GTP-ase activity (Orso *et al.* 2009). ER membrane fusion involving atlastins is mediated by the enzymatic activity of the protein by the hydrolysis of guanosine triphosphate (GTP, Saini *et al.* 2014). Atlastin localisation is generally restricted to ER tubules, however over-expression of atlastins has been shown to cause the proteins to localise in high concentrations to three-way ER junctions in mammalian, insect and yeast cells (Rismanchi *et al.* 2008; Orso *et al.* 2009; Chen *et al.* 2012). In contrast, over-expression of an atlastin mutant can result in a decreased number of three-way junctions in the network in combination with elongation of ER tubules (Hu *et al.* 2009). Over-expression of atlastin in *Drosophila melanogaster* neuronal cells has also been shown to result in ER membrane hyper fusion (Orso *et al.* 2009). These results indicate that atlastins regulate ER structure by mediating the fusion of ER tubules when they make contact with each other at locations where junctions between tubules form. The specific ER localisation of these atlastins and the homotypic ER membrane fusion they facilitate are mechanistically crucial for ER network membrane remodelling machinery, due to the ER's close association with other membrane bounded organelles in the cell.

Atlastins are specific to metazoan ER fusion and have not been precisely conserved between kingdoms in sequence similarity. However, yeast and plant orthologues that also have GTP-ase enzymatic activity have been identified. These are Sey1p (Hu *et al.* 2009) and Root Hair Defective 3 (RHD3) (Chen *et al.* 2011), in *Saccharomyces cerevisiae* and *Arabidopsis thaliana,* respectively. Alongside a large GTPase domain, both orthologues also share other signature features with atlastin, including a short C-terminal tail, a helical bundle domain and two transmembrane segments that reside in close proximity to one another (Stefano *et al.* 2014).

Expression of mutated RHD3 results in changes in ER morphology (Chen *et al.* 2011) that bare a close resemblance to the phenotype witnessed in mammalian cells upon the depletion of atlastins (Orso *et al.* 2009; Hu *et al.* 2009). The phenotype resulting from

expression of RHD3 mutants consists of a network containing fewer polygonal regions and long strands of ER (Zhang *et al.* 2013). Similar to atlastin, overexpression of Sey1p has also been shown to localise to three-way junctions when overexpressed (Chen *et al.* 2012). This phenotype has been hypothesised to be the result of disruption of the cells capacity for ER tubule fusion due to overexpression of defective RHD3 protein. The decreased tubular ER fusion during ER remodelling could be resulting in the formation of fewer polygonal regions (Zhang *et al.* 2013).

Although Sey1p has been identified as a yeast orthologue of RHD3, Sey1p did not restore wild-type ER structure in *Arabidopsis thaliana* RHD3 mutants (Chen *et al.* 2011). Nor, conversely, was expression of RHD3 in yeast cells able to compensate for defective Seyp1 protein expression to restore wild-type ER morphology in the study by Chen *et al.* (2011). This suggests the two proteins are not similar enough to be functionally interchangeable. However, further research has demonstrated that expression of RHD3 can induce ER membrane fusion in yeast Sey1p mutants (Zhang *et al.* 2013).

RHD3 appears to serve a multifunctional role in ER membrane characteristics, as demonstrated by a study of the mobility of ER membrane proteins in the lipid bilayer of *A. thaliana* leaf cotyledon cells. Cells expressing mutant RHD3 and the fluorescent protein fusion CNX-GFP (which acts as a membrane marker), in fully developed epidermal cells, exhibited a reduction in CNX-GFP membrane mobility (Stefano *et al.* 2014). Therefore, RHD3 seems to have some effect on protein mobility within ER network membranes.

Two Rab GTPases that localise specifically to the ER have also been identified recently, Rab10 and Rab18 (English & Voeltz, 2013b; Gerondopoulos *et al*. 2014). Overexpression of a Rab10 mutant and Rab10 depletion have been shown to produce an increase in cisternal ER proportional to tubules and a reduction in both ER membrane fusion and movement (English & Voeltz, 2013b), which may account for the increase in sheets. Over-expression of non-functional Rab-18 mutants have also been shown to result in an increase in ER cisternae (Gerondopoulos *et al*. 2014). These results suggest a different mechanism to atlastins for ER membrane fusion, as disruption of atlastin function has produced the opposite effect, with long unbranched ER tubules being propagated (Hu *et al*. 2009).

1.2.4 ER tubule junctions

A member of the Lunapark protein family, Lnp1p, has recently been discovered to interact with reticulons and DP1/Yop1p in yeast (discussed further in section 1.3) and shown to localise to tubule junctions of ER in both mammalian and yeast cells (Chen *et al.* 2012). Even though *A. thaliana* has two Lunapark isoforms, it is yet to be documented whether interaction with reticulons and/or localisation to ER tubule junctions occurs in plant cells (Kriechbaumer, personal communication). In yeast, Chen *et al.* (2012) demonstrated that Lnp1p appears to act antagonistically with the ER tubule fusing protein atlastin homologue Sey1p. They suggest that the two proteins function to balance the structure of the network and that Lnp1p is required for formation of the polygonal ER junctions, with synergic reticulon interaction.

1.2.5 Plasma membrane-ER anchor points

In addition to locations where the ER is incorporated into plasmodesmata in the cell wall (discussed further in section 1.5), there is additional anchorage of the ER at the plasma membrane, which was first documented by Quader *et al.* (1987) in a study of ER dynamics in onion bulb epidermis cells. Only more recently have these anchor sites, and how their persistence relates to ER structure and remodelling, been investigated in greater detail (Sparkes, *et al*. 2009b; 2009c).

In 2009, leaf cells expressing fluorescent protein fusions of ER and Golgi markers were micromanipulated using infrared optical laser trapping by Sparkes *et al.* (2009c). Golgi bodies were captured and moved, which showed that they are tethered to the ER network. Micromanipulation of Golgi bodies resulted in remodelling of the ER around certain points, revealing the fixed localities of ER referred to as anchor points. Although persistent, these anchor sites are not permanently fixed, as in regions where rapid streaming of ER occurred these sites were also found to move with the network. Sparkes *et al.* (2009c) note that they prefer to term these anchor/growth sites, as opposed to anchor sites, for this reason.

Time lapse imaging of the ER network, visualised using expression of green fluorescent protein fused to the ER retention peptide sequence HDEL (GFP-HDEL), revealed regions

of ER tubules that exist as consistent puncta, remaining static as the surrounding network remodelled (Sparkes *et al.* 2009b). These regions constituted 5 % of the otherwise spatially and structurally transient ER network. Therefore, rather than ER movement involving the network in its entirety, the dynamics are a result of the combination of the formation and fusion of new tubules and cisternae, with the simultaneous movement of existing membrane structures within a scaffold at the cell periphery.

In addition to these plasma membrane anchor points, junctions where microtubules and the ER meet have been suggested to be stable. Research had indicated that these may be locations where the transport of organelles along actin filaments is disrupted (Hamada *et al.* 2012) and the sites have been described as cortical microtubule-associated ER sites (C-MERS, Peña & Heinlein, 2013). Wang *et al.* (2014) have since demonstrated that two proteins, an actin binding protein of the NET plant specific super family known NET3C, and an ER-PM contact site protein Vesicle-associated membrane protein-associated protein 27 (VAP27), localise to these points and form complexes with both microtubules and actin. The turnover of NET3C and VAP27 at these sites has been shown to be controlled by F-actin and microtubules respectively (Wang *et al.* 2014).

1.3 Curving ER membranes

1.3.1 Introduction to the reticulon protein family

In recent years it has become clear that integral membrane components are responsible for the induction and maintenance of membrane curvature within the ER. A family of proteins known as reticulons have been discovered in a multitude of species and linked to a wide array of specific functions dependent on cell type. Despite the varied implications of reticulon proteins in cellular activity, one association has remained unanimous throughout the majority of cell types studied – a localisation to highly curved ER membranes (Nziengui *et al.* 2007).

A reticulon protein is defined as a protein which possesses a region known as the reticulon homology domain (RHD). The RHD is categorized as a 150 to 201 amino acid sequence at the carboxy-termnius of the reticulon proteins, which consists of two hydrophobic domains linked with a hydrophilic region approximately 66 amino acids in

length (Oertle *et al.* 2003). The total size of reticulon proteins can range 6-fold from 200 up to 1200 amino acids due to the high variability at the amino terminus (Yang & Strittmatter, 2007).

In excess of 250 RTN/RTNL genes have been identified across eukaryotic kingdoms, based on at least partial sequence homology of the RHD in sequences stored in the GenBank database (Oertle *et al.* 2003). Thus far there have been no homologous genes identified in prokaryotic species. The lack of reticulons in prokaryotic cells may be due to the reticulons evolving with the development of the ER membrane system, which these organisms lack (Yang & Strittmatter, 2007).

Plants possess the largest number of these proteins, with 21 different reticulon genes having been identified in *Arabidopsis thaliana* (Nziengui *et al.* 2007) compared to only four present in the human genome (Nziengui & Schoefs, 2009). Figure 1.3.1A shows the phylogenetic relationships within the *A. thaliana* reticulon family. The extent of conservation of protein sequences varies in relation to different reticulon protein domains. Between species, the most conserved region is the reticulon homology domain (RHD), by which the protein family is categorized at the C-terminus, and the N-terminal sequences between species bear little to no resemblance (Nziengui & Schoefs, 2009).

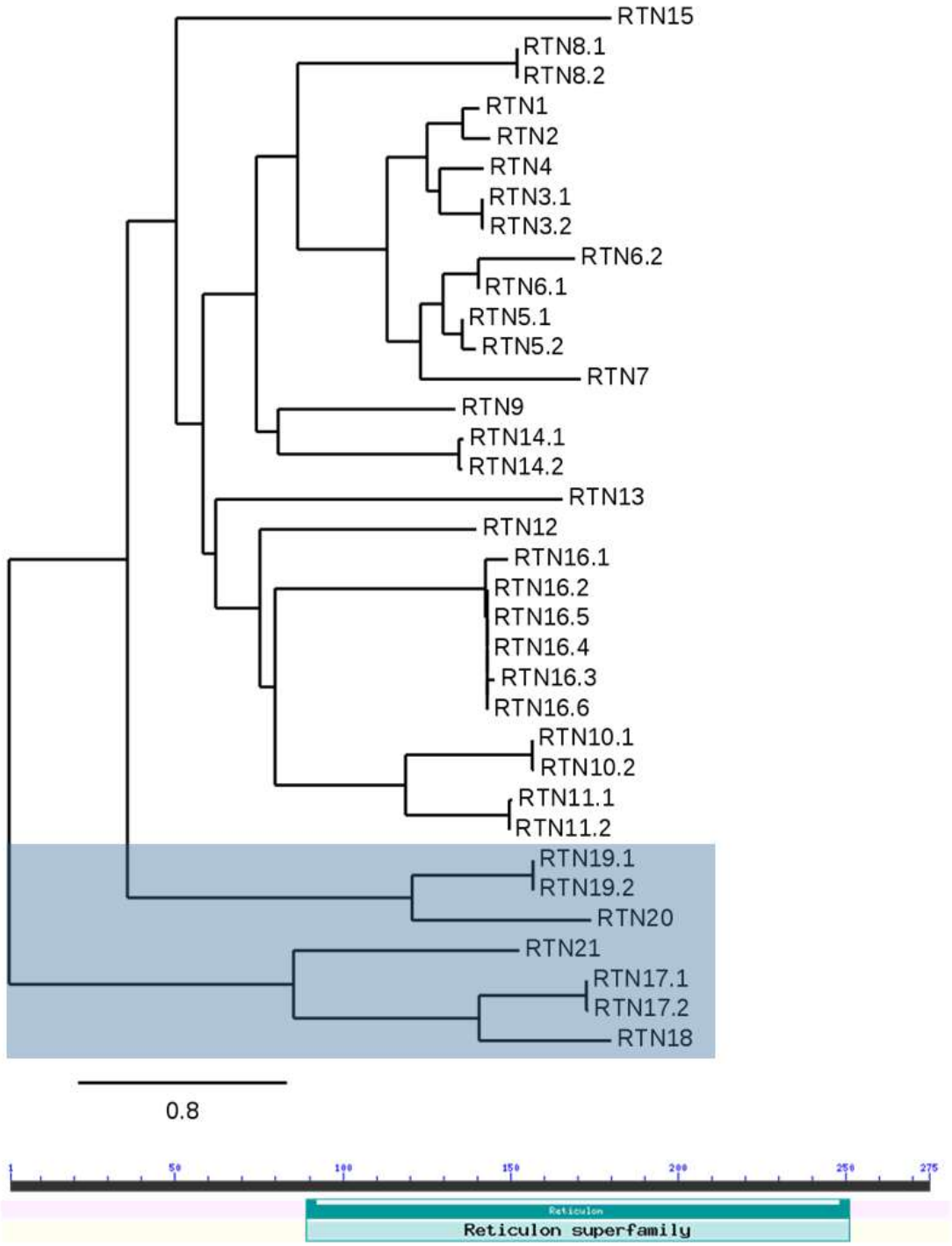


Figure 1.3.1A: Phylogenetic analysis showing relationships within the *A. thaliana* reticulon family including alternate splice isoforms. Grey shading indicates reticulon protein with an extended N-terminal domain. Bar for bootstrap value is shown and BLAST domain annotation below (Kriechbaumer *et al.* unpublished).

Plants may possess a high number of reticulon family members due to requirements for temporal and spatial regulation of reticulon gene expression depending on their functions, in addition to their shared ER membrane shaping properties. For example, a plant will have different expression requirements for proteins and their synthesis depending on the stage of maturation or seasonal cycle, temperature, availability of sunlight, and nutrition. Therefore, a high number of complementary reticulon genes coding for proteins, each with specific adaptions for specific conditions or growth stages, could explain the requirement for a plant to have such a high number of reticulon genes. The eFP Browser (available at http://bar.utoronto.ca/efp/cgi-bin/efpWeb.cgi) provides expression pattern information and maps regarding *Arabidopsis thaliana* genes (Winter *et al.* 2007). For the At1g64090 RTNLB3 gene, expression based on the eFP browser appears to be relatively ubiquitous throughout the plants developmental stages, tissues, and when subject to biotic and abiotic stress, varying light intensity, and levels of plant hormones. Therefore, RTNLB3 appears to be expressed relatively consistently regardless of conditions and developmental stages, which hints at an essential role in cell function and/or development throughout cell types and tissues (Figure 1.3.1B shows a map of RTNLB3 expression in *A. thaliana*).

Genetic redundancy may also account for the high number of reticulon family members within plants such as *A. thaliana*, which have thus far been shown to share their ER membrane curvature inducing properties for RTNLB1-4 and 13 (Sparkes *et al.* 2010). In the case of genetic redundancy, multiple genes encode for proteins acting as a buffer that carry out the same function. This can be advantageous in the event of a mutation or defect in the function of a gene that is critical to survival, as the other complementary genes can compensate for the impact this would have on the organism (Kafri *et al.* 2009).

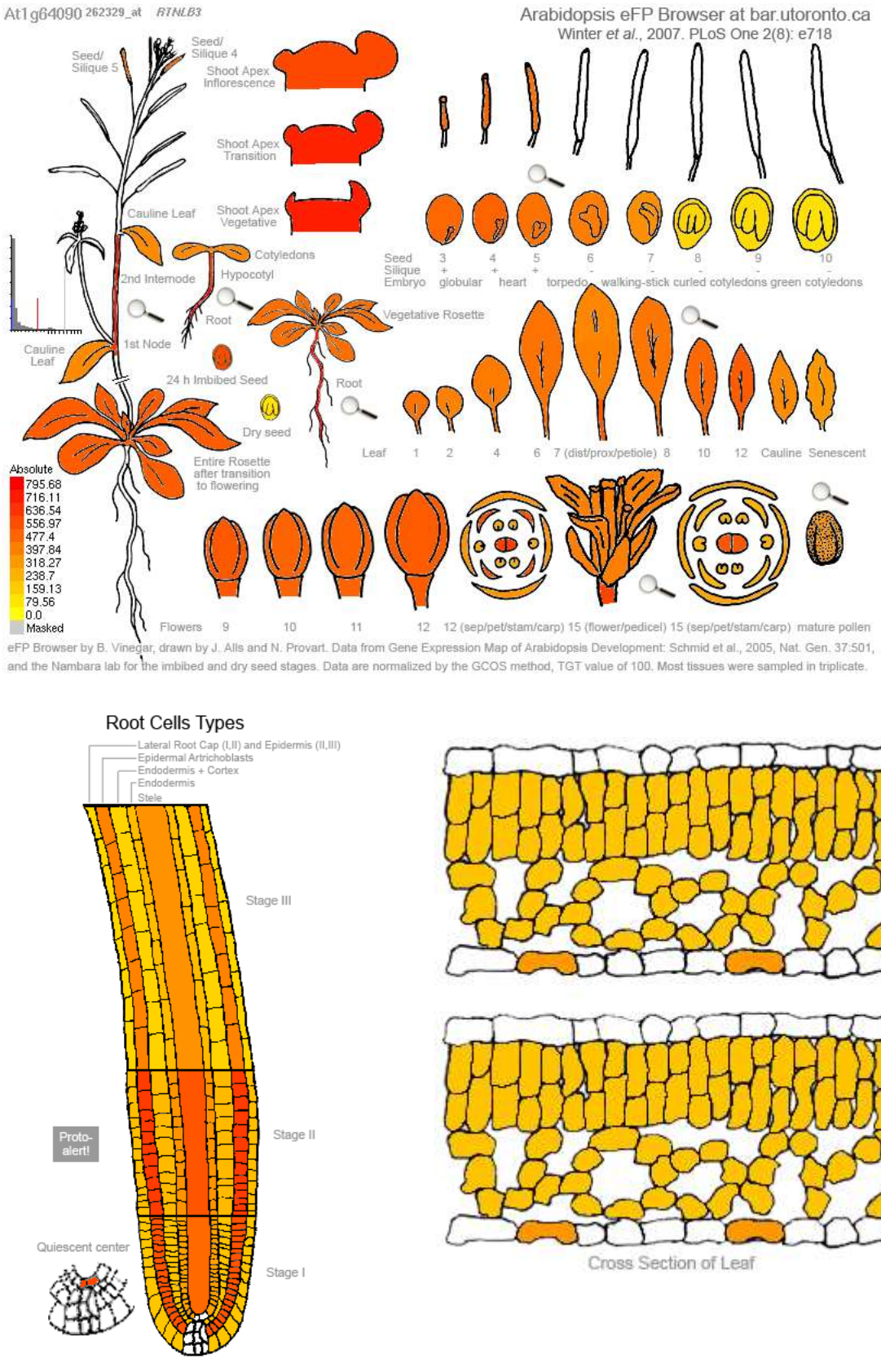


Figure 1.3.1B: Expression maps of At1g64090 RTNLB3 A. thaliana gene from eFP Browser. The gene in expressed throughout the plant tissues including cotyledonary leaves and roots.

Although reticulon proteins appear to have emerged relatively early in the evolution and divergence of species, they have continued to evolve, particularly in the non-conserved N-terminal region. For example, one of the exons of RTN4 is specific only to primates, and therefore must have evolved following the separation of this group from other mammals (Oertle *et al.* 2003). Despite this variation, as the overall structure of the RHD is conserved between species, it indicates that this structure is likely of importance to cellular function.

In 2003, Oertle *et al.* established the nomenclature now used to describe the reticulon family. They designated the abbreviation RTN for reticulons of chordate species and other metazoan reticulons as RTNL (reticulon-like), including insect, nematode and platyhelminth. Reticulons for species of other kingdoms are categorized as RTNLA, RTNLB and RTNLC for fungal, plant and protists respectively. This is followed by the number of the specific reticulon gene, and a letter denoting the splice variant if applicable.

Although a large variety of interacting proteins have been identified for members of the reticulon family, one consistent feature is localisation to curved ER membranes. This has been found in the broad range of species examined including mammalian (Van de Velde *et al.* 1994), amphibian (Kiseleva *et al.* 2007), insect (Wakefield & Tear, 2006) and plant cells (Tolley *et al.* 2008). One reticulon isoform (RTN1-C) has been recognized at the cell exterior of oligodendrocytes, however the protein was also found associated with the endoplasmic reticulum of these cells (GrandPré *et al.* 2000).

1.3.2 Reticulon proteins in vertebrate cells

Although research of reticulons as a known eukaryotic protein family is relatively recent, RTN4 was first isolated in 1988 and identified as neuronal growth inhibitor (Caroni & Schwab, 1988), however remained uncategorised until the following decade. The protein and other isoforms were initially referred to as neuroendocrine-specific proteins (NSP) due to the specific neuroendocrine tissue expression pattern that had been observed. In 1994, Van de Velde *et al.* suggested the name reticulon, after having established that two of these NSP are localised to membranes of the ER. Following this, RTN4A became

known as Nogo-A, with splice variants B and C also being assigned the Nogo prefix, a term still used throughout medical literature.

Vertebrates possess four reticulons; RTN1, RTN2, RTN3 & RTN4. Humans express at least 21 different reticulons isoforms, formed from multiple splice variants of each gene (Oertle *et al.* 2003). Initially the majority of mammalian research remained focused on RTN4/Nogo. Research implicating RTN4A in the inhibition of neurite growth (McGee & Strittmatter, 2003) has sparked much research focused on this variant in the medical field due to the potential benefits of understanding the role of this protein in neuronal growth inhibition. This work has led to RTN4A emerging as a new avenue for identifying causative agents of neurodegenerative diseases and potential therapeutic interventions for these. Indeed, interference in cellular pathways involving RTN4a is becoming an increasingly good candidate for therapeutic intervention to promote neurite growth and recovery after stroke (Wiessner *et al.* 2003; Lee *et al.* 2004; Tsai *et al.* 2007). RTN4A has also been linked to the motor neurone disease amyotrophic lateral sclerosis (ALS) and multiple sclerosis (Reindl *et al.* 2003; Jokic *et al.* 2006).

The localisation of reticulons specifically to tubular ER has been well documented, with the region of the protein determining this localisation having been identified as the RHD (Yang & Strittmatter, 2007). However, in the oligodendrocyte cells of chicks, both the N-terminal domain and the loop domain of RTN4A have been identified on the surface of the cells in culture. Therefore reticulons may on occasion have varying cellular localisations and/or topologies in relation to cell type.

The splice variant B of RTN4 (Nogo-B) has been found to be expressed in specific renal epithelial cells of mice, and that expression is up regulated in response to injury, with similar results observed in patient biopsies who have suffered damage of the renal tubules (Marin *et al.* 2010). Expression of RTN4B (Nogo-B) has also been shown to be activated in liver cirrhosis (Zhang *et al.* 2011).

A study using human neuroblastoma cells has shown that levels of RTN1C present in the ER membrane have a direct effect on how responsive the cell is to the activation of cell death pathways (Sano *et al.* 2007). The link between reticulons, the ER and apoptosis is not limited to RTN1C, as RTN3 expression has also been shown to be activated in the

event of ER stress. RTN3 was found to interact with RTN4B, and both reticulons to interact with Bcl-2, a key component of one of the major apoptotic pathways often deregulated in cancer cells (Wan *et al.* 2007).

Other studies have also found multiple reticulons capable of interacting with the same binding partner. All reticulons in humans have been identified as interacting proteins to BACE1, an enzyme that is a key factor in the neurodegenerative condition Alzheimer's, and both RTN1 and RTN3 have been shown to interact with a protein in which mutations are the most commonly identified causative agent of hereditary spastic paraplegia (Yang & Strittmatter, 2007).

C. elegans possesses one reticulon gene coding for three proteins due to alternative splicing; RTN-A, B and C (Iwahashi *et al.* 2002). The variant RTN-C is only expressed during embryogenesis and once the organism has hatched the protein is no longer detectable, suggesting involvement specifically in embryogenesis (Iwahashi *et al.* 2002). The N-terminal sequence of RTN-C is unique, based on bioinformatics comparison to other organisms whose genomes have been sequenced. This suggests that the region is very specific to the embryogenesis of this organism, and is an example of how the N-terminal sequences of reticulon isoforms have diverged between species to fulfil specific functions. This also shows great specificity in timing of expression and that difference in temporal expression pattern of individual splice variants of a single reticulon gene are possible.

1.3.3 Reticulon proteins & ER membrane conformation in yeast

Another organism in which a substantial amount of reticulon research has been carried out is the yeast model *Saccharomyces cerevisiae.* Consistent with previous findings in other organisms yeast reticulons localise to ER membranes and have been identified as proteins functionally involved in tubular ER structure (Voeltz *et al.* 2006). The interacting protein DP1/Yop1p, which shares the tubular ER localisation of reticulons and the membrane embedded hairpin topology, has also been linked to tubular membrane curvature (English *et al.* 2009). In cells where both yeast RTN1 and DP1/Yop1 have been

depleted, almost all of the ER is converted to large cisternal sheets, however when only one of these proteins is depleted there is little change to overall ER structure (Voeltz *et al.* 2006). Therefore DP1/Yop1 and RTN1 appear to both possess a capacity to curve ER membranes into tubules in yeast.

Fluorescence recovery after photobleaching (FRAP) analysis of DP1/Yop1p and RTN1p in yeast revealed that both have less mobility in the membrane than other ER membrane proteins generally exhibit, and both have also been shown to form oligomers of a range of sizes (Shibata *et al.* 2008). Mutants expressing a truncation of RTN1 no longer localised to the tubular ER and expression resulted in an impaired generation of ER tubules, greater RTN1 mobility, and decreased oligomerisation. Interestingly, Shibata *et al.* (2008) found that a decrease in the levels of ATP in both mammalian and yeast cells resulted in a decrease in the already limited mobility of reticulon proteins. They hypothesise that ATP may be required for the disassembly of reticulon oligomers, and therefore an increase in oligomer size, as a result of lack of ATP, may lead to decreased mobility.

Following this work, Shibata *et al.* (2010) also linked cisternal sheet formation to the abundance of reticulons and DP1/Yop1, with localisation of these proteins to sheet edges producing the curvature in these regions. They suggested that these proteins alone could give rise to both tubular and cisternal structures and that their abundance may determine the proportion of each morphology in the cell. However, Estrada de Martin *et al.* (2005) demonstrated that reticulons are not the only factor involved in forming and maintaining the tubular ER network in yeast, and other proteins involved in the generation and maintenance of ER cisternae have since been identified – discussed in section 1.2.2. They found that when cells lack another protein, Ice2, the tubular ER structure is affected. If the work by Voeltz *et al.* (2006) and Shibata *et al.* (2008) is confirmed, and reticulons and DP1/Yop1 in yeast are indeed sufficient to induce the generation of ER tubules, Ice2 may play a role in stabilising these structures.

A further study of yeast ER structure using transmission electron tomography and modelling during sequential stages of budding in wild-type and deletion mutant cells lacking reticulon and DP1/Yop1 membrane shaping proteins, was conducted by West *et al.* (2011). The deletions resulted in loss of curvature of the ER membranes, changes in ribosomal density, and a large increase in ER that was associated with the plasma

membrane. The authors state that the results indicate that the proteins may stabilise, as opposed to generate, curvature of yeast peripheral ER. Furthermore, the cisternal ER in the deletion mutants was found to lack fenestrations present in wild-type sheets, further indicating that reticulons and DP1/Yop1 may play a role in generating or stabilising curvature within these sites. In their study, the diameter of ER tubules in both wild-type and deletion mutant cells was also measured. The ER tubules were found to not be of a consistent diameter along the length of an individual tubule, but varied in a range of diameters. This variation in diameter was greater in the mutant cell than in wild-type and had a greater mean diameter. They noted that the results suggested that reticulon and DP1/Yop1 proteins are able to facilitate a range of degrees of curvature in membrane structure.

1.3.4 Reticulon proteins & the nucleus

It has been found that in yeast reticulon knockout mutants nuclear pore complexes (NPC) do not form, and that in a model *in vitro* vertebrate system of nuclear pore complex formation reticulon inhibition also prevented the formation of nuclear pore complexes (Anderson & Hetzer, 2008). This suggests that the requirement of reticulons for NPC formation may be conserved throughout eukaryotic organisms. As reticulons induce positive curvature in the ER membrane, the structural conformation of the mainly negative curvature of the membranes of the NPC would be opposing this. Therefore, a model with reticulons directly contributing to this curvature is not possible (such as at the edges of cisternae, Antonin, 2009). Also, enrichment of reticulons at sites of NPCs would be necessary, and RTNs are thought to generally not be present in NE membranes (Voeltz *et al.* 2006).

Other work by Dawson *et al.* (2009) has confirmed that RTN and Yop1/DP1 family members are required for NPC formation in yeast. *Saccharomyces cerevisiae* mutants expressing fluorescent RTN1-GFP and DP1/Yop1-GFP fusions showed that the proteins colocalise to NPCs and that deletion of both leads to clusters of NPCs forming. Defective importation from the nucleus was also observed. In another model system tested (*Xepopus laevis*), when RTN4a was inhibited nuclear pore complexes also failed to form (Dawson *et al.* 2009). Kiseleva *et al.* (2007) investigated RTN4A in *Xenopus* oocytes in

relation to nuclear envelope (NE) formation and demonstrated involvement of RTN4a in NE formation by disruption of RTN4a functionality, which affected NE development.

1.3.5 Reticulon proteins in plant cells

Oertle *et al.* (2003) identified in excess of 180 differing reticulon genes in plants, which share the RHD but little sequence similarity in the exon coding for the N-terminal region of the proteins. The RHD can vary 12 to 89 % in amino acid sequence, however the length of the plant RHD varies only by 15 amino acids at maximum (Nziengui *et al.* 2007). This suggests a greater evolutionary selection pressure on the structure and size of this domain as opposed to the specific molecular composition, hinting at a related structural function.

The first documentation of plant reticulons (henceforth referred to as reticulons) in the literature identified three reticulons, RTNLB1, RTNLB2, and RTNLB4, that interact with the pilin protein of *Agrobacterium tumifaciens* (Hwang & Gelvin, 2004). Overexpression of RTNLB1, referred to as BTI1, resulted in a greatly increased transformation efficiency by *Agrobacterium tumefaciens,* with interference of RTNLB1 leading to a decreased level of transformation. The exact function of these proteins in the infection process is thus far unknown. Following this, two plant reticulons were discovered to possess enzymatic activity, adding to the range of functions previously identified in other organisms. RTNLB19 and RTNLB20 encode regions capable of functioning as 3ß-hydroxysteroid dehydrogenases/C-4 decarboxylases (Rahier *et al.* 2006).

Initially, RTNLB2 and RTNLB4 were found to localise to the ER (Nziengui *et al.* 2007), with the ER localisation of RTNLB13 demonstrated shortly after, in combination with over-expression of RTNLB13 severely affecting ER morphology (Tolley *et al.* 2008). It was also discovered in this study that, in-conjunction to tubule constriction, over-expression of the seed specific RTNLB13 results in a reduction in the rate of diffusion of ER luminal proteins.

Following this work by Tolley *et al.* (2008), an extensive study by Sparkes *et al.* (2010) showed that RTNLB1, 2, 3 and 4 also co-locate to the tubular ER of *Nicotiana tabacum*

leaf epidermal cells, with over-expression of both N- and C- terminal fluorescent fusions of each causing a similar constricted phenotype of the membrane network as that of RTNLB13 over-expression. Transmembrane topology was also established for RTNLB1-4 as possessing four transmembrane domains (TMD) with cytosolic N and C termini. The cytosolic locality of the termini was demonstrated using protease protection assays, redox sensitive GFP (RhoGFP2) and BiFC (biomolecular fluorescence complementation). The latter of the techniques was also used to show the cytosolic orientation of the loop domain of RTNLB13, confirming previous topology predictions. Figure 1.3.5 summaries the membrane topology that was ascertained for these proteins.

RTNLB1-4 mutants expressing truncated proteins lacking either pair of N- or C- terminal transmembrane domains, with and without the loop domain, became distributed throughout the ER network rather than maintaining localisation to the tubular membranes (figure 1.3.5 b - e illustrates truncations). Therefore a complete RHD proved necessary to cause constriction of the ER into tubular form and for specific tubular localisation.

The transmembrane domains of plant reticulons are predicted to be five to six amino acids longer than the length of other plant ER transmembrane protein helices (Tolley *et al.* 2010). Tolley *et al.* (2010) demonstrated by analysis of cells expressing sequentially shortened TMD regions of RTNLB13 that the full length TMDs are required for RTNLB13 to localise to and constrict the ER membrane. Over-expression of RTNLB13 can cause cisternal ER to adopt a tubular morphology, which does not occur in mutants, where RTNLB13 has been modified to the predicted length of the majority of other proteins that span the ER membrane. This shows that the length of the transmembrane domains is directly related to RTNLB13's curvature inducing capability and ability to form complexes in the membrane.

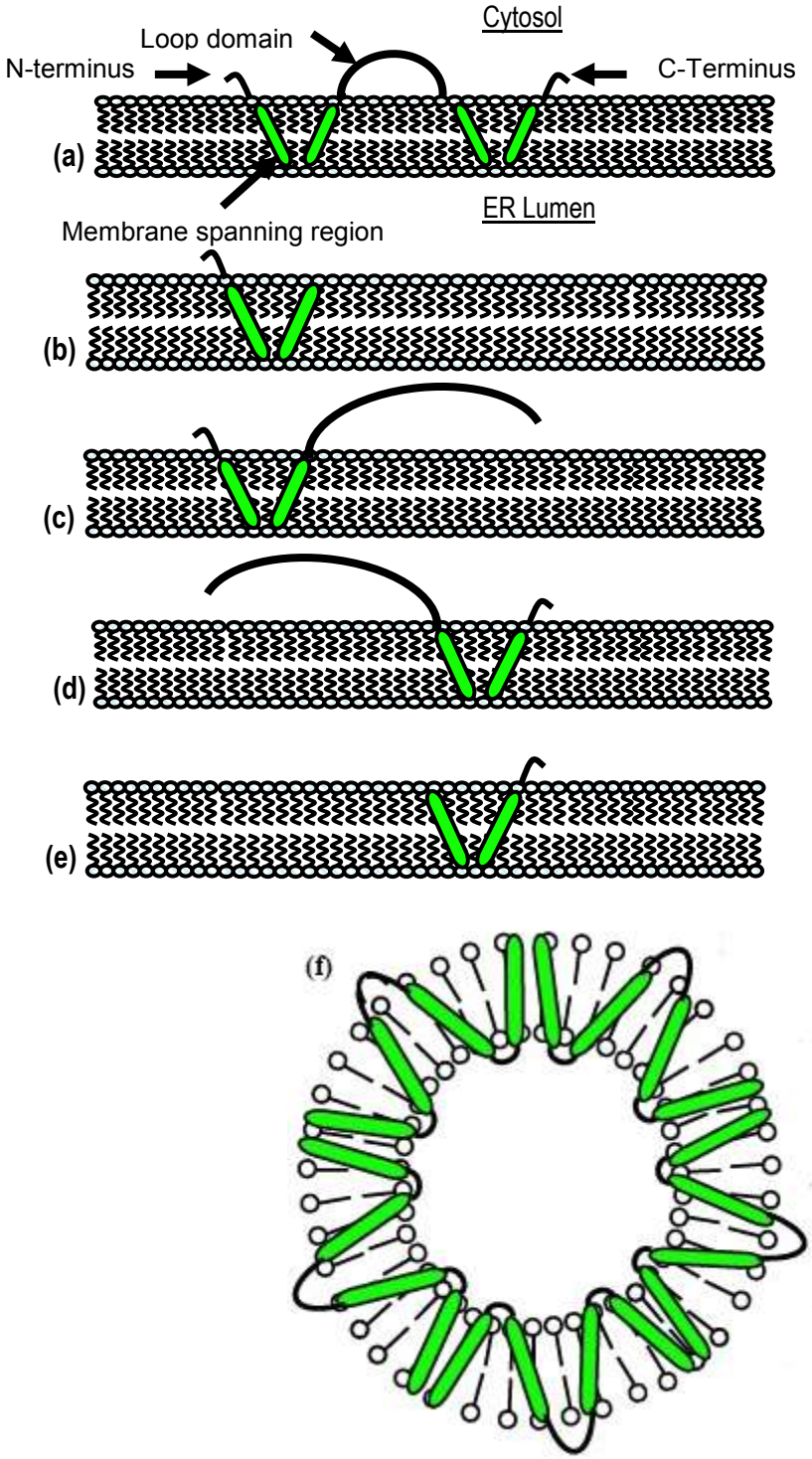


Figure 1.3.5: Full length topology and truncations of reticulon proteins tested for localisation and ER tubule constriction RTNLB1-4 and RTNLB13 (Sparkes *et al.* 2010). (a) Membrane topology of full length reticulon protein. (b) Truncation 1; N-terminus with two hydrophobic domains minus loop domain. (c) Truncation 2; N-terminus with two hydrophobic domains and loop domain. (d) Truncation 3; C-terminus with two hydrophobic domains and loop domain. (e) Truncation 4; C-terminus with two hydrophobic domains minus loop domain. (f) Model for potential membrane topology of RTN proteins within a membrane bilayer inducing curvature to form an ER membrane tubule structure.

In plants, the majority of cortical ER is tubular, however in the *A. thaliana* phosphatidate phosphatase double mutant *pah1 pah2,* the ER is predominantly in cisternal form (Eastmond *et al.* 2011). Tolley *et al.* (2010) transfected epidermal leaf cells of this mutant with YFP-RTNLB13 and RFP-HDEL constructs (HDEL is an ER retention signal and when tagged with fluorescent proteins is used as an ER luminal marker, Brandizzi *et al.* 2004). The cisternal ER partly converted to a tubular morphology, resembling the mix of cisternal and tubular ER in wild-type plant cells, demonstrating in *A. thaliana* plants *in vivo* that overexpression of RTNLB13, the smallest of the plant reticulons, is sufficient to induce the high degree of curvature in the ER membrane required for the formation of tubules.

Analysis using FRET-FLIM (fluorescence resonance energy transfer measured by fluorescence lifetime imaging microscopy) has revealed that interaction between these different plant reticulons is possible, as well as the formation of homodimers (Sparkes *et al.* 2010).

Another outcome of the 2010 study by Tolley *et al.* (2010) indicated increased mobility of RTNLB13 in tobacco cells expressing a modified RTNLB13 where all of the TMDs had been shorted. It is hypothesised that plant reticulons asymmetrically insert into the ER membrane, forming a W shaped topology, and that when inserted into the membrane the reticulons form oligomeric complexes which generate membrane curvature. If full TMDs are required for the proteins to insert into the membrane, then a lack of a full TMD may also indirectly affect oligomerisation, as the proteins cannot insert into the membrane in their usual topology to form these complexes. This could account for the increased membrane mobility witnessed when all of the TMDs of RTNLB13 are shortened, as there would be less hindrance of unoligomerised independent molecules.

More recently, Breeze *et al.* (2016) identified that reticulons possess an amphipathic helix (APH) domain within their highly conserved C-terminal regions. They demonstrated that this APH is required for RTNLB13 to perform its characteristic membrane shaping function, proposing that this is likely to apply to the entire RTN family. This is in contrast to the previously accepted model, which had accounted for the ER membrane bending properties of the RTN proteins purely through a mechanism of insertion into the lipid bilayer in a wedge-like hairpin topology and oligomerisation, forming curved arcs of

oligomers (Sparkes *et al.* 2010; Tolley *et al.* 2010). Breeze *et al.* (2016) showed that when the APH region is mutated or deleted the protein no longer functions to curve ER membranes; however the proteins capacity for oligomerisation is not affected. Breeze *et al.* (2016) conclude that their findings indicate that the APH is the mechanism through which the RTN protein family induce membrane curvature. However, they note that another study by Zurek *et al.* (2011) using human RTN4 has shown that a loss of membrane-shaping function can also result from the extension of transmembrane domain length, further indicating that transmembrane domain length is critical for reticulons to perform their membrane curvature inducing function. Therefore it appears likely that both TMD length and APH functionality are implicated in RTN proteins capacity to perform their ER membrane shaping function.

An interaction has been demonstrated between the seed-specific plant reticulon RTNLB13 and RHD3-like 2 (RL-2), a seed-specific isoform of RHD3 (a plant atlastin orthologue - discussed in section 1.2.3) involved in ER tubule fusion, by coimmunoprecipitation (Lee *et al.* 2013). Concomitant over-expression of both proteins resulted in dramatic changes in ER morphology, distinct from overexpression of RTNLB13 alone (Tolley *et al.* 2010). Overexpression of only RL-2 did not result in an altered ER phenotype (Lee *et al.* 2013), which suggests that the protein likely cooperates with the reticulon to perform its function.

Reticulon proteins have also been found to play crucial roles in the replication cycles of various viruses. In plants, Brome mosaic virus (BMV) RNA replication is inhibited following deletion of reticulon proteins that have been found to interact with the BMV protein 1a (Diaz *et al.* 2010). Viral replication compartments that consist of invaginations of the ER membrane fail to form in the absence of reticulons, where RNA synthesis would occur. Partial depletion of reticulon proteins resulted in viral replication compartments with a reduced diameter (Diaz *et al.* 2010). Interestingly the interaction between viral and reticulon proteins appears to be conserved beyond the plant kingdom as Enterovirus 71 (EV71) RNA synthesis has been found to be related to an interaction with human reticulon 3 (Shin-Ru *et al.* 2011).

A proteomic screen of the *Arabidopsis thaliana* plasmodesmal proteome has identified RTNLB3, RTNLB6 and RTNLB20 as components of plasmodesmata and the authors suggest the proteins may function in constricting ER derived membrane to form the desmotubule (Fernandez-Calvino *et al.* 2011). Desmotubules form during the process of cell plate development during cytokinesis.

RTNLB3 (TAIR locus number At1g64090) will be investigated in this study in relation to the role it plays within plasmodesmata and during cell plate formation. Out of the three RTNLB proteins identified within the plasmodesmatal proteome (Fernandez-Calvino *et al.* 2011), RTNLB3 has been chosen as it is currently the only reticulon out of the three identified that has been subject to research characterising its phenotype in plant cells. Therefore this work will build upon that carried out by Sparkes *et al.* 2010 and Tolley *et al.* 2010 using interphase cells *Nicotiana tabacum* cells.

1.4 The endoplasmic reticulum, mitosis & cytokinesis *in planta*

Selective staining using zinc iodide and osmium textroxide produces high contrast of ER and the nuclear envelope membranes and allows these membranes to be clearly visualized using electron microscopy. Zinc iodide osmium tetroxide fixation has been carried out in a range of cell types such as a study by Dauwalder & Whaley in 1973 in maize root tips that focussed on the Golgi apparatus. Harris (1979) analysed ER morphology employing the technique, however this was in relation to seed development in *Vicia faba.* One of the first thorough studies to focus on the morphology and distribution of the ER during mitosis was carried out using potassium permanganate and osmium fixation to selectively stain elements of the ER in mitotic onion root tip cells (Porter & Machado, 1960). Although their work primarily focussed on the relationship of the ER with the chromosomes and mitotic spindle, they also document observations on the association of the ER with the forming cell wall in telophase.

Porter & Machado (1960) observed how the lattice of ER tubules marks the midpoint of the phragmoplast and centrifugally grows outwards from this point to the edges of the cell. It was observed that accompanying this are small vesicles amongst this meshwork of ER. They noted how these vesicles after osmium staining appear empty and perhaps more

dense in permanganate-fixed samples compared to the cytoplasm. However, in combination with osmium impregnation, the structures are stated to be dense and vesicular. The authors reported that the vesicles increased in size and eventually fused to form the new cell wall, except where plasmodesmata have formed.

Hawes *et al.* (1981) documented the changes in ER distribution which occur during mitosis using the osmium impregnation technique and high voltage electron microscopy of thick sections of maize roots. During prophase, ER membrane was seen aggregated around the regions where the spindle poles form. Concomitant to this, the nuclear envelope began to break down and becomes indistinguishable from this aggregated ER. This membrane surrounded the mitotic spindle, with tubular ER seen crossing the region between the two poles. Once chromosomal alignment and movement to the poles had occurred, tubular ER began to aggregate in the orientation the cell plate would form.

The forming cell plate is surrounded by two bundles of microtubules orientated perpendicularly to the orientation of plate growth, collectively known as the phragmoplast (Van Damme *et al.* 2007). Since early electron microscopy based studies, such as those by Porter & Machado (1960) and Hawes *et al.* (1981), it has been confirmed that at the earliest stages of cell plate assembly during late anaphase vesicles from the Golgi aggregate in the centre of the phragmoplast where the cell plate will begin to form (Seguí-Simarro *et al.* 2004). The ER network potentially provides a scaffold for the aggregation of the Golgi derived vesicles, which become loosely associated with the ER as cell plate formation progresses. As well as retaining the vesicles in this location, the ER may also be responsible for regulation of the release of calcium ions that is necessary for fusion of the vesicles (Hepler, 1982).

Membrane tubules grow from the vesicles and fuse to form a connected tubulo-visicular membrane network (Samuels *et al.* 1995). It is suggested that the contents of these vesicles form the building blocks for the new cell wall and that the phragmoplast microtubules provide tracks along which the vesicles are transported (Seguí-Simarro *et al.* 2004). The developing cell plate is initially high in callose, following which cellulose is synthesized as the cell plate matures (Samuels *et al.* 1995).

The network progresses from tubulo-vesicular to more consistent smooth tubules as development proceeds and then forms a fenestrated plate (Samuels *et al.* 1995). The associations between the ER and the cell plate increase with plate development, occurring until the plate is covered with points where the ER is connected (Seguí-Simarro *et al.* 2004). Once this has formed some ER can be seen traversing this region trapped in the cell plate as thin tubules which remain continuous throughout (Hawes *et al.* 1981; Hepler, 1982; Seguí-Simarro *et al.* 2004).

The phragmoplast microtubules remain associated with the edges of the centrifugally developing cell plate and therefore move outwards with development (Samuels *et al.* 1995). The cell plate grows until it fuses with the existing plasma membrane through membrane projections at the edges of the plate and any remaining fenestrae are sealed (Samuels *et al.* 1995).

1.5 Plasmodesmata

1.5.1 Introduction to plasmodesmata

Initial observations of connections existing between plant cells were made in 1879 by Eduard Tangle, and in 1901 these structures were termed plasmoderma, which became plasmodesmata (Carr, 1976). Prior to when they were first documented, cells were considered to be autonomously functioning units, without the need or evident mechanism in place to function as an interconnected system. Since the discovery that cells function together in tissues, research has been ongoing to elucidate the structure and function of the connections between them.

The plant cell wall generally occupies a width of approximately 200 to 1000 nm and creates a barrier between adjacent cells, through which only few small molecules can diffuse (Lucas *et al.* 2009). Due to the complex multicellular structure of higher plants, the necessity of cell-to-cell molecular transport and communication has resulted in the evolution of structures to support this. Plasmodesmata (PD) are the primary mechanism plants evolved to facilitate this transport (Fernandez-Calvino *et al.* 2011). This evolutionary development enables the organism to co-ordinately function, which is

thought to have been necessary for the evolution of tissues, although not sufficient in isolation (Graham *et al.* 2000). Plasmodesmata have evolved independently in land plants and multiple other lineages, such as some green and brown algae (Popper *et al.* 2011).

1.5.2 Plasmodesmatal structure

In 1971, Robards speculated that "it is not difficult to envisage that there is a basic particulate, proteinaceous, subunit common to the ER membrane and desmotubule, so that modulation from the former to the latter may occur merely by an increase in the particulate component with a concomitant reduction in non-particulate protein and probable complete elimination of lipidic material". He also suggested, based on ambiguous evidence showing that the ER appeared closely associated with either side of forming plasmodesmata, that the desmotubule is derived from ER membrane.

In 1981 Hawes *et al.* produced the first clear images conclusively showing the direct association of the ER on the either side of a fully formed plasmodesma, as well as the osmicated desmotubule itself. They noted that this supports the previously made hypothesis that plasmodesmata are formed by constriction of the ER at these points during cell plate formation. Then in 1982, Hepler presented the first clear cross sectional images of the ultrastructure of a plasmodesma with clearly visible outer plasmalemma showing asymmetrical staining between the two membrane leaflets, the outer membrane exhibiting a greater degree of staining. Moving inwards this outer layer encloses a cytoplasmic space showing little staining, with the inner desmotubule visible as a solidly stained rod like structure.

Further electron microscopy analysis, such as that of freeze-substituted *Nicotiana tabacum* leaf tissue, have shown approximately 3 nm electron opaque particles evenly distributed along the space between the desmotubule and inner leaflet of the plasma membrane of the plasmodesma (Ding *et al.* 1992). These were identified as potentially proteinaceous components that extend as spoke-like extensions, protruding from the desmotubule into the plasmodesmatal central cavity (Ding *et al.* 1992). These units along the length of the desmotubule are thought to be arranged in a helical arrangement, which could serve a functional role in partially occluding the cytoplasmic sleeve and play a role in regulating transport (Roberts & Oparka, 2003).

Actin has been identified at the neck region and along the cytoplasmic sleeve, which may be involved in active transport through the channel (White *et al.* 1994). In *Nephrolepis exaltata* when the entire actin cytoskeleton was depolymerised by the addition of cytochalasin, the plasmodesmata dilated at the neck region (White *et al.* 1994). The same drug treatment has also been shown to increase the size exclusion limit for transport through the plasmodesmata of *Nicotiana tabacum* twenty fold (Ding *et al.* 1996). In contrast, stabilising the actin cytoskeleton with phalloidin treatment inhibited transport between cells. Therefore, actin may play a role in transport throughout the plasmodesma, as well as likely having a role in regulation of the degree of permeability (Roberts & Oparka, 2003). Myosins have also been identified as plasmodesmatal components and are suspected to play an active role in transport (Radford & White, 1998; Blackman & Overall, 1998; Reichelt *et al.* 1999), possibly along a scaffold of actin filaments (Roberts & Oparka, 2003).

Tilney *et al.* (1991) have demonstrated that the desmotubule remains intact when the plasma membrane is solubilized. The plasmodesmata were observed to remain in the cell wall following plasmolysis, except when the cell was fully retracted, and then broke away. When the desmotubule remained intact, the plasmodesma were noted to retain their structure. They therefore determined that the desmotubule may be a structural, cytoskeletal element within plasmodesmata.

As the cell wall is relatively thick in comparison to the small size of the plasmodesmal channel, the structure requires the support of a cytoskeletal element or similar, as well as the continuous plasma membrane. Tilney *et al.* (1991) proposed a hypothetical mechanism by which this structure would form. They suggested that during anaphase or just prior to phragmoplast formation, the transmembrane proteins required for this structure to form are synthesised in the ER. These proteins would then relocalise to accumulate in the otherwise lipid composed channel, in the region where the desmotubule will form. Tilney *et al.* (1991) hypothesised that these proteins form both oligomeric complexes with each other and also connections with other molecules in the cytoplasmic sleeve, and that this results in the formation of a proteinaceous “cytoskeletal rod”- the desmotubule. This hypothesis is yet to be confirmed or disproved, as the mechanisms underlying the formation of the desmotubule and its structural components remain

unknown. Tilney *et al.* (1991) also postulated that evolutionarily, this would have been a favourable mechanism, as it would result in plasmodesmatal structures of a fixed size, therefore regulating pore size and ensuring consistency in transport through individual plasmodesma. Plasmodesmatal transport has since been further investigated and plasmodesmata have been found to not be restricted to a fixed pore size for transport (discussed further in section 1.5.3). This proposed mechanism could also ensure a cytoskeletal element forms in each plasmodesma to provide a support structure throughout and maintain the channel, preventing membranous components from pinching into vesicles.

The continuity of the ER and its incorporation into the desmotubule, as seen in transmission electron micrographs, has also been confirmed using other experimental techniques. Oparka *et al.* (1994) plasmolysed onion epidermal cells and observed that the protoplast remains attached to the cell wall via plasma membrane connections called Hechtian strands, which form branched connections. It was also noted that following plasmolysis, large regions of the cortical ER did not incorporate into the forming protoplast, and remained fixed to the cell wall. These ER fragments become enveloped by the plasma membrane when the protoplast condenses inward towards the central region of the cell. Therefore, although the cortical ER is not incorporated into the main body of the protoplast, it is still bound within the cell's plasma membrane. In addition to these points of anchorage to the cell wall, at plasmodesmata the associated ER (and plasma membrane) remained connected at the ER of the desmotubule, although distended due to plasmolysis, remained continuous between cells. They concluded that both the plasma membrane and ER remain continuous through the plasmodesmata and the cell wall (Oparka *et al.* 1994).

In recent years, advances in light microscopy techniques have enabled "super-resolution", subdiffraction imaging; producing imaging of twice the resolution of a confocal fluorescence microscope (Fitzgibbon *et al.* 2010). Fitzgibbon *et al.* (2010) employed three-dimensional structured illumination microscopy (3D-SIM) to investigate plasmodesmatal structure in more detail than prior light microscopy studies had achieved. They studied *Nicotiana tabacum* leaf parenchyma cells expressing a GFP and viral movement protein fusion known to be targeted to plasmodesmata. The technique allowed the central cavity and neck of PD to be resolved for the first time in living cells

(Fitzgibbon *et al.* 2010), which was confirmed to be structurally similar to that previously described in this report, based on electron microscopic analysis using fixed samples.

In addition to proteins, lipids in specific combinations and arrangements are thought to be key elements of the specialised ER and plasma membrane domains of plasmodesmata, and could contribute to their functionality (Grison *et al.* 2015). The lipids of the plasma membrane have been shown to be laterally segregated within these structures in *Arabidopsis thaliana* (Grison *et al.* 2015). The plasmodesmatal plasma membranes are enriched in sterols and sphingolipids that possess very long chain saturated fatty acids in comparison to the majority of the plasma membrane. Grison *et al.* (2015) have shown that altering the sterol composition of young diving cells can result in reversible impairment of the localisation of glycosylphosphatidylinositol anchored proteins to the plasmodesmata. They found that this caused the permeability of callose mediated plasmodesmata to be altered, due to interference with the localisation of proteins required for regulation of callose mediated permeability.

Although little is known about the lipid composition of the desmotubular ER, it is suspected to be unique in comparison to other ER domains due to its extremely constricted membrane structure. Bayer *et al.* (2014) suggest, based on the degree of curvature and the electron density of the desmotubule in EM images, that the membrane may be comprised of lipid headgroups in a non-bilayer lipid phase arrangement, where there is virtually no lumen present. They note that certain types of lipids have been found to favour this arrangement, which would require a lipid composition distinct from other ER domains to form.

1.5.3 Plasmodesmatal transport

Attempts to elucidate the mechanism and route of transport through plasmodesmata and what molecules can be transported, have yielded varying and somewhat conflicting results. Transport through plasmodesmata was initially thought to be limited to hydrophilic, relatively low molecular weight molecules. Studies using water soluble dyes attached to a range of sizes of peptides suggested that only molecules within 800 D could diffuse through (Tucker, 1982; Goodwin, 1983; Terry and Robards, 1987).

Tilney *et al.* (1991) hypothesised that as the ER lumen is separate from the rest of the cell cytoplasm, and when incorporated into plasmodesmata as the desmotubules is occluded into solid rods, molecules that diffuse through plasmodesmata must do so either via the space between the plasma membrane of the plasmodesma and the central core of the desmotubule or diffusion via the plasma membrane lining the exterior of the plasmodesma. The latter route of transport is consistent with results reported by Baron-Epel *et al.* (1988), who studied the redistribution of a fluorescent phospholipid analogue using photobleaching.

Grabski *et al.* (1993) demonstrated that ER localised probes were transported between connecting cells but those they localised to the plasmalemma were not. They concluded that the continuous ER membrane is part of the route by which lipids can be transported across the cell wall. This would require transport via the desmotubule itself, and indicates that the plasmalemma of the plasmodesmata forms a barrier preventing lipid diffusion from the plasma membrane through the plasmodesma (Grabski *et al.* 1993). The transport of molecules via diffusion through the desmotubule has since been further demonstrated as a pathway for some small molecules (Cantrill *et al.* 1999).

Contrary to the preceding conclusions regarding the size exclusion limit of plasmodesmatal transport, further work has shown that selective transport of relatively large molecules through this route is possible (Overall & Blackman, 1996). A study of different cell types in leaves of *Nicotiana tabacum,* showed that plasmodesmata have the capacity to facilitate the transport of far larger molecules, up to 50 kDa in size (Oparka *et al.* 1999*)*. However, during developmental changes to the tissue, this reduced considerably, with plasmodesmata developing branched forms rather than a single straight desmotubule throughout (Oparka *et al.* 1999*)*. Therefore, there can be great variation between transport capacities of plasmodesma, depending on developmental phase of the plant and cell type, with trafficking of large molecules being possible (Oparka *et al.* 1999*)*.

Another further study into the nature of plasmodesmatal ER confirmed prior observations that the ER is continuous between cells and concluded that the size exclusion limit is below the size of GFP, 27 kD (Martens *et al.* 2006). Plasmodesmata are now known to vary greatly in size exclusion limit, depending on not only developmental and tissue

specific factors, but also due to changes in turgor pressure, environmental factors and pathogen attack (Roberts & Oparka, 2003). The primary route for molecular traffic through plasmodesmata has now been demonstrated to be via the cytoplasmic sleeve, the size of which can change dramatically (Knox & Benitez-Alfonso, 2014).

Plasmodesmata form both during cytokinesis, termed primary plasmodesmata, and during extension of the cell wall during cell expansion, which are called secondary plasmodesmata (Faulkner *et al.* 2008). Localisation throughout the cell wall varies, and they can be found in discrete clusters, or more regularly distributed throughout the cell wall (Brecknock *et al.* 2011). It has been suggested that this variation in distribution patterns may be due to differences between longitudinal and transverse cell walls in roots (Turner *et al.* 1994 ; Burch-Smith *et al.* 2011).

Plasmodesmatal structure is variable depending on cell and tissue type, and dynamic in structure between developmental stages (Overall & Blackman, 1996). The number, size, and molecular make-up can also vary between cells, as well as established plasmodesma being subject to further modification by cellular enzymes, which allows further potential control and specificity of transport between induvial cells and tissue types (Knox & Benitez-Alfonso, 2014). This allows for temporal variation during development and responses to triggers from environmental changes (Knox & Benitez-Alfonso, 2014). Additionally, plasmodesmata can be blocked by callose deposition in response to a stress factor or be dismantled if the cells developmental point means that fewer or no plasmodesmata are favourable, compared to the number that were required during cellular growth and expansion (Roberts & Oparka, 2003).

For example, regarding the range of structural variation between plasmodesmata, transmission electron microscopy analysis of the structure of plasmodesmata in the mature leaves of sugarcane found a variety of structural features between cell types, where three distinct morphological variations were identified and described (Robinson-Beers & Evert, 1991). These included a form where the desmotubule between mesophyll cells was found to vary in degree of ER membrane constriction, specific to the region within the plasmodesma. Although constricted into a rod at both the extremities, marked by electron opaque structural components, the central portion of the tubule was less constricted and had a luminal cavity (Robinson-Beers & Evert, 1991).

The cell wall around sites where plasmodesmata form is composed of callose, the turnover of which is thought to play a fundamental role in regulating the transport of molecules through plasmodesma, with pectin also found in these regions (Knox & Benitez-Alfonso, 2014). The overall size and the range of sizes a plasmodesma can dilate or contract to is dependent on the structure of the surrounding cell wall and the action of enzymes that aid in its modification (Knox & Benitez-Alfonso, 2014). The cell wall also affects the development of new secondary plasmodesma after cytokinesis has occurred, for which targeted dissolution of the cell wall is required, as well as for further development of primary plasmodesmata, such as modification resulting in branching and twinning (Knox & Benitez-Alfonso, 2014).

Plant viruses exploit the dynamic potential of plasmodesmata by a variety of mechanisms to facilitate their transport from cell to cell to establish further infection. As described in section 1.3.5, an interaction between reticulons and a plant virus has already been documented and shown to be essential for the replication cycle of Brome mosaic virus (BMV) (Diaz *et al.* 2010). Plant viruses have been known to interact with plasmodesmata for several decades prior to this, and many studies have utilised recombinant viral movement proteins fused to fluorescent protein tags to study intercellular protein transport in plants (Roberts & Oparka, 2003). Some viral movement proteins encode proteins capable of modifying plasmodesmata to facilitate their transport through them (Deom *et al.* 1992). If reticulons were responsible for formation of the desmotubule and maintenance of the high degree of membrane curvature, as they are elsewhere in the ER, interaction with reticulons and interference with desmotubule structure could provide a mechanism by which some plant viruses modify the size exclusion limit of plasmodesmata.

1.5.4 Plasmodesmata conclusions

Although the cellular origin of the plasmodesmal membranes have now been ascertained, as well as some of the other components, our knowledge to date of the molecular components of plasmodesmata remains far from complete. However, genetic and proteomic techniques have recently accelerated the rate of research into elucidating these

components, with approximately 30 proteins having been identified that are indicated to be localised to these structures (Maule, 2008). Furthermore, the “proteinaceous, subunit common to the ER membrane and desmotubule” hypothesised by Robards in 1971 that may facilitate transformation of ER membrane into this highly constricted form, has neither been identified nor excluded.

1.6 Research aims of the thesis

1.6.1 Investigate function, localisation & dynamics of RTNLB3 protein in plant cells

To expand on current limited data and investigate the role of plant reticulon 3 in endoplasmic reticulum membrane curvature.

1.6.2 Employ high-resolution 3D microscopy techniques to investigate plant ER structure

Develop methodology to enable modelling of the ER in 3D to investigate tubular and cisternal ER in plant cells in greater detail than has previously been documented.

1.6.3 Elucidate the role of RTNLB3 in cell plate formation

To investigate the role, localization and dynamics of RTNLB3 in dividing plant cells, particularly in relation to the cell plate and plasmodesmata. Elucidate the role of RTNLB3 in the structure of plasmodesmata and analyse their formation at the cell plate.

2. Materials & methods

2.1 DNA constructs used for transformations

The gene used throughout this study is the A. thaliana sequence for RTNLB3; TAIR locus number At1g64090.

DNA constructs for the RTNLB3-YFP and RTNLB3-YFP truncation in PDONR207 (Invitrogen™) vectors were provided by Imogen Sparkes and their generation is described in Sparkes *et al.* 2010. The antibiotic selection genes housed in the PDONR207 (Invitrogen™) vector confers kanamycin resistance to bacteria upon expression of the constructs and hygromycin resistance in plant cells.

The constitutive promoter sequence 35S of the cauliflower mosaic virus (CaMV) was included in each construct for over-expression of the reticulon- fluorescent protein fusions (Benfey *et al.* 1990).

The RTNLB3-YFP truncation sequence was cloned into pOpOn2.1 (Moore *et al.* 2006) with an inducible promoter. The vector was provided by Ian Moore (Oxford University) and cloning of the reticulon truncation DNA into the vector was carried out by Verena Kreichbaumer (Oxford Brookes University). The construct carries spectinomycin antibiotic resistance to bacteria, and kanamycin and hygromycin antibiotic resistance to plant cells.

The DNA for the GFP-HDEL construct (Saint-Jore *et al.* 2002) in a pVKH18En6 vector was sourced from the clone collection belonging to the School of Life Sciences at Oxford Brookes University. The antibiotic resistance the construct confers to bacteria is to kanamycin and to hygromycin for plant cells.

2.2 Bacteria

2.2.1 Bacterial culture medium

Bacteria were grown in either LB or YEB culture medium, as described in tables 2.2.1 and 2.2.2.

Table 2.2.1: LB culture media

Reagent	Concentration (g/l)
Bacto-tryptone (Sigma-Aldrich, UK)	10
Bacto-yeast extract (DIFCO)	5
NaCl (Sigma-Aldrich, UK)	10

pH was adjusted to 7.0 with NaOH and the medium autoclaved. For solid medium 1 % agar (Sigma-Aldrich, UK) was added prior to autoclaving.

Table 2.2.2: YEB culture medium:

Reagent	Concentration
Beef extract (DIFCO)	5 g/l
Bacto-yeast extract (DIFCO)	1 g/l
Peptone (Sigma-Aldrich, UK)	5 g/l
Sucrose (Sigma-Aldrich, UK)	5 g/l
$MgSO_4 \cdot 7\ H_2O$	2 mM

Medium was autoclaved. For solid medium add 1 % agar (Sigma-Aldrich, UK) was added prior to autoclaving.

2.2.2 Antibiotics used for selection of bacteria and constructs

Antibiotics and concentrations used for selection of bacteria and constructs are listed in table 2.2.3.

Table 2.2.3: Selection antibiotics

Antibiotic	Concentration (µg/ml)
Gentamycin (Melford, UK)	10
Kanamycin (Sigma-Aldrich, UK)	10
Rifampicin (Sigma-Aldrich, UK)	25
Hygromycin (Melford, UK)	40

2.2.3 Transformation of competent *Escherichia coli* and DNA extraction

Plasmid DNA was transformed into *Escherichia coli* (*E.coli*) strain DH5α (Subcloning Efficiency™ Competent Cells, Invitrogen, UK) cells using heat shock transformation.

Cells were cultured in liquid Luria-Bertani (LB) medium or on solid LB medium (with 1 % agar) plus the appropriate selection antibiotic. Aliquots of *E.coli* cells (one aliquot of 50 µl per single reaction as prepared by the manufacturer) were removed from -80 °C storage and thawed on ice for 10 minutes. 1 µl of DNA was added to each aliquot tube containing DNA for each construct to be transformed. Tubes were flicked to mix contents and tapped to bring contents to the bottom of the tube. Tubes were then incubated on ice for 30 minutes. Next, cells were heat shocked by placing tubes for 45 seconds in a 42 °C water bath, then incubated on ice for a further 2 minutes.

Following incubation, 800 µl of LB liquid medium was added to each tube and tubes shaken at 37 °C in a shaking incubator for 50 minutes. Cells were then pelleted in a centrifuge tube at 4000 rpm for 2 minutes. 700 µl supernatant was removed from each and the pellets were resuspended in the remaining supernatant. Each tube of resuspended cells was spread onto a round 9 cm plate (Thermo Scientific, UK) containing solid LB medium with suitable antibiotic for selection.

DNA for each construct was extracted from the transformed *E. coli* for use in further work using the Wizard® *Plus* SV Minipreps DNA Purification System (Promega, UK), according to the manufacturer's instructions.

2.2.4 *Agrobacterium tumifaciens* strains

For stable BY-2 cell and *Arabidopsis thaliana* transformation with binary vectors, GV3101 (pMP90) *A. tumifaciens* strain (Koncz & Schell, 1986), with chromosomal rifampicin antibiotic resistance, and containing a helper Ti plasmid which carries gentamycin antibiotic resistance, was used.

For transient BY-2 cell transformation with binary vectors EHA105 *A. tumifaciens* strain (Buschmann *et al*. 2011) with chromosomal rifampicin resistance was used.

2.2.5 Preparation of competent *Agrobacterium tumifaciens* cells

Agrobacterium tumifaciens cells were streaked onto a round 9 cm plate (Thermo Scientific, UK) of solid YEB medium containing appropriate antibiotic selection for the strain (Gentamycin and rifampicin for GV3101, rifampicin only for EHA105). Cells were grown for 24 to 48 hours at 28 °C. A well isolated colony was used to inoculate a 5 ml culture of liquid YEB medium plus appropriate antibiotics for selection, and grown at 28 °C in a shaking incubator for 6 to 8 hours.

200 ml culture of liquid YEB medium were inoculated with the 5 ml starter and the 200 ml culture was grown overnight at 28 °C in a shaking incubator. Optical density of the culture was measured in the morning using a NanoDrop ND-1000 UV-Vis Spectrophotometer (NanoDrop Products, USA) to ensure the culture had reached an OD_{600} of 0.4-0.6 overnight. Cells were split into four sterile 50 ml falcon tubes and harvested by centrifugation at 4 °C for 10 minutes at 3600 rpm, and then the supernatant removed from cell pellets.

Under sterile conditions in a laminar flow cabinet, 1 ml of sterile, cold, 100 mM $CaCl_2$ was added using a chilled pipette (both refrigerated prior to 4 °C). Each falcon tube of cells was resuspended by gently pipetting up and down within the chilled pipette until a smooth suspension was achieved, then an additional 19 ml of cold 100 mM $CaCl_2$ was added. Suspended cells were combined into two 40 ml volumes and held on ice for 30 minutes. Cells were harvested by centrifugation at 4 °C for 10 minutes at 3600 rpm and supernatant was removed from cell pellets. Cells were resuspended in 850 µl of ice cold sterile 85 mM $CaCl_2$ and 150 µl of sterile glycerol. The cell suspension was immediately aliquoted to 50 µl aliquots in sterile microfuge tubes, frozen in liquid nitrogen and stored at -80 °C.

2.2.6 Transformation of *Agrobacterium tumifaciens* cells

One 50 µl aliquot of competent bacteria was used per transformation. Cells were put on ice from -80 °C storage, and 5 µl DNA added to frozen cells. Cells and DNA were incubated on ice for 5 minutes or until thawed, then frozen in liquid nitrogen. Cells were then incubated at 37 °C for 5 minutes, after which 1 ml of liquid YEB medium was added and cells were incubated for 2 to 4 hours at 28 °C in a shaking incubator. Cells were harvested by centrifugation at 3000 rpm for 3 minutes and the supernatant was removed. Cell pellets were then resuspended in 500 µl of liquid YEB medium and spread onto plates of solid YEB medium containing the appropriate antibiotics for selection.

2.3 Bright-Yellow 2 *Nicotiana tabacum* cell culture and modification

All plant cell culture work was carried out under sterile conditions in a laminar flow hood, used specifically for plant cell culture work separate from bacterial culture handling areas.

2.3.1 Source of BY-2 cell line

BY-2 cells used for this project were provided by:

Derek Goto, PhD
Research Faculty of Agriculture
Hokkaido University
Sapporo 060-8589, Japan

2.3.2 Culture of *N. tabacum* BY-2 suspension cells

For liquid culture medium 0.43 % Murashige and Skoog basal salt (Sigma-Aldrich, UK), 3 % sucrose (Sigma-Aldrich, UK) and 0.02 % of 1 mg/ml 2,4D (dichlorophenoxyacetic acid) (Sigma-Aldrich, UK) were added to distilled water and the pH adjusted to 5.2. 100 ml conical flasks were prepared with 50 ml medium in each and the openings covered with squares of pre-cut foil, which were secured around the tops of the flasks. Flasks were then autoclaved, stored at 4 ° C, and allowed to return to room temperature prior to use.

All flasks were flamed at the top of the flasks where the foil lids were located prior to opening. The foil lid of a flask containing fresh medium was gently loosened and lifted up

to allow appropriate antibiotics for selection to be added if required. The foil lid was then similarly loosened on the original culture flask, and 1ml of old cell culture transferred to the new subculture flask. Foil lids were then placed back over the flasks and resealed. The old culture was kept as a back-up for the following week. Cultures were grown in the dark, shaking at 130 rpm at 27 °C, and subbed weekly from the recent week old subculture flask, unless contamination required use of the backup flask.

2.3.3 Establishment of BY-2 suspension culture from calli

Half of an individual cell callus was transferred from a plate to a fresh flask containing 50 ml BY-2 media, as detailed in section 2.3.2 for suspension cells. The plate with remaining callus was resealed with Parafilm® and stored as a back-up in the dark at 27 °C. For callus growth maintenance, to create a fresh back-up plate half of an existing cell callus from the previous plate was transferred to a new BY-2 plate (the preparation of which is detailed in section 2.3.5) containing relevant selection antibiotics and sealed with Parafilm®.

2.3.4 Transient transformation of *N. tabacum* BY-2 cells

Fifty ml 3 day old BY-2 culture (wild-type or culture expressing a reticulon construct), which had been subcultured weekly, were used for transient transformations. All of the protocol was carried out under sterile conditions in a laminar flow cabinet. This protocol has been based on that described by Buschmann *et al.* (2011).

The cells were allowed to settle at the bottom of the flasks and supernatant was removed to leave approximately 10 ml concentrated cell culture. The concentrated cell culture was then washed twice in 50 ml sterile Paul's medium (0.43 % Murashige & Skoog Salts without vitamins (Duchefa) plus 1 % sucrose (Sigma-Aldrich) at pH 5.8, autoclaved), allowing cells to settle between each wash step. Following the final wash, excess Paul's medium was removed to produce an approximately 10 ml concentrated cell culture at 5 x original cell density.

Ten ml overnight *Agrobacterium tumifaciens* strain EHA105 cultures were grown at 180 rpm, at 28 °C in LB medium plus antibiotics for selection of the bacterial strain and the construct to be transformed.

One ml overnight culture was subcultured in 5 ml fresh LB medium, without antibiotics, with 250 µM acetosyringone (3',5'-Dimethoxy-4'-hydroxyacetophenone, Sigma-Aldrich, UK). Cells were grown for several hours, again at 180 rpm at 28 °C, and the optical density (OD) was measured using a NanoDrop ND-1000 UV-Vis Spectrophotometer (NanoDrop Products, USA) until an OD_{600} of approximately 0.8 was reached.

For each construct being transformed, 1 ml of each corresponding *Agrobacterium tumifaciens* culture was transferred to a 1.5 ml Eppendorf tube and harvested by centrifugation at 10,000 rpm at RT for 1 minute. Supernatant was removed from the cell pellet and the cells resuspended in 30 µl of sterile Paul's medium.

One ml of concentrated BY-2 culture was then transferred to each Eppendorf tube with acetosyringone at a final concentration of 250 µM and agitated for 1 minute at 100 rpm. Each Eppendorf of mixed cell suspension was plated out onto round 9 cm plates (Thermo Scientific, UK) containing solid Paul's medium (0.43 % Murashige & Skoog Salts without vitamins (Sigma-Aldrich, UK) plus 1 % sucrose (Sigma-Aldrich, UK) at pH 5.8 plus 0.5 % agar (Phytagel, Sigma-Aldrich, UK), autoclaved.

Plates were sealed with micropore tape, covered in foil and incubated in the dark at 27 °C. Cells were checked for expression using a Leica MZFLIII stereomicroscope (Leica Microsystems, Germany) from two days post transformation and analysed using a Zeiss LSM 510 Meta (Zeiss, USA) confocal scanning laser microscope once expression was evident (2-4 days).

For analysis cells were scraped from the agar surface and mixed on a 25 x 75 mm glass microscope slide with a drop of fresh Paul's medium and a 22 x 55 mm glass cover slip gently applied, excluding air bubbles.

2.3.5 Stable transformation of wild-type *N. tabacum* BY-2 cells

Liquid medium was prepared as detailed in section 2.3.1 up to pH adjustment to 5.2. Medium was allowed to cool to room temperature, then appropriate antibiotics were added. For solid medium, 0.8 % Bacto-agar (Difco) was added following pH adjustment, and medium was autoclaved. Medium was allowed to cool until hand hot but thoroughly molten, and appropriate antibiotic for selection of constructs were added if required. Medium was poured onto 9 cm round plates (Thermo Scientific, UK) and allowed to cool until set.

Ten ml cultures of *Agrobacterium tumifaciens* GV3101 strain, containing the constructs to be transformed, were grown in LB medium with appropriate antibiotic selection, shaking at 180 rpm at 28 °C overnight.

The following procedure was carried out entirely under sterile conditions in a laminar flow cabinet. 1 ml of each overnight bacterial culture was transferred to a 1.5 ml Eppendorf tube and pelleted at 5000 g for 5 minutes at RT. Supernatant was removed and the cells resuspended in 1 ml LB medium containing 200 µM acetosyringone (3',5'-Dimethoxy-4'-hydroxyacetophenone (Sigma-Aldrich, UK) working stock solution contained 100 mM acetosyringone in ethanol). Centrifugation was repeated to wash the cells of previous medium, and then was repeated for a further two washes. Following the final wash, cells were resuspended in another 1 ml of LB medium with acetosyringone and incubated for 1 hour at RT.

Seven ml of 3 day old wild-type BY-2 culture was transferred to a 15 ml sterile falcon tube for each construct to be transformed, and 100 µl of corresponding bacterial solution added with 1.2 µl of acetosyringone stock solution. Tubes were gently inverted several times to mix the cell culture solutions and then poured onto round 9 cm plates (Thermo Scientific, UK) containing solid BY-2 medium without antibiotics. Plates were sealed with micropore tape, covered in foil, and incubated in the dark at 27 °C for 3 days without shaking.

Following incubation, BY-2 cells were transferred from each plate for washing by gently tapping the plate to loosen cells and pipetting the solution up and down using a 10 ml pipette. The cell suspension was then placed in a sterile 15 ml falcon tube. Remaining cells were rinsed from the plate with an additional 5 ml liquid BY-2 medium, and transferred to the same falcon tube.

Cells were washed three times with approximately 12 ml liquid BY-2 medium (total volume 15 ml), containing 100 µl/ml carbenicillin (Sigma-Aldrich, UK) and 20 µ/ml timentin (Melford, UK) to kill *A. tumifaciens* used for transformation, with cells left to settle in the falcon tube for 15 minutes between each wash step. Following a final wash step, cells were resuspended in a total of 10 ml liquid medium. One ml of resuspended cells were transferred onto plates of solid BY-2 medium containing 100 µl/ml carbenicillin, 20 µ/ml timentin plus appropriate antibiotic for selection of the construct. This was repeated for all of the cell solution. Plates were gently rotated to spread the cells over the surface of the solid medium and sealed with Parafilm®. Plates were then incubated in the dark at 27 °C for 4 – 6 weeks without shaking, until calli appeared.

Calli were screened for expression using a Leica MZFIII stereomicroscope and if fluorescent, transferred to suspension culture as per section 2.3.3. Cells were cultured in liquid culture for four weeks at 27 ° C, shaking at 130 rpm, prior to use for downstream applications.

2.3.6 Synchronisation of *N. tabacum* BY-2 cell cultures

Liquid medium was prepared as per section 2.2.1, up to pH adjustment to 5.2. Seven day old BY-2 culture was used, and 7 ml of culture was placed into 50 ml fresh, sterile BY-2 liquid medium with 5 µl of 5 mg/ml (working solution in filter sterilised DMSO) aphidicolin from *Nigrospora sphaerica* (Sigma-Aldrich, UK) under sterile conditions, and incubated for 24 hours at 130 rpm at 27 °C.

Following incubation, cells were washed with 10 x 50 ml fresh liquid BY-2 medium using a sintered glass funnel (porosity 3), ensuring the majority of medium drained

through the funnel between each step, avoiding the cells drying out. Following washing, cells were resuspended in 50 ml liquid BY-2 medium and returned to the incubator.

2.4 *Arabidopsis thaliana* plant growth and transformation

2.4.1 MS plates for *Arabidopsis thaliana* plant culture

Murashige and Skoog (MS) medium (0.22 %) was added to DW, and the PH adjusted to 5.2. Bacto agar (0.8 %) was added and the media autoclaved. 120 mm square plastic petri dish plates were poured in a laminar flow hood once the media had cooled to a warm temperature to touch, but was still thoroughly molten. Appropriate antibiotic selection was added to the medium just prior to pouring onto plates, as required. Plates were allowed to set and cool to room temperature before use.

2.4.2 Sterilisation of *Arabidopsis thaliana* seeds and plating onto MS plates

Seeds were placed in 1.5 ml Eppendorf tubes and prior to sterilisation were stored at 4 °C for at least two days. Following refrigeration, 1 ml bleach solution was added to each tube of seed (bleach solution contained 10 % sodium hypochlorite (NaClO) (Fisher Scientific, UK) solution in DW plus 0.02 % Tween 20 (Fisher Scientific, UK)). Tubes were shaken continuously at approximately 150 rpm on a shaker for 10 minutes. Seeds were allowed to settle to the bottom of the Eppendorf tubes, and bleach solution was removed under sterile conditions in a laminar flow hood. Sterile DW was added, and seeds were washed for 5 minutes, then again in fresh sterile DW 2 x 10 minutes, all with continuous agitation.

Following the final wash step, 700 µl of DW was removed and the seeds re-suspended in the remaining DW, then transferred onto sterile filter paper. This was left to partially air dry in the laminar flow hood. A sterile toothpick was then used to pick up and transfer the seeds onto 120 mm square MS agar plates, containing appropriate antibiotic selection if required, in a grid formation.

2.4.3 Growth of *Arabidopsis thaliana* seedlings up to seven days

Plates were transferred to a growth cabinet and grown at 21 °C, 16 hours light, 8 dark. For root studies plates were orientated vertically during growth or flat for cotyledon analysis. Plants were either used at 7 days old as seedlings or grown further for mature plants.

2.4.4 Growth of *Arabidopsis thaliana* from seedlings to whole plants in soil for seed harvesting

Seedlings were transferred after two to three weeks growth on plates to small pots containing a compost-vermiculite mixture and grown in the greenhouse at 21 °C, 14 hours light, 10 hours dark. Plants from which seed was to be harvested were grown until siliques had begun to mature, and Aracons (Betatech, Belgium) were placed around each plant to harvest the seed as the siliques began to dehisce. Once seeds had matured the plants were no longer watered and left until they had thoroughly dried out. Seeds were collected and sieved to separate seeds from other dry plant material, then stored at room temperature in Eppendorf tubes.

2.4.5 Transformation of *Arabidopsis thaliana* wild-type Columbia plants

For floral dipping (Bent, 2006), nine Columbia (Col-0) *Arabidopsis thaliana* plants were grown per large pot. Plants were grown in the greenhouse at 21 °C, 14 hours light, 10 hours dark, until they began to grow bolts. Bolts were cut off, and the next set of bolts was allowed to grow. Plants were selected as ready for dipping once they had developed a mixture of open and closed buds on the bolts.

Agrobacterium tumifaciens (GV3101) that had been transformed with the desired construct was grown in 5 ml of LB medium with the appropriate antibiotic for selection at 28 ^{o}C overnight at 180 rpm. 200 ml of LB medium including appropriate antibiotics for selection was inoculated with 2 ml of the overnight culture and incubated at 28 ^{o}C, for 20 – 24 hours. The culture was transferred to 50 ml falcon tubes, and the bacteria pelleted by centrifugation at 5000 rpm for 15 minutes, following which the supernatant was removed

and the bacteria re-suspended in an equal volume of infiltration medium. Infiltration medium contained Murashige and Skoog (MS) Medium basal salt mix (Sigma-Aldrich, UK) at 2.165 g/L, 5% sucrose (Sigma-Aldrich, UK) and 250 µl Silwet L-77®.

Each pot of *Arabidopsis thaliana* plants was dipped for approximately 45 seconds in the bacteria and infiltration media solution. Two pots were dipped per each different construct used. Plants were placed on their side in a tray and covered with a plastic bag overnight in the dark, uncovered the following morning and pots placed upright in the greenhouse to grow to seed (approximately 4 weeks post dipping).

2.4.6 Generation of stably transformed *Arabidopsis thaliana* lines

Positive transformants (T0) were selected by germinating the seed on MS plates containing the relevant antibiotic selection and Timentin, 20 µg/ml (Melford, UK), to kill *A. tumifaciens* used for transformation. Due to the number of seed, seeds were re-suspended in sterile DW water following the final wash step after sterilisation, poured and spread over the plate, as opposed to the toothpick method described in section 2.4.2 for plating out seed.

Plates were transferred to a plant growth cabinet and grown at 21 °C, 16 hours light, 8 hours dark for 2 - 3 weeks. Positive transformants were then grown to seed as per section 2.4.4 and seed harvested (T1). Seed from each T1 plant was again grown employing the same methodology and seeds from these plants (T2) were grown without selection to 7 day old seedlings and screened to select for highly expressing lines using an Zeiss LSM 510 Meta (Zeiss, USA) confocal fluorescence laser scanning microscope.

2.5 Electron microscopy preparation

2.5.1 Standard fixation of BY-2 cells

Six day old *N. tabacum* BY-2 suspension cultures were synchronised as detailed in section 2.3.6. Cells were allowed to settle and approximately 40 ml of excess BY-2 media was discarded. 1.5 ml samples of the concentrated, synchronised BY-2 culture were

placed in a 1.5 ml Eppendorf tube and allowed to settle. 1 ml of the supernatant media was removed and 1 ml of fixative added. Primary fixative contained 1 % glutaraldehyde (Agar Scientific, UK), 1 % paraformaldehyde (Agar Scientific, UK), 1 % sucrose (Fisher Scientific, UK), 0.1 % Cl_2 (Fisons Scientific, UK) and 0.02 % Brij35 non-ionic surfactant (BDH, VWR Analytical) in NaCaC (TAAB Laboratories Equipment Ltd, UK) buffer (0.1 M, pH 6.9). Following 10 minutes incubation allowing cells to settle, 1 ml of supernatant fixative was replaced with fresh fixative, and cells fixed for a further 50 minutes (total primary fixation of 1 hour).

Once primary fixed, samples were washed in four changes of NaCaC buffer (0.1 M, pH 6.9), 10 mins per wash. The final wash solution was removed from cells, exchanged for secondary fixative of 1 % aqueous OsO_4 (TAAB Laboratories Equipment Ltd, UK), and cells incubated for 1 hr at RT. Cells were washed four times in UP water following secondary fixation and block stained in 0.5 % aqueous uranyl acetate (TAAB Laboratories Equipment Ltd, UK) overnight at 4 °C. Cells were returned to room temperature, uranyl acetate was removed and cells rinsed in UP water for 10 minutes prior to dehydration in an ethanol series (section 2.5.4) and resin embedding (section 2.5.5).

2.5.2 Standard fixation of *Arabidopsis thaliana* roots

Seven day old *Arabidopsis thaliana* seedlings were screened for expression of constructs (excluding control for inducible plants and wild-type) using a Leica MZFLIII stereomicroscope (Leica Microsystems, Germany) prior to fixation. For plants containing fluorescent constructs, only plants exhibiting high expression of YFP in the roots were used for electron microscopy.

Seedlings were transferred from plates to 10 ml glass vials containing primary fixative (recipe as per section 2.5.1) and fixed for one hour on a rotator providing gentle mixing. Once primary fixed, samples were then fixed in zinc iodide osmium tetroxide as per section 2.5.3, then dehydrated in an ethanol series (section 2.5.4) and embedded in resin (section 2.5.5). Plant roots were dissected from whole seedlings and the rest of the plant

discarded during the 70 % ethanol step of dehydration. Following this only roots were processed.

2.5.3 Zinc iodide osmium textroxide fixation

Fixation was followed up to and inclusive of incubation in primary fixative as per section 2.5.1 for BY-2 cells and 2.5.2 for *Arabidopsis thaliana* roots. Once fixed samples were washed twice in NaCaC buffer (0.1M, pH 6.9), 10 mins per wash, followed by 10 mins wash in DW.

For the ZIO solution, 3 g powdered zinc and 1 g resublimed iodine (BDH, VWR Analytical) were added to 20 ml DW in succession while stirring. Solution was stirred for a further 10 minutes and then filtered. The solution was mixed 1:1 with freshly prepared 2 % aqueous OsO_4 (TAAB Laboratories Equipment Ltd, UK), immediately prior to adding to the samples.

The DW wash was removed from samples and replaced with ZIO solution. BY-2 cells were incubated at RT for 90 minutes and *Arabidopsis thaliana* roots for 5 hours, on a rotator providing gentle mixing. Once incubation was complete, the ZIO solution was removed and samples dehydrated in an ethanol series (section 2.5.4) and then embedded in resin (section 2.5.5)

2.5.4 Dehydration of fixed samples in ethanol series

Samples were dehydrated using a series of ethanol (and UP water) of 10 %, 20 %, 30 %, 50 % , 70 % 90 %, 100 % and 3 X 100 % ethanol dried over a molecular sieve, at RT for 30 minutes per step. Samples were incubated overnight at 4 °C in 70 % ethanol rather than 30 mins at RT if required (*A. thaliana* roots were dissected from whole plants while submerged in 70 % ethanol at this stage). BY-2 cells were centrifuged for 1 min at 3000 rpm to pellet cells from the solution between each dehydration step. Samples were immediately embedded in resin following full dehydration in the ethanol series.

2.5.5 Infiltration of fixed samples in SPURR's resin

Following dehydration, samples were embedded in a series of 100 % ethanol dried over a molecular sieve combined with Spurr's resin (TAAB Laboratories Equipment Ltd, UK) in solutions of 1:3, 1:1, 3:1 for 1 hour each, followed by 100 % resin 1 hour, 100 % overnight, 100 % 8 hrs, 100 % overnight, 100 % 8 hrs, all on a rotator at RT. A final fresh 100 % resin change was carried out prior to polymerising cells in the Eppendorf tubes, or in embedding moulds for roots, for 10 hours at 70 °C. For suspension cell embedding cells were centrifuged until pelleted between each 100 % resin change using a Beckman microfuge B centrifuge with 6 position rotor.

2.5.6 Sectioning of resin embedded samples

Resin embedded samples were all sectioned using a Powertome XL ultramicrotome (RMC Boeckeler, USA). Thick sections for screening samples were cut with glass knives and ultrathin sections and semi-thick sections were cut using a diamond knife. Sections were placed on 200 square mesh 3.05 mm copper grids (TAAB Laboratories Equipment Ltd, UK) after sectioning. Grids used for semi-thick sections prepared for tomography were coated in formvar (TAAB Laboratories Equipment Ltd, UK) as a support film prior to use.

2.5.7 Staining of samples prior to TEM imaging

Sectioned samples on grids were stained prior to imaging by floating the grids sample face down on small droplets of solutions, filtered onto dental wax as a surface. Lead citrate staining was carried out in a closed Petri dish with sodium hydroxide pellets (Sigma-Aldrich, UK), surrounding the dental wax and solution droplets (to absorb atmospheric CO_2). Grids were stained for 5 minutes with lead citrate, followed by the droplets of ultra-pure water for one minute each. Grids were then stained with 2 % aqueous uranyl acetate for 8 minutes followed by 3 droplets of ultra-pure water for one minute each. The grids were dried of solutions between each step by touching the edge of the grid at a 90 ° angle against filter paper (Whatman®).

Samples for tomography, following prior staining for contrast, were also incubated on a drop of 10 nm colloidal gold fiducial solution (Sigma-Aldrich, UK) for 30 seconds each side, and then allowed to dry in a grid box prior to imaging.

3. Characterisation of full length and truncated RTLNB3 phenotypes in *Nicotiana tabacum* Bright Yellow 2 (BY-2) mono-culture cells

3.1 Introduction

To study reticulon localisation and dynamics in both interphase cells and during cell division, the *Nicotiana tabacum* Bright Yellow 2 (BY-2) cell line has been employed as the model organism of choice in this chapter. The cell line, derived from the cultivar Bright Yellow 2, was initially developed by the Japan Tobacco Company at the Hatano Tobacco Experimental Station in 1968, and described as a cell line in 1972 (David & Perrot-Rechenmann, 2001; Santos *et al.* 2016). It has since become the most widely used tobacco suspension cell line. The BY-2 cell line was first recognised to be a potentially valuable tool for advancing plant cell studies by Nagata *et al* in 1992, who described its high homogeneity and dramatically higher growth rate in comparison to any other previously established plant cell line. Suspension cultures of the cell line have a doubling time of approximately 16-24 hours under optimal conditions and within seven days can multiply up to 100-fold (Santos *et al.* 2016).

Obtaining cell lines from plants has been relatively straight forward, with many having been established from a range of plant species including rice (*Oryza sativa)*, carrot (*Daucus carota*) and tobacco (*Nicotiana tabacum*), and of tissue specific cell types (David & Perrot-Rechenmann, 2001; Santos *et al*. 2016). Prior to the BY-2 cell line other tobacco suspension cell lines were used including XD (Filner, 1965). Although *Arabidopsis thaliana* has become a model organism for research of entire plants, suspension cultures derived from *A. thaliana* possess poor capacity for synchronization (Geelen & Inze, 2001). This limits the use of this cell type in suspension when synchronized cultures are needed for cell level morphological and molecular investigation. Therefore the BY-2 cell line established from *N. tabacum*, with a relatively short doubling time from which highly synchronized cultures can be obtained, is the optimal candidate of a model organism for use as an undifferentiated plant suspension culture line, particularly in relation to cell cycle studies (Geelen & Inze, 2001). The cells differ from those in *N. tabacum* plants *in situ,* as they lack the surrounding cells housed within intact tissues of the whole multicellular organism. However, it is difficult to observe high numbers of dividing cells in plants at sufficiently high resolution *in situ* using fluorescence microscopy, and the BY-2 cell line provides a model system to

facilitate this for use in this study. Were a higher resolution light microscope available for use, this would allow for the analysis carried out in this study to be carried out in intact plant tissue.

To overcome the limitations of working with whole plants, the generation and adoption of the *N. tabacum* BY-2 cell line as the organism of choice for cell cycle studies, with its highly synchronisable potential, has allowed study of cell cycle dependent changes (Nagata & Kumagai, 1999). For example, for the characterization of cyclins and their functions during the cell cycle a highly synchronized mitotic population of homogenous culture was required (Nagata & Kumagi, 1999). The cyclins involved in plant cell division have now been characterized and assessed to be similar to their mammalian homologues (Setiady *et al*. 1995; Reichheld *et al*. 1996). Previously, cultures with mitotic indexes of a peak of 10% were cited in the literature as being synchronized populations. Since Nagata *et al.* (1992) published work using the BY-2 cell line it has become the standard model for plant cell cycle studies throughout the world. There is also no prerequisite of making protoplasts in order to transform BY-2 cells (David & Perrot-Rechenmann, 2001) with a range of successful transformation techniques available.

The aim of this work is to use the over-expression of full length and mutant RTNLB3 protein tagged with YFP in BY-2 cells to study RTNLB3 localisation and function during cell plate formation and plasmodesmatal development in comparison to interphase. Thus far work has been carried out elucidating the ER phenotype and function of RTNLB proteins in interphase *Nicotiana tabacum* cells using transient expression of full length and truncated proteins in leaves (Tolley *et al.* 2008; Sparkes *et al*. 2010). However the stable expression of RTNLB constructs in plant cells and their phenotype during plant cell division is yet to be documented. Furthermore, RTNLB3 having been recently identified in a plasmodesmatal proteome screen suggests the protein may be incorporated into these structures (Fernandez-Calvino *et al.* 2011). Thus, due to the proteins ER membrane shaping properties (Sparkes *et al*. 2010), RTNLB3 is a promising candidate for a protein that may play a role in plasmodesmatal formation. Furthermore, the mechanism by which the inner cores of plasmodesmata known as desmotubules form is yet to be elucidated. As over-expression of reticulon proteins has been shown to cause constriction of tubular ER and the desmotubule is composed of highly constricted ER membrane, if RTNLB3 is a structural component of plasmodesmata it is possible this protein may play a role in desmotubule formation. If RTNLB3 were to become concentrated at the cell

plate during cell division, in particular at the sites where plasmodesmata form, the proteins could act to constrict the ER membrane at these sites to form the desmotubule cores and may remain incorporated within these structures as curvature stabilising proteinaceous components.

This chapter aims to investigate this hypothesis further, initially by employing fluorescence microscopy to investigate the localisation of RTNLB3 and truncated RTNLB3 (the over-expression of which has been shown to interfere with ER tubule formation by Sparkes *et al.* 2010) during cell plate formation. In addition to this the stable over-expression phenotype of the constructs within interphase cells will be investigated. If the results indicate that RTNLB3 is active during cell plate formation in this region, electron microscopic techniques will be developed that will enable further investigation of the potential role of RTNLB3 in cell plate and plasmodesmatal formation at an ultrastructural level.

3.2 Materials & methods

Preparation of BY-2 cells up to imaging analysis is detailed in chapter 2, section 3.

3.2.1 Mitotic index count of synchronisation efficiency with DRAQ5 staining

To establish the time period for the peak mitotic index post wash from aphidicolin after synchronisation of cells (synchronisation protocol in section 2.3.6), from 5 hours of incubation onwards, 1 ml of cells was removed each hour for screening.

The initial screen for the optimum time to obtain peak mitotic index post synchronisation and washing the cells of aphidicolin was carried out using DRAQ5 (1,5-bis{[2-(di-methylamino) ethyl]amino}-4, 8-dihydroxyanthracene-9,10-dione) stain (Thermo Fischer).

For DRAQ5 staining, 100 µl of cells were combined with 0.2 % Triton X (Sigma Aldrich) and 10 µM DRAQ5 and incubated for 1-2 minutes prior to imaging with a Zeiss 510 Meta CLSM, using x10 dry and x40 oil immersion objectives, excitation laser 488

and excitation captured in LP650. Slides were prepared by placing the sample on a 25 x 75 mm glass microscope slide and a 22 x 55 mm glass cover slip gently applied, excluding air bubbles.

3.2.2 Screening for expression of BY-2 cultures and image analysis

For screening of transient transformations, plates were analysed using a Leica MZFLIII stereomicroscope (Leica Microsystems, Germany) from 2 days post transformation and analysed using a Zeiss LSM 510 Meta (Zeiss, USA) confocal scanning laser microscope. Analysis method is described in section 2.3.4.

For analysis of liquid BY-2 culture (screening described in section 2.3.5), 500 µl of cell culture was transferred onto a 25 x 75 mm glass microscope slide and a 22 x 55 mm glass cover slip gently applied, excluding air bubbles. Slides were analysed using a Zeiss LSM 510 Meta (Zeiss, USA) confocal scanning laser microscope with x 10 dry, x 40 oil and x 60 immersion objectives.

3.2.3 Preliminary analysis of ER luminal diameter from thin section transmission electron micrographs

Thin sections (80 nm) of both samples embedded in Spurr's (Spurr, 1969) resin were stained for 8 minutes with uranyl acetate and 5 minutes lead citrate prior to data collection (as per section 2.5.7). All cells were imaged at 100 KV with a Hitachi A-7650 tomographic transmission EM, after allowing the section a few minutes to stabilise in the electron beam. For wild type and RTNLB3-YFP over-expressing cells, five different cells of each were used and ten ER tubule diameter measurements recorded from each cell. A portion of ER was identified to be a continuous membrane bounded structure with a consistent lumen, with over 300 nm visible longitudinally, of a relatively narrow and consistent diameter. Individual measurements were taken at a 90 degree angle to this longitudinal orientation, across the tubule diameter spanning from the outside of the high level of contrast of one stained lipid bilayer membrane to the beginning of the parallel lipid bilayer membrane.

3.3 Results

3.3.1 Development of a rapid transient over expression system of fluorescent protein fusions in BY-2 cells

Transient over–expression of both GFP-HDEL (figure 3.3.1 A) and RTNLB3-YFP (figure 3.3.1 B) that labelled the ER network was successfully achieved within 3 days, with peak over-expression present at 3-4 days post transformation. Numbers of transformed cells varied somewhat between transformations, however a rate of approximately 30% for successful transformations was achieved using this methodology. Unsuccessful transformations were identified to be due to human error or suboptimal factors during the optimisation stages of experimentation, such as excluding acetosyringone from the protocol.

Very few cells undergoing division were found in any of the samples analysed from the plates. Attempts were made to return the cells from the solid Paul's medium to liquid BY-2 culture medium (as detailed in section 2.3.3), with Timentin and carbenicllin to kill the *Agrobacterium,* and the appropriate antibiotic for selection of the construct included to select for positive transformants. However, healthy cultures of cells expressing the construct and undergoing division failed to be established. Cultures were also set up (as detailed in section 2.3.2), without selection antibiotic for the construct, but even when transfer was carried out upon expression detected at three days, returned to the incubator and checked 24 hours later, although expression was still present, few cells undergoing division could be found. These cultures also failed to establish into healthy growing liquid cultures when incubated for a further week, despite the lack of antibiotics.

3.3.2 RTNLB3 labels the ER in interphase BY-2 cells, exhibiting constriction of ER lumen in comparison to wild-type and is specifically recruited at a high concentration to the cell plate during telophase

Stably transformed *Nicotiana tabacum* BY-2 suspension cells over-expressing RTNLB3-YFP and truncation 2 (figure 1.3.5) of RTNLB3-YFP that had been previously established (Pengwei Wang, Oxford Brookes University), were transiently transformed with an ER luminal marker consisting of green fluorescent protein with an N-terminal signal peptide (GFP-HDEL).

Cells over-expressing RTNLB3-YFP possessed a highly tubular ER phenotype, which did not co-localise with GFP-HDEL in some regions of ER tubules (figure 3.3.2, A -C). In contrast the majority of ER in cells over-expressing the truncated RTNLB3-YFP was cisternalised, with co-localization of the construct with GFP-HDEL consistent though-out the ER (figure 3.3.2, D – E).

Cells in late telophase undergoing cell plate development were also analysed. Control images using the ER membrane stain DiOC6 (figure 3.3.3, A) in WT BY-2 cells and those expressing GFP-HDEL (figure 3.3.3, B) show the ER distribution in cells undergoing cell plate development during telophase. DiOC6 staining of WT cells showed the ER phenotype in the cell without genetic modifications, revealing the cell plate as a clearly defined linear region of ER across the cell. The stain also labelled some other intracellular components besides ER, however the ER network and cell plate remained clearly distinguishable. As an additional control, cells stably over-expressing the ER luminal marker GFP-HDEL were utilised to specifically label the ER. The results were similar to those obtained using DiOC6 staining, revealing the cell plate as an ER rich fine liner region, where GFP-HDEL was localised, with the intensity of labelling of the plate by the fluorescent fusion remaining consistent to that seen in other regions of the cell with a high density of ER.

In contrast to the fluorescence distribution described for WT cells and those over-expressing GFP-HDEL, during cell plate formation RTNLB3-YFP becomes highly enriched at the cell pate in relation to the rest of the ER network (figure 3.3.3, C). This enrichment was not to a consistent degree throughout the cell plate. A strongly labelled defined linear region was present in the centre of the plate, with fluorescence intensity increasing centrifugally outward towards the less mature, developing edges. This cannot be attributed to a larger proportion of ER membrane alone, as this distinctive fluorescence distribution is not present in either controls (figure 3.3.3, A & B). The ER network not associated with the cell plate is highly tubular throughout the cell, as seen in interphase cells over-expressing this construct (figure 3.3.2, A-C).

Truncation 2 of RTNLB3-YFP was also found to localise at a greater degree to the cell plate in comparison to the rest of the ER network (figure 3.3.3, D), although the contrast was to a lesser degree than that seen for the full length construct. The localisation to this region was a less defined liner region than that seen for the mature central portion of the

cell plate labelled by full length RTNLB3-YFP (figure 3.3.3, C), or the localiation of ER membrane seen in the controls (figure 3.3.3, A & B). Although the construct was localised to the region corresponding to the cell plate, the pattern was diffuse in comparison. The intensity of labelling within areas of the plate itself, unlike the variation seen in cells over-expressing the full length construct, was relatively consistent throughout.

3.3.3 Generation of stably transformed BY-2 lines over-expressing RTNLB3-YFP and truncation 2 of RTNLB3-YFP

Following obtaining the initial results presented in sections 3.3.1 and 3.3.2, both stably over-expressing reticulon cell lines were not able to be further maintained, and were lost. This required the generation of new stably expressing BY-2 cell lines for further experimental work.

Transformations of WT BY-2 suspension cultures cells were carried out with either full length RTNLB3-YFP or truncation 2 of RTNLB3-YFP. A new BY-2 cell line and liquid culture was established successfully, yielding a monoculture of cells highly over-expressing the full-length RTNLB3-YFP construct, which exhibited the same phenotype as previously documented (section 3.3.2).

Establishment of a new stably transformed BY-2 line over-expressing the truncated RTNLB3-YFP construct proved unsuccessful, despite concurrent attempts employing identical methodology to the full length RTNLB3-YFP construct, as well as following repeat attempts. The few cells which exhibited fluorescence in the samples resulting from the transformations had a plasmolysed phenotype indicative of cell death (figure 3.3.4, A).

Transient over-expression of truncated RTNLB3-YFP was carried out to confirm the viability of the *A. tumifaciens* containing the construct used in transformation attempts. Transient transformation was successful, and many cells exhibited the predicted highly cisternal ER phenotype (as described in section 3.3.2), 48 to 72 hours post transformation (figure 3.3.4, B, C, D & E). In some cells, nuclear envelopes became clearly labelled with the truncated RTNLB3-YFP construct (figure 3.3.4, H), or cells became highly vacuolated (figure 3.3.4, G). A range of unusual phenotypes not reminiscent of characteristic plant organelles were also observed in the cell samples analysed. Following 72 hours

incubation or more, some cells exhibited high levels of very irregular fluorescent labelling not consistent with the structure of a continuous reticulated network. These appeared to be substantial deformities to the structure of the ER network in intact cells, and highly inconsistent localisation of the truncated fluorescent construct within it (figure 3.3.4, F), or cells appeared plasmolysed, indicative of cell death (figure 3.3.4, I).

In some cells that highly transiently over-expressed the truncated RTNLB3-YFP, as expression levels increased, large aggregates of fluorescence began to form in the cells. However the rest of the ER remained as a consistent network surrounding these bodies and throughout the cell. With the laser set to a level where the rest of the ER was still distinguishable these bright areas were unresolvable (figure 3.3.4 H, J & L). However when the laser intensity was reduced, a "sponge" like structure was revealed (figure 3.3.4, K). Figure 3.3.4, image L shows a cell expressing the mutant reticulon 3 protein with multiple fluorescent bodies such as these. This was not observed in cells transiently over-expressing the full length RTN3-YFP construct, which was used as a control to rule out artefacts being due to other factors in the transformation that could have resulted in an unexpected expression phenotype. This same observation was also noted in *N. tabacum* leaf epidermal cells transiently expressing high levels of the construct as result of infiltration (data not shown).

3.3.4 Establishment of timescale, synchronisation efficiency and optimal protocol for the synchronisation of a BY-2 suspension cell culture

Before analysis of cells by TEM, *Nicotiana tabacum* BY-2 cultures needed to be synchronised to increase the percentage of cells simultaneously in later stages of division in a single culture. A trial synchrony and cell count was carried out with the aid of DRAQ5 as a chromosomal stain (figure 3.3.5) to establish the percentage of synchronisation and the time frame required post cell cycle release to achieve the greatest number of cells in late mitosis.

BY-2 suspension culture cells often grow in chains, which can vary greatly in cell number (Figure 3.3.5. A, B & C). Chromosomes and therefore the nuclei of cells were consistently and clearly labelled by the DRAQ5 stain in cells (figure 3.3.5. A – F), enabling accurate identification of the stages of the cell cycle and recording of the mitotic

index of the culture. Cells in metaphase exhibited labelled chromosomes aligned in the central region of the cell (figure 3.3.5. D & E), with synchronisation of the cell culture yielding many cells concurrently progressing through the same stage of the cell cycle (figure 3.3.5. E). Cells in late telophase were clearly identifiable from the DRAQ5 labelled daughter nuclei with the maturing cell plate in between them labelled with a high concentration of RTNLB3-YFP fluorescence (figure 3.3.5. F).

The mitotic index and cell counts obtained from this synchrony are shown in Table 3.3.1. The mitotic index was calculated using the following equation.

Mitotic Index Calculation:

$$\frac{(P+M+A+T)}{(P+M+A+T+C+I)} \times 100 = \text{Mitotic Index (\%)}$$

P – Prophase
M – Metaphase
A – Anaphase
T –Telophase (cell plate formation)
C – Cytokinesis (late telophase)
I - Interphase

Table 3.3.1: Cell counts and mitotic index at a range of time points following aphidicolin wash from a BY-2 tobacco suspension culture stably over-expressing RTNLB3-YFP

Time (h)	Prophase/Pro Metaphase (P)	Metaphase (M)	Anaphase (A)	Telophase (cell plate formation) (T)	Cytokinesis (late telophase) (C)	Interphase (I)	Mitotic Index (%)
6	7	3	4	0	0	92	13.2
7	4	2	0	3	0	90	9.0
8	20	4	7	8	0	82	32.0
9	10	11	5	7	1	70	31.7
10	11	11	3	7	5	69	30.2
11	8	7	3	1	5	102	15.1
12	2	2	0	3	8	127	4.9

3.3.5 Preliminary analysis of ER luminal diameter from thin section transmission electron micrographs of interphase *N. tabacum* BY-2 cells

Based on the results obtained in section 3.3.4, cell cultures were prepared for electron microscopy following synchronisation and 9 hours incubation after cell cycle release (by washing of aphidicolin from the cells). ER morphology in interphase wild type and RTNLB3-YFP over-expressing cells was analysed using thin section transmission electron microscopy. Images were produced using the TEM, and those of good quality selected with clearly defined contrast of membrane labelling and clear resolution, such as that shown in figures 3.3.6 A & B, for wild-type and RTNLB3-YFP over-expressing cells, respectively. The ER luminal diameter was measured (as detailed in section 3.2.3) to assess if this can provide an indication of whether there is a significant difference in ER structure between the two cell types.

Figure 3.3.7 shows results of measurements recorded from the transmission electron micrographs. The two data sets of 50 measurements each were analysed and divided into groupings to show how many of the measurements for each cell type fell into a specific size range. When plotted as a histogram, it became apparent that the frequency in which measurements appeared in each size range varied between the two samples. There was a

far greater frequency of smaller diameter measurements in the measurements obtained for cells over-expressing RTNLB3-YFP in comparison to wild-type. None of the measurements for cells over-expressing the RTNLB3-YFP construct were above 30 nm in diameter, as opposed to 16% of wild type samples. Also, whereas only 4% of wild type measurements were below 15 nm, 32% of measurements taken from cells over-expressing RTNLB3-YFP were under 15nm. The narrowest diameter recorded was 9 nm in width amongst these measurements.

An unpaired two tailed t-test was used on the data values to see if there is a statistically significant difference between the two data sets. The samples of 50 measurements from wild type cells were tested against the 50 measurements from RTNLB3-YFP over-expressing cells. The test yielded a P-value result of 8.1366E-08. This test value confirms that the difference in diameters recorded is statistically significant at a level of 99.9% certainty. The average measurement for wild-type was 23.26 nm and 17.00 nm for RTNLB3-YFP over-expressing cells.

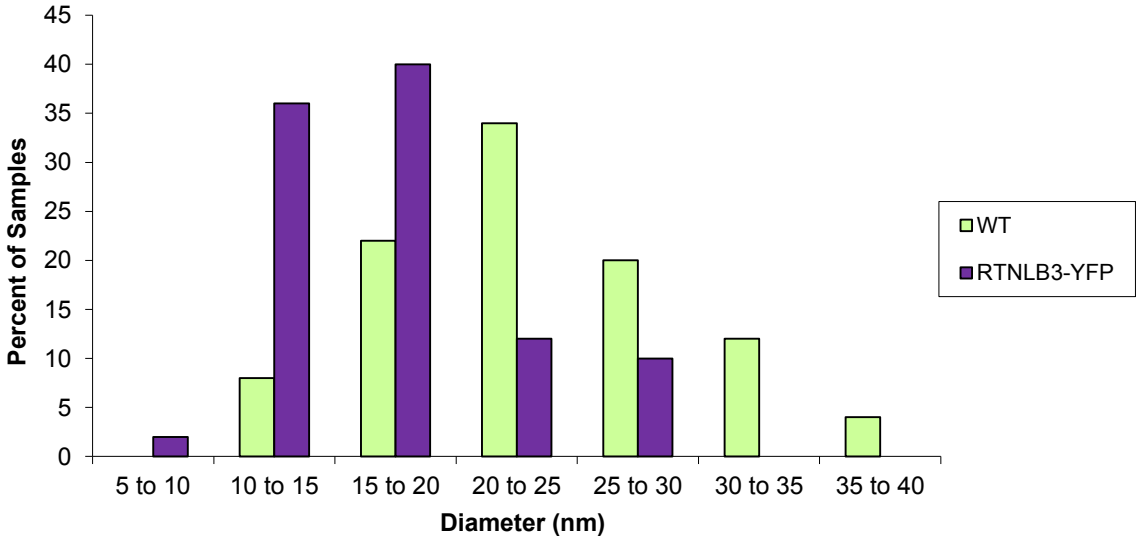


Figure 3.3.7: Diameter of cross sections of ER in Wild Type & RTNLB3 over-expressing BY-2 suspension cells.

3.3.6 Transmission electron microscopy of the ER & RTNLB3 during cell plate formation

Cell plates for both wild type and RTNLB3-YFP over-expressing cells were imaged. The developing edges of cell plates at an active stage of centrifugal development and growth towards the existing cell wall were analysed (figure 3.3.8). Microtubules were visible in both samples as a supporting network perpendicular to and traversing the forming cell plate in this region (figure 3.3.8, A & B).

The edge of wild type cell plates such as figure 3.3.8, A, had a dense accumulation of ER in the region of the developing cell plate at this resolution and magnification. In comparison, full length RTNLB3-YFP had less visible ER in the thin sections at the edge of the developing cell plates (figure 3.3.8, B).

In both samples cell plate material deposited at a more central, mature site of cell plate formation was observed fusing to form the new cell wall and plasma membrane (figure 3.3.9). Although the exact morphology of cell plate fusion events varied between cells and stage of maturation in both samples, the maturing cell plates also shared similarities that appear in both cell types.

The vesicular matter at the cell plate appears to fuse into larger aggregates as the cell plate matures, as shown in figure 3.3.9 A & B. ER was also visible in close proximity to the cell plate and in what appeared to be similar levels in both the wild-type (figure 3.3.9, A) and RTNLB3-YFP over-expressing cells (figure 3.3.9, B). There are regions where either ER tubules have become merged with the cell plate material or membranes extend from the cell plate region outward as tubules. In samples produced with this preparation technique we cannot distinguish between these two potential options.

Other observations noted during data collection from several cells included that many Golgi bodies were seen around the region of cell plate development, some with vesicles seen budding from them, presumably providing cell plate material (data not shown). Thi is as expected based on the literature, as Golgi bodies are known to locate to the periphery of the cell plate in a Golgi belt during the early stages of division, contributing the material that will form the cell plate in the division zone (Nebenführ *et al*. 2000).

The difference in staining and therefore contrast seen between the two cell plates was not specific to the cell type. This appeared to vary randomly between individual cells in the

samples and no relationship between cell type or stage of cell plate development was observed in relation to contrast from staining.

3.3.7 Transmission electron microscopy employing zinc iodide osmium textroxide fixation to stain ER membranes in BY-2 cells

Due to the difficulties in contrasting and identifying ER in conventionally fixed and stained material, the zinc iodide osmium tetroxide (ZIO) fixation was carried out (discussed further in chapters 5 & 6). The technique produces specific contrast on the endomembrane system for transmission electron microscopy, without labelling the plasma membrane. This is due to the fact that the inner surface of the plasma membrane has a strongly negative electrostatic charge in plants (Molnár *et al*. 2016) and the ER has a high level of positively charged Ca^{2+} ions stored within the lumen and released from the membrane surface into the cytosol (Voeltz *et al.* 2002). Therefore ZIO does not stain the plasma membrane but Zn^{2+} of the ZIO solution can replace Ca^{2+} to stain the ER.

Samples of wild type cells were impregnated for a range of time points following 1 hour aldehyde fixation, embedded in Spurr's (Spurr, 1969) resin and stained following sectioning for 8 minutes in uranyl acetate and 5 minutes lead citrate. The optimal level of contrast was obtained when the cells were incubated in fresh zinc iodide osmium tetroxide solution for 90 minutes (figure 3.3.10 A & B). Note high electron opacity of ER membranes.

Cell plates were also screened for during sectioning of samples. Although the cultures had been synchronised (with an estimated potential peak of up to approximately 30% of cells in telophase during fixation, as documented in section 3.3.4), cells in this stage of division were labour and time intensive to find. Despite optimisation of the embedding protocol to concentrate the cells as much as possible by centrifugation, and without the use of prior embedding in agar (which was also trialled, data not shown), the cells remained relatively sparse in the resin block. At the stage of utilising the ZIO fixed BY-2 cell samples for testing the selective staining technique, it was decided to not continue collecting samples of cell plates for 3D electron microscopy from these samples. It had become apparent that for further imaging work a different model system employing *Arabidopsis thaliana* would

need to be employed instead of BY-2 cells, due to several difficulties with this model (discussed further in section 3.4.7).

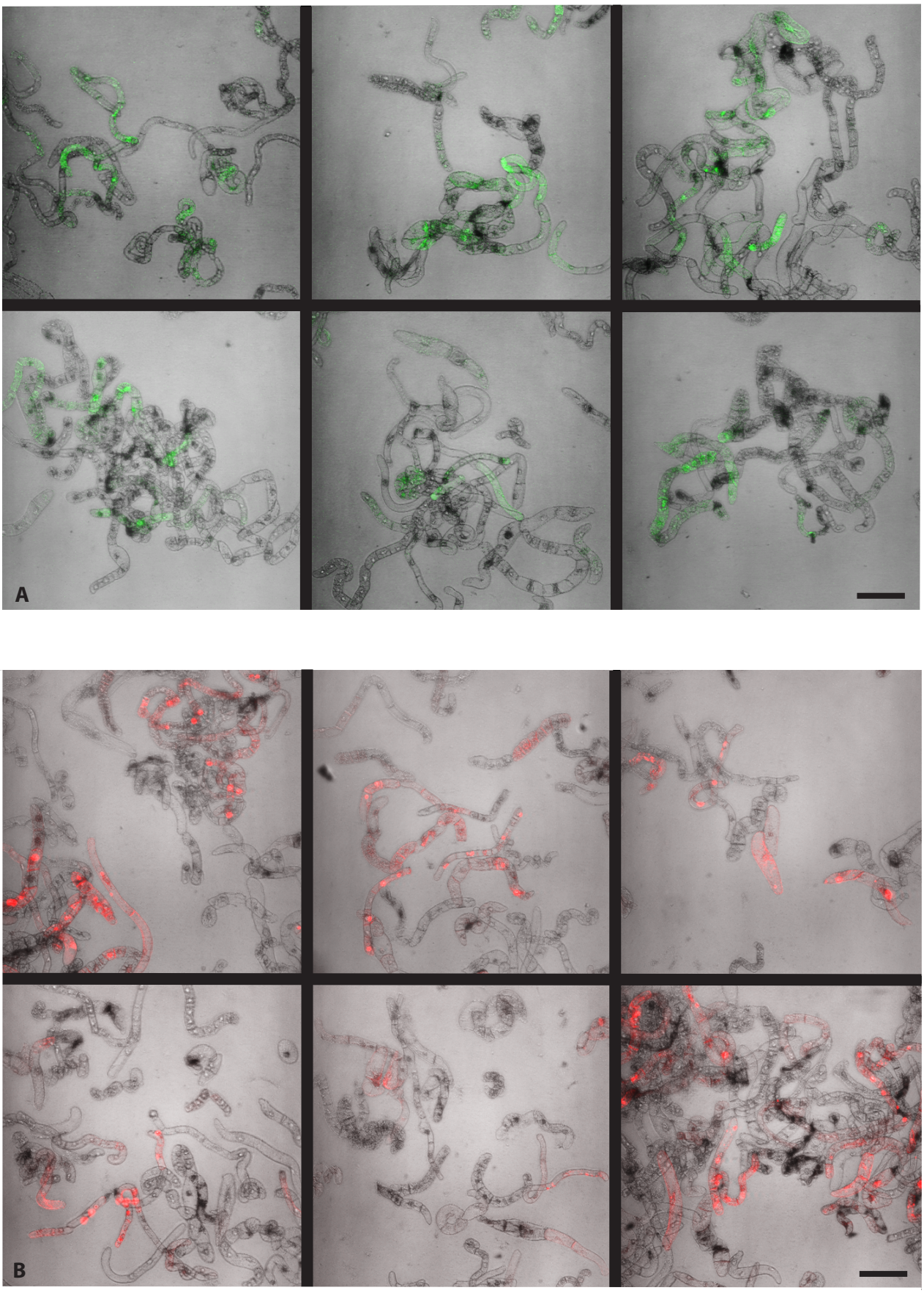


Figure 3.3.1: Transient over-expression of fluorescent constructs in *N. tabacum* BY-2 cells following 4 days incubation. (Scale bars - 200 µm)

A) Transient over-expression of GFP-HDEL (green).
B) Transient over-expression of RTNLB3-YFP (red).

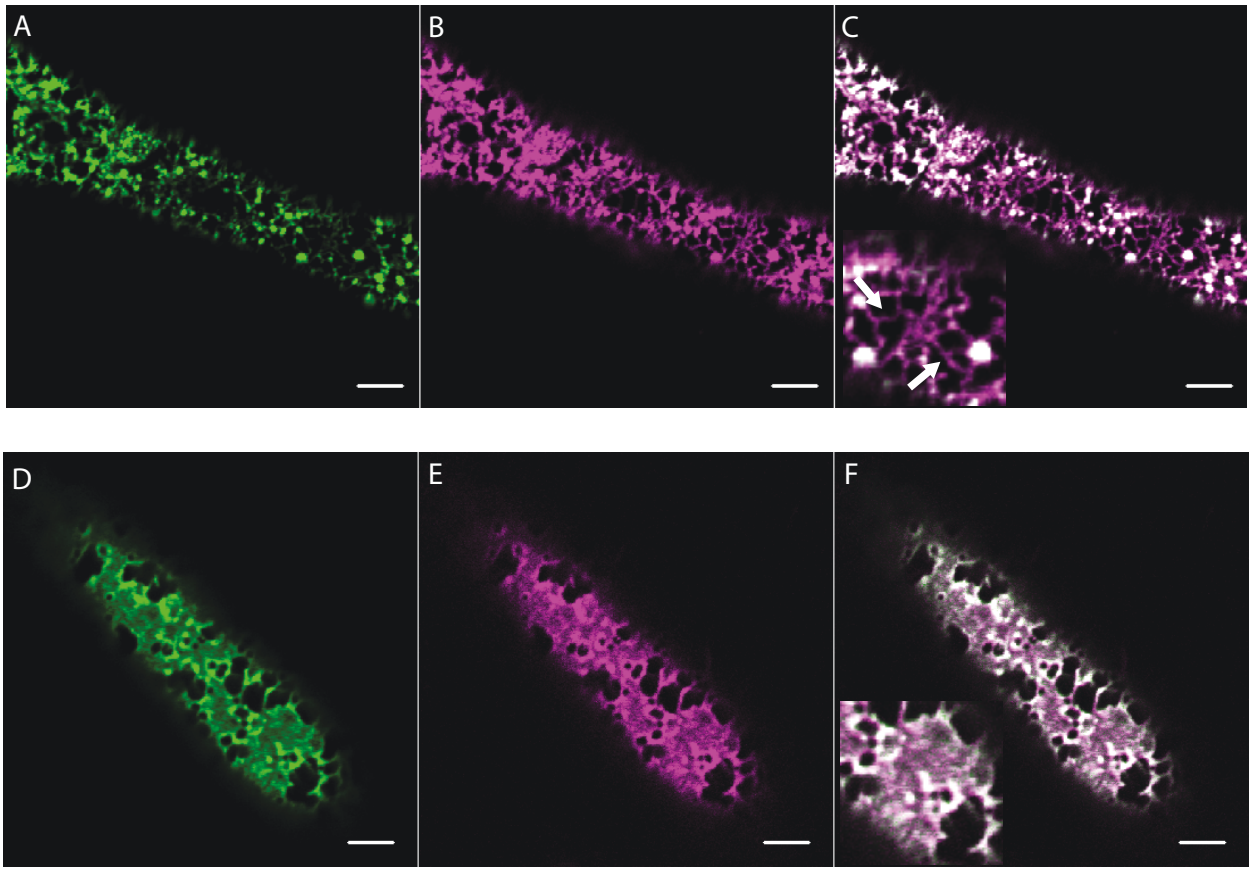


Figure 3.3.2: Confocal micrographs of *N. tabacum* BY-2 cells in interphase, stably over-expressing RTNLB3-YFP (magenta) and transiently over-expressing GFP-HDEL (green). (Scale bars - 5 µm).

A) Luminal ER marker GFP-HDEL.

B) Full length RTNLB3-YFP.

C) Merged image. White arrows indicate examples of tubules from which GFP-HDEL is excluded and therefore does not colocalise with RTNLB3-YFP fluorescence. Aggregates of GFP-HDEL are present in distinct punta, which colocalise with RTNLB3-YFP labelling (white).

D) Luminal ER marker GFP-HDEL.

E) Truncated RTNLB3-YFP exhibiting highly cisternal ER phenotype.

F) Merged image. Truncated RTNLB3-YFP labelling is present across cisternae, colocalising with luminal GFP-HDEL (white).

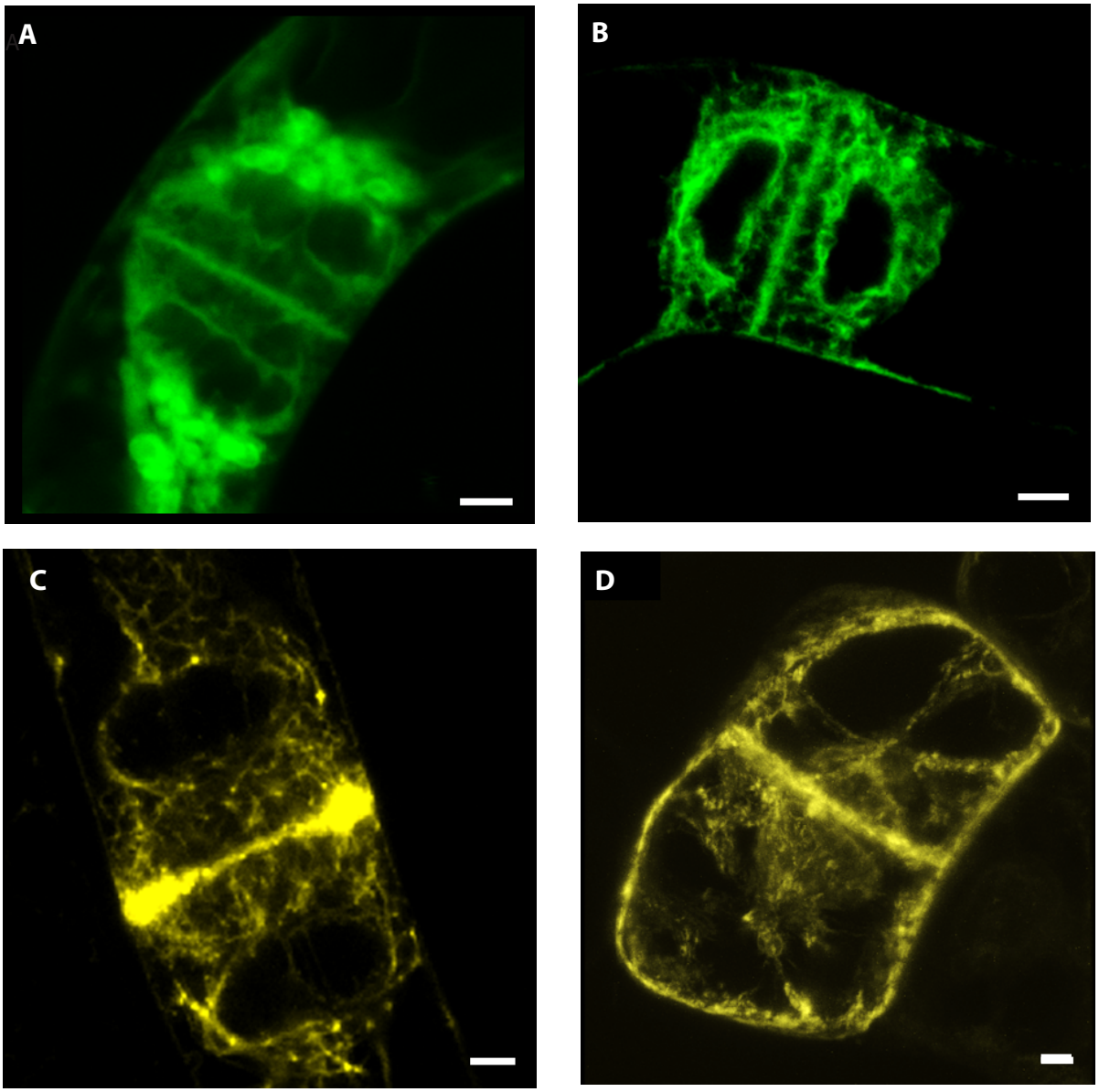


Figure 3.3.3: Confocal micrographs of *N.tabacum* BY-2 suspension cells undergoing cell plate formation in telophase (scale bars - 5 µm).

A) Wild-type BY-2 cell ER stained with Dioc6.

B) BY-2 cell stably over-expressing luminal ER marker GFP-HDEL.

C) BY-2 cell stably over-expressing full length RTNLB3-YFP.

D) BY-2 cell stably over-expressing truncation 2 of RTNLB3-YFP.

Figure 3.3.4: Confocal micrographs of *N.tabacum* BY-2 cells over-expressing truncated RTNLB3-YFP. All images show transient over-expression, except for image A (stable).

A) Failed attempts at producing a stable truncated RTNLB3-YFP cell line did result in some expressing but plasmolysed cells in some samples screened (scale bar - 50 μm).

B, C, D & E) 48 - 72 hours following transient transformation most over-expressing cells exhibit a primarily cisternal ER phenotype with labelling by the truncated RTNLB3-YFP construct throughout. Some cells also have many clearly defined tubules present comprising part of the network (B) (scale bars - 50 μm).

F) Following 72 hours incubation or more some cells begin to exhibit irregular fluorescence patterns not consistent with the structure of a continuous reticulated network and appear damaged (scale bar - 20 μm).

G) Following 72 hours incubation some highly vacuolar cells were also observed (scale bar - 20 μm).

H) In some cells nuclear envelopes became clearly labelled with the truncated RTNLB3-YFP construct (scale bar - 50 μm).

I) 72 hours post transformation some cells contained high levels of the truncated RTNLB3-YFP construct but appeared damaged and plasmolysed (scale bar - 20 μm).

J) 48 hours post transformation some cells develop large aggregations of ER fluorescence, which are excessively bright to resolve when other ER is visible (scale bar - 20 μm).

K) The laser intensity and gain were lowered to reveal structural detail in areas of high intensity aggregated fluorescence, such as that shown in image J (scale bar - 20 μm).

L) In cells where several bright fluorescent aggregations were present, they were presented in a wide range of number between cells and varied in size, shape and density within each cell in which they were observed (scale bar - 50 μm).

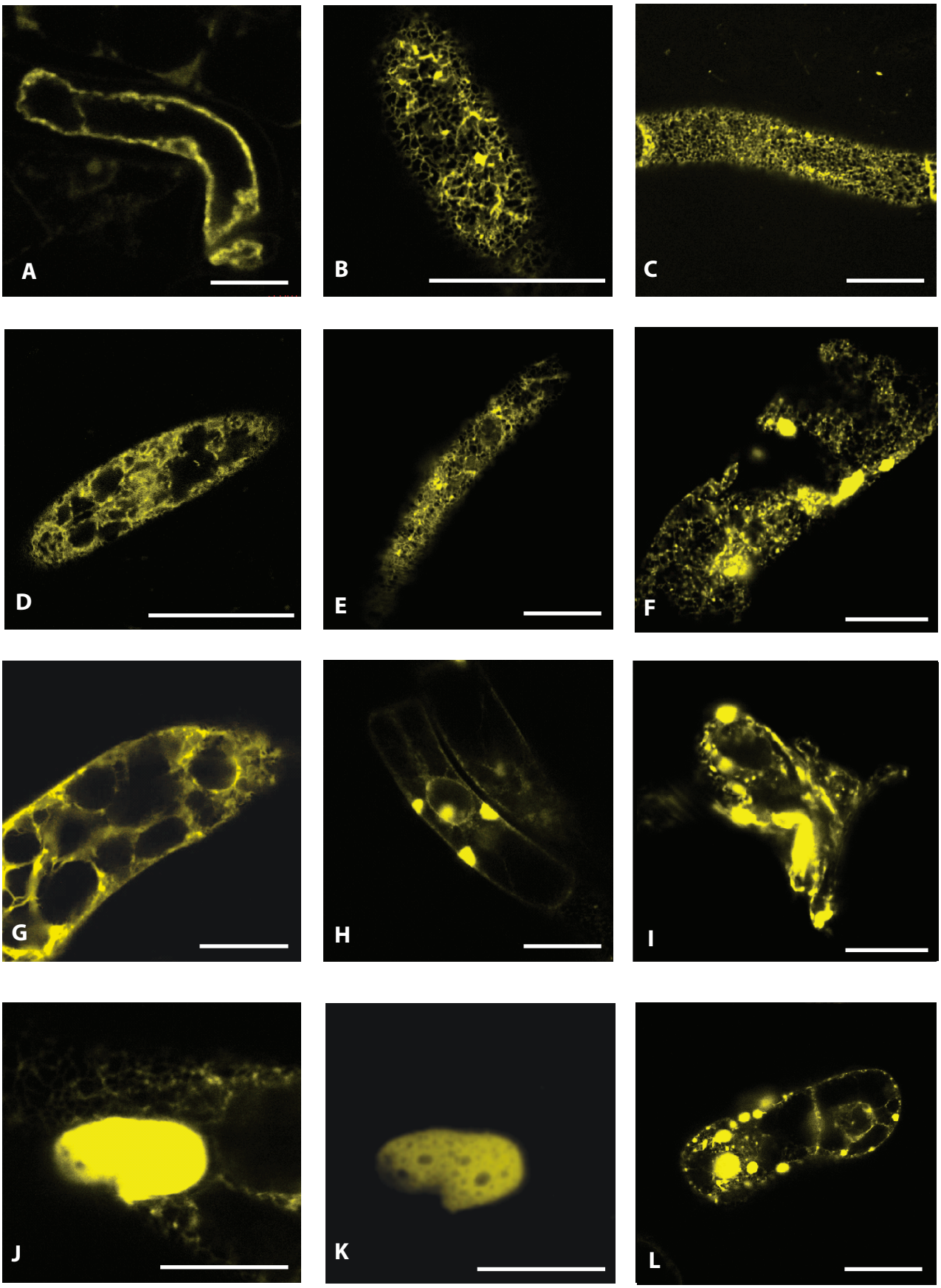


Figure 3.3.4

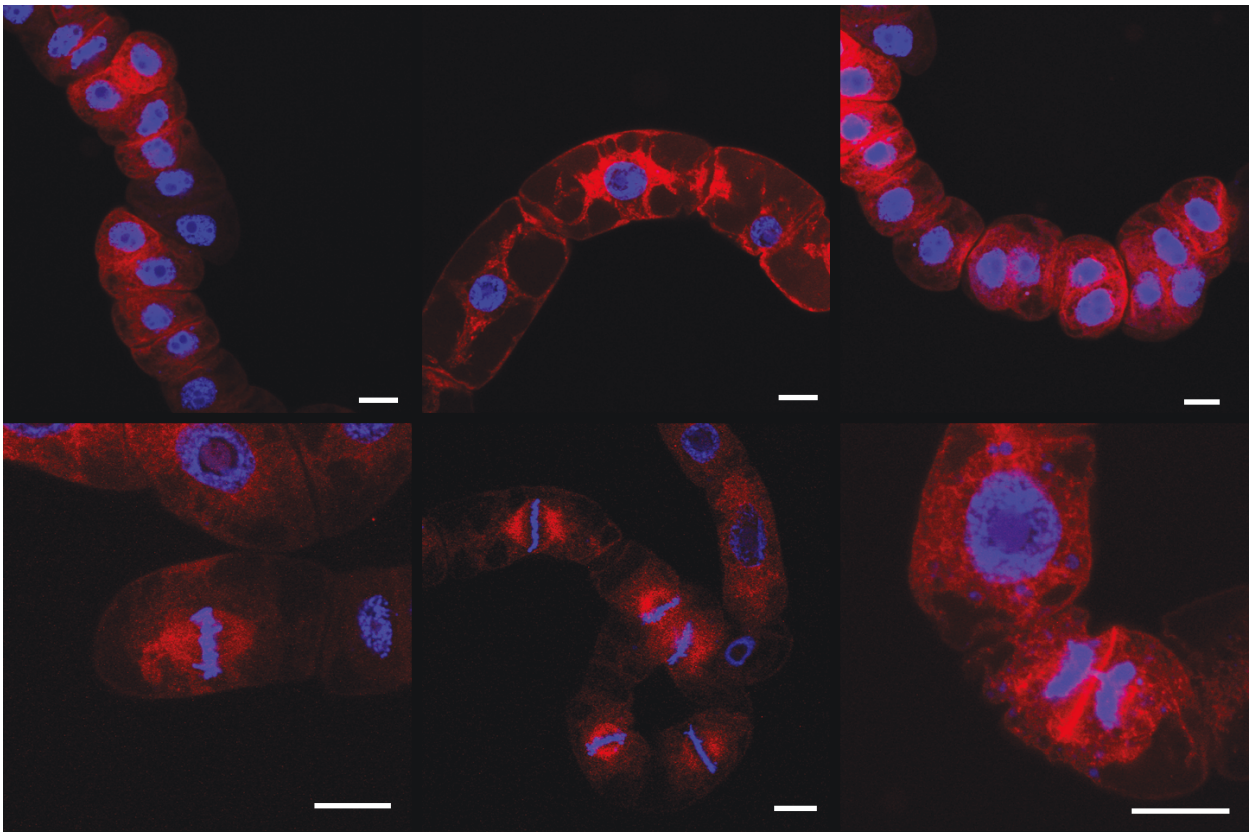


Figure 3.3.5: Synchronised BY-2 cell culture stably over expressing RTNLB3-YFP (red) and chromosomes stained with DRAQ5 (blue) (scale bars - 20 µm).

A, B & C) BY-2 suspension culture cells often grow in chains, which can vary greatly in cell number. Chromosomes and therefore nuclei are consistently and clearly labelled by DRAQ5, enabling accurate identiication of the stages of the cell cycle and recording of the mitotic index of the culture.

D & E) Chromosomes align along the central region of the cell in metaphase. Synchronisation of the cell culture yields many cells cocurrently progressing through the same stage of the cell cycle.

F) In late telophase two opposing daughter nuclei are clearly visibile with chromosomes beginning to decondense. The maturing cell plate exhibits a high level of RTNLB3-YFP fluorescence and is apparent as a defined liner structure in between the two opposing daughter nuclei undergoing formation.

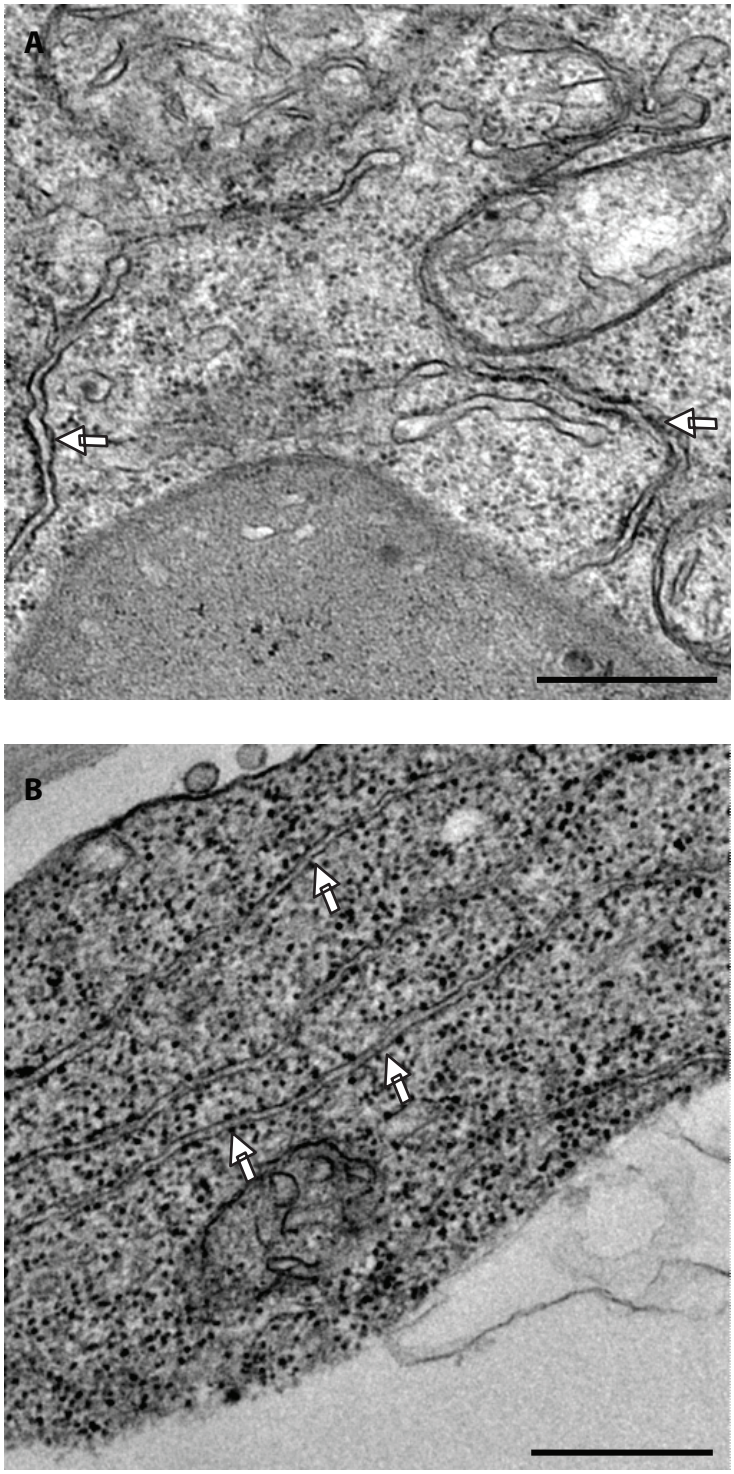


Figure 3.3.6: 80 nm thin section transmission electron micrographs of interphase *N. tabacum* BY-2 suspension culture cells showing endoplasmic reticulum morphology (scale bars - 500 nm).

(A) Wild -type cell ER (arrows indicate ER).

(B) RTNLB3-YFP over-expressing cell ER (arrows indicate ER).

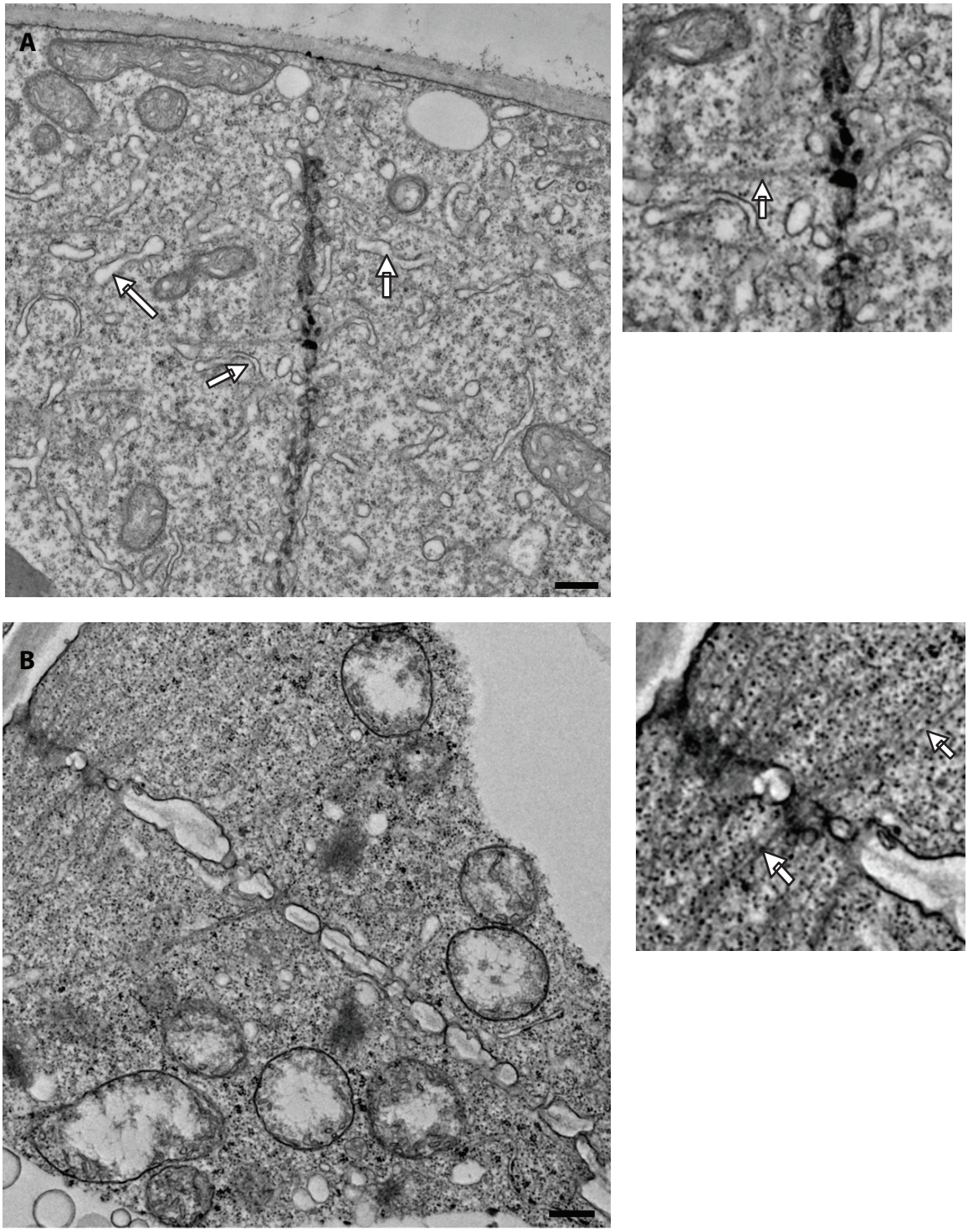


Figure 3.3.8: Transmission electron micrographs of *N. tabacum* BY-2 suspension culture cells showing the developing edges of a cell plate (scale bars - 500 nm).

A) Wild type cell with cell plate close to completion of centrifugal growth towards the current cell wall. A high concentration of cross sections of ER are visible (arrows indicate examples). Microtubules traverse the cell plate (in enlargement arrow indicates a microtubule).

B) RTNLB3-YFP over-expressing cell showing a comparable stage of cell plate development as figure A of a wild-type cell (in enlargement arrows indicate microtubules).

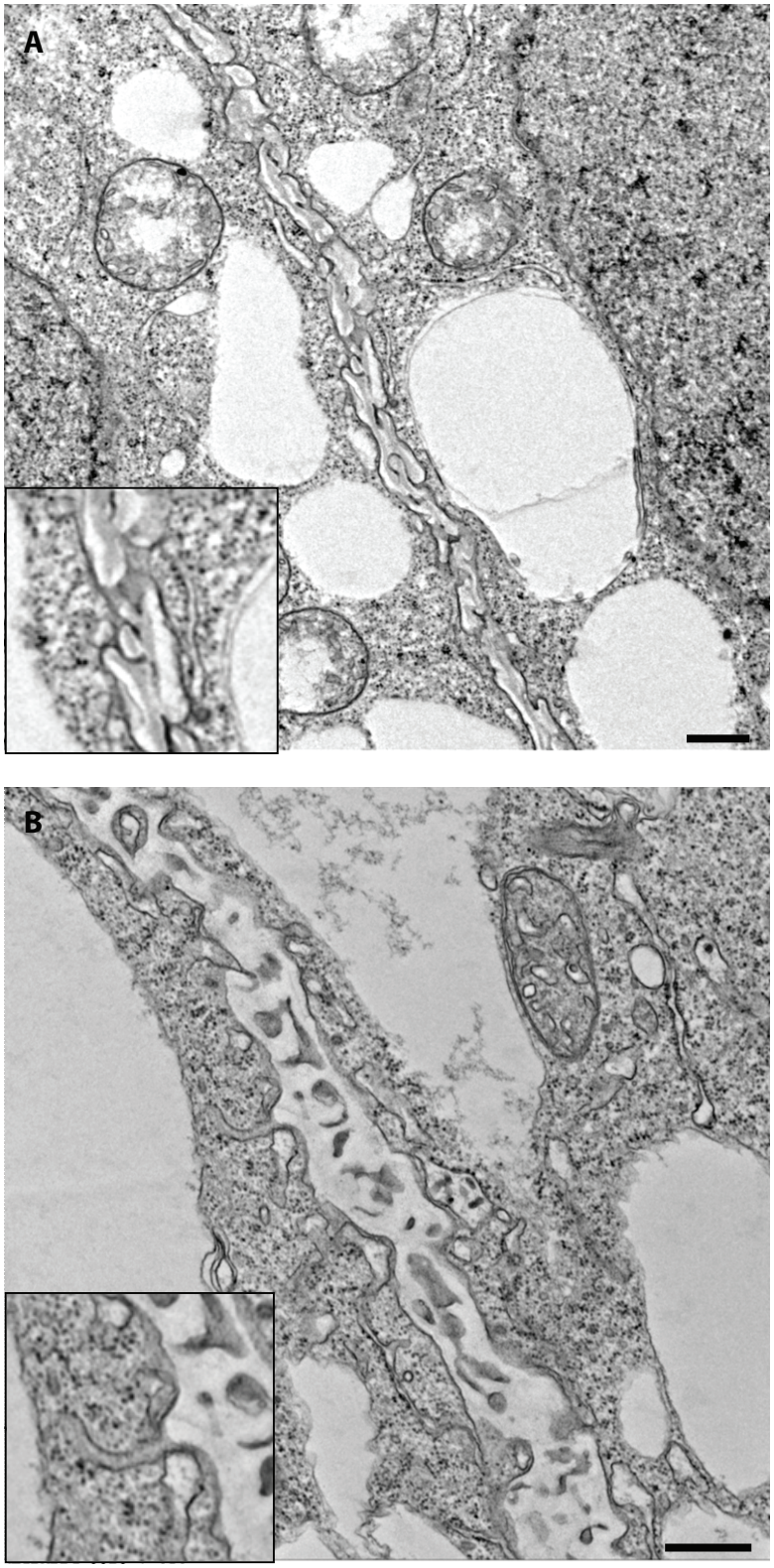


Figure 3.3.9: Transmission electron micrographs of *N. tabacum* BY-2 suspension culture cells showing maturing regions of cell plates with ER in contact with new cell wall material (scale bars - 500 nm).

A) Maturing central portion of wild-type cell plate undergoing fusion to form a new cell wall. In some areas it is unclear which material the connecting region between the cell plate and ER is composed of (inset).

B) Maturing portion of a cell plate in an RTNLB3-YFP overexpressing cell showing connections between the cell plate and surrounding ER (inset).

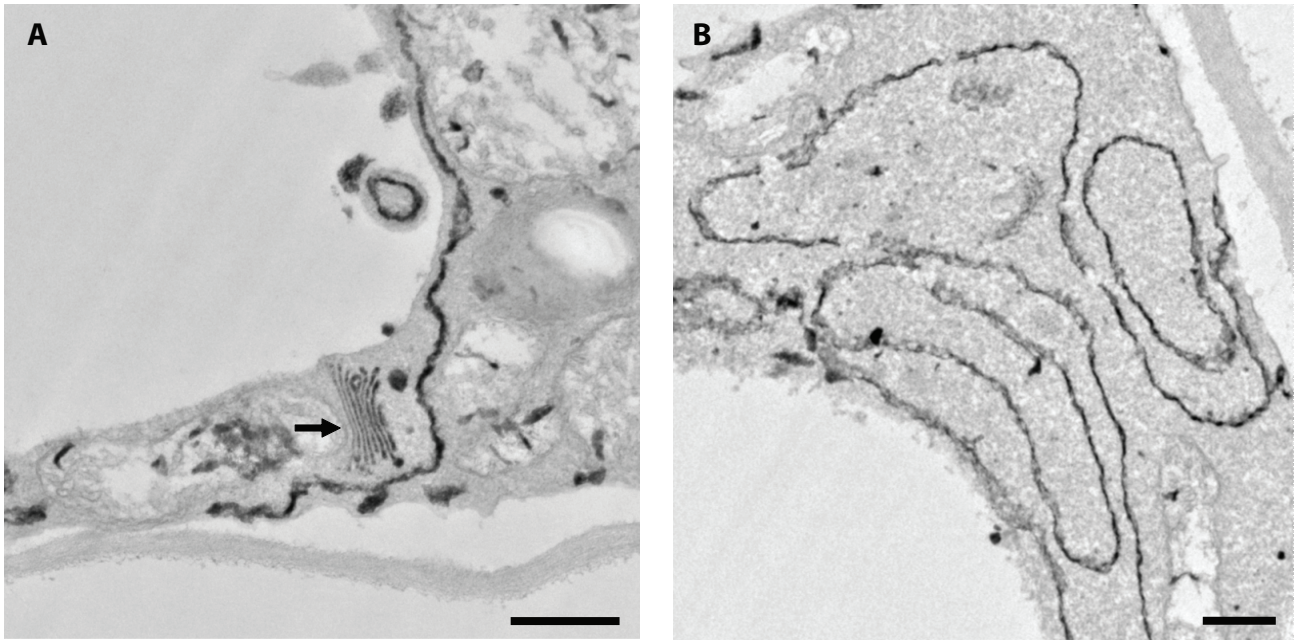


Figure 3.3.10: Thin section transmission electron micrographs of zinc iodide osmium textroxide fixed wild-type *N. tabacum* BY-2 suspension culture cells (scale bars - 500 nm)

A) Cell exhibiting optimum ER contrast with ZIO staining. The membranes of a Golgi body are also clearly defined (arrow).

B) Image showing an area of ER staining. Some regions of the interconnected ER appear larger with less contrast than others. These may be cisternal domains that have been cut through at an angle, resulting in a larger surface area of less eletron dense material in the sample section in comparison to ER membrane regions that exhibit higher levels of contrast.

3.4 Discussion

3.4.1 Development of a rapid transient over-expression system of fluorescent protein fusions in BY-2 cells.

To aid in the efficient analysis of *Nicotiana tabacum* BY-2 suspension culture cells expressing reticulon constructs, a rapid method of transient transformation was employed. The commonly used technique for transient transformation of *N. tabacum* requires infiltration of whole leaves; however, in this study, monoculture suspension cell lines were chosen as a model. Therefore a method of rapid transient expression of constructs for phenotypical analysis in these cells was a desirable tool, as the generation of cell lines stably over-expressing a construct takes approximately 2-3 months to yield a suspension culture that is ready for further experimental work. Based on the protocol described by Buschmann *et al* (2011), a protocol was adapted and refined to facilitate this. Following multiple experiments, an average transformation rate of approximately 30% following 3 to 4 days incubation with the transformed *Agrobacterium tumifaciens* bacteria was achieved (figure 3.3.1).

Despite the method developed by Buschmann *et al.* (2011) providing an efficient transient transformation technique for the study of fluorescent construct expression in BY-2 cells, very few divisions were observed in any of the samples analysed. The rate of cell division that occurs may be reduced on solid medium in comparison to growth in liquid culture. Division rates were insufficient to use samples from this technique for further cell cycle related studies. Attempts to develop a method to facilitate this proved unsuccessful. Therefore this protocol, although enabling rapid over-expression of constructs in BY-2 cells on solid medium, could not be developed further to facilitate the study of the cells in a liquid culture with a high rate of division occurring. This was trialled as a novel approach, although it had not been reported previously by Buschmann *et al.* (2011) who devised the transient transformation protocol. Subsequently there have been no reports of stably transformed lines being established from cells transformed employing this transformation methodology or studies published using the method to study BY-2 cells undergoing division. Therefore it was decided not to pursue attempting this further, as several different approaches had been tested without success.

3.4.2 RTNLB3 labels the ER in interphase BY-2 cells, exhibiting constriction of the ER lumen in comparison to wild-type and is specifically recruited at a high concentration to the cell plate during telophase

In agreement with the phenotype documented for RTNLB1-4 and RTNLB13 over-expression by Sparkes *et al* (2010) in *Nicotiana tabacum* leaf epidermal cells, over-expression of RTNLB3 in BY-2 cells caused increased tubulation of the ER and tubular constriction. This results in the exclusion of luminal GFP-HDEL from some tubules, an ER luminal marker consisting of green fluorescent protein N terminally fused to the amino acid sequence HDEL, which targets the protein to the ER (GFP-HDEL) (Runions *et al.* 2006). The phenotype of the truncated RTNLB3-YFP construct is also indistinguishable in the BY-2 suspension cell line for that recorded previously in leaf epidermal cells, with a highly cisternal network exhibiting colocalisation throughout with the luminal ER maker.

Unlike if a native promoter was used, where other reticulons that share the ER curvature inducing phenotype with RTNLB3 would compensate for expression of the truncation, over-expression driven by the 35S promoter used in this study reveals the impact that the truncated form of RTNLB3 has on ER structure when present at high enough levels to outcompete the other endogenous reticulons. This is evident from the cisternalised ER phenotype that occurs upon over-expression of the truncation in comparison to the full length protein.

Both full length and truncated RTNLB3-YFP localised preferentially to the cell plate in comparison to the rest of the ER network during cell division. Localisation of the full length construct resulted in a defined region of fluorescent labelling in the location of the more mature central portion of the cell plate. This is similar to the fluorescent labelling of the cell plate in WT cells by DiOC6 and in cells over-expressing the luminal marker GFP-HDEL. However unlike these two controls, localisation of the RTNLB3-YFP construct to the cell plate was further enriched at the developing edges of the cell plate. As the cell plate develops, ER that traverses the cell plate becomes trapped and constricted to form the inner cores of the desmotubules of plasmodesmata that form at these sites (Hawes *et al*. 1981). RTNLB3 may be recruited specifically to the regions where this process is occurring, becoming incorporated into these structures as the cell plate matures. Therefore as the cell plate develops centrifugally outwards, the highest concentration of RTNLB3 protein would remain associated with the sites of active

growth, where the protein continues to be recruited to this region as the cell plate develops. Regions where the cell plate has been established and is maturing, particularly at plasmodesmatal sites, could remain enriched with the protein but without further additional recruitment to this region. This hypothesis would account for the localisation identified for RTNLB3-YFP during cell plate development and provides further evidence for the fact that RTNLB3 may play a role in the formation of plasmodesmata. Truncated RTNLB3-YFP was also found to be enriched at the cell plate, however in comparison to the full length construct and controls the enrichment was more diffuse in this region and lacked variation in intensity in relation to cell plate maturation. This may be due to the mutant protein being recruited to the plate but it is not able to be incorporated into the cell plate structure and plasmodesmata due to its lack of curvature inducing properties. Both constructs appear to be localised to the ER throughout the cells and are likely to be confined to the ER at the cell plate. However, as the constructs are over-expressed with a 35S promoter, the levels of the construct and therefore concentration of the fluorescent constructs within the cells will be greater than if the construct was expressed using a native promoter. Therefore the amount of RTNLB3-YFP seen recruited to the region of the cell plate here will be in a quantity exceeding that which would occur at natural levels. However, the amount of RTNLB3 required for cell plate formation when expressed at endogenous levels may be at a relatively low level, which would be difficult to observe using this technique. Therefore the over-expression of the constructs demonstrates clearly that the protein is recruited to the region of the cell plate, and that the full length construct localises preferentially to the developing edges as the plate develops. When the brightness was reduced on the microscope to reveal more detail of the localisation of the construct at the cell plate, both full length and truncated RTNLB3-YFP constructs appeared to be confined to ER membranes, indicative of the bright regions of fluorescence not being over-expression artefacts in the region. However, the resolution capacity of the confocal microscope used for this experiment was not sufficient to resolve this in precise detail. If a higher resolution confocal microscope such as a super-resolution LSM with Airyscan (Zeiss, Germany) were available, this could be confirmed using imaging with far greater accuracy.

A fluorescently labelled protein construct consisting of a dynamin-like protein known as phragmoplastin, fused with GFP and expressed in BY-2 cells, has been previously demonstrated to exhibit a similar localisation phenotype during cytokinesis (Gu & Verma,

1997). Phragmoplastin, which is involved in cell plate formation, has been found to first localise to the central region of cell plate formation and then redistribute to the growing edges of the cell plate as it develops centrifugally outwards (Gu & Verma, 1997). Gu and Verma (1997) have suggested that phragmoplastin is involved in membrane fusion events during early cell plate formation. Therefore, if RTNLB3-YFP is also involved in the early stages of cell plate formation, in this case at the sites where plasmodesmata develop, this would account for the similar localisation pattern to that identified for phragomoplastin during cytokinesis.

Recently, a study has been published by Knox *et al.* (2015), who obtained data using the same cell lines also used in this study, with their results corroborating the observations presented here. In agreement with conclusions drawn from the data presented here, the truncation of RTNLB3-YFP interferes with specific recruitment of RTNLB3-YFP to the cell plate during development.

To investigate this further Knox *et al.* (2015) performed fluorescence recovery after photobleaching (FRAP) analysis on the two cell lines and bleached cells undergoing cell plate formation in the central region of each cell plate and the two leading edges. RTNLB3-YFP mobility was found to be reduced in the central region of the plate in comparison to the developing edges. The regions with the higher degree of RTNLB3-YFP mobility at the edges corresponded to the regions where higher fluorescence intensity has also been observed. RTNLB3-YFP mobility is affected by oligomerisation of reticulon proteins, which is required for the proteins to be able to constrict ER membrane into tubules or curved structures. This has previously been demonstrated for reticulon family proteins by Shibata *et al*. 2009 and Tolley *et al.* 2010. Therefore their FRAP data suggests that a higher proportion of oligomerised RTNLB3-YFP proteins are present in the central, more mature region of the cell plate, than at the developing edges (Knox *et al.* 2015). This in turn suggests that during maturation of the cell wall RTNLB3-YFP proteins are incorporated into, or resulting in, sites of high membrane curvature that are rich in reticulon oligomers. Knox *et al.* (2015) also present data showing significant enrichment of RTNLB3-YFP at plasmodesmata, imaged by three-dimensional structured illumination microscopy (3D-SIM). They conclude that RTNLB3 localises preferentially to ER strands that traverse the cell wall at plasmodesmata sites, forming oligomeric complexes and that their data suggests that during the formation of primary

plasmodesmata, reticulons are involved in shaping the ER membrane into desmotubules at the cell plate. The data also showed similar results for RTNLB6, which has also been identified in a plasmodesmatal proteomic screen (Fernandez-Calvino *et al*. 2011).

When cell plates in cells over-expressing truncated RTNLB3-YFP and GFP-HDEL were subject to FRAP, the fluorescence recovery rate for the truncated reticulon construct was faster than the rate of recovery of GFP-HDEL, which both exhibited a more rapid rate of recovery than full length RTNLB3. The truncated RTNLB3 lacks a hydrophobic domain required for oligomerisation of the protein into complexes and therefore interferes with the proteins capacity to shape membranes (Sparkes *et al.* 2010). They state that this accounts for the lack of specific recruitment to the cell plate and increased mobility of the protein in the cell plate region in comparison to full length RTNLB3.

3.4.3 Truncation 2 of RTNLB3-YFP is poorly tolerated and high levels of over-expression are lethal to BY-2 cells

A new BY-2 cell line stably over-expressing RTNLB3-YFP (section 3.3.3) was generated, which was found to be suitable for downstream applications, and exhibited the expected phenotype previously identified in the initial equivalent stably transformed BY-2 line (section 3.3.2).

A new stably transformed line expressing truncated RTNLB3-YFP could not be established. The high levels of over-expression of the construct by transient transformation confirmed the viability of the *A. tumifaciens* cultures used for the attempted stable transformations. It also demonstrated that transient expression of the construct results in a primarily cisternal ER network as previously described in cells stably over-expressing the construct (section 3.3.2). High levels of over-expression also resulted in some large aggregations of the fluorescent construct, although the rest of the ER network remained reticulated in structure with a fluorescence distribution characteristic of prior observations (section 3.3.2, Sparkes *et al*. 2010). These aggregates are suspected to be comprised of ER membrane, as the protein has been shown to localise specifically to the ER, however these aggregates lacked the expected reticulated pattern of the ER network.

Labelling of the nuclear envelope by the construct was also observed. As the truncated RTNLB3-YFP construct localises preferentially to lower curvature membranes, it is possible that the construct could insert into the membranes that comprise the nuclear envelope, a relatively low curvature ER domain (English & Voeltz, 2013a).

A range of other observations were made, not consistent with the structure of the cisternalised ER network previously documented to result from truncated RTNLB3-YFP over-expression (Sparkes *et al.* 2010). The range and number of abnormalities in the cell samples analysed increased with duration of over-expression, indicating that these changes were likely due to high levels of over-expression of the mutant protein. Observations included highly vacuolated cells, deformed ER networks with a highly irregular distribution of the fluorescent construct within them, and some cells showing signs of plasmolysis, which is indicative of severe cellular disruption and potentially cell death.

Although a stably transformed BY-2 cell line over-expressing the reticulon 3 truncation had previously been obtained (Pengwei Wang, Oxford Brookes University), the success rate of establishing a stably transformed cell line from experiments had been noted to be very low in comparison to the full-length construct. The previous line was the product of approximately 20 separate attempts until a cell line was successfully established (Pengwei Wang, personal communication). The over-expression level of the stably transformed line was also lower, based on fluorescence intensity, than that of the stably transformed full length RTNLB3-YFP culture. Therefore, although it is possible for stable transformation to occur and the over-expression of the construct be tolerated in a BY-2 cell, it appears that this is a rare occurrence in comparison to what would be expected from using the stable transformation protocol employed in this study, when compared to the successful transformation and stably transformed cell line generation using the full length RTNLB3-YFP construct.

Therefore it is apparent that a high level of expression of this truncated form of RTNLB3-YFP is very poorly tolerated long-term by BY-2 cells and as a result is lethal on most occasions. This is supported both by the fluorescent but dead cells identified in samples taken from attempted stable transformations and from the observations made regarding some of the damaging effects of high-levels of transient over-expression to the structure of the ER in transformed cells.

The changes in ER morphology due to a high level of expression could be structurally so disruptive to the ER network that normal cellular processes can no longer be maintained, which are essential for cell survival and proliferation. The shift to a permanently cisternal network could disrupt cell function to a degree that the cells find difficult to tolerate, due to interfering with ER processes isolated to tubular regions of ER. For example, the *A. thaliana* mutant line *pah1 pah2* exhibits an almost entirely cisternal ER morphology (Nakamura *et al*. 2009) and presents an altered growth phenotype that exhibits a greater sensitivity to phosphate concentration in the growth medium than wild-type plants. In the case of mutant RTNLB3 over-expression, although cells may continue to be viable in interphase and the ER continues to function proficiently enough for cell survival and growth, cells may be unable to undergo mitosis without severe structural defects to the cell plate, possibly resulting in the cell wall being unable to form correctly due to disruption caused at plasmodesmatal sites by the mutant construct.

There may also be other changes in cellular morphology that result from over-expression of the truncated construct that are currently unknown, which affects the likelihood of long-term cell survival and proliferation. If reticulons were to be involved in the formation of nuclear pore complexes in plants, as has been shown to be the case in some organisms (Anderson & Hetzer, 2008; Antonin, 2009; Dawson *et al*. 2009), disruption of function by over-expression of a truncated reticulon protein may result in the failure of new nuclear pores to correctly assemble, which could result in a lethal phenotype. This has been shown to be the case for numerous *null* mutants of plant nucleoporins (NUP), proteins that are components of nuclear pore complexes, which exhibit lethal embryonic phenotypes in *A. thaliana* (Parry, 2014).

3.4.4 Establishment of timescale, synchronisation efficiency and optimal protocol for the synchronisation of a BY-2 suspension cell culture

Synchronisation of cell suspensions is required to achieve high levels of mitotic cells in a single culture for the efficient analysis of stages of the cell cycle. The technique enables a culture to be halted in S phase by addition of the cell cycle inhibitor aphidicolin, a metabolite of *Nigrospora oryzae* (Kumagai-Sano *et al.* 2006). The cells are then released from S phase by washing the aphidicolin infused media from the cells, allowing them to progress through G2 to the mitotic phase.

The high peak mitotic index achieved in the results shown in section 3.3.4 is sufficient for use of this technique in further experimental work, with the optimum time window for experimental work having been established. From the results shown in table 3.3.1, this is between 8 to 10 hours following washing the cells of aphidicolin for peak mitotic index (highest achieved was 32.2%), with the same time points being optimal for studying cells in telophase (cells in telophase peaked at 8 % 8 hours post cell cycle release and remained at 7 % for the following two hours in this data set). The technique was employed in the preparation of cell cultures for transmission electron microscopy analysis of the RTNLB3-YFP over-expression phenotype.

3.4.5 Preliminary analysis of ER luminal diameter from thin section transmission electron micrographs of interphase *N. tabacum* BY-2 cells

The initial numerical data gathered of ER diameter indicated that there was an overall shift to a significantly narrower diameter in RTNLB3 over-expressing as opposed to wild type cells. This demonstrates, alongside confocal microscopy data where GPF-HDEL is excluded from some ER tubules when this construct is expressed (section 3.3.1 & 3.4.1), that constriction of the ER tubule diameter is induced and therefore results in a decreased luminal capacity. For TEM this is only a preliminary indicator based on the comparison of the two data sets. Longitudinally sectioned ER tubules cannot be conclusively differentiated from cross sections of ER cisternae from thin section electron micrographs, due to both domains exhibiting similar luminal diameters in this orientation (Shibata *et al*. 2006). ER tubules visible in transverse in the section cannot be measured, as these cannot be accurately differentiated from other small structures that have a round membrane bounded appearance in cross section, such as Golgi derived vesicles. With the methodology employed the exact location that the section that has been cut may also be through at any point and angle along a longitudinal tubule or cross sectional cisternal sheet. Therefore these values cannot be deemed as true representations of actual cross sectional ER liminal diameter. However, these variables are equally true for both data sets, and therefore such a significant difference towards a higher number of smaller luminal capacities (which is as expected based on other data gathered thus far), it can be concluded that there is a significant phenotype worth investigating further. This will be carried out using more accurate electron microscopic techniques such as TEM tomography, SBFSEM and 3D reconstruction. Furthermore, due to the inability to

conclusively identify tubular and cisternal ER, no conclusions about cisternal compared to tubular ER ratios or how they differ between samples can obtained using this method. Therefore three-dimensional imaging techniques at this resolution are necessary for further detailed ultra-structural data collection and analysis, which will be discussed in detail in chapters 5 & 6.

3.4.6 Transmission electron microscopy of the ER & RTNLB3-YFP during cell plate formation

The bundles of microtubules shown in figures 3.3.8 A & B have previously been documented to move with the actively growing region of the cell plate as it develops (Van Damme *et al.* 2007). Therefore we can tell that regions with this structure identified are undergoing active growth. In the wild-type cells there is a large aggregation of ER around this region and in contrast there appears to be less in the RTNLB3-YFP over-expressing cells. As ER tubules are suspected to be narrower in these cells, with a far lower proportion of the ER in cisternal form, it is logical that less ER would be visible in each thin section micrograph of these cells than in the wild-type samples. This is due to the decreased probability of cutting through ER in an 80nm section if the overall volume the ER occupies in the cell is significantly less. However it is also possible that this difference could be due to differences in the distribution of the ER during cell plate formation between wild-type cells and those over-expressing the RTNLB3 construct.

During cell plate development ER that traverses the cell plate in its vesicular form becomes incorporated into the fusing cell plate, and plasmodesmata, as they develop to become desmotubules (Hawes *et al*. 1981; Hepler, 1982). Therefore such sites, as present in figure 3.3.9, A & B, show these associations of the ER with the cell plate, however cannot accurately be analysed due to the cell plate material and ER membrane exhibiting similar levels of staining that cannot be differentiated between. This is particularly unclear during the fusion of the new cell wall material when the ER becomes incorporated into the forming cell wall. Therefore this is highly problematic to achieving the aims of this study as it is not possible to identify which material is ER that will become the desmotubles of plasmodesmata at these points. Therefore a specific staining technique for either the ER or cell plate material is required for further analysis, the

optimisation process of which is discussed in section 3.3.7 and 3.4.7 of this chapter and will be applied further in chapters 5 and 6.

3.4.7 Transmission electron microscopy employing zinc iodide osmium textroxide fixation to stain ER membranes in BY-2 cells

Zinc iodide osmium textroxide impregnation is used to selectively stain the membranes of membrane bounded organelles but does not stain the plasma membrane, mitochondrial and plastid envelopes, or the cell wall (Hall & Hawes, 1991). The technique produces material suitable for electron microscopy with the ER specifically stained at extremely high electron opacity and therefore contrast (as demonstrated in the fixations achieved and results presented in section 3.3.7). This resolves the limitations of analysis of the ER in relation to cell plate development identified and discussed in sections 3.3.6 and 3.4.6, respectively.

Although the ZIO technique provides the capacity to distinguish ER from cell plate material in thin section electron micrographs, where ER is identified it still remains unclear as to whether this is tubular or cisternal ER that has been sectioned in cross section. The location and angle at which the section has been cut in relation to the opposing ER membranes also cannot be determined. This is problematic, as the resulting image of a section that has not been cut exactly through the midpoint of a tubule in transverse section is not representative of the tubule diameter. A cisternal sheet that has not been sectioned at an exact 90° angle to the two opposing membrane bilayers will also not depict the true cisternal luminal diameter. Therefore to fully gain an understanding of ER morphology and the changes which occur during cell division, another approach in combination with ZIO fixation is required. TEM tomography will be employed to obtain high resolution three dimensional data of the stages of cell plate formation in wild-type, RTNLB3-YFP and truncated RTNLB3 over expressing cells in *Arabidopsis thaliana* root tips.

In combination with the ZIO preparation, this provides a methodology that will enable the collection of data from which the interactions between the ER and the cell plate can be clearly identified and analysed as it develops. ER fully incorporated into the new cell wall as desmotubules in mature plasmodesmata will retain staining, therefore showing the

continuity of the ER between cells. As the plasma membrane does not stain, this other plasmodesmatal membrane component will not hinder accurate identification and analysis of the desmotubule membrane cores.

Therefore comparison between the wild-type, full length and truncated RTNLB3 over-expressing cells, with regards to the structural characteristics during cell plate development, and incorporation of the ER during desmotubule formation, will be possible. The interactions between the ER and the cell plate during the formation of the new cell wall and plasmodesmata have thus far not been fully documented in this level of detail. Although work has been carried out on an ultra-structural level (discussed in sections 1.4 and 1.5), this has also been subject to the limitations met and discussed thus far in this study. Therefore, the intricacies of the relationship between the ER and the forming cell plate are still unclear. In addition the molecular component responsible for transforming the ER into such a highly constricted membrane rod, with an occluded lumen that is not seen elsewhere in the plant cell, remains to be confirmed.

Further work in this thesis will be carried out using *Arabidopsis thaliana* root tips as a model plant system as opposed to BY-2 cell cultures. Failure to establish a new stably transformed line of BY-2 cells over-expressing truncated RTNLB3-YFP, due to suspected lethality of the construct in this cell model, prevented further investigation of this construct alongside WT cells and those over-expressing full length RTNLB3-YFP. The mutant phenotype could be further investigated in this cell model by employing a new construct, containing the truncated RTLB3-YFP sequence with an inducible promoter that activates expression only with the addition of a stimulus. However it was decided that rather than switch to an inducible truncated construct in this system, that the existing constructs would be further investigated using *Arabidopsis thaliana* plants.

The phenotypes of the RTNLB3 constructs have not yet been established in a stably over-expressing whole plant model, with phenotypical data of any plant reticulons investigated having thus far been derived from transiently transformed tobacco leaves (Tolley *et al.* 2010; Sparkes *et al.* 2010). Due to the phenotype observed in this chapter for the non-inducible truncated RTNLB3-YFP construct when stable over-expression was attempted, it would be interesting to investigate this construct further and to ascertain whether the observed lethality is isolated to stable over-expression in BY-2 monoculture cells, or if stable over-expression also results in a lethal phenotype in a different model system.

Additionally, *A. thaliana* root tips provide an excellent well-established and relatively simple plant model system for investigating cell division (Beemster & Baskin, 1998; Hayashi *et al.* 2013; Heidstra & Sabatini, 2014; Zhang *et al.* 2016), due to the growing meristematic region of the root where undifferentiated cells undergo division (Nakajimaa & Benfey, 2002). The use of *Arabidopsis thaliana* as a model organism for plant research also has other advantages, which will be discussed further in chapter 4, section 1.

The *A. thaliana* system also has the potential to overcome some of the impracticalities of preparing samples of cells undergoing cytokinesis for electron microscopy analysis, which were encountered when using BY-2 cell cultures in this study (described in section 3.3.7). Unlike the cells in these samples, which were unable to be tightly packed together when embedded in resin blocks (thus requiring the sectioning and screening large quantities of material to cut), fixed and embedded *A. thaliana* root tips will consist of plant tissue, therefore containing many interconnected cells within each section of root cut.

4. Generation and confocal microscopy analysis of stably transformed *Arabidopsis thaliana* plants over-expressing RTNLB3 constructs

4.1 Introduction

Arabidopsis thaliana has gained popularity as a model organism since the 1980's and has become one of, if not the, most commonly used plant for scientific research (Müller & Grossniklaus, 2010). Its relatively simple and small genome has proved ideal for genetic and molecular studies, with five chromosomes comprising a genome totalling 119 Mb in size (Rensink & Buell, 2004). The species is representative of a flowering plant, with the benefits of a short life cycle and high yield of seed. This makes genetics studies involving the generation of stably transformed lines practical for research time scales (Müller & Grossniklaus, 2010). This model organism has been chosen for use in this study due to these factors, as well as the rapid rates of cell division that occur in the root meristem during growth (Beemster & Baskin, 1998). Therefore the generation of stably transformed lines expressing the full length and truncated RTNLB3 constructs would be suitable for the investigation of the expression phenotype in a range of cell types, for analysis of the ER during cell pate development, and plasmodesmatal formation.

The floral dip method for stably transforming *Arabidopsis thaliana* plants has been well established and optimised, having been used widely in plant research for several decades (Clough & Bent, 1998; Bent, 2006; Zhang *et al*. 2006). The technique does not require any plant tissue culture, is relatively simple, low in cost of reagents and minimal in the amount of labour it requires (Zhang *et al*. 2006; Bent, 2006). Arabidopsis plants are grown until flowering and then either sprayed or dipped in a solution containing *Agrobacteria tumefaciens* that have been transformed with the desired construct for expression. The plants are then grown to seed and these collected for germination on media containing the appropriate antibiotic for enabling selection of plants expressing the construct. The dipped plants are referred to as "T_0" plants, with positively transformed plants grown from these designated "T_1". The transformation efficiency of the technique is typically between 0.1-3 %, with most commonly about 1% of the T_1 generation having been transformed (Wang, 2006). Thousands of seeds can be collected from each Arabidopsis plant and therefore a single floral dip experiment is sufficient to obtain transformed plants in the next generation (Zhang *et al.* 2006).

T_1 plants are hemizygous as T-DNA insertion following floral dipping occurs after the male and female gametophyte cells have diverged in the T_0 plants. Positive T_1 transformants contain the construct in all cells, as each expressing plant is the result of a germline transformation (Wang, 2006). The eco-type of Arabidopsis most commonly used by researchers is Col-0 ("Columbia"), which was the first full Arabidopsis genome to be sequenced (Wang, 2006). For the floral dip method various *Agrobacterium* strains have been successfully used, with the most common and especially amendable for Arabidopsis transformation being GV3101 pMP90 (Wang, 2006).

T_2 plants resulting from the self-fertilisation of the T_1 generation will result in some plants that do not contain the construct, as the parent generation from the floral dipped plants is hemizygous. This can be overcome so that the T_2 generation can be utilised for phenotypic studies by germinating the plants under selection for positive transformants and those in which the construct has not been silenced, or by screening for expression (Wang, 2006). In this study individual plants were manually screened and accurately identified as over-expressing or not, as the constructs used were fluorescent fusions containing YFP fused to the protein of interest. To generate stably transformed lines that are homozygous, T_2 generation plants can be grown to seed and T_3 plants grown from each, so that lines in which all individuals express the construct can be identified.

Brefeldin A (BFA) induces ER cisternae by causing Golgi membranes to be reabsorbed into the ER, due to the drug blocking secretion at the ER/Golgi interface. This also leads to an accumulation of secretory products within the ER due to retrograde transport from the Golgi bodies (Boevink *et al*. 1999). Treatment with the drug can therefore be employed to artificially induce sheet formation in an ER network. As the over-expression phenotype of RTNLB3-YFP is predicted to be highly tubular in any successful plant lines created, this can be employed to analyse whether the construct remains restricted to curved membranes or if it does distribute over the ER sheets formed.

Callose has been shown to be specifically located at plasmodesmatal sites (Fitzgibbon *et al.* 2010). Analine blue which stains for callose can therefore be used as a specific marker for PD in cell walls (Zavaliev & Epel, 2015). This technique was employed to attempt to

identify any co-localisation between RTNLB3-YFP at the cell surface and plasmodesmata.

4.2 Materials & methods

For Arabidopsis plant growth and transformation methods, with full-length RTNLB3-YFP, truncated RTNLB3-YFP and dexamethasone inducible truncated RTNLB3-YFP, please refer to chapter 2, (section 2.4).

4.2.1 Treatment of leaves with Brefeldin A and Rhodamine hexyl B staining

Brefeldin A was dissolved in DMSO at 10 mg/ml and stored at -20 °C. Individual cotyledonary leaves were cut from 7 day old seedlings and incubated in a freshly prepared working solution of 100 µg/ml BFA and DW for 3 hours. Following BFA treatment leaves were incubated in a freshly prepared working solution of 1 µg/ml Rhodamine hexyl B for 15 minutes.

4.2.2 Confocal microscopy imaging of *Arabidopsis thaliana* plants

Individual leaves or roots were placed on a drop of water on glass microscope slides (0.8 – 1.0 mm, Fischer, UK), followed by an additional drop of water on the surface, with the abaxial leaf side facing upwards. A cover slip (22 x 50 mm, Scientific Laboratory Supplies Ltd, UK) was placed over the leaf, ensuring air bubbles were excluded.

Samples were imaged using a Zeiss LSM 880 (Zeiss, USA) confocal fluorescence laser scanning microscope with 10 x air and x 40, x 63 and x 100 oil immersion objectives.

4.2.3 Screening of *Arabidopsis thaliana* plants using a fluorescence stereomicroscope

Plates of germinated seedlings were screened at 7 days old for fluorescent plants using a Leica MZFLIII stereomicroscope.

4.2.4 Dexamethasone induction of an inducible truncated RTNLB3-YFP construct

T_2, 6 day old Arabidopsis seedlings, from floral dipping with the inducible truncated RTNLB3-YFP construct, were induced in a solution of 20 μM dexamethasone (Sigma-Aldrich, UK) and 0.02 % Silwett L-77® in DW. A 20 mM stock solution of dexamethasone was prepared in DMSO (Sigma-Aldrich, UK) and stored at 4 °C for a maximum for two weeks for each use.

For induction seedlings on agar plates were covered in dexamethasone solution (8 ml) and swirled to distribute the excess solution around the plants over the agar plate 20 hours prior to the beginning of an experiment. Plates were sealed with microscope tape and placed back horizontally in an Arabidopsis plant growth cabinet. Plates were agitated to re-disperse solution that had not yet been absorbed by the plants or agar plate 4-6 hours after initial induction. A plate of control plants was also prepared with each experiment, with identical preparation except the solution contained 1 μl per ml DMSO, as opposed to 20 mM dexamethasone in DMSO.

4.2.5 Analine blue staining of leaves for callose

Individual cotyledonary leaves were cut from 7 day old seedlings and incubated in 0.01% aqueous analine blue solution for 15 minutes prior to imaging (as per section 4.2.2).

4.3 Results

4.3.1 Confocal microscopy analysis of stable over-expression of full-length and truncated RTNLB3-YFP in seven day old *Arabidopsis thaliana* leaf cotyledonary cells

Arabidopsis thaliana eco-type Col-0 plants stably over-expressing RTNLB3-YFP were successfully generated and highly expressing T_2 plants were selected for confocal microscopy analysis. The fluorescence intensity in cotyledonary leaves in these plants was shown to be relatively consistent between epidermal cells (figure 4.3.1, A & B). High levels of expression were also present in stomata. The YFP labelled ER was observed to

be a highly tubular interconnected network throughout each individual cell, with very few visible cisternae (figure 4.3.1, C & D). Larger, thicker strands exhibiting high levels of YFP fluorescence were also present in the majority of cells analysed, although these varied in size, number and fluorescence intensity between individual cells, exhibiting more variation than the YFP expression present in the rest of the ER network (figure 4.3.1 B, C & D). Larger aggregates of fluorescence were also observed in some cells, which may be bundles of the same structures (such as figure 4.3.1, B). Using this method of observation, it is not possible to differentiate these strands from the rest of the labelled ER network. However linear strands that traverse almost the entire length of some cells are not consistent with the reticulated pattern of the majority of the RTNLB3-YFP labelled ER network (figure 4.3.1, C & D). No nuclear envelope labelling by the over-expressed fluorescent RTNLB3 construct was observed in leaf cells.

Arabidopsis thaliana eco-type Col-0 plants were also floral dipped for transformation with the truncated RTNLB3-YFP construct. When seeds collected from the T_0 dipped plants were grown on appropriate selection media for the construct no positive transformants were obtained. Seeds were also grown on media in the absence of antibiotic selection. Seedlings that germinated were screened for fluorescence and no expression was observed in any plants. It can therefore be concluded that the truncated RTNLB3-YFP construct is likely lethal when stably over-expressed in *Arabidopsis thaliana* plants, as the transformation with full-length RTNLB3-YFP that was carried out in parallel yielded many highly expressing transformants per floral dipped T_0 plant.

To enable analysis of the over-expression phenotype of truncated RTNLB3-YFP in *A. thaliana* plants, and to overcome the suspected lethal phenotype of consistent over-expression within transformed plants, a new inducible construct was employed. Plants were floral dipped and stably transformed with truncated RTNLB3-YFP and a dexamethasone inducible promoter within the construct. Positive T_1 transformants were identified and grown to T_2 seed. Plants were grown and over-expression was successfully induced prior to confocal microscopy analysis.

Following 20 to 24 hours of induction of the truncated RTNLB3-YFP construct, leaf cotyledonary cells exhibited high levels of expression (figure 4.3.1, E & F). YFP labelled ER was present throughout the cells as an interconnected, primarily tubular network

(figure 4.3.1, E & F). Within some cells aggregates of YFP were present, as were strands exhibiting high concentrations of YFP fluorescence that were very large in size compared to ER tubules (figure 4.3.1, E).

Plants transformed with the inducible truncated RTNLB3-YFP construct were also treated with the components of the induction solution (DMSO and Silwett-77 in distilled water), excluding dexamethasone, for 20 hours as a control for expression. The plants were then stained with hexyl-rhodamine B to label the ER network. Plants that had not been treated with dexamethasone should not express the inducible construct and therefore have a wild-type phenotype with no YFP expression anywhere in the plants. The ER in individual cotyledonary leaves (figure 4.3.2, A), large areas of leaf cotyledons at low magnification (figure 4.3.2, B) and roots (figure 4.3.2, C) were screened for YFP expression. None was detectable and hexyl-rhodamine B staining revealed an intact interconnected ER network within cells of a mix of tubules and cisternae (figure 4.3.2, A).

4.3.2 Confocal microscopy analysis of stable over-expression of full-length RTNLB3-YFP in seven day old *Arabidopsis thaliana* roots

Plants stably transformed with RTNLB3-YFP exhibited over-expression of the construct throughout all root cells (figure 4.3.3). Intensity of fluorescence varied between cells and the roots of some plants with very high levels of over-expression containing large aggregates of RTNLB3-YFP (figure 4.3.3, A & B). Except for these large concentrations of over-expression of the construct, RTNLB3-YFP over-expression appeared relatively consistent between root tip cells observed, with a similar pattern, but differences in the precise localisation of labelling (figure 4.3.3, C). These could correlate to different arrangements of labelled ER networks within the cells. The labelled membrane thought to be ER was present in the greatest concentration at the cell periphery and in some cells surrounding the nuclei, although not appearing to consistently label the nuclear envelope (figure 4.3.3, D). The detail of the structure of the networks within the root tip cells in the meristematic region was unable to be resolved using the confocal microscope, even with the highest magnification objective (figure 4.3.3, E).

4.3.3 Confocal microscopy analysis of stable over-expression of induced truncated RTNLB3-YFP in seven day old *Arabidopsis thaliana* roots

Over-expression of the truncated RTNLB3-YFP construct was observed throughout the root tips of highly over-expressing plants when viewed throughout by adjusting the plane of focus to scan through the root. At low magnification in a single plane of focus, fluorescence was not visible in all cells (figure 4.3.4, A & B). The ends of the root tips exhibited very high levels of concentrated YFP fluorescence throughout this region (figure 4.3.4, A).

When root tips were observed focused approximately mid-way longitudinally through the root in the meristematic region, truncated RTNLB3-YFP fluorescence was present throughout the cells at varying levels of intensity (figure 4.3.4 C, D, E & F). The greatest concentration of the construct in this region was present in the cells towards the end of the root tip (figure 4.3.4, C). Individual cells were identifiable in most root tips from a concentration of RTNLB3-YFP fluorescence outlining the regions of the cell peripheries resembling cortical ER (figure 4.3.4 C, E & F). At the end of some lateral roots, which that had grown from the parent root, the shape of individual cells was found to be irregular. Individual cells were difficult to differentiate based on truncated RTNLB3-YFP fluorescence (figure 4.3.4, D).

Fluorescence intensity varied greatly between some cells in the same root tip, with some exhibiting very low levels of truncated RTNLB3-YFP expression and other nearby cells a high concentration (figure 4.3.4, E & F). When meristematic cells were viewed focused close to the cell surface truncated RTNLB3-YFP labelling was present throughout this region. This corresponds to cortical ER labelling (figure 4.3.4, E & F). However, the structure of the labelling could not be resolved in detail in meristematic cells. Nuclear envelope labelling was also present (figure 4.3.4, E & F).

Cell further up the root in the elongation zone were also observed. The ER in these larger cells could be resolved, revealing interconnected networks of ER consisting of both tubular and cisternal structures, consistently labelled with truncated RTNLB3-YFP (figure 4.3.4, G & H). When the cisternal sheets were able to be resolved within a cell they appeared to have fenestrations visible within the cisternae (figure 4.3.4, G); these,

however, could not be imaged in further detail at higher resolution with the highest objective on the confocal microscope.

4.3.4 Localisation of full length & truncated RTNLB3-YFP in *Arabidopsis thaliana* leaf cotyledonary cells treated with Brefeldin A and stained with hexyl-rhodamine B

Arabidopsis cotyledonary leaves over-expressing either the full length or inducible truncated RTNLB3-YFP construct were treated with BFA to induce cisternal sheet formation in the ER and stained with hexyl-rhodamine B.

Following BFA treatment cisternae were successfully induced in RTNLB3-YFP over-expressing *Arabidopsis thaliana* plants (figure 4.3.5), which exhibit a highly tubular ER phenotype without treatment (figure 4.3.1). RTNLB3-YFP localisation to cisternal rims highlights these regions (figure 4.3.5, B).

Cisternal regions of ER exhibited high levels of hexyl-rhodamine B fluorescence (figure 4.3.5) with tubular ER appearing less prominent with a lower concentration of fluorescence. In comparison, RTNLB3-YFP brightly labelled a tubular network (figure 4.3.5, A). RTNLB3-YFP fluorescence appeared dominant on tubules in comparison to hexyl-rhodamine B staining (figure 4.3.5, A & B). Some aggregations of a high density of colocalised RTNLB3-YFP and hexyl-rhodamine B staining were present on thick ER strands (figure 4.3.5, A & B), which may correspond to bundles of ER tubules or transvacuolar stands. When merged, the fluorescence localisation highlights preferential staining of cisternae by the ER labelling stain. Although there was some RTNLB3-YFP labelling on large cisternae, labelled by hexyl-rhodamine B, RTNLB3-YFP did not colocalise fully with the staining across these structures (figure 4.3.5, A).

Leaves over-expressing induced truncated RTNLB3-YFP also exhibited large cisternae in the ER network following BFA treatment, in comparison to the ER phenotype of the construct previously observed in leaves (figure 4.3.1), which was primarily tubular. However, unlike full length RTNLB3-YFP labelling, which did not colocalise across cisternae throughout the ER network labelled by hexyl-rhodamine B staining (figure 4.3.5, A & B), the truncated construct was present throughout most ER sheets (figure

4.3.5, C & D). In some sheets truncated RTNLB3-YFP and hexyl-rhodamine B did not co-localise entirely, and the YFP labelling pattern showed regions that had the appearance of holes in the cisternae, despite these regions being labelled throughout by hexyl-rhodamine B staining (figure 4.3.5, D).

4.3.5 Staining for callose with analine blue hints at co-localisation of RTNLB3-YFP at plasmodesmata in *Arabidopsis thaliana* leaf epidermal cells.

Attempts to image the location of plasmodesmata using analine blue to stain callose yielded limited results when observed in a single focal plane.

Focusing on the cell periphery however, some punctate regions of high intensity RTNLB3-YFP localisation (figure 4.3.6, A) and callose staining (figure 4.3.6, B) were observed, with exact co-localisation of fluorescence at these points (figure 4.3.6, C).

Z-stacks of images from a series of focal planes were collected to attempt to resolve structures in greater detail. The RTNLB3-YFP localisation to the tubular ER of two adjacent cells could be seen. The ER appeared to connect with the cell perimeter in the two adjacent cells in opposing localities, with discontinuity of the network between the two cells. This region lacking in labelling, surrounded by the cortical ER of the two cells, is indicative of the locality of the cell wall (figure 4.3.6, D). High intensity puncta of analine blue labelling were also present (figure 4.3.6, E). When merged, two of these points of callose staining correspond to two opposing sides of the cell wall between two adjacent cells (figure 4.3.6, F).

Figure 4.3.1: Confocal micrographs of the expression phenotypes for stable over-expression of full length RTNLB3-YFP (A - D) and induced truncation 2 of RTNLB3-YFP (E & F) in seven day old *Arabidopsis thaliana* cotyledonary leaves.

A) Over-expression of RTNLB3-YFP is relatively consistent in fluorescence in the leaf cells of cotyledons, in highly expressing plants. High levels of expression are present in both stomatal and epidermal cells. With the level of focus close to the underside of the leaf, YFP expression highlights the perimeters of cells due to presence of expressing cortical ER (scale bar = 50 μm).

B) ER is consistently labelled with the RTNLB3-YFP construct present in the leaf cotyledons. Some thicker strands with high levels of YFP fluorescence are also present. These vary in number, size, and density of fluorescence between cells. In some cells these form large aggregates of fluorescence (scale bar = 20 μm).

C & D) RTNLB3-YFP labelling of ER appears as a consistent interconnected network throughout the cells. Nuclear envelope labelling is not present. The YFP labelled network is highly tubular in structure with few cisternal regions present. It is difficult to distinguish whether the thicker strands highly fluorescent with the YFP construct are continuous with the labelled ER network. These straight non-reticulate strands that traverse the length of the cell are not consistent with the structure of the rest of the ER network labelled (scale bars = 10 μm).

E & F) Leaf cotyledonary cells of plants with induced over-expression of truncated RTNLB3-YFP exhibit high levels of fluorescence. The construct labels an interconnected network of ER within the cells, with some aggregations of fluorescence distinct from this network and thick fluorescent strands within some cells (scale bars = 10 μm).

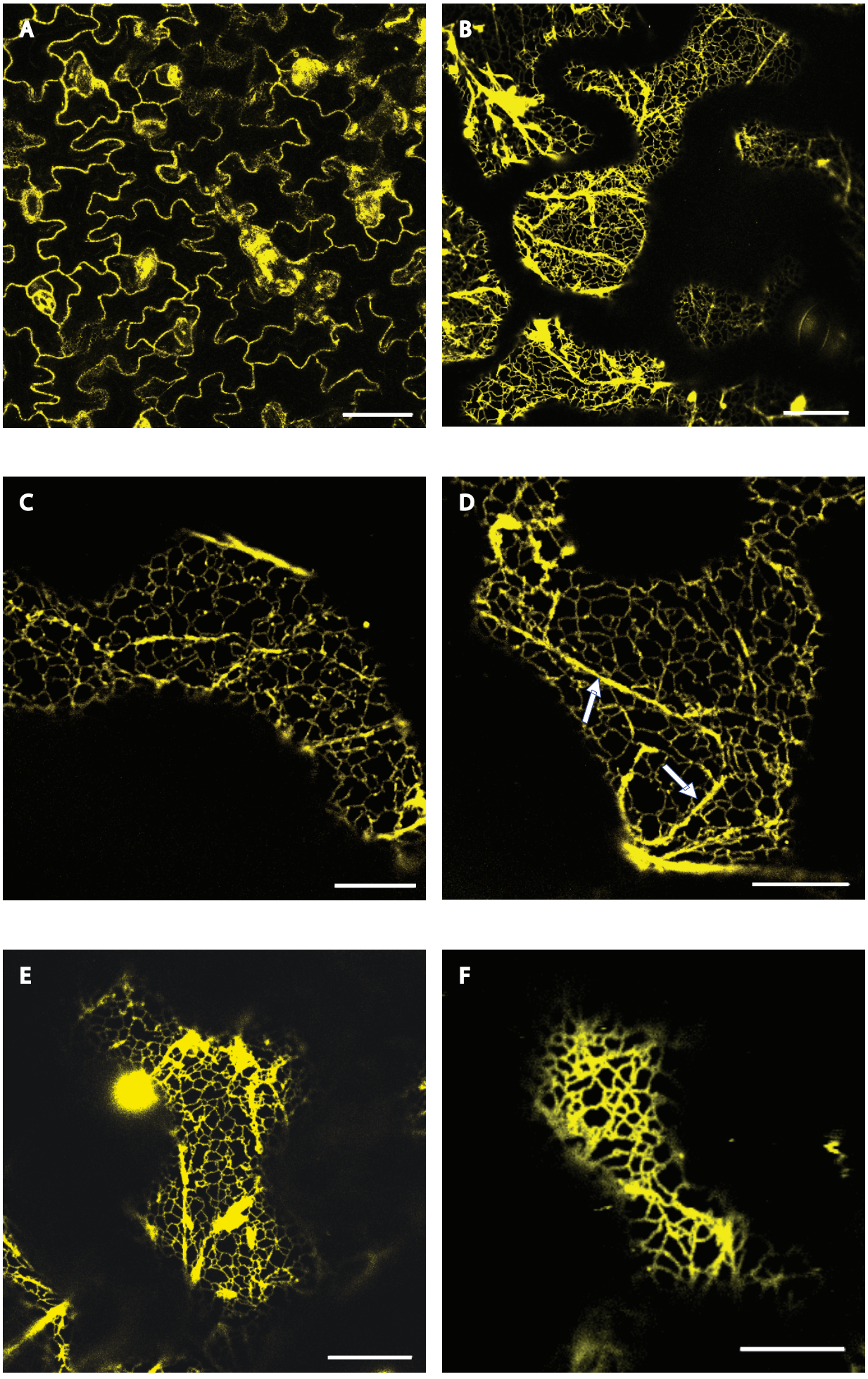


Figure 4.3.1

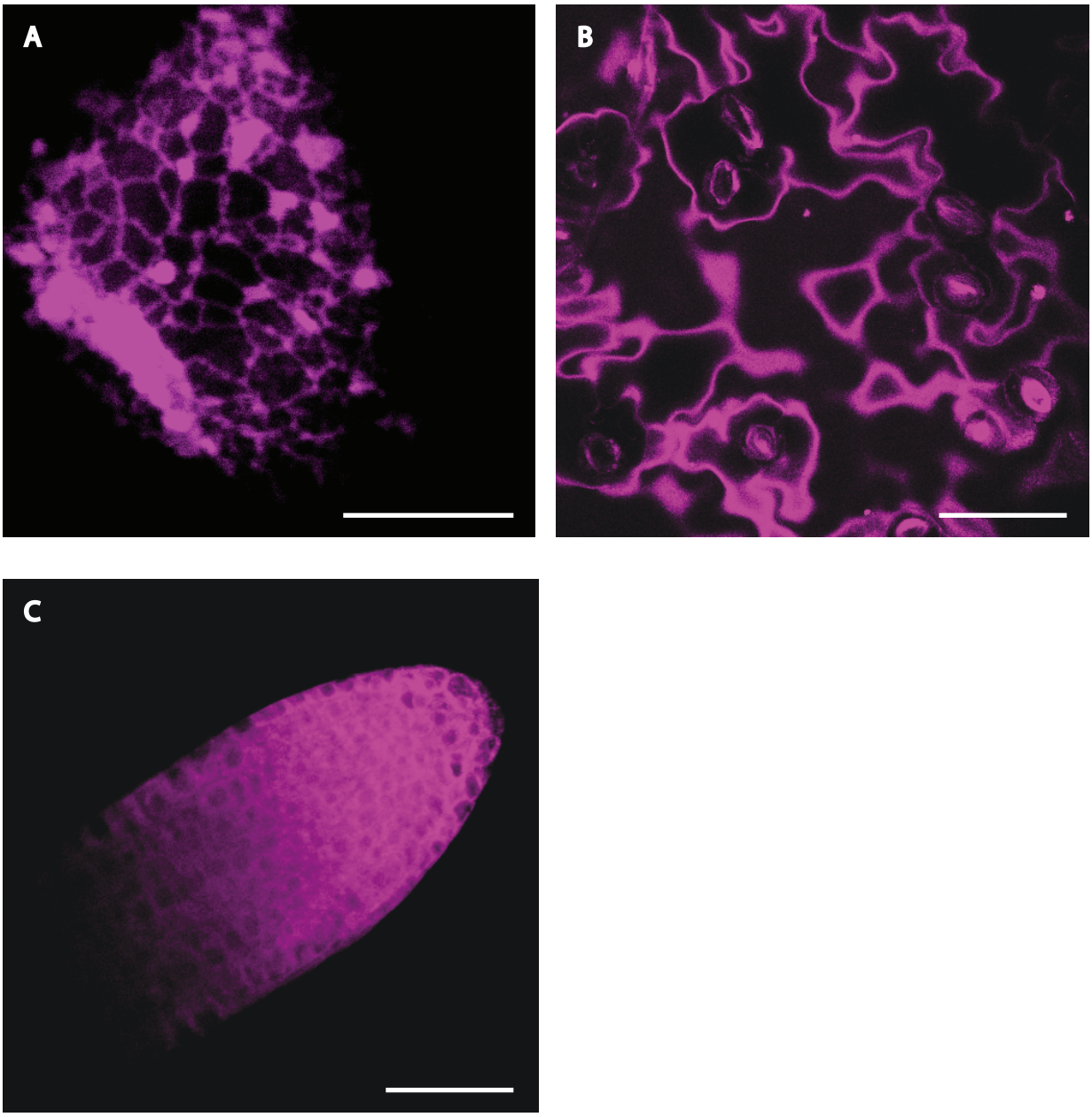


Figure 4.3.2: Confocal micrographs of seven day old *Arabidopsis thaliana* plants, stably transformed with an inducible truncated RTNLB3-YFP construct, following 20 hours incubation with DMSO and Silwett-77 solution in the absence of dexamethasone, stained with hexyl-rhodamine B.

A) Hexyl-rhodamine B staining of the ER within a leaf cotyledonary cell, highlighting an interconnected ER network of sheets and tubules. No RTNLB3-YFP expression is present within the cell (Scale bar - 20 μm).

B) Low magnification image of leaf cotyledonary cells, with the cell peripheries and stomata highlighted by hexyl-rhodamine B staining of the ER. No RTNLB3-YFP expression is present in any of the leaf cells (Scale bar - 20 μm).

C) Low magnification image of a root tip exhibiting hexyl-rhodamine B staining throughout. No RTNLB3-YFP expression is present within the root tip. (Scale bar - 50 μm).

Figure 4.3.3: Confocal micrographs of the phenotype for stable over-expression of full length RTNLB3-YFP in seven day old *Arabidopsis thaliana* root tips.

A & B) Expression of the fluorescent RTNLB3-YFP construct is visible throughout the root tips of highly over-expressing plants. There is apparent variation between individual cells fluorescence intensity, however this varies depending on the plane of focus used to take the image. When observed through different planes of focus through the roots over-expression appeared to be relatively consistent between the cells observed (scale bars – A: 50 μm, B: 20 μm).

C & D) RTNLB3-YFP fluorescence is visible at a relatively consistent level inside of root tips between cells. When cells are viewed towards the cell surface YFP labelling appears more concentrated in some regions of the cells than others (C). When cells are viewed at a plane of focus towards the middle of cells, some nuclei are highlighted by surrounding YFP labelling, in addition to the cell periphery. Aggregates of very high fluorescence intensity of YFP are also present in some root tip cells.

E) RTNLB3-YFP labelling appears to be present on a membrane network reminiscent of ER within the cells, however proved difficult to resolve in detail within the root tips (scale bars - 10 μm).

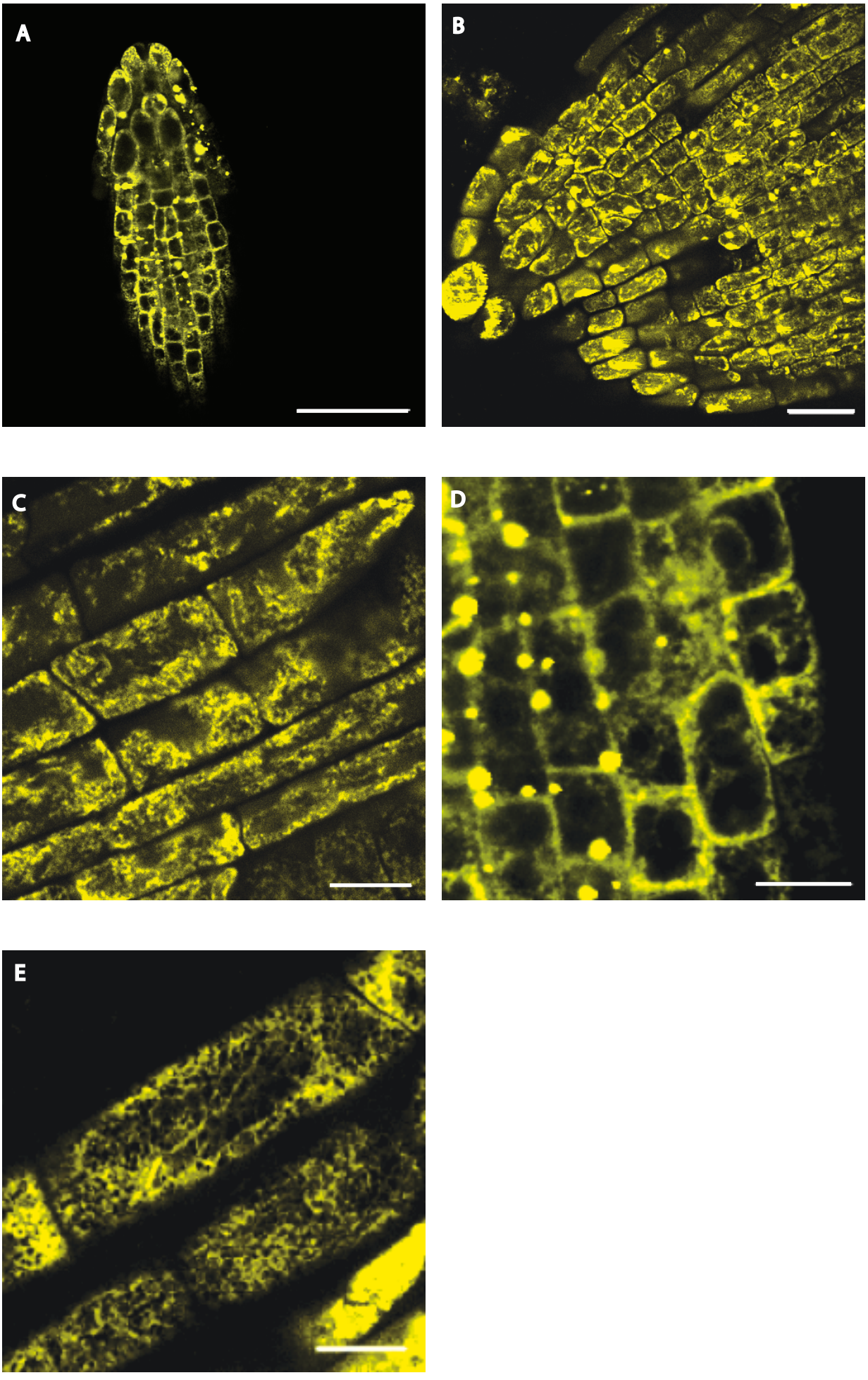


Figure 4.3.3

Figure 4.3.4: Confocal micrographs of the expression phenotype of induced truncated RTNLB3-YFP in seven day old *Arabidopsis thaliana* root tips.

A & B) At low magnification, viewing the entire root tip, expression of the truncated RTNLB3-YFP construct is visible throughout the root tips of highly over-expressing plants when observed throughout by adjusting the plane of focus to scan through the root. However, when imaging in a single plate of focus, fluorescence is not visible in all cells in images. The ends of the root tips exhibit very high levels of concentrated YFP fluorescence throughout the region (A). (Scale bars - 50 μm).

C) When expressing root tips are observed focused approximately mid-way longitudinally through the root, viewing the meristematic region, YFP fluorescence is present throughout the cells at varying levels of intensity. The greatest concentrations of truncated RTNLB3-YFP over-expression in this region are present in the cells towards the end of the root tip. Individual cells are identifiable from a concentration of RTNLB3-YFP fluorescence outlining the regions of the cell peripheries (scale bar - 20 μm).

D) At the end of some root tips the shape of individual cells is irregular and individual cells are difficult to differentiate based on truncated RTNLB3-YFP over-expression (scale bar - 10 μm).

E & F) Fluorescence intensity varies between cells in root tips, with some cells exhibiting very low to undetectable levels of truncated RTNLB3-YFP expression and other cells within the same root containing a high concentration. Cells focused close to the cell surface have fluorescent labelling throughout this region, which may correspond to cortical ER labelling, however the structure of this could not be resolved in detail in meristematic cells. Large round structures highlighted by YFP labelling within approximately the centre of cells were present, which correspond to the cell nuclei (scale bars - 20 μm).

G & H) Further up the root in the elongation zone, the ER in larger cells could be resolved, revealing interconnected networks of ER consistently labelled with truncated RTNLB3-YFP. The ER network structure labelled by the construct is a mix of tubular and cisternal forms. In some cells cisternal sheets appear to have fenestrations visible; however these could not be imaged in further detail at higher resolution (scale bars – G: 10 μm, H: 20 μm).

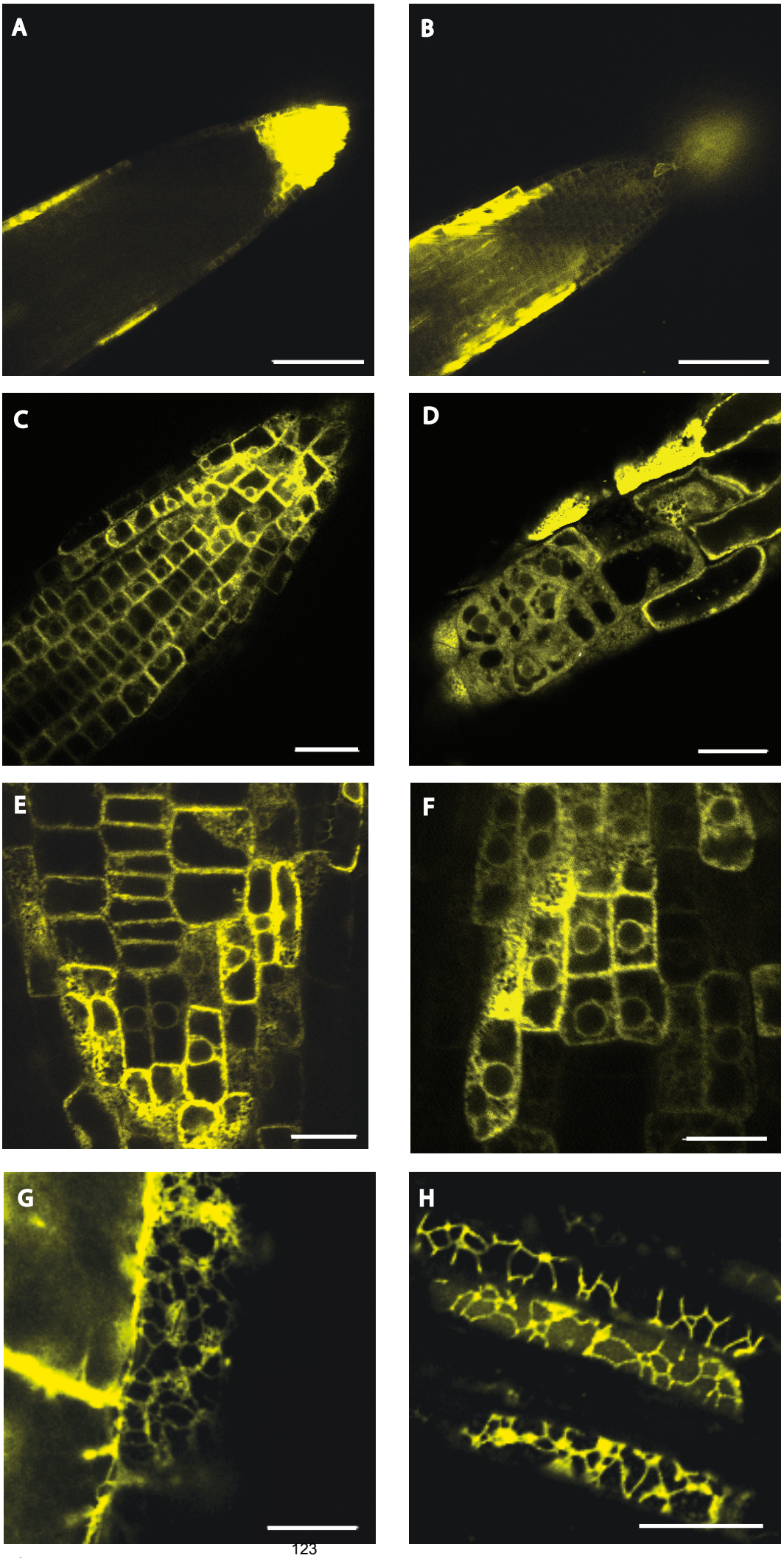


Figure 4.3.4

Figure 4.3.5: Confocal micrographs of seven day old *Arabidopsis thaliana* cotyledonary leaves over-expressing RTNLB3-YFP constructs, following Brefeldin A treatment and hexyl-rhodamine B staining.

A & B) Full length RTNLB3-YFP over-expression in leaf cotyledonary cells (green) in comparison to the ER network stained (magenta). High levels of RTNLB3-YFP labelling are present throughout the tubular ER network and cisternal rims, however is excluded from some cisternal regions labelled by hexyl-rhodamine B staining (scale bars - A: 20 μm, B: 10 μm).

C & D) Induced truncation of RTNLB3-YFP over-expression in leaf cotyledonary cells (green) in comparison to the ER network stained (magenta). High levels of truncated RTNLB3-YFP labelling are present throughout the ER network, colocalising (white in merged image) with labelling by hexyl-rhodamine B staining (scale bars - 10 μm).

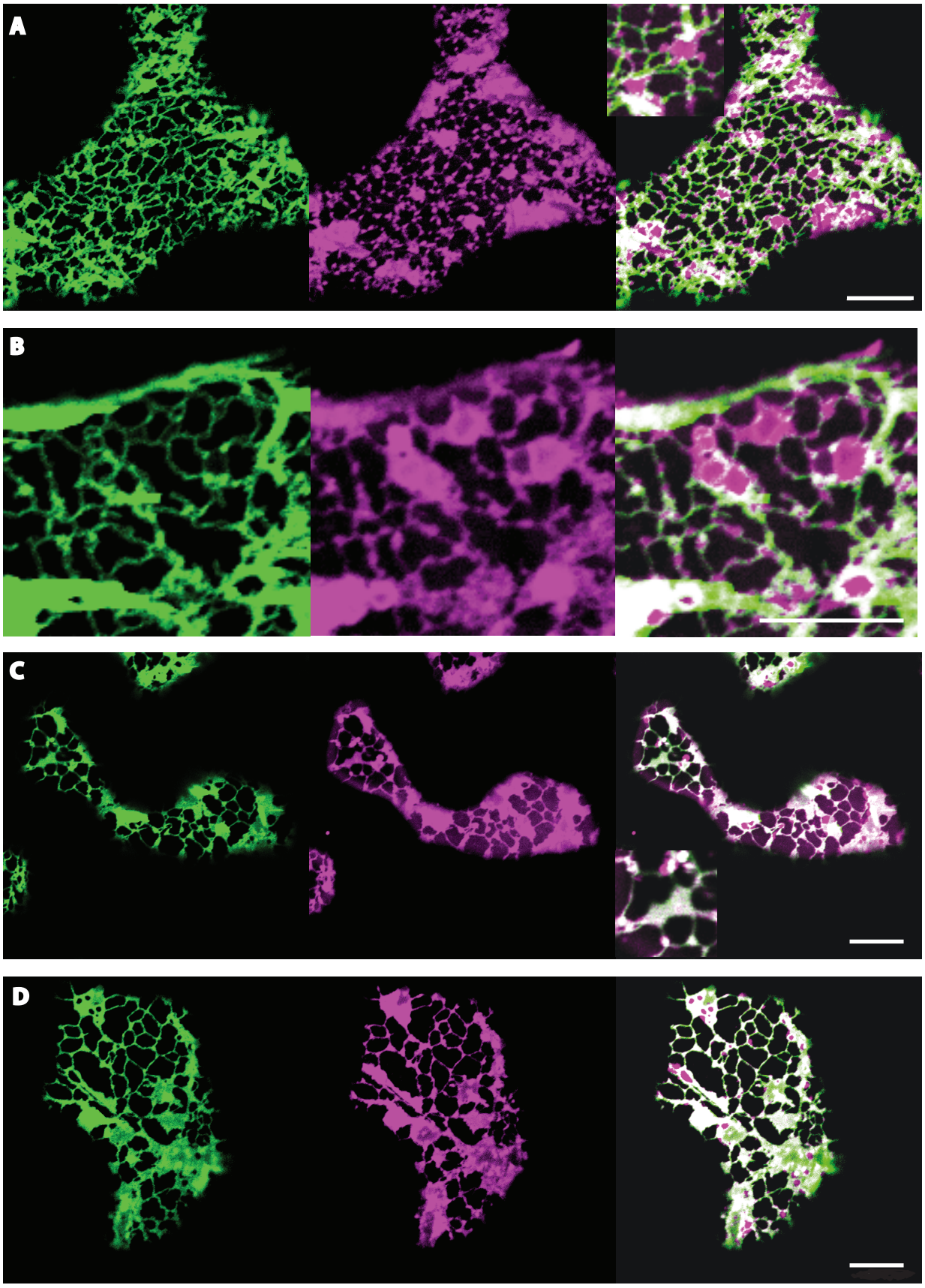


Figure 4.3.5

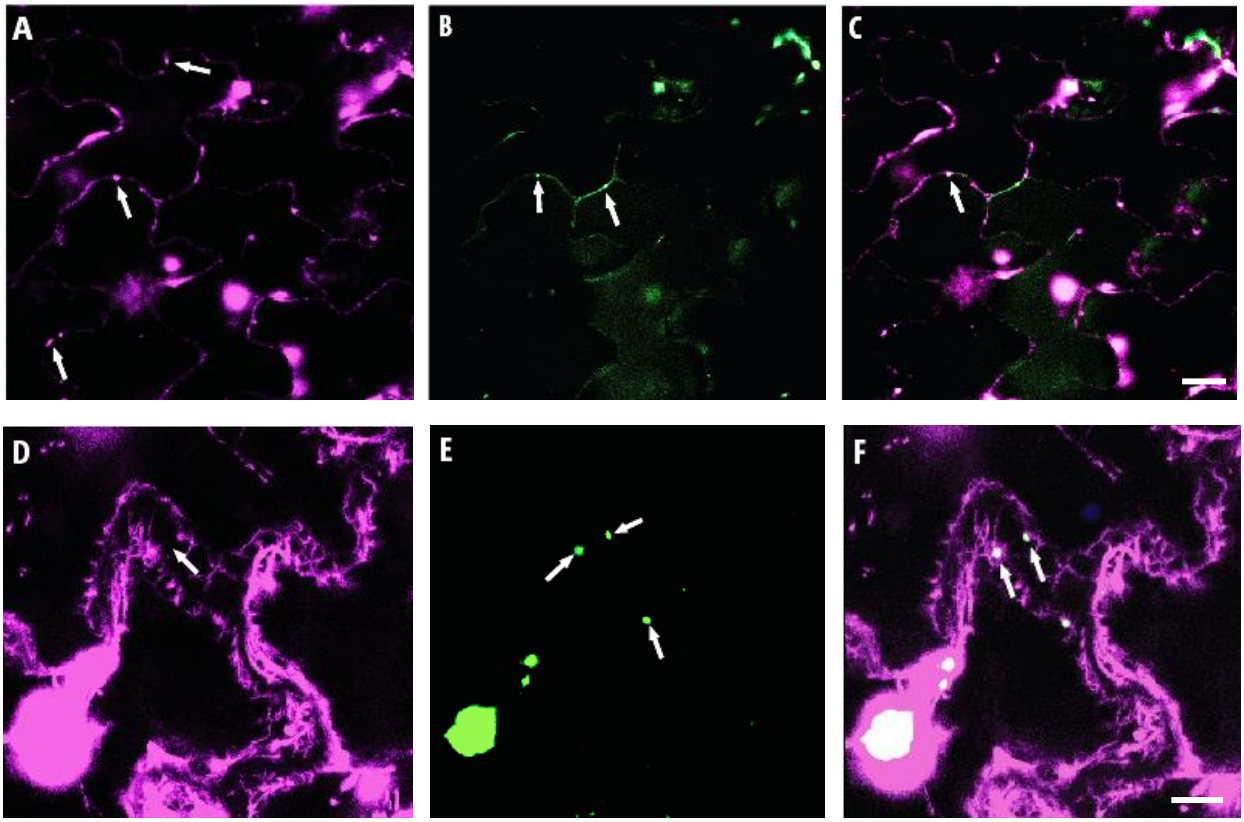


Figure 4.3.6: Analine blue staining of seven day old *Arabidopsis thaliana* plants stably over-expressing RTNLB3-YFP.

A) Over-expression of RTNLB3-YFP in the leaf cells of a cotyledon. Punctate regions along the cell periphery of high intensity RTNLB3-YFP expression are evident (arrows).

B) Analine blue staining in the leaf cells of a cotyledon. Punctate regions along the cell periphery of analine blue staining are evident (arrows).

C) Merged image of A & B. Punctate region of co-localisation of high RTNLB3-YFP fluorescence and analine blue staining along cell periphery between two adjacent cells (scale bar = 20 μm).

D) Image of a compiled Z-stack showing over-expression of RTNLB3-YFP in the leaf cells of a cotyledon. Gap between adjacent cells where cell wall is located shows a lack of RTNLB3-YFP expression present, where ER is discontinuous but present either side (arrow highlights a region such as this).

E) Image of a compiled Z-stack of analine blue staining in the leaf cells of a cotyledon. Punctate regions of analine blue staining are present (arrows).

F) Merged image of D & E. Punctate regions of analine blue staining and RTNLB3-YFP colocalisation. Two such points are located along the periphery of two adjacent cells, in opposing locations, with an inner region lacking continuous RTNLB3-YFP labelling indicating the presence of the cell wall in between (scale bar = 10 μm).

4.4. Discussion

4.4.1 Confocal microscopy analysis of stable over-expression of full-length and truncated RTNLB3-YFP in seven day old *Arabidopsis thaliana* leaf cotyledonary cells

The results of the floral dip with the RTNLB3-YFP construct, and subsequent screening, yielded multiple highly over-expressing lines that could be employed for further study. The ER phenotype of the over-expressed construct presented a highly tubular ER network consistent with the results shown by Sparkes *et al.* (2010) in transiently transformed *Nicotiana tabacum* leaves (utilising the same construct). This is the first study where the *Arabidopsis thaliana* RTNLB3 sequence, fused to a fluorescent protein, has been confirmed to exhibit this phenotype in the same species that the DNA sequence of the construct is derived from. Additionally, it is the first demonstration of this employing stable expression in a whole plant, grown from germination through developmental stages from seed to whole plants while over-expressing the RTNLB3-YFP construct. The stable over-expression phenotype for the construct in a BY-2 monoculture cell model was characterised in chapter 3. These results demonstrate that an artificially induced highly constricted ER network is not a lethal or developmentally disruptive factor for plant growth. No morphological abnormalities in comparison to wild-type plants grown alongside the stably expressing lines were observed.

Other observations from the initial analysis of the stably transformed plant lines are also consistent with previous research findings. Studies utilising other fluorescent protein constructs tagged to GFP have shown that strands that traverse the cell, such as those described in section 4.3.1, have identified these structures as transvacuolar strands (Brandizzi *et al.* 2003).

These consist of large strands of ER that move relatively rapidly in comparison to the reticulated network, which have been shown to traverse the central vacuole or be co-planar to the rest of the ER (Runions *et al*. 2006). These structures therefore, that the stably expressed RTNLB3-YFP construct also localises to, appear to be consistent with that expected of the over-expression distribution pattern of an ER localised fluorescent protein. However, this may be as a result of over-expression, with excess fluorescent

construct resulting in strand labelling, as the preferential localisation of RTNLB3-YFP to tubular regions of ER may contradict this.

In cotyledonary leaf cells full length RTNLB3-YFP did not label nuclear envelopes within the cells, which is in contrast to the phenotype observed in *Nicotiana tabacum* leaf cells for RTNLB3-YFP and other reticulon constructs when over-expressed by Sparkes *et al*. (2010). This is inconsistent with the finding that RTNLB3-YFP localises preferentially to ER membranes of high curvature, as the nuclear envelope is a low curvature ER domain (Voeltz & Prinz, 2007). Nuclear envelope labelling may occur despite preferential localisation of RTNLB3 to the ER because high levels of over-expression of the construct could result in saturation of the tubular ER with RTNLB3 and/or YFP. In this event, if the construct was to localise to another ER domain, as the nuclear envelope does exhibit some curvature in comparison to the surfaces of ER cisternae the construct may then localise to this region in the event of saturation of tubular ER and cisternal rims. Therefore the labelling observed by Sparkes *et al*. (2010) in infiltrated tobacco leaf cells may be due to higher levels of expression of the construct using their transient transformation method than occurs when the construct is stably expressed in *Arabidopsis thaliana* plants. How over-expression of the construct is tolerated within cells and the point of saturation of ER membranes may differ between plant species (such as the endogenous Arabidopsis gene over-expressed in this system), cell and tissue types.

Stable over-expression of truncated RTNLB3-YFP proved to be lethal in *Arabidopsis thaliana* plants and no stably expressing plant lines could be obtained in parallel to those over-expressing full length RTNLB3-YFP. This is consistent with the lethal phenotype found when attempts were made to stably over-express the construct in BY-2 cells (as detailed chapter 3). Reasons for lethality of over-expression of the construct in plant cells were hypothesised and discussed in section 3.4.3, which are also applicable to over-expression in *Arabidopsis thaliana* plants. The finding that the construct proved lethal to whole plants is not surprising, as the construct was not tolerated in a monoculture cell model, with cells failing to divide successfully to establish a culture. Therefore the lack of germination and growth of truncated RTNLB3-YFP over-expressing whole plants is consistent with the construct being severely disruptive to cellular processes, which may include cell plate and plasmodesmatal formation, ER function, and/or nuclear envelope structure and formation.

As discussed in section 4.3.1, a new truncated RTNLB3-YFP construct which includes an inducible promoter for expression was transformed by floral dipping into *Arabidopsis thaliana* plants. Stably transformed plants were obtained that exhibited no fluorescent construct expression prior to exposure to the inducing compound. Expression of the construct was successfully induced and observed at a high level with 20 hours of exposure to dexamethasone. The over-expression phenotype appeared primarily tubular in leaf cotyledonary cells. Similar highly fluorescently labelled strands were present as in full length RTNLB3-YFP over-expressing cells, which have been identified as transvacuolar stands and were discussed earlier in this section. Large aggregates of YFP fluorescence were present in some cells, which were also present in BY-2 cells over-expressing this construct (section 3.3.3). These may be an artefact due to high levels of over-expression of the fluorescent protein itself, similar to those identified in other studies utilising high levels of fluorescent construct expression (Ma *et al*. 2007 ; Latijnhouwers *et al*. 2007), or large bundles of ER membrane in which the structure of the network has been disrupted by over-expression of the truncated construct.

4.4.2 Confocal microscopy analysis of stable over-expression of full-length and inducible truncated RTNLB3-YFP in seven day old *Arabidopsis thaliana* roots

The root tips of plants stably over-expressing RTNLB3-YFP exhibited relatively consistent over-expression of the construct throughout root cells, labelling the ER network. However, the structure of the membrane labelling inside of the small meristematic cells within the root tips could not be resolved in detail using confocal microscopy. Therefore in addition to not being able to document the ER phenotype in detail in these cells, no further analysis of cell plates and ER in dividing cells in *A. thaliana* root tips expressing this construct could be undertaken using this imaging method.

Over-expression of the truncated RTNLB3-YFP was also present throughout the roots of plants in which expression had been induced, however there was substantial variation in expression levels between individual cells. Based on the method of plant transformation utilised (floral dip methodology discussed in section 4.1), all plant cells are expected to

contain the inducible construct. Therefore the variation may be attributed to an uneven diffusion of dexamethasone into the root tissues and cells from being applied externally to the plants, resulting in varying levels of induction. Despite this variation, the majority of cells exhibited over-expression of the construct at a medium to high-level. As with roots over-expressing the full length construct, the ER phenotype of labelling by the truncated construct in meristematic cells could not be resolved. Due to this no further ER or cell plate analysis could be carried out using this method.

The ER phenotype was observed in larger cells further up the root in the elongation zone of roots over-expressing the inducible truncation of RTNLB3-YFP, which showed a tubular and cisternal ER pattern. This confirmed the ER localisation of the truncated construct in root cells. The ER phenotype contained more cisternae than had been observed for over-expression of the construct for the same time period of induction in cotyledonary leaves. This may be due to the ER of root cells that is labelled by the fluorescent construct having a larger ratio of cisternae in this cell type, or due to over-expression of the construct promoting sheet formation (as has been observed in chapter 3 for truncated RTNLB3-YFP over-expressed in BY-2 cells, and the study by Sparkes *et al.* (2010)).

As noted in chapter 3 for the phenotypes observed in BY-2 cells, over-expression of the truncated RTNLB3 protein driven by the 35S promoter can result in sufficient levels in the ER to outcompete the other endogenous reticulon family members that perform a complimentary membrane curving function. Therefore, this could also account for the large cisternae present in some of the *A. thaliana* root cells observed here.

In some cells at high magnification the cisternal sheets had the appearance of being highly fenestrated; this, however, could not be resolved in fine detail for further image analysis using the confocal microscope. The nuclear envelopes within the cells appeared to be consistently brightly labelled with the construct. As the truncated construct does not localise preferentially to high curvature membranes, localisation to the nuclear envelope as a semi-curved ER domain is not unexpected, although this was not observed during the same period of induction of the construct in cotyledonary leaves. The concentration of truncated RTNLB3-YFP, in relation to the amount of ER membrane within the cell for the construct to distribute to, may be higher in root cells. This could result in a difference

in expression phenotype between cell types. A lower ratio of truncated RTNLB3-YFP to ER may localise preferentially to the tubular and cisternal ER network and only localise to the nuclear envelope when there is an abundance of the construct throughout these membranes.

Some lateral roots that had grown from the parent root of plants with induced over-expression were also observed. Unlike the parent root tips, the shape of cells appeared irregular and the cells were difficult to differentiate from each other based on YFP labelling. The maximum resolution obtainable of these cells with the microscope was not sufficient to investigate the ER in more detail. Based on viewing the cells at low magnification, the irregular structure could be due to over-expression of the construct disrupting cell plate formation and interfering with the development of new cell walls. It could also be a result of smaller lateral roots not being orientated completely flat for imaging under the coverslip and slide in between which the larger parent root is sandwiched. A different angle of the lateral root would alter the appearance of cells in a single plane of focus compared to the parent roots, as may imaging cells within a smaller amount of tissue. Finally, some cells further up in the elongation zone appeared slightly plasmolysed, which could be the result of damage when applying the cover slip to the fragile tissue or drying out during imaging.

Although some root cells showed irregularity in levels of fluorescent protein expression and some, primarily round, bright aggregates (such as in figure 4.3.3. A), this is not unexpected. Several studies employing fluorescent protein fusions have documented that very high levels of expression can result in large aggregates of the fluorescent construct in cells (Ma *et al*. 2007; Latijnhouwers *et al*. 2007). Therefore, this is a potential consequence of using a 35S as opposed to native promoter to induce over-expression. These kinds of large aggregates have been previously described as cytoplasmic in nature (Ma *et al*. 2007) and appear very distinct from any structures that could be identified as ER. Therefore if any samples used further in this study have such high levels of expression that this occurs, they are highly likely to be easily identifiable as artefacts caused by this, thus not interfering with the results or conclusions drawn from the use of these stably expressing lines.

4.4.3 Localisation of full length & truncated RTNLB3-YFP in *Arabidopsis thaliana* leaf cotyledonary cells treated with Brefeldin A and stained with Rhodamine hexyl B

The results described in section 4.3.4 confirm that RTNLB3-YFP preferentially localises to high curvature ER membranes in *Arabidopsis thaliana* seedlings, whereas the truncated RTNLB3-YFP construct distributes across the ER membrane network including cisternae. This is in agreement with conclusions drawn by Sparkes *et al.* (2010) from transiently transformed tobacco leaf epidermal cells co-expressing RTNLB3-YFP with GFP-CXN. The latter construct induces sheet formation when over-expressed, as well as acting as an ER membrane marker. Their study showed that in cisternal regions of the ER, the majority of full length RTNLB3-YFP labelling was preferentially localised to the rims of the cisternae, whereas the truncated constructs were no longer confined to these regions and were distributed over cisternal sheet surfaces. In their work, these phenotypes were also present for RTNLB1, RTNLB2 and RTNLB4 when over-expressed in combination with GFP-CXN. Their study also employed BFA to induce sheet formation; however they only conducted this experiment in conjunction with RTNLB13. The results for this protein produced a similar RTNLB enrichment pattern to those observed for full length RTNLB3 in this study.

The results from confocal microscopy analysis of the stable over-expression of the full length construct and induced over-expression of the truncation demonstrate a sufficient level of over-expression of the constructs for phenotypic analysis. The localisations observed with confocal microscopy analysis show that in this model system the full length protein but not the truncated form, specifically localise to high curvature ER membranes. This provides further evidence that these phenotypes are representative of the membrane curvature inducing properties of RTNLB3 in the cell. However, analysis of the ER in cells undergoing cell plate formation in root tips in the meristematic region where a high number of division events occur was not possible, due to a high enough level of resolution being unobtainable using confocal microscopy. Despite this, based on the analysis carried out thus far using this methodology, these plant lines provide an excellent model system to employ for the ultra-structural analysis discussed in section 3.4.7, to study the effects of RTNLB3 on ER structure and further investigate the suspected role of the protein in desmotubule formation.

4.4.4 Staining for callose with analine blue hints at co-localisation of RTNLB3-YFP at plasmodesmata in *Arabidopsis thaliana* leaf epidermal cells

Although results were limited from this experiment, due to limitation of the resolution that can be obtained using the confocal laser scanning microscope (Zeiss LSM 510 Meta) they did provide some further support toward the hypothesis that RTNLB3 localises to plasmodesmata and therefore may play a role in plasmodesmatal structure. The few points of co-localisation that were able to be resolved and focused accurately for a sufficient time for images to be recorded, showed exact co-localisation to regions that would be likely to be plasmodesmata, due to the high level of specific callose staining. The Z-stack presented in figure 4.3.6 shows the staining to be at the periphery on opposing points of a cell wall, either side to where callose deposition would be expected and a plasmodesmata is likely to be present (Zavaliev & Epel, 2015).

The ER labelling by the RTNLB3-YFP construct also corresponds with this, with the ER appearing to meet the plasma membrane at this point either side but not visibly traverse this region. With the maximum capacity of this equipment individual desmotubles cannot be resolved, therefore even if RTNLB3 were present throughout this structure any presence of the construct would be unlikely to be detected. If RTNLB3 is present throughout the desmotubule, it is also possible that due to the YFP tag the fluorescent protein fusion could be excluded from this region. This could occur due to other components of the structure resulting in a physical blockade of diffusion into this portion of the membrane, or due to the highly constricted shape of the membrane itself. The protein could feasibly also only be present at either side of a plasmodesmata, as some have been shown to be composed of tightly constricted desmotubule regions with a less constricted central cavity (Burch-Smith *et al.* 2011).

Following this part of the study being carried out, co-localisation of RTNLB3 and a plasmodesmatal marker, in this case a GFP tagged viral movement protein, have been shown to co-localise at similar points in transiently transformed *Nicotiana benthamiana* plants (Knox *et al*. 2015). Furthermore, the recent study by Knox *et al* employed a higher resolution light microscopy technique, three-dimensional structured illumination

microscopy (3D-SIM), to investigate these localities. Their observations were obtained using the BY-2 cell line as employed in parts of this study (chapter 3). Knox *et al.* (2015) plasmolysed BY-2 cells expressing RTNLB3-GFP and stained the cell wall using calcofluor (blue). The Hechtian strands of plasmolysed BY2 cells that traversed the cell wall showed consistent labelling with RTN3-GFP throughout the plasmodesmata. In addition to this, they resolved individual desmotubules, clearly labelled with RTNLB6-GFP, across the cell walls.

Chapter 5. Transmission electron microscopy analysis of ZIO stained *Arabidopsis thaliana* root tip cells

5.1 Introduction

The first transmission electron microscope was developed in 1931 by Ernst Ruska and Max Knoll, which possessed 400 X magnification (Chatterjee *et al.* 2012), followed by the first electron micrograph of a eukaryotic cell being published in 1945 by Keith Porter (Mielańczyk *et al.* 2015). TEM is an invaluable tool in modern biology for the visualisation of cell ultrastructure and has remained one of the primary methods employed for visualisation and analysis of biological samples at high resolution (Hughes *et al.* 2014). Conventional transmission electron microscopy generates two dimensional data of a relatively thin sample (50 – 250 nm) through which a beam of electrons is projected (Hughes *et al.* 2014). The high energy electrons, for which the wavelength decreases with increasing accelerating voltage, are diffracted by atomic planes inside of a material and can penetrate ultrathin solid samples. The beam is focused through electromagnetic fields in a vacuum, which act as lenses to focus the beam onto the sample (Chatterjee *et al.* 2012). The sample is then observed on a fluorescent screen or via a camera on a computer.

A mixture of sodium iodide and osmium textroxide was first introduced as a stain for biological samples by Champy in 1931 (Dağdeviren *et al.* 1994). The technique has since been adapted for use in TEM sample preparation as an osmium impregnation step during fixation, employing zinc iodide in place of sodium (Reinecke, 1981). Hawes *et al.* (1981) employed the technique to enhance the electron opacity of the endoplasmic reticulum and nuclear envelope in maize to investigate the structure and distribution of these membranes during mitosis, imaging thick sections with a high voltage electron microscope. The zinc iodide osmium impregnation (ZIO) technique stains the nuclear envelope, endoplasmic reticulum, Golgi bodies, plastid thylakoids, mature cell tonoplast and may stain mitochondrial membranes on occasion (Hall & Hawes, 1991). The mechanism by which ZIO impregnation results in staining of these membranes has not been thoroughly investigated; however reduction of the osmium during the fixation has been shown to

result in the deposition of the zinc osmate ($ZnOsO_4$). The regions where this occurs have been associated with high affinity $Ca2^+$ sites, where Ca^+ is replaced and/or displaced by Zn^+, due to its higher binding affinity for these sites (Gilloteaux & Naud, 1979).

In this chapter the ZIO technique was employed in the transmission electron microscopy preparation process for *Arabidopsis thaliana* root tips, with the aim of staining the ER membranes so that they exhibit high electron opacity to aid ultrastructural analysis of ER localisation and structure. Analysis of wild-type and RTLB3-YFP construct over-expressing plant cells where the ER can be clearly imaged, will facilitate further investigation into the role of RTNLB3-YFP in shaping the ER and the role the protein may play in cell plate and plasmodesmata formation.

Since the techniques inception, three dimensional imaging in electron microscopy has relied upon serial-section TEM and electron tomography for data collection (Linberg & Fisher, 1986; Mishchenko, 2009; Bock *et al.* 2011; Takemura *et al.* 2013). The earliest method used to obtain 3D data using an electron microscope was serial section TEM (ssTEM), introduced in the late 1950's (Bang & Bang, 1957). This was followed by the imaging of relatively thick sections of 1-5 µm using high and medium voltage TEM's combined with stereoscopic imaging and computation methods in the early 1970's (Favard & Carasso, 1973). Studies first describing the theory and demonstrating basic application of electron tomography were published in 1968, however due to the computing power required to reconstruct the data not being readily available until several decades later, it wasn't until the 1990's that electron tomography began to be widely implemented as a tool for researching cell ultrastructure (Weyland & Midgley, 2004).

The word *tomography* means the representation of slices or sections, and is used to describe the 3D representation of a sample achieved through tilting the specimen to multiple angles (Joachim, 2006). Electron tomography involves the imaging of thick (up to 500 nm) sections of resin embedded samples at a range of angles using a high-voltage TEM and digital image collection. From this three-dimensional data can be reconstructed from the tilt series data set (McEwen & Marko, 2001). Although use of the term is now broader, specifically the word refers to data sets obtained from single-axis tilt geometry, such as when a sample in the electron microscope is tilted around a single axis and the beam direction is fixed (Joachim, 2006). TEM tomography has the potential to be able to achieve a high enough resolution to allow for imaging and modelling of detail as small as

the structure of plasmodesmata (Nicolas *et al*. 2017). Therefore, in this study single-axis TEM tomography of ZIO impregnated samples of *Arabidopsis thaliana* root tips was employed to analyse the relationship between the ER and developing cell plate, and sites of plasmodesmatal formation, in three-dimensions.

5.2 Materials & methods

Generation of stable *Arabidopsis thaliana* lines, growth of plants, fixation and preparation of samples for TEM imaging and tomography are detailed in Chapter 2.

The methodology for the induction of the truncated RTNLB3-YFP construct in *Arabidopsis thaliana* plants is detailed in Chapter 4, section 4.2.4.

5.2.1 Transmission electron microscopy and tomographic imaging

All samples were imaged at 120 KV using a Hitachi A-7650 tomographic transmission EM (Hitachi, UK), after allowing the section a few minutes to stabilise in the beam. Images were recorded using an AMT 2k62k CCD camera (Advanced Microscopy Technologies, UK).

For tomography all samples were imaged at 100 KV after allowing the section a few minutes to stabilise in the beam. Tilt series of 200 nm sections were collected between −60° and +60° at 2° intervals. Images were recorded using an AMT 2k62k CCD camera (Advanced Microscopy Technologies, UK).

5.2.2 Processing of tomographic datasets

Each tilt series dataset was converted from tif files to mrc files using the Cygwin command line interface for Microsoft Windows. Files were then aligned using the standard gold-bead tracking of 10 fiducials and reconstructed to generate 3D tomograms using eTomo (IMOD, USA). Noise in the tomograms was reduced by filtering using the median function of the clip IMOD program. Segmentation and image processing were conducted using Amira (version 6.0.1) (Visualisation Sciences Group, Germany).

5.3 Results

5.3.1 80nm thin section electron microscopy of ZIO stained *Arabidopsis thaliana* root tip cells

Thin section samples of ZIO impregnated wild-type *Arabidopsis* root tip cells and those over-expressing truncation 2 of RTNLB3-YFP were analysed using transmission electron microscopy. All cells observed were within the meristematic regions of the root tips. Control root tips of stably transformed plants containing the inducible truncated RTNLB3-YFP construct were also prepared and analysed, which would be expected to exhibit a wild-type phenotype. The plants were also treated with the components of the induction solution, consisting of DW water, DMSO and Silwet® in the absence of dexamethasone. This was to check that the other components of solution used to induce the over-expression of the construct did not have an impact on cell morphology in isolation. RTNLB3-YFP over-expressing root tips were also successfully prepared for electron microscopy, however these samples were not analysed in detail and results collected for comparison in this section, the reasons for which will be discussed in section 5.4.1. These samples were utilised for SBFSEM data collection and analysis, for which the results are presented in chapter 6.

Electron micrographs of wild-type root tip cells are shown in figures 5.3.1 & 5.3.2. The staining imparted the highest level of contrast to ER membranes and nuclear envelopes, with the cell walls and vacuoles devoid of staining. Nuclei were located in the central region of each cell, which were stained to the same high degree as ER membranes in the cell cytoplasm (figure 5.3.1, A & B). At sites where ER extended out from the nuclear envelope no significant difference in staining of the different ER domains could be seen by eye. Cell walls were easily distinguishable as low electron opacity boundaries compartmentalising each cell with a mostly linear shape, in a grid like network throughout the root tip (figure 5.3.1, A & B). ER in both tubular and cisternal forms was present within the cells, with ER in direct association with the cell walls appearing primarily tubular (figure 5.3.1, C, D, E & F). Cross sections of cisternae, however, may appear as tubules in thin section electron micrographs. ER with the morphology present within the cells does not penetrate into the cell walls, therefore appearing as an accumulation of ER membrane on either side of a barrier of cell wall material (figure 5.3.1, C, D, E & F).

Electron micrographs of cells from control root tips, of plants stably transformed with the inducible construct of truncation 2, are shown in figure 5.3.1 G & H. Analysis of the root tip cells resulted in no observable distinct difference in cellular, tissue or ER morphology to the wild-type *Arabidopsis* root tip cells analysed (figures 5.3.1 A - F and 5.3.2). The level of contrast of staining did differ from the wild-type samples in appearance, however, similar to the wild-type samples, the ER and nuclear envelopes exhibited the highest degree of contrast within the cells as a result of the ZIO impregnation. The ER membranes and nuclear envelopes were clearly distinguishable from other organelles within the cells, with the cell walls also being clearly defined due to the lack of staining present. ER was present in tubular and cisternal forms, with some cisternae identifiable as sheets of membrane. The relationship between the ER and cell walls was consistent with that observed in wild-type root tips. ER incorporated into the cell walls did not maintain the same structure as cytoplasmic ER (figure 5.3.1, H), with some sites identifiable as plasmodesmata where the ER traverses the cell wall and faint staining is present across this region.

At higher magnification sites where ER is present on opposing sides of a cell wall, and traverses this region at plasmodesmata, could be identified (Figure 5.3.2, A – D). At these sites, faint lines of ZIO staining, narrower than the ER not incorporated into the cell wall, can be seen to connect the ER membrane on opposing sides across the cell wall (Figure 5.3.2, A – D). The appearance of the point at which the ER contacts the cell wall varies, from a blunt discontinuation of the highly contrasted ER membrane at the cell wall (Figure 5.3.2, C), to a structurally distinct transition zone. At some of these sites the highly osmicated ER membrane appears to pinch off into a point at the interface of where the membrane is incorporated into the cell wall, just before the interior of wall where no highly electron opaque material is visible (Figure 5.3.2, D).

Thin section micrographs of root tip cells over-expressing induced truncated RTNLB3-YFP are shown in figure 5.3.3. As with wild-type cells and the control, the level of contrast resulting from the preparation varied from the other samples, however the proportional staining with regards to the degree of electron opacity imparted to the organelles was consistent. Again, nuclear envelopes and the ER exhibited the highest degree of staining within the cell, and the cell walls and vacuoles the least, rendering the organelles clearly identifiable (figure 5.3.3, A & B). Most of the cross walls were present in a grid like formation throughout the root tip, with a linear structure (figure 5.3.3, A),

but some cell walls with varying curved morphologies were also observed (figure 5.3.3, B). Some root cells contained large dense aggregates of osmium staining, which were distinct in structure from other cellular morphologies (figure 5.3.3, C). Some cell walls also contained small concentrations of ZIO staining within them (figure 5.3.3, D), which weren't present at such a high electron opacity in aggregates in the cell walls of wild-type cells. Similar observations were made regarding the association of the ER and the cell wall within wild-type and control plant cells. ER in close association with the cell wall in neighbouring cells at opposing points appeared continuous, observable as distinct but faint staining within the cell wall material, and not consistent with the cytoplasmic ER in structure and electron opacity (figure 5.3.3, E & F).

5.3.2 200 nm thick section electron microscopy of ZIO stained *Arabidopsis thaliana* root tip cells

The same set of samples as for thin section TEM (section 5.3.1), from the same preparation for control, wild-type and truncated RTNLB3-YFP over-expressing plant roots, were also cut and observed as thick sections prior to tomography. Observations for the result of the ZIO impregnation of organelles were consistent from those observed in section 5.3.1 in thin section.

Figures 5.3.4, 5.3.5 and 5.3.6 show electron micrographs of wild-type root tip cell samples. At low magnification tissue architecture resembled that observed for wild-type root tips as thin sections (figures 5.3.1 A - F and 5.3.2). Nuclei were located within the central region of the cells and not directly associated with the cell walls (figure 5.3.4, A, B & C). ER and cell walls remained distinctly identifiable in thick sections, due to their high and low levels of electron opacity, respectively. Where cells were sectioned in thick section with the cross walls perpendicular to the plane of the section (figure 5.3.5), results were also similar to those documented for wild-type thin section samples (figures 5.3.1 A - F and 5.3.2). Sites where the ER crosses the cell wall, connecting ER in adjacent cells exhibited some membrane continuity present as faint staining distinct from the rest of the ER (figure 5.3.5, A & B). Due to the larger amount of material within each section more ER membrane was observable around the cross walls, with a greater quantity identifiable as cisternal ER (figure 5.3.5, C & D). At some sites ER membrane appeared increasingly compressed the further into the cell wall it was incorporated, and remained consistent as a

fine line of ZIO staining to the opposing side (figure 5.3.5, E). An unusual cross wall phenotype was also observed at this orientation with ER of consistent cytoplasmic morphology and staining crossing the cell wall from one cell to the one adjacent (figure 5.3.5, F).

Cross walls that appeared thicker than those shown in figure 5.3.5 were also observed. As in figure 5.3.5 F, ER is present throughout these cell walls and retains the morphology of cytoplasmic ER (figure 5.3.6, A – D). Based on the shape of the cells in relation to those surrounding them within the tissue, these cross walls appear to be orientated in the section at an angle that may not be perpendicular to the longitudinal plane of the cell wall (figure 5.3.6, A). Both tubular (figure 5.3.6, B) and cisternal (figure 5.3.6, C) morphologies of ER were observed within regions of cell wall material (figure 5.3.6, D). Despite this, not all ER that was associated with either side of such cross walls remained consistent throughout, with some not visible across these regions (figure 5.3.6, E) or only appearing to persist in morphology partially into the cell wall material but not continuously throughout (figure 5.3.6, F).

Thick section samples of control root tips yielded similar results and observations as those obtained for wild-type root tips. Figure 5.3.7 A - E show electron micrographs of the roots of plants stably transformed with the truncated RTNLB3-YFP construct and incubated in the control induction solution without dexamethasone to induce over-expression.

Electron micrographs of thick section samples of induced truncated RTNLB3-YFP over-expressing root tips are shown in figures 5.3.8, 5.3.9 and 5.3.10. Most cells in the root tips observed were compartmentalised by complete cell walls with a linear morphology (figure 5.3.8, A), containing highly electron opaque ER and nuclear envelopes (figure 5.3.8, B). The structure and amount of ER traversing cell walls varied between individual cross walls (figure 5.3.8, B). Some cross walls were devoid of ER membrane staining within the cell wall material except for faint contrast (figure 5.3.8, C & E), whereas others had large amounts of ER that was structurally consistent with intracellular ER spanning these regions (figure 5.3.8, D). Some cross walls had large cisternae in direct association with the cell wall but which remained isolated to the cell interior (figure 5.3.8, E).

The localisation of nuclei within the cells and their association with the cell wall also varied (figure 5.3.9). In the majority of cells the nuclei were in the central region of the

cell, with no direct association with the cell wall (figure 5.3.9, A). However, in some cells nuclear envelopes were found to be located very close to or in direct association with the cell wall, with nuclear envelope and/or ER membranes incorporated into the cell wall material (figure 5.3.9, B, C, D & E). This phenotype was not observed in the cells of wild-type or control root tips. Unusual cell wall formations not present in wild-type or control root tips were also present in samples over-expressing the truncated RTNLB3-YFP construct (figure 5.3.10). Although most of the root tip consisted of cells surrounded by fully formed cell walls, which formed a grid like network of cross walls compartmentalising the cells, some cells lacked clearly defined boundaries separating the cell cytoplasm and contents (figure 5.3.10, A & B). In regions where cell walls appeared poorly defined or missing, many large cisternal sheets of ER were also present with tubular ER and/or cross sectional cisternae (figure 5.3.10, C). In samples of cells within the root tissue of wild-type and control samples, and the majority of the cells samples over-expressing truncated RTNLB3-YFP, cross walls were present between neighbouring cells in an interconnected, lattice like matrix. In some cells lacking a complete cell wall, fully formed nuclei were present within the section and no observable cell plate was present (figure 5.3.10, D). This indicates that the cells are in interphase, as opposed to undergoing division. Additionally, some extensions of dense cell wall material were observed extending from neighbouring cell walls, which appeared to dissipate into the cell cytoplasm (figure 5.3.10, D). As cell plate formation in wild-type cells progresses centrifugally outwards from the cell interior, this also suggests that these cell wall formations cannot be attributed to normal, incomplete cell plate formation.

5.3.3 Transmission electron tomography of ZIO stained *Arabidopsis thaliana* root tip cells

Tomographic data sets were collected, reconstructed and modelled of developing cell plates in Arabidopsis root tip meristems. Figure 5.3.11, A, shows a transmission electron micrograph image of a 200 nm thick section, taken at 0° tilt, of a cell plate undergoing formation. Detail of developing plasmodesmata at sites where the ER is incorporated into the cell plate material is not discernible, with the cell plate appearing as a solid mass of low contrast. A dense accumulation of ER is present either side of the developing cell wall, the structure of which is unclear in two dimensions.

An image taken from the reconstructed tomographic dataset of the tilt series obtained from the section (figure 5.3.11, A) presents more detail within this region (figure 5.3.11, B). For clarity of the surrounding ER structure, only the high density cell plate material is included in the modelled reconstruction. Figure 5.3.11, C, shows a site where the ER can be seen continuous across the cell plate, where it is becoming incorporated into the developing cell wall, presumably forming the desmotubule of a plasmodesmata. The structure of the ER is revealed to consist of both cisternal and tubular forms (Figure 5.3.11 D & E). The size of the cisternae and further structure of the surrounding network cannot be determined from the relatively small 200 nm thickness of the sample. The ultrastructure of desmotubules, seen in mature regions of the cell plate (such as shown in figure 5.3.11, C) proved too fine to be modelled and displayed accurately in these images. ER that is yet to be constricted into these structures is evident in areas where the cell wall material is yet to fuse.

Figure 5.3.12, A, shows a transmission electron micrograph taken at 0° tilt from a tomographic dataset of another developing cell plate within a cell over-expressing RTNLB3-YFP. The phenotype of the ER and cell plate material is similar to that described for the WT samples shown in figure 5.3.11. Figure 5.3.12 B & C show the cell plate and ER reconstruction. Although less ER membrane is present in the surrounding region than that observed for the wild-type sample, ER surrounds the cell plate material and traverses regions where it is yet to be constricted into desmotubules.

Figure 5.3.1: Transmission electron micrographs of 80 nm sections of ZIO stained wild-type and control (treated with DMSO and Silwett-77™) *Arabidopsis thaliana* root tip cells at low magnification.

A & B) Low magnification images showing wild-type cells separated by linear cross walls, containing highly contrasted ER (arrows), with nuclei in the centre of cells (stars) surrounded by nuclear envelopes exhibiting similar levels of staining as ER membranes (scale bars - 2 μm).

C, D, E & F) Tubular and cisternal ER is prominent in wild-type cells, with cross walls identifiable between cells as linear boundaries lacking staining. ER is present up to the edges of cross walls but does not appear continuous as the same structure and staining across these regions. Arrows show examples of ER surrounding cross walls (scale bars - 500 nm).

G) Overview of several control cells, separated by linear cross walls. The ER and nuclear envelopes exhibit the highest degree of contrast (arrows, scale bar - 500 nm).

H) Where ER is present on either side of the cross wall in control cells, at some points faint contrast is present continuously across the cell wall between two opposing sites of highly contrasted ER membrane either side (arrow, scale bar - 500 nm).

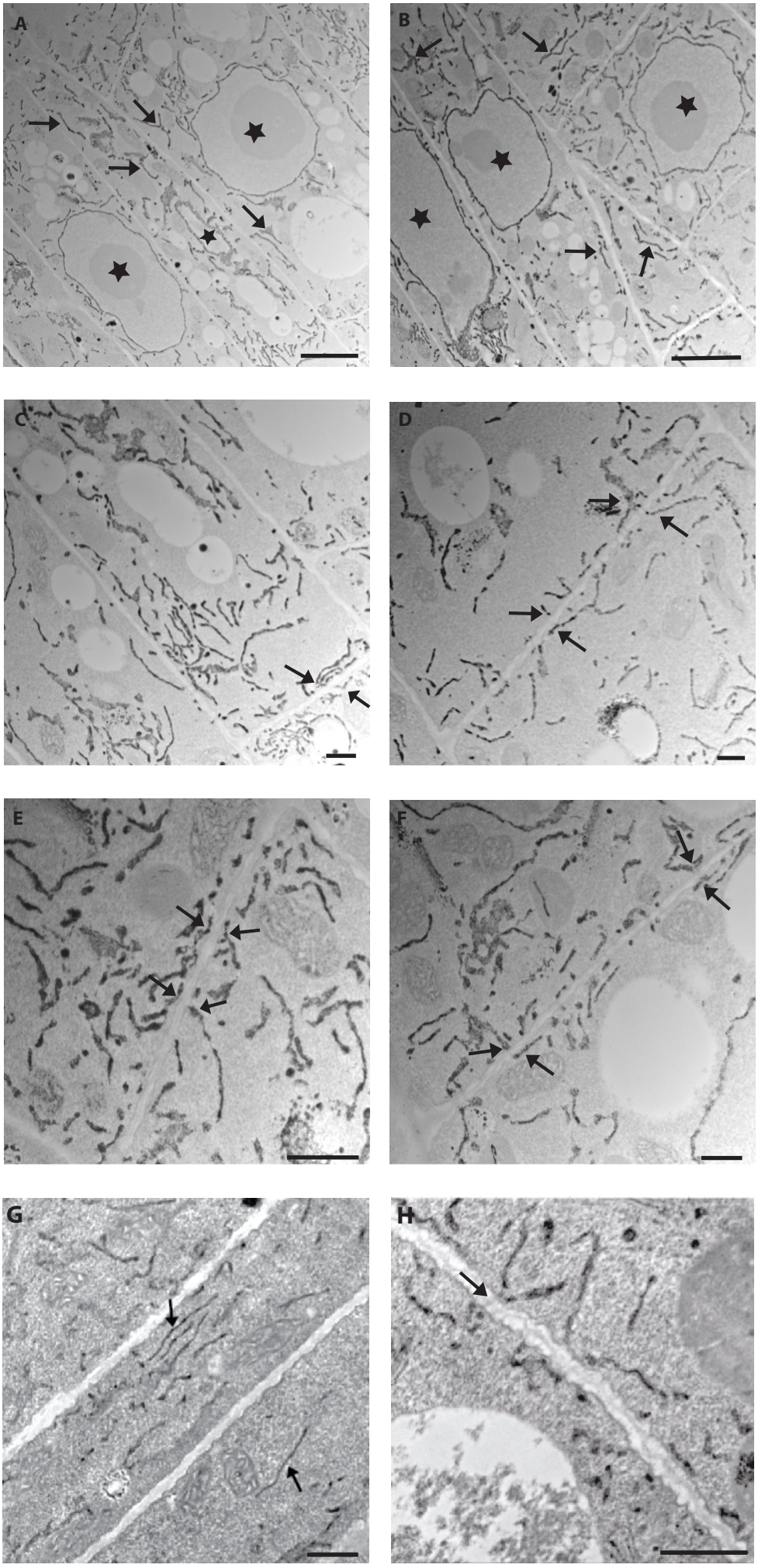


Figure 5.3.1

Figure 5.3.2: Transmission electron micrographs of 80 nm sections of ZIO stained wild-type *Arabidopsis thaliana* root tip cells showing cross walls and ER at high magnification.

A) ER is present either side of the cross wall at opposing points in some localisations along the length of the cross wall (arrows show examples of ER at such sites, scale bar - 500 nm).

B) At some sites where ER is present on opposing sides of the cross wall there is some contrast present across the cell wall material (arrows show examples of ER at such sites, scale bar - 500 nm).

C) Highly electron opaque ER in contact with a cell wall. The ER membrane does not continue across the cell wall material at the same size and density of staining (arrow, scale bar - 100 nm).

D) In some locations where ER meets the cross wall, the highly electron opaque ER membrane appears to narrow prior to this point (scale bar - 100 nm).

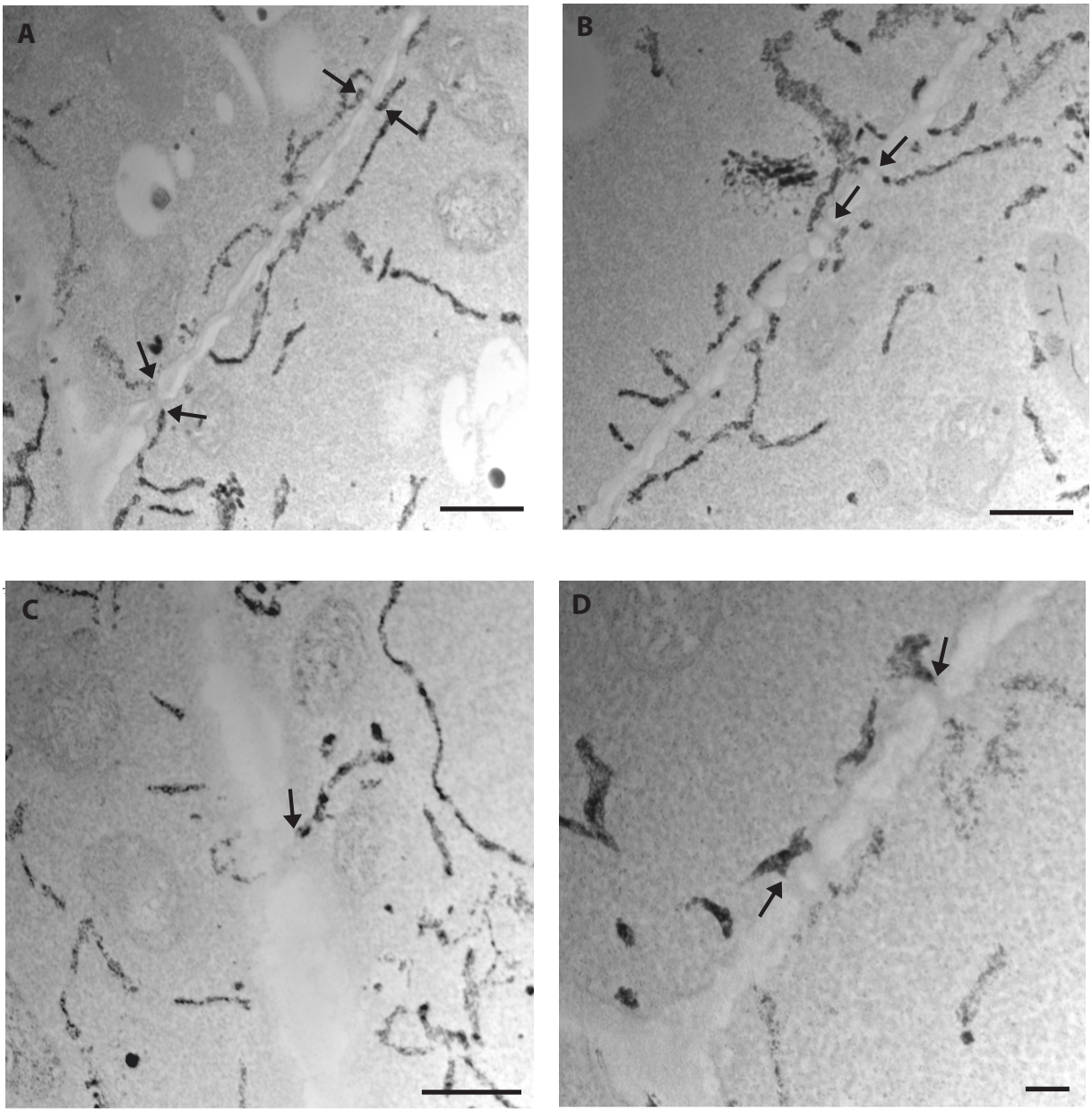


Figure 5.3.2

Figure 5.3.3: Transmission electron micrographs of 80 nm sections of ZIO stained *Arabidopsis thaliana* root tip cells of plants following 20 hours induction of truncation 2 of RTNLB3-YFP over-expression.

A & B) Low magnification images showing cells compartmentalised by mostly linear cross walls containing highly contrasted ER, with nuclei in the centre of cells (stars) surrounded by nuclear envelopes exhibiting similar levels of staining as ER membranes. Highly electron opaque deposits of ZIO are present inside of some cells, which appear as black aggregates. A cross wall with less uniform structure is also present (arrow, scale bars - 2 μm).

C) A cross wall surrounded by ER membrane with some highly concentrated deposits of ZIO also present within the cells (arrows, scale bar - 500 nm).

D) A cross wall surrounded by highly stained ER with some sites of heavy ZIO staining also present within the cell wall material (arrows, scale bar - 500 nm).

E & F) In some regions where ER is present on opposing sides of the cross wall there is faint staining connecting the membranes across the cell wall material (arrows, scale bar - 500 nm).

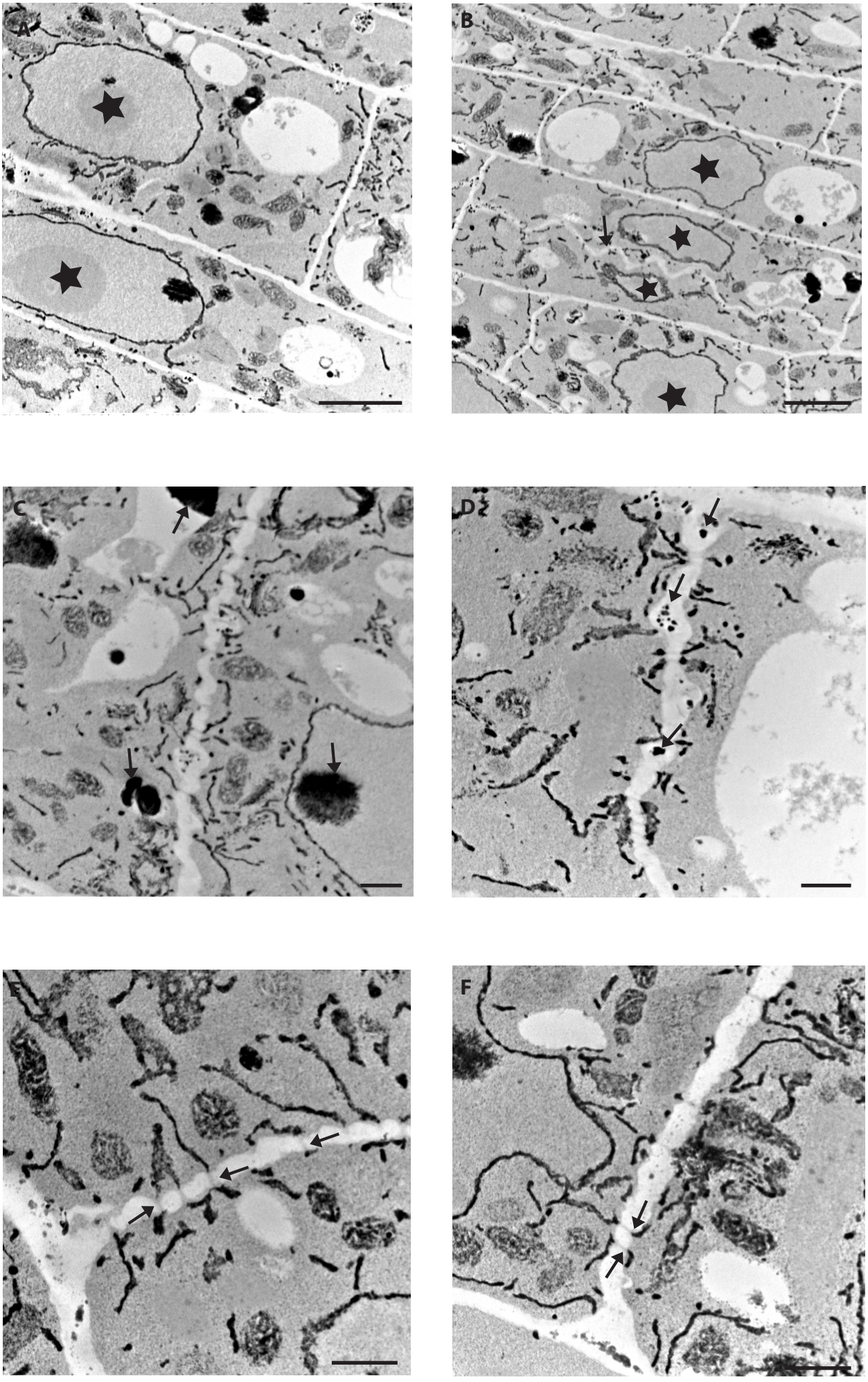


Figure 5.3.3

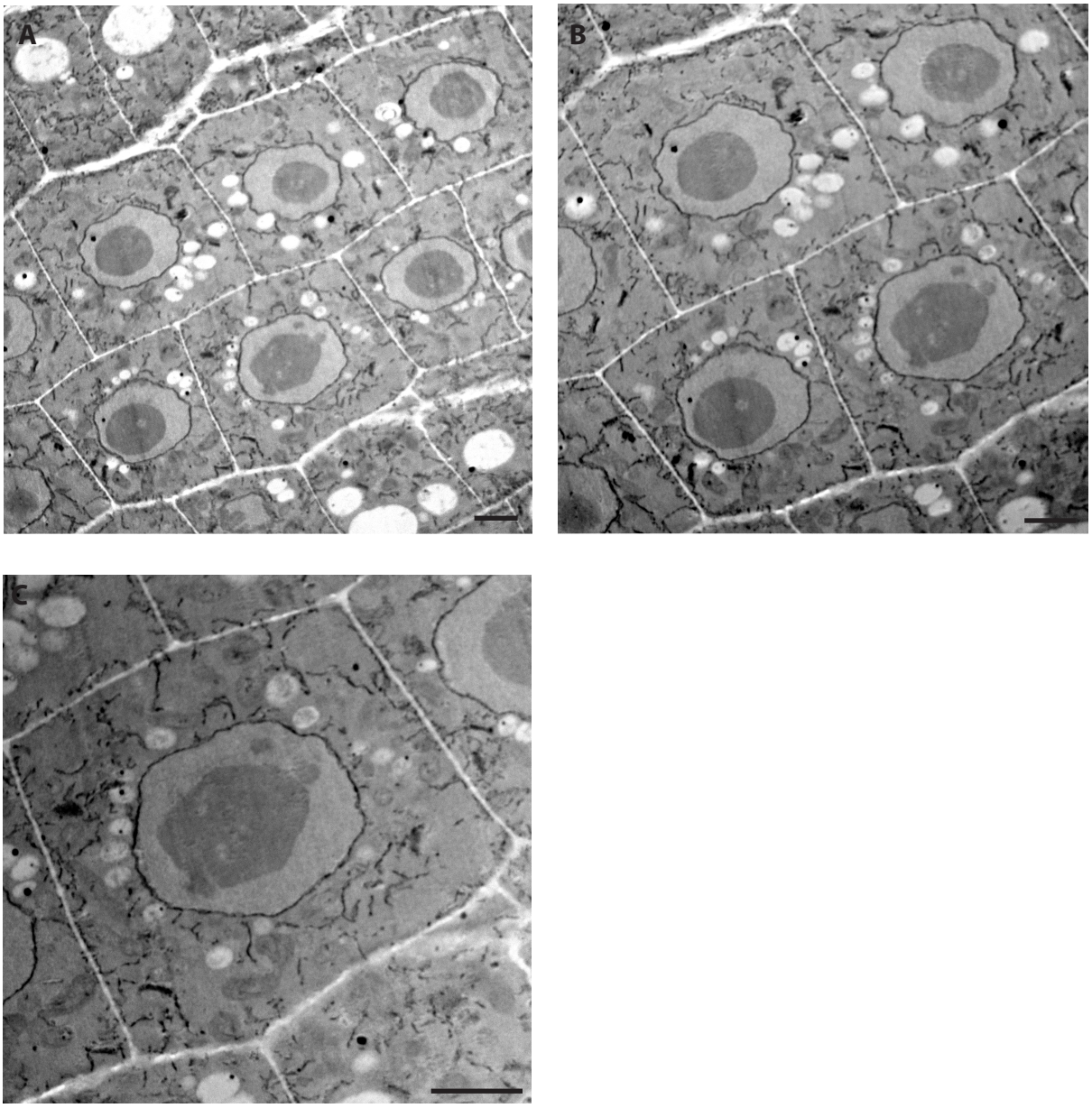


Figure 5.3.4 – Transmission electron micrographs of 200 nm sections of ZIO stained wild-type *Arabidopsis thaliana* root tips showing an overview of cells (arrow, scale bars - 2 μm).

A & B) Low magnification images showing multiple cells compartmentalised by surrounding cell walls with nuclei visible in the centre. ER membranes and nuclear envelopes exhibit a high degree of contrast with ZIO staining.

C) Higher magnification image of a cell surrounded by the cell wall around the periphery. Cell wall material exhibits little to no contrast from ZIO staining.

Figure 5.3.5: Transmission electron micrographs of 200 nm sections of ZIO stained wild-type *Arabidopsis thaliana* root tip cells with sections cut perpendicular to orientation of the cross walls visible (scale bars - 500 nm).

A & B) Cross walls surrounded by highly contrasted stained ER in adjacent cells. Arrows show sites at which the ER is incorporated in the cell wall and exhibits continuity between cells with staining evident across the cell wall.

C) A cell wall with a high concentration of ER within the cells either side in close proximity to the cross wall.

D) ER in association and close proximity to a cross wall, with ER cisternae distinguishable from ER tubules and/or cross sections of cisternae (arrows).

E) A cell wall with ER either side, with a site at which the ER is incorporated into the cross wall as a desmotubule (arrow).

F) A cell wall through which ER membrane appears to pass through without a high level of modification to its structure in relation to the ER membrane on either side of the cell wall material (arrows).

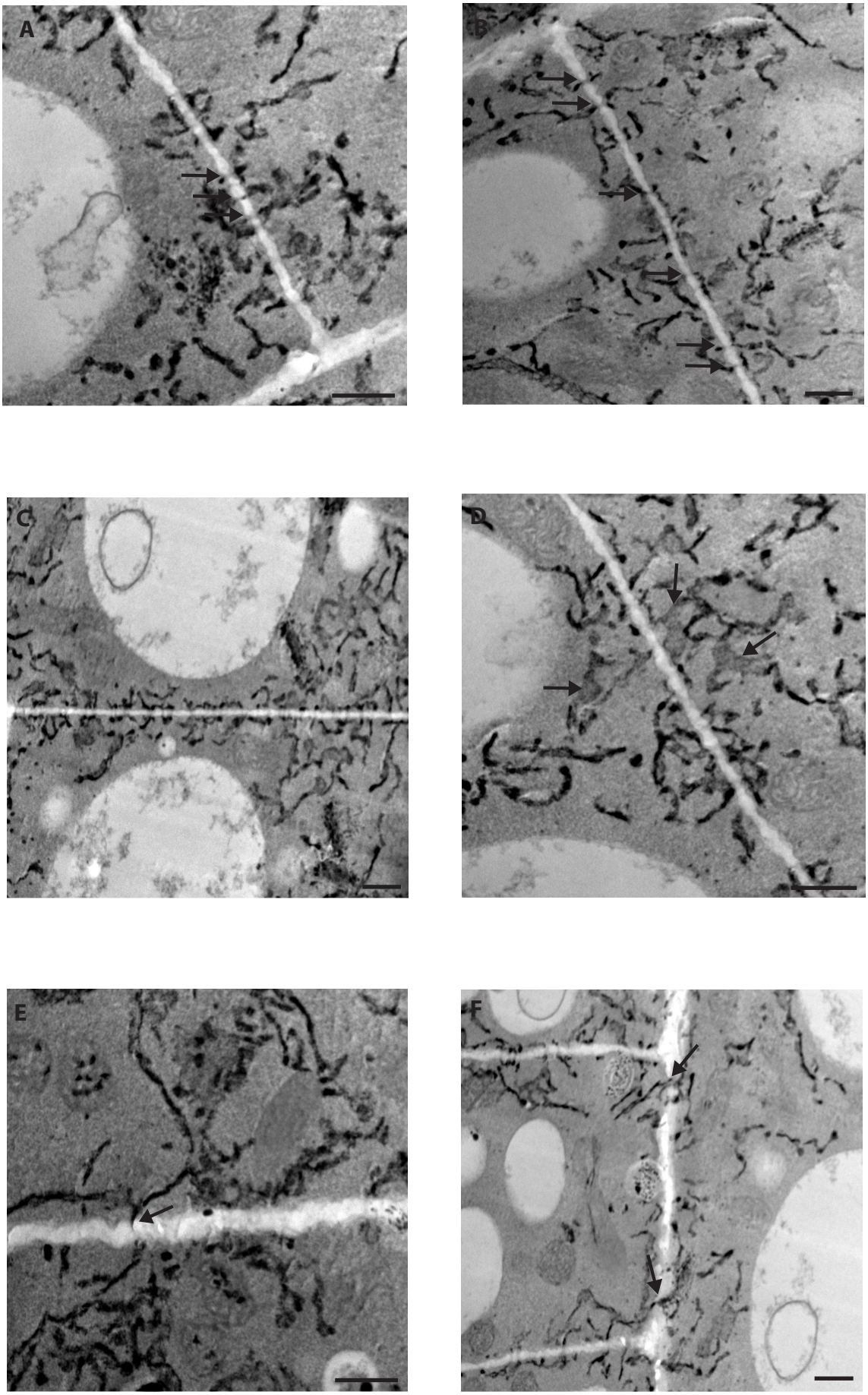


Figure 5.3.5

Figure 5.3.6: Transmission electron micrographs of 200 nm sections of ZIO stained wild-type *Arabidopsis thaliana* root tip cells showing sections through cross walls and ER (scale bars - 500 nm).

A) Across some cell walls ER can be seen incorporated into the cell wall material at the same contrast and size as the ER present within the surrounding cells. This is only the case for some cross walls, which appear to be orientated in the section at an angle that is not perpendicular to the longitudinal plane of the cell wall. Arrows indicate cell walls throughout which ER is present and continuous between adjacent cells.

B & C) Cells with sites at which ER, exhibiting consistent morphology and staining, appears to persist between adjacent cells throughout the cross wall.

D, E & F) Some cross walls show ER incorporated into the cell wall to varying degrees but the ER membrane does not traverse the region with consistent morphology to the opposing side.

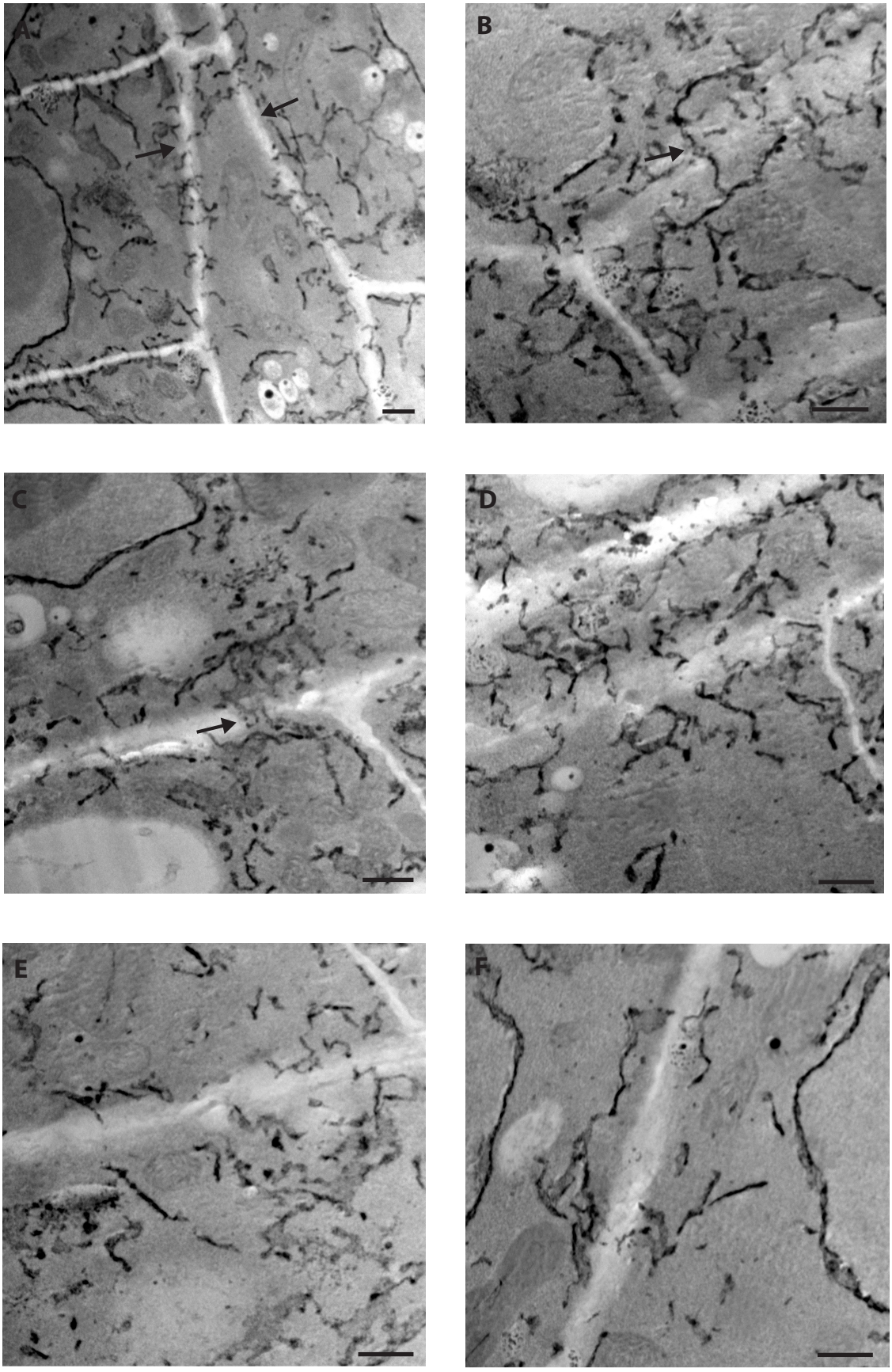


Figure 5.3.6

Figure 5.3.7: Transmission electron micrographs of 200 nm sections of ZIO stained wild-type *Arabidopsis thaliana* root tip cells treated with DMSO and Silwett-77™. Images show ER in relation to cross walls.

A) A cell surrounded by the cell wall at the periphery with the nucleus in the centre. Cell wall material exhibits little to no contrast, whereas ER membranes and nuclear envelopes exhibit a high degree of contrast with ZIO staining (scale bar - 2 μm).

B) Cells containing tubular and cisternal ER exhibit a high degree of contrast with ZIO staining in comparison to other organelles. Cells are separated by liner cross walls cut perpendicular to the plane of the section, with ER with cellular morphology not present across these regions (scale bar - 500 nm).

C) Cross walls cut at a perpendicular orientation in the section with highly stained ER within the cell and in association with cell wall material but not continuous in structure between cells (scale bar - 500 nm).

D) Region of adjacent cells with cross walls sectioned at an angle that is not a perpendicular cross section. ER with similar morphology and staining to that within the cells is present throughout the cell walls (scale bar - 500 nm).

E) Higher magnification image showing cross walls cut perpendicular to the plane of the section, with ER in association either side and sites. Some contrast is visible correlating to where the membrane is continuous between the cells as a desmotubule and the morphology is altered to what appears as a narrow line, in comparison to the cellular ER membranes (example – arrow, scale bar - 500 nm).

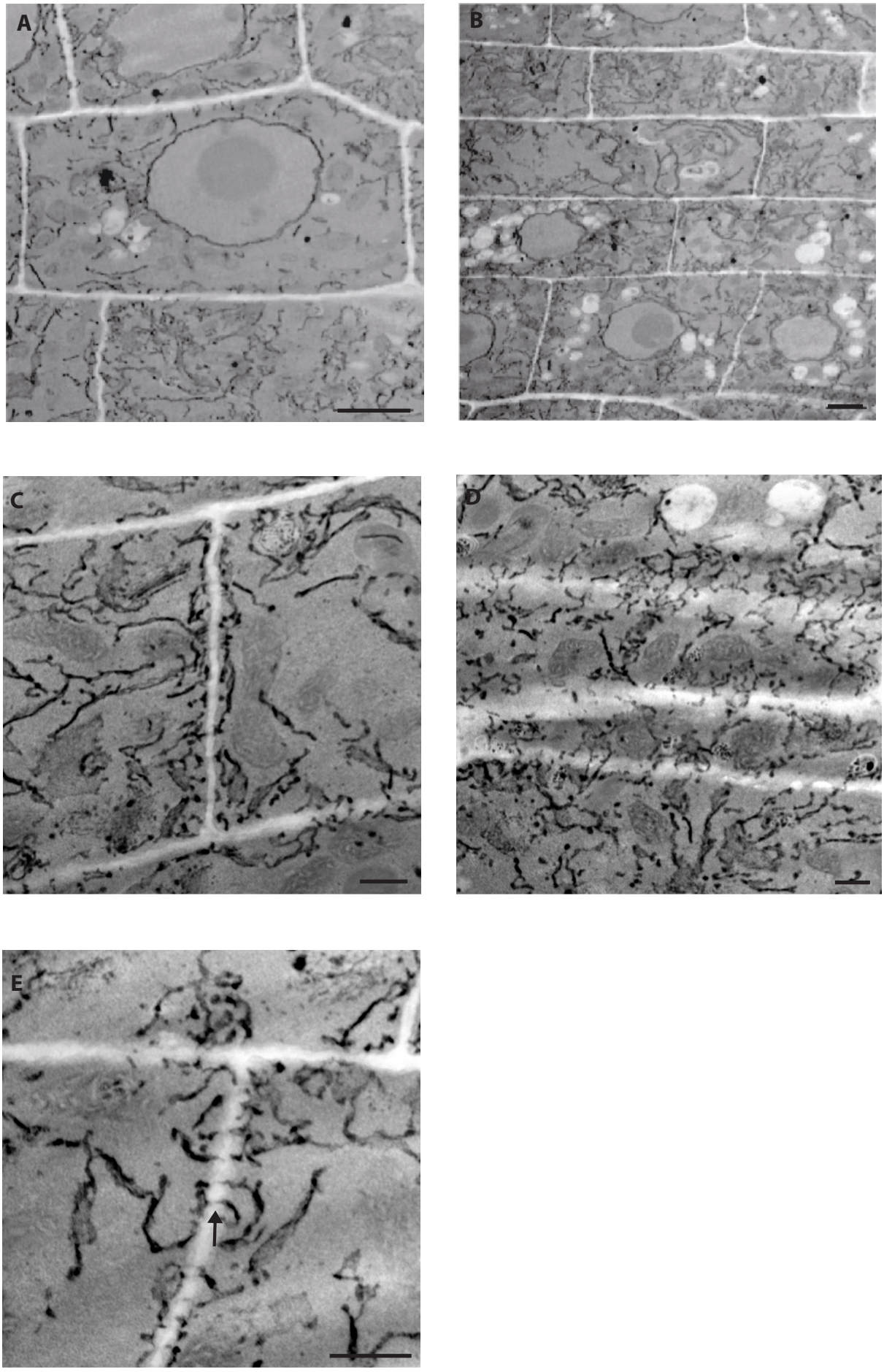


Figure 5.3.7

Figure 5.3.8: Transmission electron micrographs of 200 nm sections of ZIO stained *Arabidopsis thaliana* root tip cells following 20 hours induction of truncation 2 of RTNLB3-YFP over-expression.

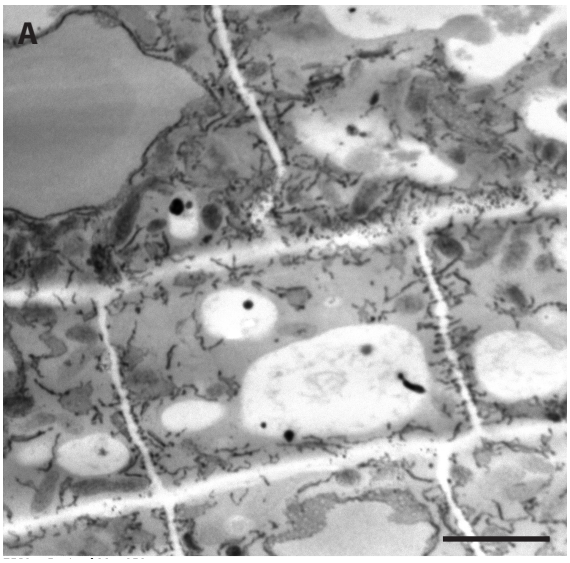
A) Low magnification overview showing cells containing highly contrasted ER and nuclear envelopes with cells compartmentalised by linear cross walls surrounding them (scale bar - 2 μm).

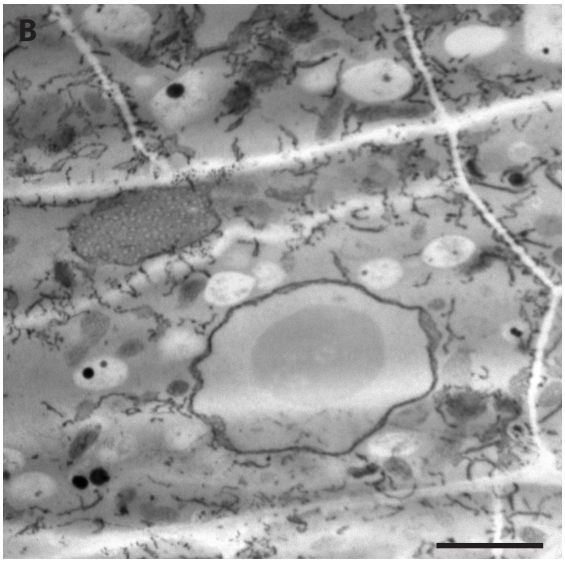
B) Low magnification image of cells with cross walls separating them containing heavily contrasted ER and nuclear envelopes. There is variation between cell walls in degree of ER membrane visible across these regions (scale bar - 2 μm).

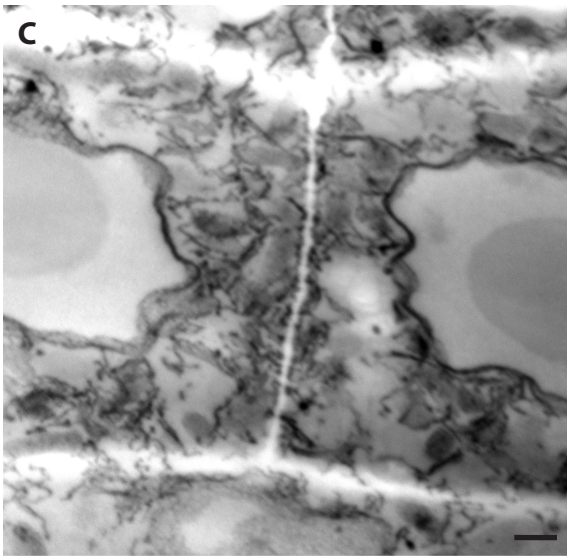
C) Some cross walls appear devoid of visible ER membrane except for fine lines of contrast, with concentrations of highly contrasted ER membrane either side of the cell wall (scale bar - 500 nm).

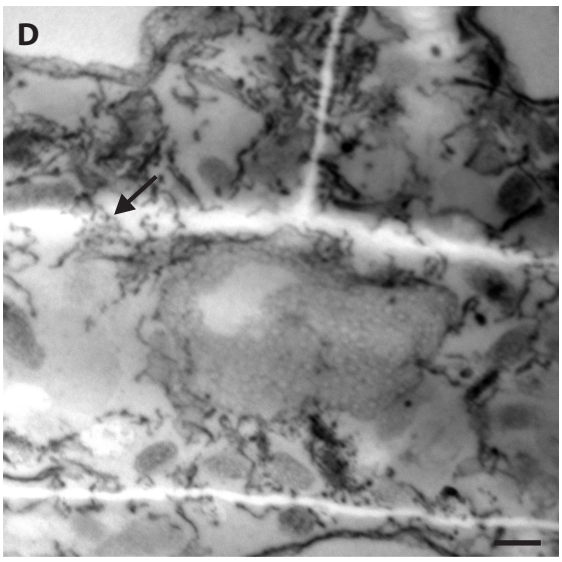
D) In some cross walls ER membrane is visible across cell wall material, which is continuous and consistent in morphology between adjacent cells (example – arrow, scale bar - 500 nm).

E) Higher magnification image of a cross wall cut perpendicular to the plane of the section, with ER associated either side of the cell wall. ER with the same morphology and level of contrast as within the cells is not present across this region (scale bar - 1 μm).









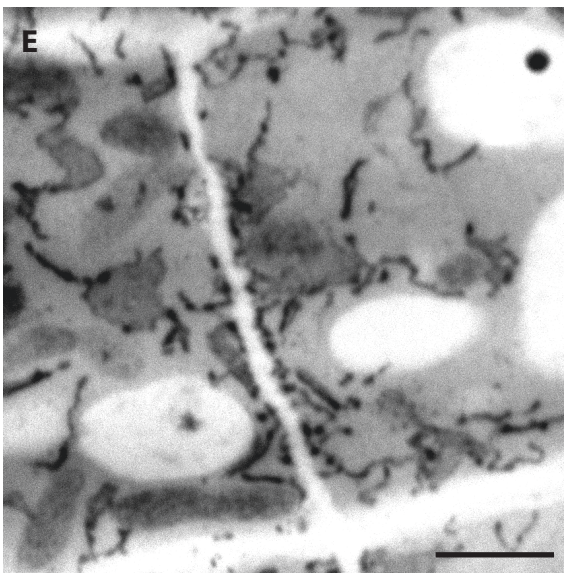


Figure 5.3.8

Figure 5.3.9: Transmission electron micrographs of 200 nm sections of ZIO stained *Arabidopsis thaliana* root tip cells of plants following 20 hours induction of truncation 2 of RTNLB3-YFP over-expression (scale bars - 500 nm), showing the association of nuclear envelopes with cell walls.

A) Cell with a nucleus in the central region of the cell with a high concentration of ER membrane between the nuclear envelope and cell wall.

B - E) Cells with nuclear envelopes in close association with cross walls. ER membrane originating from the nuclear envelope surfaces appears to be incorporated into the cell wall material.

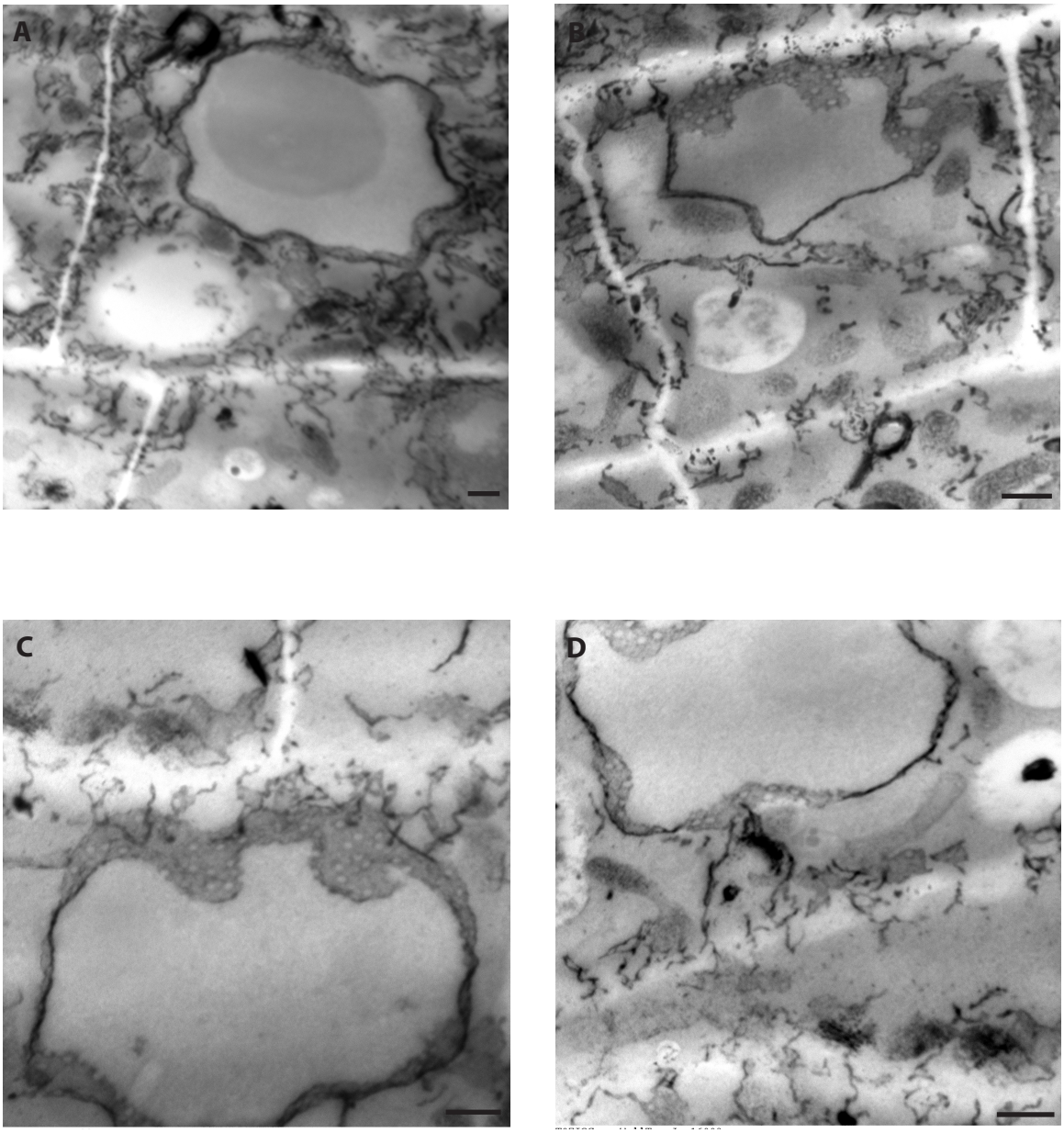


Figure 5.3.9

Figure 5.3.10: Transmission electron micrographs of 200 nm sections of ZIO stained *Arabidopsis thaliana* root tip cells of plants following 20 hours induction of truncation 2 of RTNLB3-YFP over-expression, showing cells with abnormal formations of cross walls (scale bars - 500 nm).

A & B) Some cells lack continuous, clearly defined cross walls surrounding their periphery. Arrows indicate regions where cell wall material becomes difficult to distinguish or does not appear to be present as a consistent boundary between cells.

C) A high proportion of the ER within regions where cross walls appear poorly defined is present as large cisternal sheets.

D) Nuclei are visible within some cells lacking fully formed cell walls, with some cell wall material extending from existing cell walls into the cytoplasm, which then appears to dissipate so that the cell is not compartmentalised from the neighbouring cells interior.

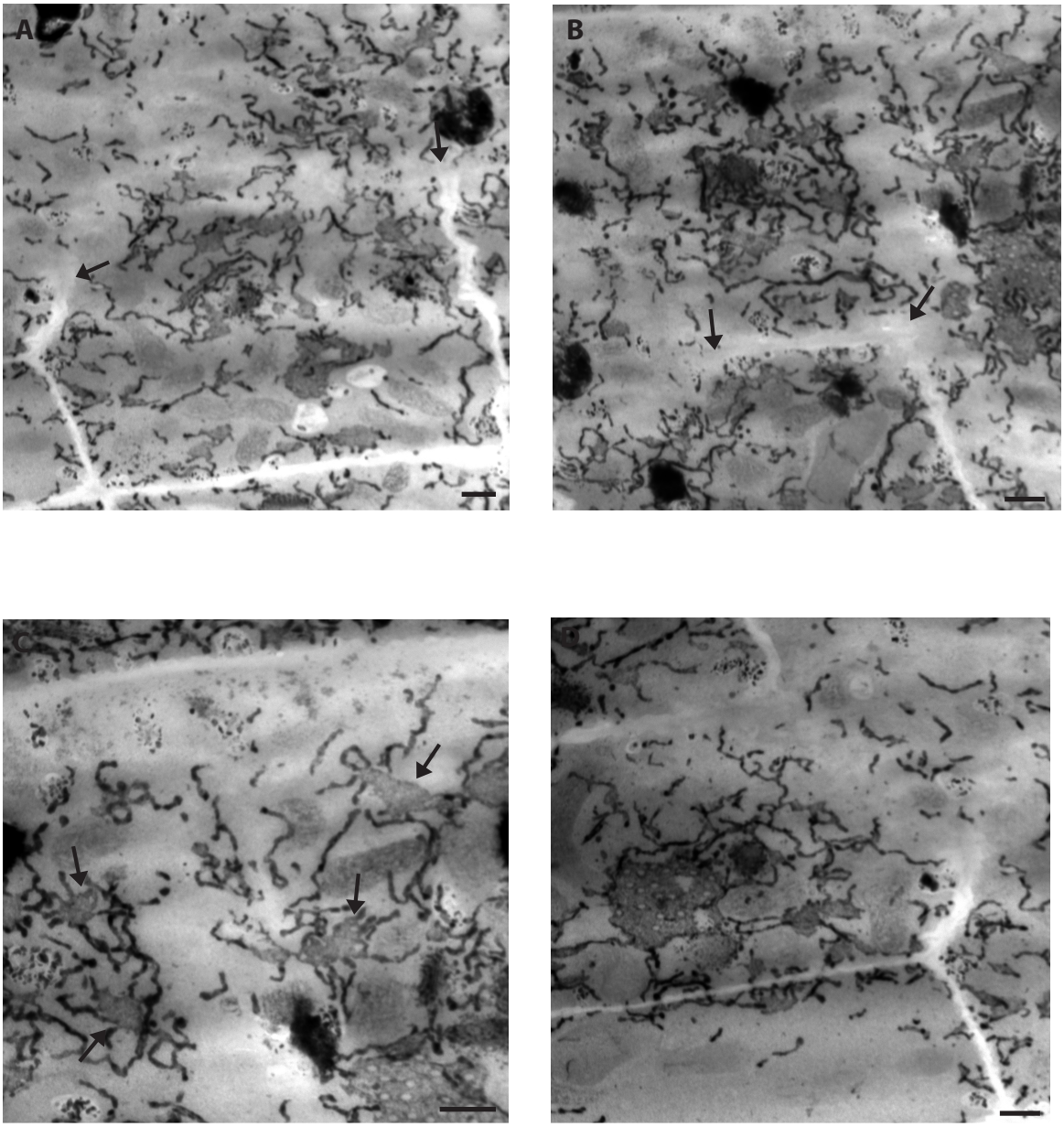


Figure 5.3.10

Figure 5.3.11: Tomographic data of a cell plate undergoing development in a wild-type *Arabidopsis thaliana* root tip meristematic cell.

A) Transmission electron micrograph of a thick section taken at a 0° tilt angle, showing a cell plate at a late stage of maturation, with surrounding ER exhibiting high contrast from ZIO staining (scale bar - 500 nm).

B) Image taken from within the three dimensional reconstruction of a tomographic data set, obtained from the sample shown in figure A (scale bar - 500 nm).

C) Higher magnification image showing the site of a plasmodesmata forming within a mature region of the cell plate in the tomographic data set (scale bar - 200 nm). ZIO stained ER can be seen passing through the cell plate material and becoming constricted at each opposing side, with the fine structure of the desmotubule appearing narrower and fainter in staining than the rest of the ER membrane.

D) Modelled ER (green) and dense cell plate material (yellow) shown as an overlay with the tomographic reconstruction data that the model was based on (scale bar - 500 nm).

E) Modelled ER (green) and dense cell plate material (yellow) of the tomographic data set reconstruction (scale bar - 500 nm).

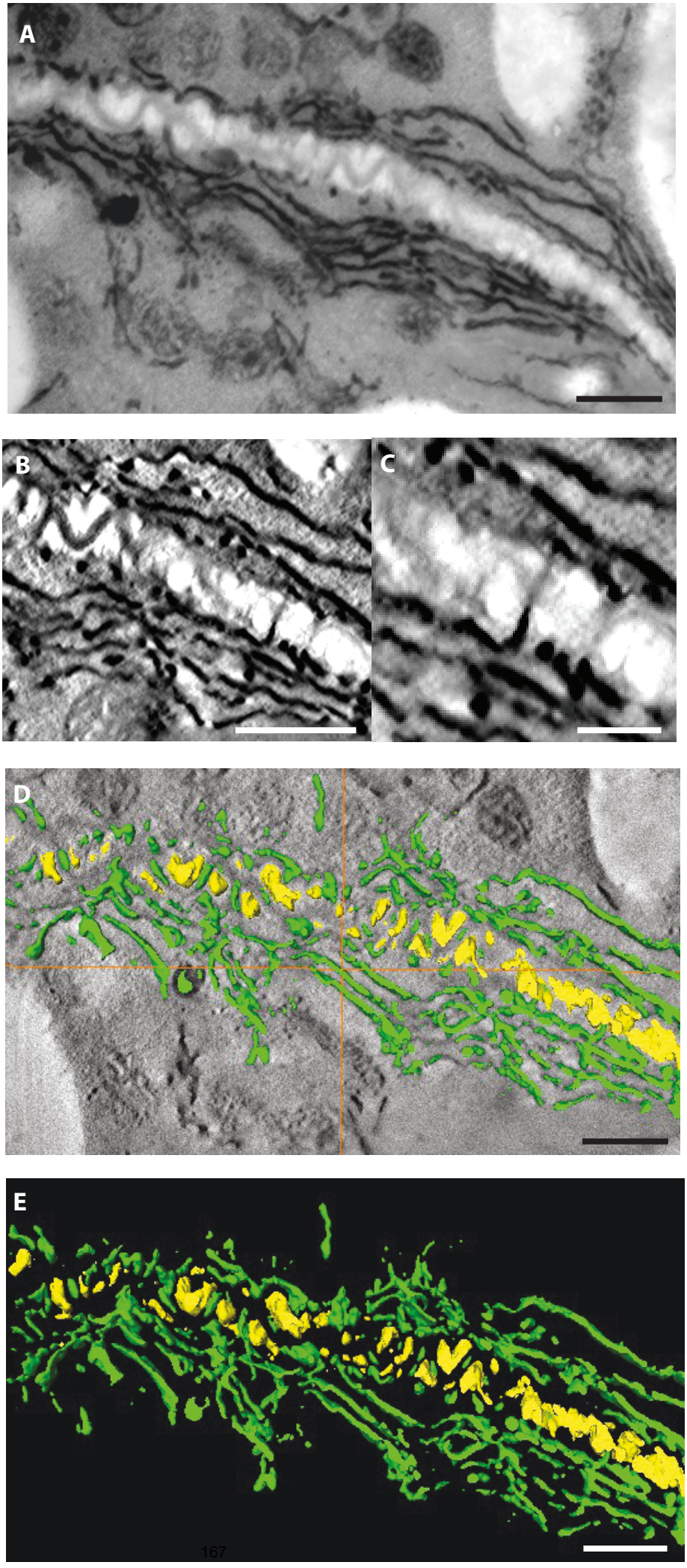


Figure 5.3.11

Figure 5.3.12: Tomographic data of a cell plate undergoing development in an *Arabidopsis thaliana* root tip meristematic cell over-expressing RTNLB3-YFP (scale bars - 500 nm).

A) Transmission electron micrograph of a thick section taken at a 0° tilt angle, showing a developing cell plate, with surrounding ER exhibiting high contrast from ZIO staining.

B & C) Three dimensional model from the tomographic reconstruction of tilt-series data set taken of the sample shown in figure A, with ER (green) and cell plate material (yellow).

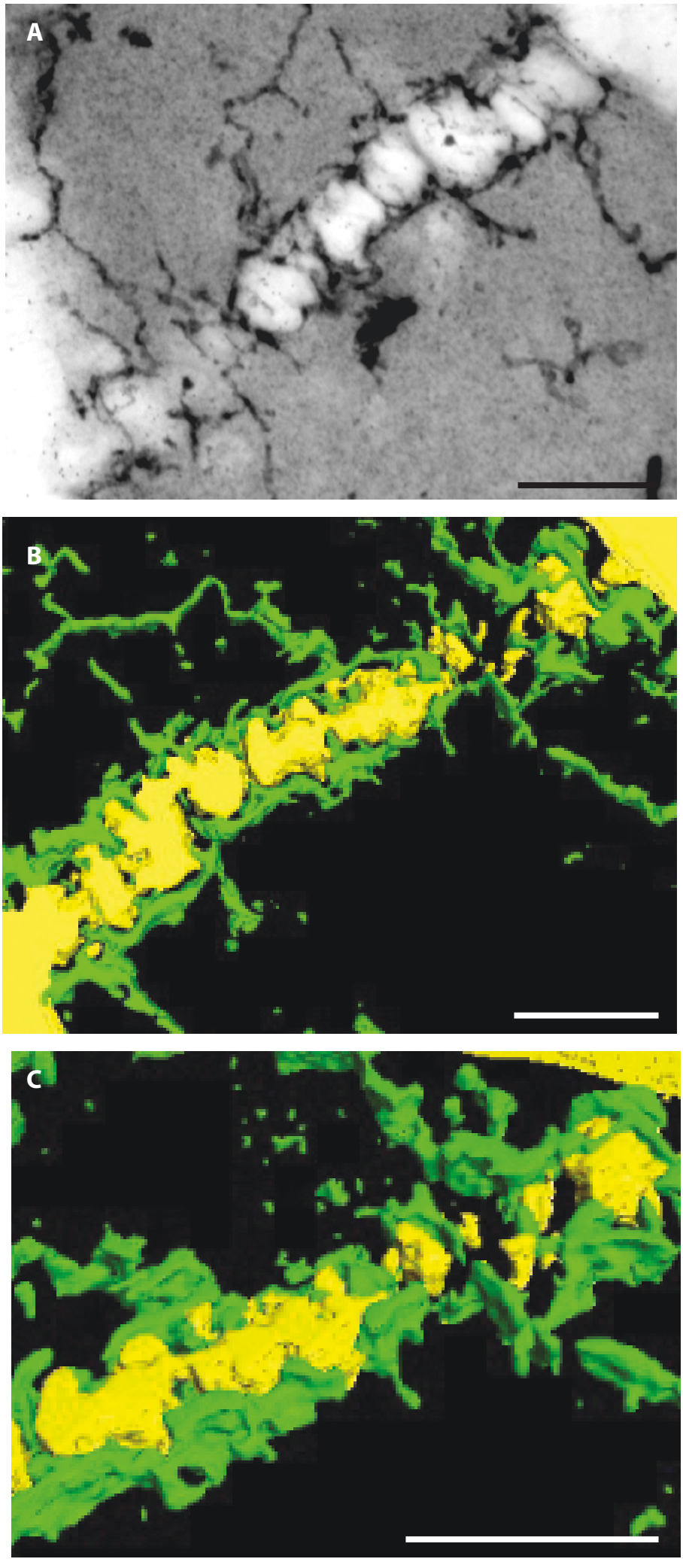


Figure 5.3.12

5.4 Discussion

5. 4. 1 80nm thin section electron microscopy of ZIO stained *Arabidopsis thaliana* root tip cells

Wild-type, control and truncated RTNLB3-YFP over-expressing *Arabidopsis thaliana* root tips were successfully prepared for electron microscopy analysis, employing the ZIO impregnation method. ZIO impregnation was optimised to establish the amount of time required for incubation of the roots in ZIO solution to produce a sufficient degree of contrast of ER membranes to enable structural analysis, without large quantities of unspecific osmium deposition obscuring the ultrastructural detail of the cells (unsuccessful fixation data not shown). There was some variation in the level of staining when comparing the different sample sets (which were prepared in the same experiment with roots of the same kind together in glass vials with the solution), individual roots within the same sample set, and level of staining within tissues of root. This variation is expected, firstly due to the differences between root size and tissue types, as these have an effect on the extent of osmium penetration and impregnation within any specific time frame. Additionally, although sample sets were prepared synchronously in the same experiment, due to the sensitive nature of the ZIO reaction slight differences in the result can occur between sample vials. This may be due to the exact volume of material proportional to the amount of ZIO solution within each vial, or some other unknown factor that has not been elucidated. Another potential variable is the subsequent sectioning and secondary staining of the material prior to imaging. For example the degree of secondary staining achieved may vary due to the properties of the surface of the section being slightly altered by exposure to any contaminants, such as traces of oils within the water of the knife boat when cutting or from storage.

Despite these differences in levels of staining in the resulting images, the proportional electron opacity of organelles within cells in the meristematic region of the root tips remained consistent between sample sets and individual roots within them. ER and nuclear envelopes possessed the highest degree of electron opacity and contrast within all three sample sets, and cell walls and vacuoles the least. Some Golgi membranes also exhibited high levels of contrast, however are sufficiently distinct in structure

from the ER to not impede ultrastructural analysis. Other organelles that are stained by the ZIO technique (Hall & Hawes, 1991) exhibited substantially less contrast than the ER and nuclear envelope membranes, and were therefore easily distinguishable from these.

The cells within the meristematic regions of all sample roots were compartmentalised by linear cross walls that formed an interconnected, lattice-like structure when observed as thin sections cut from the tissue. A few cross walls exhibiting greater variation in shape, with higher degrees of curvature, were present in an induced root tip over-expressing truncation 2 of RTNLB3-YFP. However the cross walls were otherwise morphologically intact, and based solely on this evidence it cannot be concluded whether this may be a phenotype of over-expression of the construct. This is due to some variation in cross wall shape having been occasionally observed in wild-type *Arabidopsis* root tips during the optimisation process. Therefore further analysis of the samples is required to establish whether differences in cross-wall morphology are a phenotypic feature of root cells over-expressing this construct or a natural anomaly.

Tubular and cisternal forms of ER were present in the cells of all sample types, although cross sections of cisternae cannot be distinguished from tubules in two-dimensional TEM images. The phenotype of the association between the cellular ER and the cell walls of all root samples observed was also similar. ER membrane was directly associated with cross walls in all cells. At sites where ER was present on both sides of the cross wall, at the same point in neighbouring cells, continuity of staining across the cell wall was present. However, this appeared as a faint line of staining directly crossing the cell wall material between the ER either side, as opposed to retaining the same morphology and intensity of contrast as the intracellular ER. These sites have been identified as localisations of plasmodesmata based on previously published electron microscopy data (Hawes *et al.* 1981; Helper, 1981), where the ER is connected between the cells in a highly constricted morphology as the desmotubule when incorporated into the cell wall. At some plasmodesmatal sites observed the ER membrane can be seen becoming increasingly constricted as it intersects with the cell wall, until it appears to disappear into a pinched off point.

In the truncated RTNLB3-YFP overexpressing root sample set, some cells contained large, dense deposits of osmium distinct from other organelles. These are suspected to be an artefact of the ZIO impregnation due to having identified similar deposits, in far greater quantities, in wild-type plants that were subject to longer osmium impregnation times during optimisation of the protocol. As this set of samples exhibited the highest level of contrast of ZIO staining of ER membrane out of the three compared in this experiment, it is expected that these samples would be the most likely to contain some artefacts of osmium impregnation.

Some smaller concentrations of dense ZIO staining within some cell walls of roots over-expressing truncated RTNLB3 were also observed. This may correspond to ER membrane that has not been fully constricted into desmotubules due to the mutant construct, but has become incorporated into the cell wall. The ZIO solution is thought to heavily stain ER membranes by the deposition of zinc ions in place of calcium ions, which are present in high levels on the positively charged ER membrane (Gilloteaux & Naud, 1979; Voeltz *et al.* 2002). Further analysis of the samples in thick section and in three dimensions will allow their morphology and distribution to be investigated in more detail, which may aid in elucidating this.

As the data that can be obtained from thin and thick section TEM is limited to two dimensions, due to time constraints RTNLB3-YFP over-expressing root tips were not analysed in detail with image collection using these techniques, prior to progressing to tomography and SBFSEM. However, thin section samples were observed to confirm that the samples possessed the desired level of ZIO staining for further imaging, which was comparable to the other samples described previously. No dramatic phenotypic differences from wild-type and controls in ER and cell structure were observed during the preliminary thin-section TEM analysis.

5.4.2 200nm thick section electron microscopy of ZIO stained *Arabidopsis thaliana* root tip cells

Analysis of thick sections of the samples revealed further detail of the ER within the cells, the structure of the cell walls and their association with each other. A striking difference between cross walls within root tips for all sample types was found in comparison to the observations made from thin sections. In some cross walls ER

membrane consistent in morphology and electron opacity to within the cells was found to be present throughout this region between adjacent cells. Why this was not evident in the thin section samples may be due several reasons. These cross walls may be a structurally distinct form within the root tip that is more apparent with a greater thickness of material present in the section imaged, as this observation is only present in a minority of cross walls within these samples. Another possibility is that these cross walls are the same in structure as other cross walls within the roots, however due to a combination of the amount of material present within these samples and the orientation of the cut through the cross wall, the phenotype is only observable in some cells. This result is unexpected based on what is documented in the literature regarding plasmodesmatal structure in higher plants (Hawes *et al*. 1981; Hepler, 1982; Ding *et al.*1992; Oparka *et al.* 1994; Knox *et al.* 2015). Based on two dimensional images it is difficult to draw further conclusions regarding this and therefore the structure of the ER across cell walls in these samples was further investigated using three dimensional imaging techniques.

In thick sections of truncated RTNLB3-YFP over-expressing root tip cells a phenotypic difference between this construct and the wild-type and control samples was revealed. Although the majority of cells were similar to those observed in in wild-type and control cells in this regard, in some cells in these sample roots the nuclei had a strikingly different localisation and association with the cell wall. In such cells, the nuclear envelope appeared almost embedded within the cell wall, either directly with nuclear envelope membrane incorporated into the structure or via short extensions of ER extending from the nuclear envelope which was in contact with the cell wall. As the construct is induced for only 20 hours prior to fixation, as opposed to being consistently over-expressed throughout the plants life-time (due to the lethal phenotype that occurs), only some cells within the meristem will have undergone and completed division within this time frame. Therefore it is to be expected that structural abnormalities that result from over-expression of the construct would only be present in a few cells within the root.

In this study RTNLB3-YFP has been primarily hypothesised to be involved in the formation of the cell plate and incorporation of the ER within it to form the desmotubules of plasmodesmata. However, the protein may have other roles with regards to aiding the correct assembly of the cell wall, as well as other aspects of cell

structure and function. Reticulons have been previously linked to nuclear envelope formation (as discussed in section 1.3.4), with over-expression of RTN3 and RTN4 in mammalian cells having been demonstrated to inhibit nuclear envelope expansion and formation and nuclear assembly found to accelerate in knockdown mutants (Anderson & Hetzer, 2008). If nuclear envelope assembly is also accelerated when a truncated form of RTNLB3-YFP, comparable to a knockdown with regards to being a non-functional mutant form of the protein, is over-expressed in plant cells, this may account for this observed phenotype. If the nuclear envelopes were to reassemble at an accelerated rate when the cell undergoes division, in combination with a more diffuse region of cell plate formation (such as that indicated by the confocal microscopy results of over-expression of the construct in BY-2 cells in section 3.3.2), the ER could become incorporated into the cell wall or remain in very close association with it via connecting ER membrane. This could occur because the nuclear envelopes reform at a stage where the chromosomes around which they assemble have not segregated as far into the daughter cells prior to reassembly to evade becoming trapped within the forming cell wall.

Another possibility or contributing factor to the previous hypothesis, may be that the distribution and structure of the ER that will form the nuclear envelope membranes is altered so that the nuclei reassemble in a different localisation closer to the cell plate than usual. Furthermore, the induced truncated RTNLB3-YFP construct, when observed in root cells using confocal microscopy (section 4.3.3), labelled nuclear envelope membranes. A high concentration of the non-functional reticulon may be interfering with nuclear envelope reformation and/or disrupting the relationship between what become the nuclear membranes and the rest of the ER network, with an impact on the localisation of the reassembled nucleus within the daughter cell.

Some nuclear envelope labelling was also observed in root tip cells highly over-expressing the full length RTNLB3-YFP construct (section 4.3.2). Therefore it is also plausible that, although not observable in all cells, some RTNLB3 is localised to the nucleus but generally at a low concentration, where it plays a role in regulating nuclear envelope reformation. As nuclear envelope reassembly has been found to slow down in mammalian cells over-expressing RTN3, and knockdown of the protein resulted in accelerated nuclear envelope assembly, this indicates that the endogenous level of RTN3 may be a required regulatory factor for the nuclear envelope to reform

at the correct rate and time during cell division (Anderson *et al.* 2009). If this is the case, over-expression of the truncated form would out-compete the native full-length RTNLB3-YFP proteins present and interfere with this function, which could result in the nuclear envelope reassembling at an altered time and rate during the cell cycle, rendering the membranes susceptible to being trapped by the cell plate as it develops.

In mammalian cells observations have indicated that nuclear envelope membranes are directly derived from cisternal, as opposed to tubular ER and that an absence of ER tubules, such as in the event of truncated reticulon over-expression, should not interfere with reassembly of the nuclear envelope during mitosis (Lu *et al.* 2011). It has also been suggested that ER tubules form connections with the chromosome mass during cell division and then expand laterally around the surface of the chromosome to form the nuclear envelope (Anderson *et al.* 2009). However, although this had been found to be the case in an in vitro study (Anderson *et al*. 2009) and has been supported by thin-section TEM data (Puhka *et al.* 2007), subsequent work by Lu *et al.* (2011) has demonstrated that this hypothesis is unlikely. They showed that in mitotic cells the majority of the ER forms a network of fenestrated, interconnected cisternae, lacking tubules. Therefore, regulation of reticulon protein and the structure and amount of cisternal ER present in the region of the chromosomal mass during mitosis may be essential for temporal control of nuclear envelope assembly. This could account for phenotype observed in the results presented here and those previously documented in mammalian cells.

In samples over-expressing the truncated construct, some structural abnormalities to cell walls within the root tissue were also observed, including cross walls that appeared to be partially formed or missing entirely (figure 5.3.10). As these cells contained fully formed nuclei with no evidence of cell plate formation, they did not appear to be in telophase undergoing division. In addition to this, cell wall material was present originating from the cell walls of neighbouring cells but not spanning the whole region where a cross wall would be expected to be located (based on wild-type and control samples).

If the cell plate was incomplete but undergoing formation as in wild-type cells, as the cell plate forms centrifugally outwards from a central point towards the existing cell walls, cell wall material would be expected to be in this location. Therefore over-

expression of the construct appears to be dramatically interfering with the formation of a new cell wall in its entirety and thus plasmodesmatal formation in combination. This could be the result of the inability of ER membranes to become highly compressed at the sites where plasmodesmata form (Hawes *et al.* 1981; Hepler, 1982; Seguí-Simarro *et al.* 2004), and therefore a large volume of membrane is present in the region where the cell plate develops. This excess of membrane could physically obstruct the fusion of the cell wall material, which is deposited in this region during cell plate formation in a vesicular form, into a compact solid cell wall structure (Samuels *et al.* 1995). This would account for the fact that in some parts the cell wall appears to have formed but not in others, and the fact that some diffuse cell wall material appears to be present in this area, excluding other organelles from the region. If this was the case ER would be expected to be seen trapped within this region, however although in a high concentration near these localities at some sites observed, in others the area was also devoid of ER membranes. Another mechanism therefore, may be responsible for this phenotype in cells that undergo division following over-expression of the mutant construct and RTNLB3-YFP may have multiples roles in the formation of the architecture of the cell plate.

The abnormalities observed regarding nuclear envelope localisation, potentially temporal regulation of its formation, and disruption to cell wall architecture, may all contribute to the lethal phenotype found for stable over-expression of the truncated construct in both BY-2 cells and *Arabidopsis thaliana* plants, or one of the mechanisms that results in these defects may be a dominant factor.

5.4.3 Transmission electron tomography of ZIO stained *Arabidopsis thaliana* root tip cells

To further investigate the 3D structure of the ER, cell plate formation and plasmodesmata within wild-type, full length and truncated RTNLB3-YFP over-expressing cells, a tomographic and SBFSEM study was undertaken (see chapter 6 for SBFSEM).

Limited tomographic data was collected and analysed of wild-type and full length RTNLB3-YFP over-expressing meristematic root tip cells undergoing division, before it was decided that SBFSEM possessed greater potential as a technique for investigating the

questions presented in this study. Tomography has the potential to resolve the fine structure of individual PD, such as in the recent study by Nicolas *et al.* (2017), who used electron tomography to produce three-dimensional reconstructions of plasmodesmata in an unprecedented level of detail. Their work has revealed that contact between the ER and plasma membrane within plasmodesmata undergoes remodelling during cell growth and differentiation. Directly following cytokinesis there was contact with the plasma membranes of plasmodesmata along the entire length of the desmotubule, which widened to produce an open cytosolic sleeve, a gap with tethers between the membranes, during cell expansion. However, the volume of material that can be imaged and modelled in three dimensions is confined to a very small region of the cell in each tomogram. Therefore, it is not feasible in a single study to image numerous cell plates in their entirety with large volumes of the surrounding ER in three dimensions using TEM tomographic data collection. As the questions posed in this study relate to the involvement of the ER in the process of cell development as a whole, in addition to the development of the desmotubules within it, and the role that RTNLB3 plays in these processes and regulation of ER structure, SBFSEM as a technique will serve to answer more of the questions posed in this study than further TEM tomography.

Also, with the aim of modelling comparable cell plates undergoing development within each sample set, due to the highly abnormal and irregular cell wall phenotype observed for the truncated RTNLB3-YFP samples during thick section TEM analysis (described in section 5.3.2), obtaining representative comparable tomograms of a defined cell plate region was not deemed practical. In addition to this, for the other phenotypes observed (section 5.3.2) and described (section 5.4.2) previously in the TEM analysis to be investigated further, larger volumes of 3D data required analysis. This included greater volumes of ER and cross walls than can be obtained from tomographic sections, and large volumes of cells to observe the localisation of nuclei within the context of the rest of the cell.

Furthermore, the range of abnormal cell wall structures identified in the mutant dataset thick section samples (section 5.3.2) suggested that the phenotype resulting from over-expression of the truncated construct results in dramatic changes to the formation and structure of the cell wall in cell undergoing division. Therefore SBFSEM, which can collect datasets throughout the entire volume of a root tip in a single sample run, provides

a far more efficient method for obtaining and identifying cells with abnormal morphologies within a tissue. Also it allows for the entire cell volume to be analysed if desired. Although serial sections for tomography of a larger volume than a single tomogram can be collected, it is difficult to obtain sufficiently high quality sections from a single sample. There is a high chance of many sections not being of a sufficiently high quality to be imaged as serial tomograms and thus being lost. This is also an incredibly time consuming approach, as it is impossible for an individual to manually thick section and screen all of the material in a block within a relatively short single study. For these reasons the transmission electron tomographic approach was not deemed practical and SBFSEM imaging was employed to further this research.

The tomographic data analysed for a wild-type and RTNLB3-YFP over-expressing cell plate revealed no significant phenotypic differences. The structure of the ER and cell plate was as expected for wild-type in both samples, reminiscent of that described by Hawes *et al.* (1981) and Hepler (1982) in their transmission electron microscopy based studies. At this stage further conclusions relating to the aims of this thesis cannot be drawn from the limited data presented in section 5.3.3 and therefore the SBFSEM data collected thereafter will be discussed in detail in chapter 6.

Chapter 6. SBFSEM, 3D reconstruction and analysis of ZIO stained *Arabidopsis thaliana* root tip cells

6.1 Introduction

Until recently, three dimensional imaging in electron microscopy has relied upon serial-section (ss) TEM and electron tomography for data collection (Linberg & Fisher, 1986; Mishchenko, 2009; Bock *et al.* 2011; Takemura *et al.* 2013). Relatively large volumes can be reconstructed in high resolution using a combination of ssTEM with tomography (Soto *et al*. 1994; Donohoe *et al*. 2006; Marsh 2007; Hughes *et al.* 2013) and through the use of sub-tomogram averaging (Nicastro *et al*. 2006; Lučič *et al*. 2013). However the technique is very time and labour intensive. For example, for the reconstruction of 379 neuronal cells, Takemura *et al.* (2013) needed to collect over 200,000 individual micrographs from which to reconstruct the whole cells. In addition to this, the technique requires a high level of prior training and skill to accomplish, due to the difficulty in obtaining continuous sections to a consistently high standard (Hughes *et al.* 2014; Kittelmann *et al.* 2016). Therefore, although in combination with ssTEM it is possible to employ transmission electron tomography for whole cell imaging, the technique has not become a routine method of 3D analysis for this volume of detail. Similar conclusions regarding the impracticalities of employing ssTEM and tomography for the analysis of large volumed cells were also drawn from the preliminary tomographic work carried out in this study (section 5.3.3).

Over the past two decades, researchers have begun to use SEM combined with novel techniques to obtain three-dimensional data. These methods employ blocks of materials embedded in resin similarly to those prepared for TEM, as opposed to conventional SEM preparation techniques. Through the use of focused ion beams (FIB), and later automated ultramicrotomes, large volumes of 3D data from block faces at high resolution have been collected using SEM, with greater efficiency than any of the previously used TEM techniques employed for the same aim (Kremer *et al.* 2015). Recently, serial block face scanning electron microscopy (SBFSEM) has emerged as a viable technique for rapidly and reliably obtaining high-quality electron microscopy datasets of large volumes of tissue, which can be further processed for 3D reconstruction and analysis.

SBFSEM was developed into its current form by Denk and Horstmann (2004), since which it has become rapidly implemented as a technique for collecting high resolution biological data (Borrett & Hughes, 2016). Only in the past few years has the technique begun to be employed for imaging plant data (Furuta *et al.* 2014; Scheuring *et al.* 2016).

It is when combined with selective staining techniques that result in a high degree of contrast between organelles in the sample, that the potential of the method for analysing the organisation and connections of organelles in plant tissue is fully harnessed (Hughes *et al.* 2014; Kittelmann *et al.* 2016). Although the technique has not yet been implemented for in depth morphological plant studies, publications assessing the technique have reported that the resolution that can be obtained using ZIO impregnated material is comparable to thin section TEM and that 3D reconstruction of datasets obtained from such samples is relatively efficient, with regards to the subsequent digital processing required (Hughes *et al.* 2014). Hughes *et al.* (2014) concluded in their analysis of the applications of the technique that it is ideally suited for imaging highly contrasted plant material subject to this preparation.

It is possible to obtain data of whole tissues or cells and their internal organisation by using SBFSEM imaging, and reconstruct their 3D morphology (Hawes & Hummel, 2015). Unlike TEM, which is limited even in the thickest sections observable to under a 1 µm in range, in Z thickness SBFSEM is only restricted by the maximum Z range of the stage, which is approximately 600 µm and can be reset during the course of a single data collection series (Kittelmann *et al.* 2016). The quality of the micrographs obtained is equivalent to intermediate magnification images of thin section TEM images (Kittelmann *et al.* 2016). The SEM specimen chamber contains an automated microtome with a diamond knife, similar to that for TEM sectioning, and slices of a set thickness are sectioned in increments through the resin block of the sample (Borrett & Hughes, 2016; Kittelmann *et al.* 2016). The images of the block faces are captured using backscattered electrons, producing images similar those obtained with TEM. As with TEM, samples require enough density to provide sufficient contrast within the sample to allow for differentiation between structures in the resulting images (Borrett & Hughes, 2016). The resin also needs to be sufficiently stable to withstand the electron beam and sectioning of

the microtome, so as not to become distorted in structure during image collection (Borrett & Hughes, 2016).

The ZIO stained and resin embedded samples prepared for TEM analyses in this study are suitable for this purpose. It has also recently been documented that for selective analysis of membranes within SBFSEM samples, ZIO impregnation is an excellent technique to enable identification, segmentation and analysis of the ER, nuclear envelopes and other organelles if desired, within plant tissues (Borrett & Hughes, 2016). The results of SBFSEM data collection and 3D reconstruction of the samples prepared and analysed using TEM imaging techniques in Chapter 5 will be presented in this chapter.

6.2 Materials & methods

Generation of stably transformed *A. thaliana* lines containing the full length and inducible truncated RTNLB3-YFP constructs, growth of plants, fixation and preparation of samples for TEM imaging and tomography are detailed in Chapter 2.

The methodology for the induction of the truncated RTNLB3-YFP construct in *A. thaliana* plants is detailed in Chapter 4, section 4.2.4.

6.2.1 SBFSEM data collection

Resin-embedded samples, as prepared for TEM imaging (detailed in chapter 2, section 2.5) were trimmed and sectioned using a Powertome XL ultramicrotome (RMC Boeckeler, USA) until root tissue in the resin block was reached, with the root orientated longitudinally in relation to the block face. Samples were placed into a Field Emission SEM is a Zeiss Merlin Compact with a Gemini column fitted with the Gatan 3View2XP for serial block face sectioning. Scanning electron micrograph images of the block face were recorded using Digital Micrograph (Gatan, UK) at 100 nm intervals of automated microtome cut sections.

6.2.2 SBFSEM data processing

The micrographs obtained for each SBFSEM dataset were combined from the series of DM4 files into a single mrc stack file format using IMOD. Regions of interest were isolated and cropped out to produce individual mrc files using the extract volume function of Digital Micrograph (Gatan, UK). Files were aligned using the automated serial section alignment function in IMOD.

To generate the 3D models of the data, Amira 6.0.1 (FEI, USA) was used to segment the organelles of interest within the dataset. Thresholding was used to isolate material possessing a high degree of contrast from ZIO staining (ER, nuclear envelopes and organelles) or a very low degree of contrast (cell walls, cell plate material and vacuoles), in relation to the rest of the sample. Specific organelles from those thresholded were manually selected within each section, then "constrained smoothing" applied to reduce noise within the sample and to interpolate the structures in three-dimensions between the series of two dimensional aligned sections. Images of the models, with and without sections of the original SBFSEM data included, were taken using the "snapshot" function and movies produced using the "movie maker" within Amira 6.0.1, which were saved as final mpg files.

6.3 Results

6.3.1 SBFSEM, 3D reconstruction and analysis of wild-type, ZIO stained *Arabidopsis thaliana* root tip cells

Datasets of two wild-type *A. thaliana* root tips including the meristematic tissues were collected using SBFSEM, analysed as aligned series of images viewing the cells within the samples, and regions of interest cropped out for further processing and 3D reconstruction.

Interphase cells with both a relatively regular rectangular cuboid shape and cells with angular cross-walls and asymmetric morphologies were isolated, and cell walls, ER and nuclear envelope membranes were segmented and reconstructed to produce three-dimensional models. The modelled data could be viewed within the mrc file cube of electron micrograph derived image data to observe the structures within the context of the

surrounding material. In some images in these results, slices from this data have been included with the images of the modelled organelles to show the structures within the context of the original dataset. An example of a low magnification cropped region of an SBFSEM micrograph, containing many cells of varying shapes within the meristematic region of the root tip, is shown in figure 6.3.1, A. The ER, nuclear envelopes and cell walls are clearly identifiable as distinct structures, based the degree of contrast within the sample tissue resulting from the ZIO staining technique used to prepare the samples.

Figure 6.3.1 B - F show sample images of modelled data from interphase meristematic cells that possessed approximately linear cell walls, forming square or rectangular cuboid cell shapes. The peripheral ER morphology in these cells was a mixture of tubular and cisternal forms, with many large sheets (figure 6.3.1, B, C & D; Appendix disc files CrossWallWT1 & WTCrosswall2). ER was present in a high concentration surrounding the cross walls, including cisternal sheets across the surface (figure 6.3.1, E; Appendix disc file WTCrosswall2), with ER observed to be predominantly cisternal in structure in these regions. Although ER was localised in a high concentration throughout the cell peripheries, the highest density was often observed to be in direct or very close association with both cross and lateral cell walls (figure 6.3.1, D & F, respectively).

Sites where the ER is incorporated into the cell walls and traverses through as the constricted cores of plasmodesmata were also analysed within the SBFSEM datasets. The structures appeared consistent with the results described and discussed in chapter 5, presenting as thin continuities of staining through the cell wall material distinct from the morphologies of intracellular ER. The level of staining of the structures was also distinct, exhibiting a lower level of contrast and appearing as less sharply defined structures than other ZIO stained ER membranes. Due to this limiting factor regarding resolution of these structures, and their very small size that would be difficult to see in a reconstruction viewing large volumes of cells, plasmodesmatal sites were not modelled in the 3D reconstructions. However, cross wall regions within the 3D models were also observed without the inclusion of modelled cell wall material. This confirmed that no ER in an intracellular, non-constricted morphology is incorporated into nor traverses these boundaries between the cells (figure 6.3.1, C).

Interphase cells with a less uniform structure than those discussed previously were also analysed. It was observed earlier in this study during TEM analysis of thick sections that

some cell walls, which appeared to be thicker and/or sectioned at an angle, had ER of an intracellular morphology incorporated within them, and ER passed through the region without constriction into desmotubule structures (section 5.3.2). This was investigated further through analysis of the SBFSEM data sets and using 3D reconstruction. Analysis of the electron micrographs of the SBFSEM datasets resulted in similar observations of the apparent structure of these cell walls and associated ER membranes. Adjacent cells and cell walls where this was identified were isolated from the datasets for 3D modelling and the ER and cell wall material reconstructed. When the models were viewed, in the majority of orientations of the model (viewing all of the ER within the region), the membrane did appear to be continuous in structure between the cells (figure 6.3.2, A). However, upon further analysis of the 3D models, with and without the context of the SBFSEM image data stack, continuous regions devoid of ER membrane were found (figure 6.3.2, B). These correlated with the cell wall material identified in the original data sets and the location of the modelled cell wall (not included for the model shown in figure 6.3.2, A & B), such as the angled cross walls between the cells shown in figures 6.3.2 C & D and movie files WTDiagonalCrossWall1 and NECrosswallWT (Appendix disc). ER was modelled on both sides of cross walls in these reconstructions, although the images show a single orientation of each. The ER morphology in close proximity to these asymmetrical cell walls (such as figure 6.3.2, C & D) was reminiscent of that described for the more uniformly shaped cells, of which examples are presented in figure 6.3.1. When observing the models of cell volumes inside all of the enclosing cell wall, it was also noted that the distribution of ER membrane was densest at the cell periphery in comparison to the central region of the cell (figure 6.3.2, D).

The phenotype of nuclear envelopes closely associated with or appearing almost embedded within the cell walls of some truncated RTNLB3-YFP over-expressing cells, that were observed during TEM analysis of thick sections, was also further investigated. Initial analysis was conducted with wild-type samples. In the micrographs of SBFSEM datasets of the root tips similarly localised nuclei were observed, which were previously only observed in the mutant cell samples. Reconstructions of the nuclear envelopes, ER and surrounding cell wall material within two of these cells are shown in figures 6.3.2 E & F. The nuclei are located in very close proximity to the cell walls, however nuclear envelope membranes were not found to be embedded within them. Short extensions of ER membrane originating from the nuclear envelope were associated with the cell walls,

and observed to be incorporated into plasmodesmata based on the SBFSEM image data. In addition to this, the nuclear pores of the nuclear envelopes proved to be very defined in the SBFSEM datasets and subsequent 3D reconstructions. The structure of the nuclear envelopes with the pores included in these data sets cannot be observed in such clear detail with other techniques, as such clear reconstructions of nuclei including the pores are absent from the literature. Other observations within these cells were consistent with those made for other interphase cells, as previously described for those shown in figure 6.3.1 and figure 6.3.2 C & D.

Cells undergoing cell plate formation were also found in the SBFSEM datasets. Three cells in this stage of cell division were identified, isolated from the WT datasets and the ER, nuclear envelopes and cell plate material of each was reconstructed to produce three-dimensional models. Images of the data obtained from one of these cells are shown in figure 6.3.3 and the movie file WTPlate1 (appendix disc).

A montage of SEM micrographs of the SBFSEM data of the cell, for which images of the 3D reconstructions are presented in figures 6.3.3 B – D, is shown in figure 6.3.3 A. When the entire volume of reconstructed ER, and nuclear envelopes within the central portion of the cell surrounding the cell plate, is viewed it is difficult to observe the detail of the plate structure and the relationship of the ER membranes with this material (figure 6.3.3, B). When the reconstructed plate material is viewed in the absence of the reconstructed ER membranes, the structure is revealed to be a particulate cell plate that extends almost to the existing walls at the cell periphery but is yet to fuse into a solid structure (figure 6.3.3, C). When smaller cropped volumes of the model are observed with the ER membrane reconstruction included, a higher concentration of ER consistently lining the developing cell plate becomes distinguishable from the rest of the surrounding ER, which is present in a predominantly cisternal form (figure 6.3.3 D). As cell plate associated ER is primarily cisternal, tubular ER spanning this region may likely correspond to ER membrane that will become increasingly constricted to form the desmotubules within the cell plate.

The reconstructed WT cell shown in figure 6.3.4 A – D appears to be at a slightly earlier stage of maturation than the cell for which results are shown in figure 6.3.3. The cell plate material can be seen surrounded by a dense network of ER, housed in the centre of the cell (figure 6.3.4, A & B), with the cell plate not having yet developed into the most

peripheral regions of the cell. When a smaller volume of the modelled ER in the region is isolated, it becomes evident that the ER membranes, retaining their structure, traverse much of this region (figure 6.3.4, C), rather than being restricted to the cell plate periphery. Viewing the model with the ER membrane reconstruction set to high transparency with the cell plate material opaque, further reveals how the ER surrounds and weaves through this region (figure 6.3.4, D).

Figures 6.3.4, E – H, show images of reconstructions from another wild-type cell that is undergoing cell plate formation, which was identified in the datasets. The whole cell model shows the ER network, which consists of both tubular and cisternal morphologies, surrounding the cell plate that is developing within the cell (figure 6.3.4, E). When the cell plate is viewed without the reconstructed ER, in combination with the SBFSEM data for context of the plate orientation and shape within the cell, the plate is revealed to have a curved, wave-like structure, and is orientated diagonally across the cell (figure 6.3.4, F). When the modelled cell plate was observed in isolation, the more central regions of the plate can be seen to have undergone a greater degree of fusion of the cell plate material than areas towards the edges of the plate, which is comprised of more sparsely distributed, smaller particles (figure 6.3.4, G). This correlates with the more mature portion of the developing cell plate being located in the central zone, from which the plate is developing centrifugally outwards. When viewed at a different axis, the plate can be seen to be a relatively regular thickness throughout, exhibiting some curvature along its length (figure 6.3.4, H).

6.3.2 SBFSEM, 3D reconstruction and analysis of induced truncation 2 of RTNLB3-YFP over-expressing ZIO stained *Arabidopsis thaliana* root tip cells

Datasets of two *Arabidopsis thaliana* root tips over-expressing induced truncation 2 of RTNLB3-YFP, and two control roots of plants stably transformed with the inducible construct were collected using SBFSEM, analysed and further processed for 3D reconstruction. Control plants were treated with the induction solution (DMSO and Silwett[77] in DW), in the absence of dexamethasone.

Two cells in late stages of division undergoing cell plate formation were identified in the control datasets. One of these cells possessed a cell plate in a relatively late stage of maturation (figure 6.3.5, A), which had extended to an existing cell wall in closest proximity to the orientation of cell plate growth on one side (figure 6.3.5, B). The other cell plate analysed was at a very early stage of development, with a small but distinct region of cell plate material and surrounding ER present in the central region of the cell (figure 6.3.5, C). From the 3D reconstruction of the ER membranes it was apparent that the nuclear envelopes had begun to reassemble from the ER membrane; however, they had not yet completed reformation (figure 6.3.5, D). Reconstruction of the ER, nuclear envelopes and cross walls within several interphase cells in the dataset revealed fully formed nuclear envelopes, cell walls, and ER networks consisting of a mixed tubular and cisternal phenotype, all of which resembled wild-type cell samples (figure 6.3.5, E).

In the induced truncated RTNLB3-YFP over-expressing root tip samples, two cells of interest that appeared to be in the process of cytokinesis were identified. The first of these cells possessed two fully formed nuclear envelopes, however no distinct cross wall was evident, nor a developing cell plate (figure 6.3.6). In the SBFSEM dataset the nuclear envelopes are clearly identifiable, with a region between them present that exhibits lower contrast than the rest of the cytoplasm, which is evident in some of the micrographs (figure 6.3.6, A). This would be expected to correspond to cell wall or cell plate material, however the region and surrounding ER does not resemble the cell plates observed in wild-type and control cells (figures 6.3.3., 6.3.4 & 6.3.5).

Reconstruction of the ER membranes, nuclear envelopes and ZIO stained organelles revealed the 3D organisation of these structures within the cell (figure 6.3.6, B). The ER membranes present consisted primarily of a dense cisternal morphology, with some large aggregates that no longer resembled wild-type and control ER sheets (figure 6.3.6, B). The two nuclei were located in close proximity to each other in the central portion of the cell. The region of lower contrast than the cytoplasm indicative of cell wall material identified in the SBFSEM data (figure 6.3.6, A), did not differ to a sufficient degree in contrast to be reconstructed, especially as it appeared to diffuse into the surrounding cytoplasm rather than possessing defined boundaries, such as those observed in wild-type, control cells and between other cells in this sample. However, if a cell wall was present, ER in the structure of the intracellular network that is not constricted into desmotubules would not be expected to span this region. Analysis of the 3D model from different

orientations revealed that the ER membranes emanating from the nuclear envelopes had many thick membrane connections between them (figure 6.3.6, C). Therefore, either a cell wall is not present, the cell wall material has not fused into a cell wall structure, the ER has been incorporated into the cell wall material but has failed to become constricted to form desmotubules, or a combination of these factors. The presence of two fully formed nuclei in the absence of an identifiable cell plate without ZIO stained ER membranes highlighting this region, as observed in wild-type (figures 6.3.3 & 6.3.4) and control cells (figure 6.3.5), suggests that this cell has undergone cytokinesis and is in interphase.

Another cell possessing two nuclei within the same cell was identified in the SBFSEM data collected from an induced truncated RTNLB3-YFP over-expressing root tip, which unlike the cell described previously (figure 6.3.6) also contained a cell plate (figure 6.3.7, A – E). When the ER, nuclear envelopes and cell plate were reconstructed into a 3D model, the cell plate appeared to span the circumference of the cell in the orientation of cell plate growth (figure 6.3.7, A & B), indicative of a late stage of maturation. When the region of the cell plate within the modelled data was observed at higher magnification, the ER could be seen to traverse across this region, which was present in a high density in all of the surrounding area (figure 6.3.7, B).

To analyse the region of the developing cell plate in further detail, the ZIO stained organelles, ER membranes and cell plate material were reconstructed in this area (figure 6.3.7, C & D). In addition to the prior observations made regarding the association of the ER with the cell plate, mitochondria and plastids were present that were partially situated within the developing cell plate (figure 6.3.7, C & D). This had not been observed in the dividing wild-type and control cells analysed, where this region was devoid of other organelles. When the modelled cell plate material was viewed in isolation of the ER and other organelles (figure 6.3.7, E), the cell plate, despite having matured to span the entire cell to the existing cell walls, possessed large areas devoid of any cell plate material in the centre (figure 6.3.7, E). Some of the cell plate surrounding this region had fused to form large solid regions of cell plate material, which is also indicative of a late stage of cell plate maturation, with the remaining material mostly consisting of medium sized interconnected aggregates.

Interphase cells from these datasets were also analysed, and ER and cross walls reconstructed. Some cells contained a very high density of ER membrane in comparison to wild-type and control cells, comprised of both tubular and cisternal ER (figure 6.3.7, F).

6.3.3 SBFSEM, 3D reconstruction and analysis of RTNLB3-YFP over-expressing, ZIO stained *Arabidopsis thaliana* root tip cells

An SBFSEM dataset of a root tip over-expressing RTNLB3-YFP was also collected, analysed as a series of SEM micrographs, and further processed using 3D reconstruction. A cell with a cell plate in the process of development was identified in the dataset, in which the cell plate was well defined in the central region of the cell and surrounded by ZIO stained ER membrane (figure 6.3.8, A), as observed in the wild-type and control samples. Reconstruction of the entire volume of the ER, nuclear envelope membranes and ZIO stained Golgi bodies, plastid and mitochondria within the cell revealed a dense network of ER throughout the cell, with a fully formed nuclear envelope (figure 6.3.8, B). Observation of the cell plate region of the model revealed a high concentration of ER in association with the cell plate, which consisted of both tubules and cisternae, however no large cisternal sheets were present (figure 6.8.3, C).

Several cross walls between interphase cells and the ER present in the adjacent cells were also reconstructed from the SBFSEM data. A high density of ER was localised in close association with the cross walls, which in some consisted primarily of densely packed tubules and small cisternae (figure 6.3.8, D). Peripheral ER in two cells, with a cross wall in between, was also reconstructed without the wall material, where the ER structure was observed to be primarily in the form of highly fenestrated, small, interconnected sheets (figure 6.3.8, E). The reconstruction of the peripheral ER in another interphase cell revealed a high density of ER that was predominantly in the form of small, densely packed tubules with some small cisternae (figure 6.3.8, F).

Figure 6.3.1: SBFSEM data and images of 3D reconstructions from the datasets, showing cross walls and ER in interphase wild-type *Arabidopsis thaliana* root tip cells (cell wall material - yellow, ER - green).

A) A large cropped region from an SEM micrograph of a single SBF section, showing an area of numerous cells within the root tip. The ER, nuclear envelopes and some organelles exhibit the greatest degree of contrast in the sample as a result of ZIO staining. Cell walls exhibit the lowest levels of contrast within the imaged tissue.

B) A model of interconnecting cell walls separating cells within the root tissue, with the ER membrane either side of a cross wall in two adjacent cells. The ER morphology consists of a mix of tubules and large sheets.

C) The ER from the cell shown in figure B, without the cell wall material. The region of the cross wall is devoid of visible ER membrane, with no ER maintaining intracellular morphology across this area. ER is present in a dense accumulation against both opposing sides of the cross wall.

D) A model of a cross wall separating two adjacent cells, with the ER membrane either side of the cross wall also reconstructed. The ER morphology consists of predominantly large cisternae with some tubules.

E) An image of a different orientation of the reconstruction shown in figure D, without SBFSEM data included. Large ER cisternae are present across the surface of the cross wall.

F) A portion of a reconstructed cross wall and ER membrane, with an accumulation of ER in tubular and cisternal morphologies in close association with the cross wall.

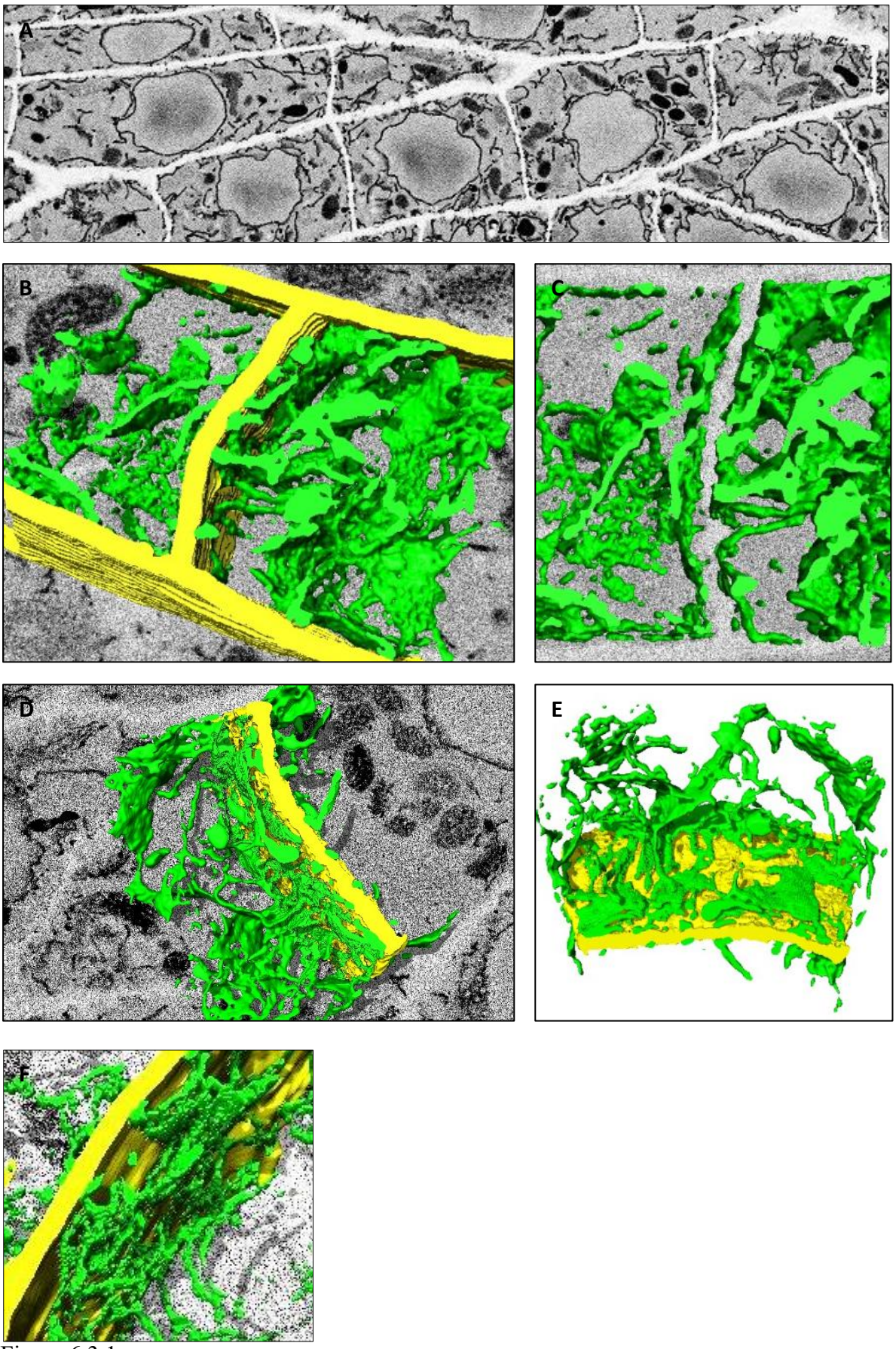


Figure 6.3.1

Figure 6.3.2: SBFSEM data and images of 3D reconstructions from the datasets, showing cross walls, nuclear envelopes and ER in interphase wild-type *Arabidopsis thaliana* root tip cells (cell wall material – yellow, ER – green).

A) A model of the reconstructed ER membrane in two adjacent cells. The site of the cell wall separating the cells is not evident from the overview of the ER from this orientation, as the membranes appear present and interconnected throughout the region without a clearly identifiable boundary indicating the presence of a cell wall. Arrows indicate areas in the locality of a cell wall where ER is present throughout, spanning two adjacent cells.

B) Image shows a crop of the reconstruction in figure A, from a different angle. A zone devoid of ER membrane spanning across it is evident, which corresponds to the region of low contrast within the SBFSEM data, indicative of cell wall material.

C) A model of a reconstructed asymmetrical cell wall and the surrounding cortical ER of two adjacent cells. A large amount of predominantly cisternal ER is present in close association with the cell wall.

D) A model of the cell wall material surrounding a single cell, with ER membrane within the cell reconstructed. Additionally, some ER in a neighbouring cell that is in close proximity to the dividing cross wall is also included in the reconstruction. ER within the cell is predominantly localised to the cell periphery near the cell walls, present as a mixture of tubular and cisternal morphologies.

E & F) Images show reconstructions of nuclear envelope, ER and cell wall material in two cells within which the nuclear envelopes are in close proximity to the cell wall. Short extensions of ER membrane extend from the nuclear envelopes to the cell walls. The ER within the cells is a mix of predominantly large cisternal sheets and tubules, with a large quantity of ER membrane lining the cell walls.

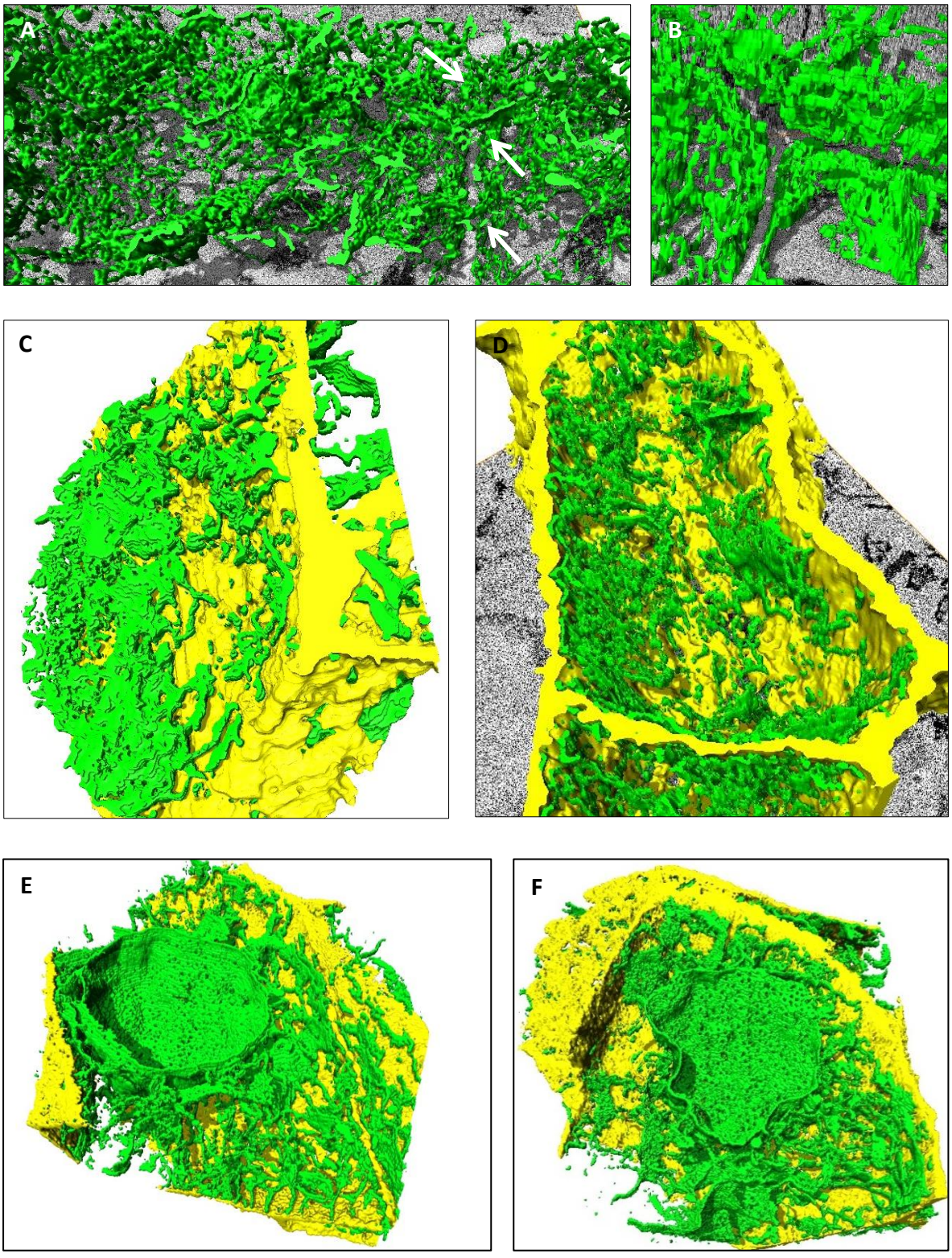


Figure 6.3.2

Figure 6.3.3: SBFSEM data and images of 3D reconstructions from the datasets, showing ER and cell plate material in a wild-type *Arabidopsis thaliana* root tip cell undergoing division (cell plate material – yellow, ER – green).

A) A montage of SEM images of SBF sections through a cell undergoing cell plate formation. The cell plate, consisting of low contrast cell wall material, is highlighted by ZIO stained ER membrane surrounding the developing plate. Arrows indicate the location of cell plate within each section. The cell pate is most developed in the central region of the cell, where it extends to the existing cell walls on either side. (Scale bar – 1000 nm).

B) Image of the central portion of the reconstruction of the dividing cell, with the ER, nuclear envelopes and cell plate material modelled. There is a dense accumulation of ER surrounding and interlacing with the cell plate material in the centre of the cell.

C) Image showing the modelled cell plate material in isolation from the ER, with a section from the SBFSEM dataset shown.

D) The modelled ER and cell plate shown in figure B, with a section from the SBFSEM dataset situated a quarter into the total volume to isolate a smaller portion of the reconstructed ER and cell plate. The ER is present in predominantly cisternal form and is highly concentrated around the cell plate.

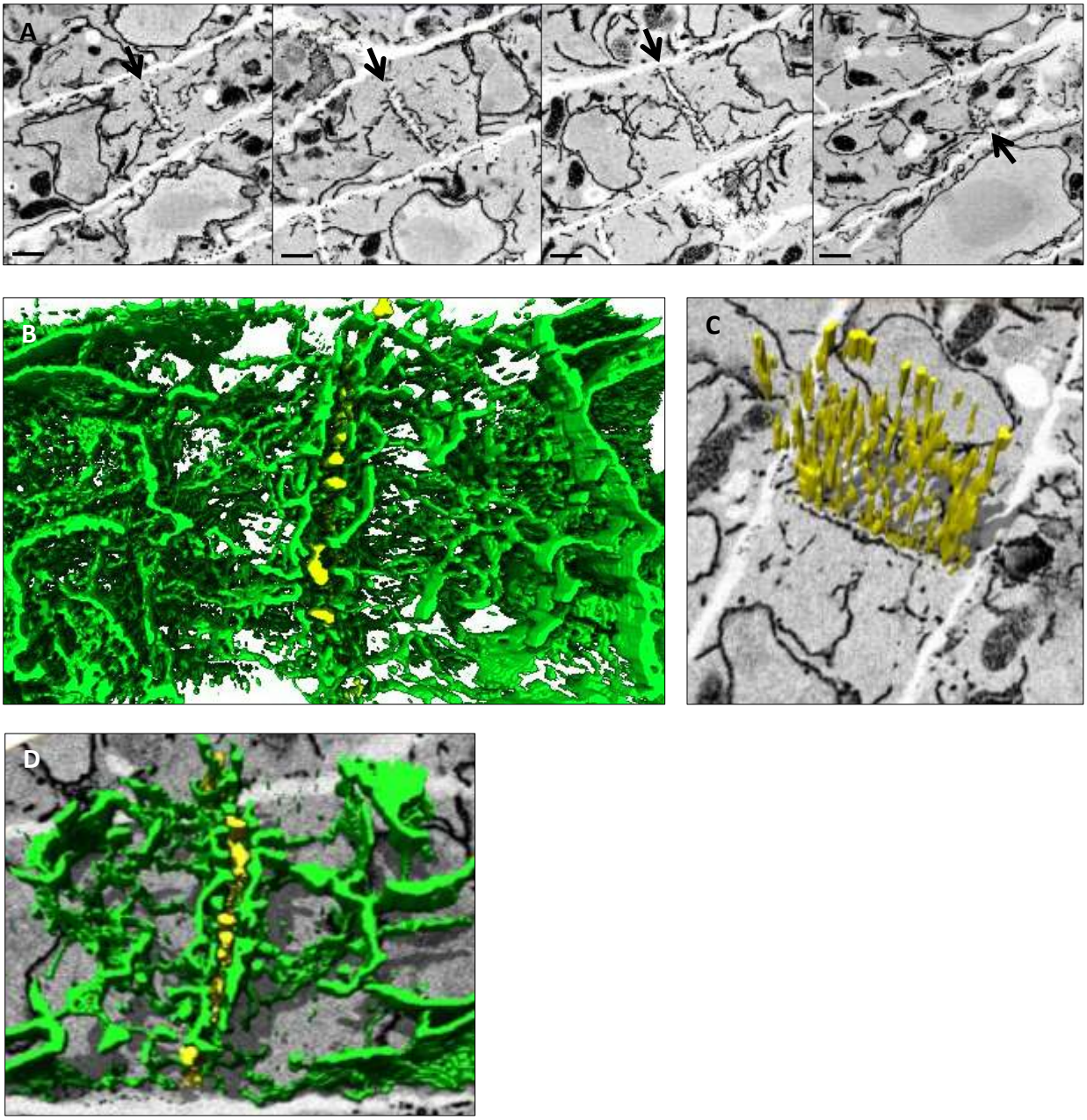


Figure 6.3.3

Figure 6.3.4: SBFSEM data and images of 3D reconstructions from the datasets, showing ER and cell plate material in wild-type *Arabidopsis thaliana* root tip cells undergoing division (cell plate material – yellow, ER – green).

A) A reconstruction of the ER, nuclear envelopes and cell plate material within a whole dividing cell, with a slice from the SBFSEM dataset shown from underneath the cell.

B) A magnification of the cell plate shown in figure A. The ER network surrounds the cell plate material in the central region of the cell.

C) A slice from the SBFSEM dataset with the 3D volume of ER modelled above it shown, which consists of a mixture of tubules and cisternae.

D) An image of the modelled cell plate material as shown in figures A & B, with the ER material set to high transparency.

E) A reconstruction of the ER, nuclear envelopes and cell plate material within a whole dividing cell.

F) The modelled cell plate material from the cell in figure E, with a slice from the SBFSEM dataset shown from approximately halfway through the cell volume. The cell plate is curved and positioned diagonally across the length of the cell.

G) Image of the entire modelled cell plate material in isolation, which consists of particles of varying sizes. In the more mature region of the cell plate towards the centre a higher density of larger interconnected regions of cell plate material are present compared to at the edges of the plate.

H) A different angle of the model shown in figure G, in which the cell plate can be seen to be a narrow defined region that exhibits curvature along its length.

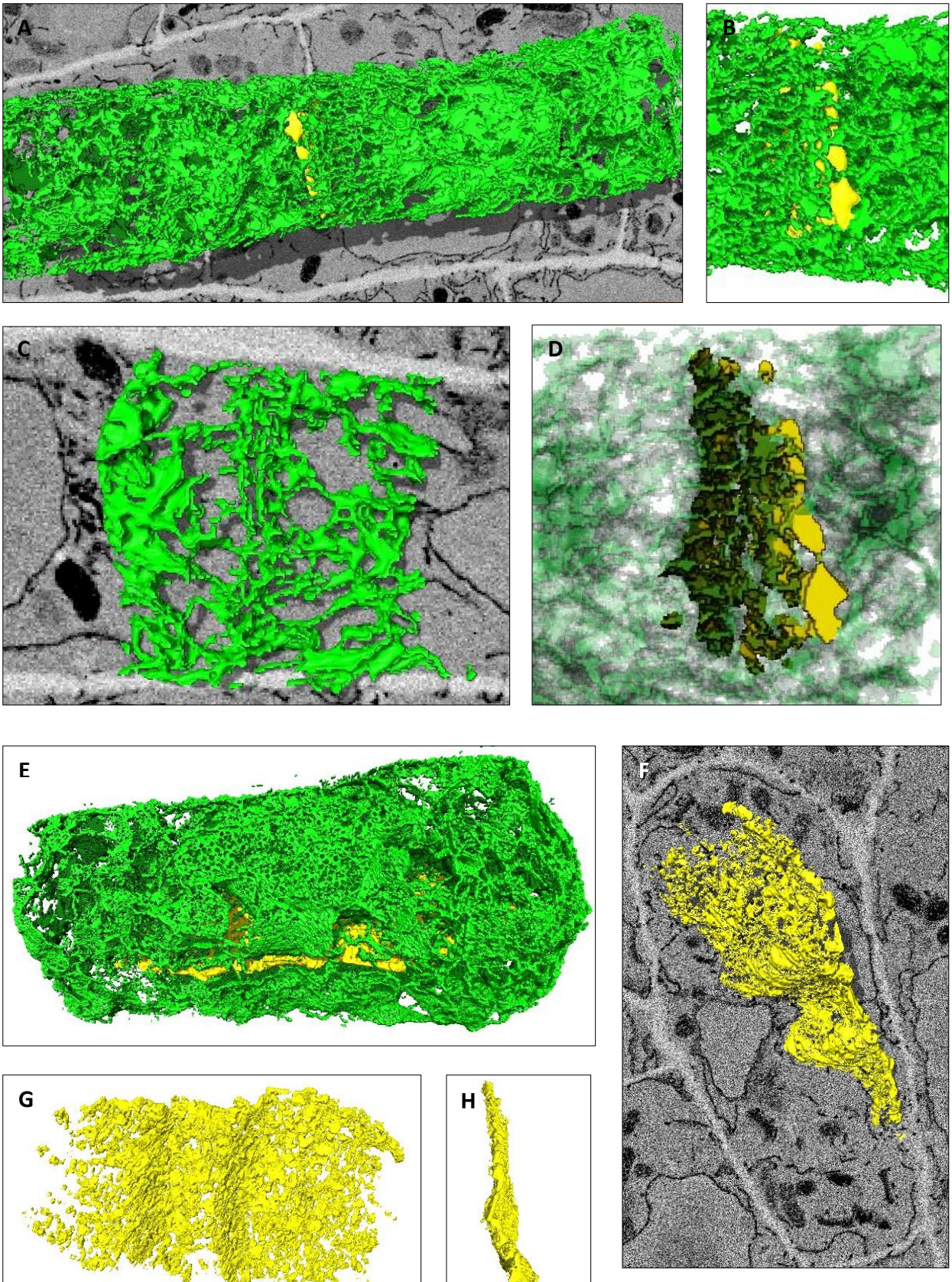


Figure 6.3.4

Figure 6.3.5: SBFSEM data and images of 3D reconstructions from the datasets, showing cross walls, developing cell plates and ER in control DMSO and Silwett[77] treated *Arabidopsis thaliana* root tip cells (cell plate material – yellow, ER – green).

A) An SEM micrograph of a single SBF section of a dividing cell, cropped from an SBFSEM root dataset, with nuclear envelopes, ER and Golgi exhibiting high levels of contrast from ZIO staining. Cell wall material and vacuoles are evident from having the lowest levels of contrast within the tissue. Cell plate material with ER membrane surrounding and traversing this region is present within the central portion of the cell (arrows, scale bar – 1000 nm).

B) An image of the reconstructed ER and cell plate material of the cell shown in figure A. The cell plate is at a late stage of maturation with much of the material fused, also having extended to the cell periphery and begun to fuse with the existing cell wall on one side. A high density of ER is associated with the cell plate over its surface, with some tubular ER traversing regions where the cell plate material is yet to fuse.

C) An SEM micrograph of a single SBF section of a cell at an early stage of cell plate formation, cropped from an SBFSEM dataset. The nuclear envelopes are yet to complete reformation and the region of the cell plate is poorly defined by the presence of highly contrasted ER and low contrast cell plate material, although distinguishable (arrows, scale bar – 2000 nm).

D) A portion of the modelled ER from the cell in figure C, with a slice from the SBFSEM dataset shown below. Nuclear envelopes have begun to reform from the ER either side of the site of where the new cell plate will develop however are incomplete at this stage (arrows), indicative of the cell being in telophase during the early stages of cytokinesis.

E) An overview of the reconstructed ER and nuclear envelopes from a portion of the SBFSEM dataset, consisting of three neighbouring cells within the root tissue. A section from the SBFSEM dataset is included from below the region of modelled membrane.

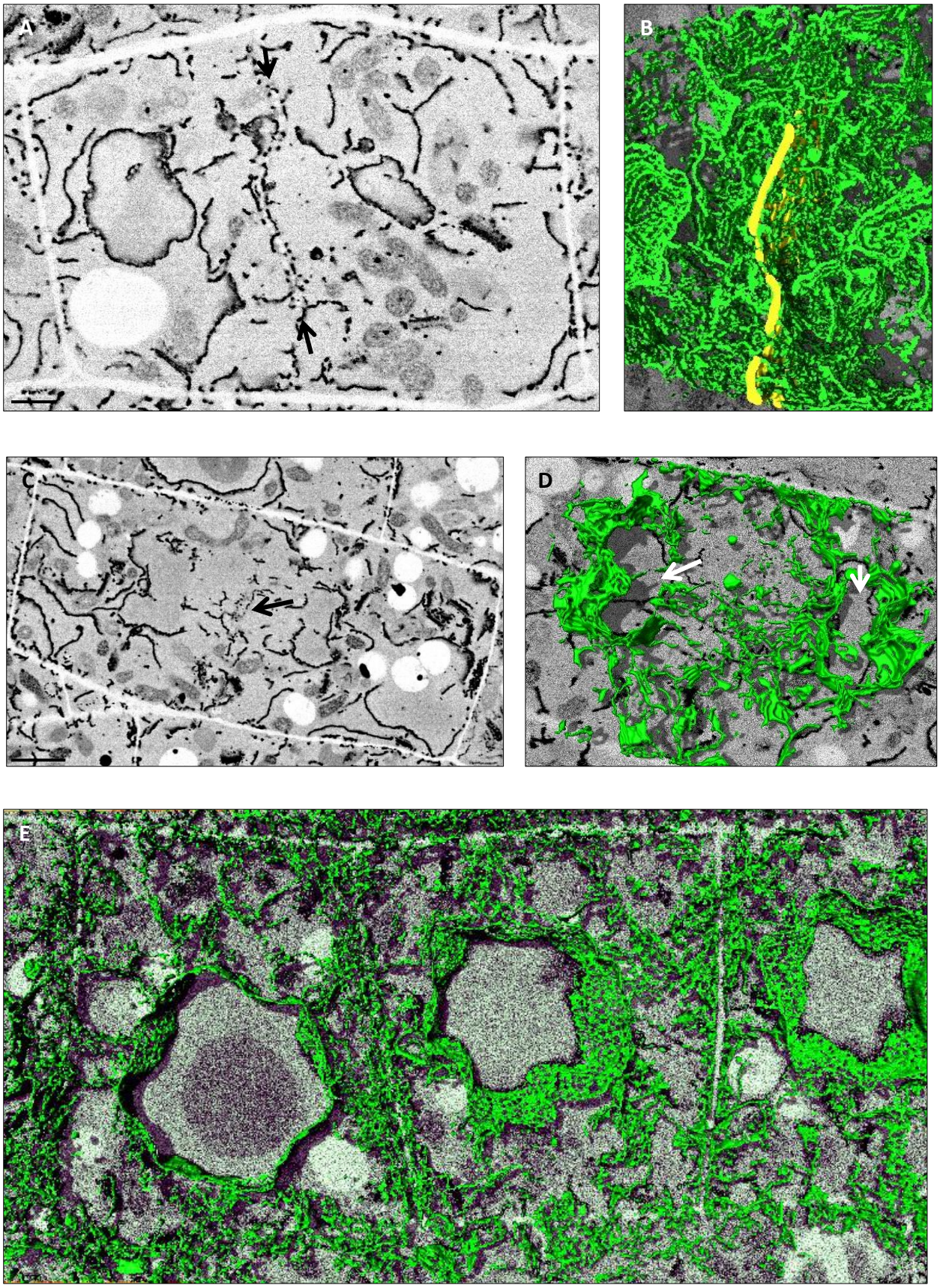


Figure 6.3.5

Figure 6.3.6: SBFSEM data and images of the 3D reconstruction of a mutant cell in an *Arabidopsis thaliana* root tip induced to over-express truncation 2 of RTNLB3-YFP (cell plate material – yellow, ER – green).

A) A montage of SEM images of SBF sections through a cell with two fully formed nuclear envelopes (triangles) with an absence of a cell wall. Within the centre of the cell, a region exhibiting a slightly lower degree of contrast, which is devoid of other organelles, is present (arrows; Scale bars – 1000 nm).

B) A model of the ER, nuclear envelopes and ZIO stained organelles within the cell shown in figure A, with images from the SBFSEM dataset framing the cell periphery. Dense aggregations of ER membrane and two nuclear envelopes in close proximity to each other are present within the cell.

C) A crop of the model shown in figure B, at an angle to show a cross section of the region between the two nuclear envelopes. Areas where ER membrane is continuous between the two nuclear envelopes are present (arrows), indicative of the absence of a cell wall separating the two nuclei, or lack of ER constriction to form desmotubules across cell wall material.

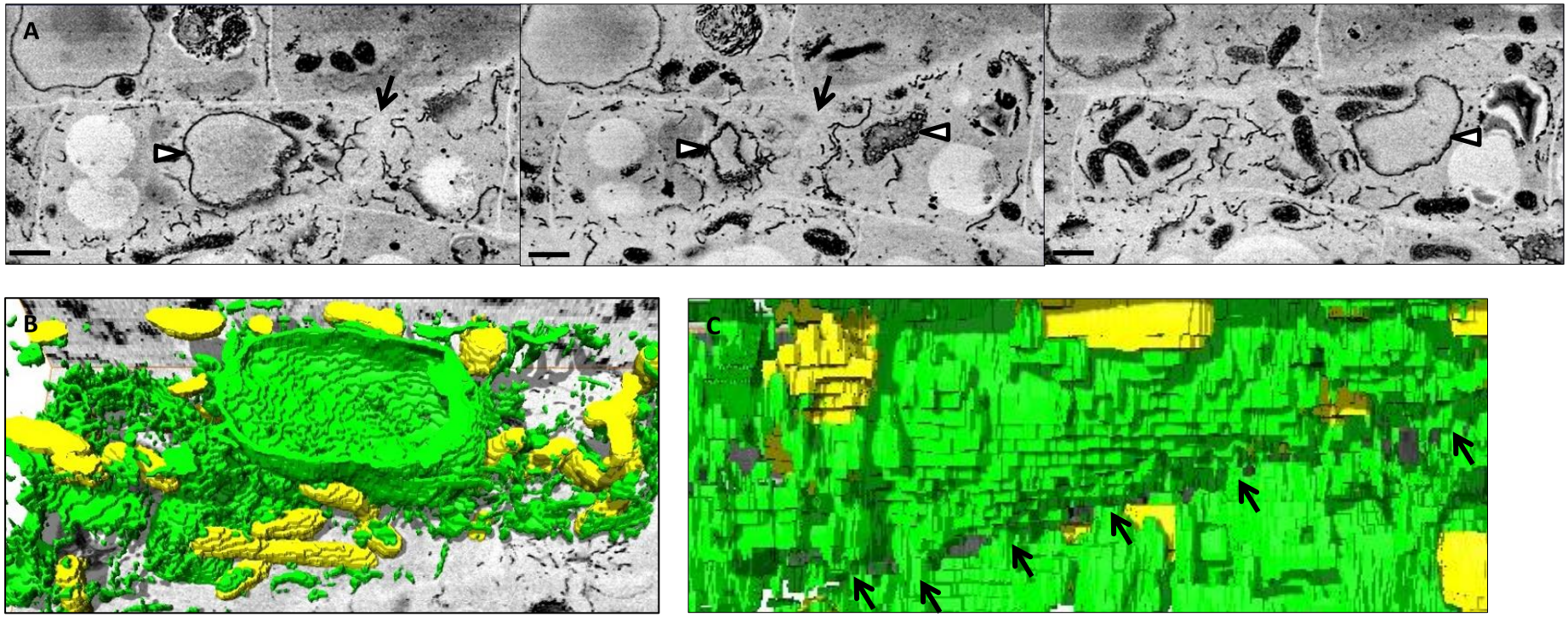


Figure 6.3.6

Figure 6.3.7: SBFSEM data and images of 3D reconstructions from the datasets, showing cross walls, developing cell plates and ER in *Arabidopsis thaliana* root tip cells induced to over-express truncation 2 of RTNLB3-YFP (cell plate material – yellow, ER – green, other organelles - purple).

A) A reconstruction of the ER, nuclear envelopes and cell plate material within a whole dividing cell, with a section from the SBFSEM dataset shown from underneath the cell. The cell plate appears to span the entire circumference of the cell and therefore be in a late stage of development.

B) A magnification of the cell plate region shown in figure A. The cell plate material is yet to fuse into a solid structure, with a high density of ER membrane present in this region that traverses across the cell plate.

C & D) Images showing reconstructions of the ZIO stained organelles, ER and cell plate material in the area of the cell plate, of the cell show in figure A. Other organelles are present in the region, which are housed within the structure of the forming cell plate. A high density of ER membrane is present either side of the cell plate material.

E) A model of the cell plate only from the cell shown in figures A-D, framed by images from of the SBFSEM dataset. The cell plate periphery corresponds with the existing cell wall at the edges of the cell, with the plate material having undergone varying extents of fusion, therefore consisting of a mixture of large sheets, smaller interconnected fragments, and isolated particles. The central portion of the cell plate is devoid of cell plate material, appearing as a large hole in the centre (stars).

F) Image showing a reconstructed cross wall and ER in two adjacent interphase cells, with a section from the SBFSEM dataset from below this region. The cell contains a very high density of ER membrane, consisting of both tubular and cisternal morphologies, surrounding the cross wall and throughout the rest of the cell volume.

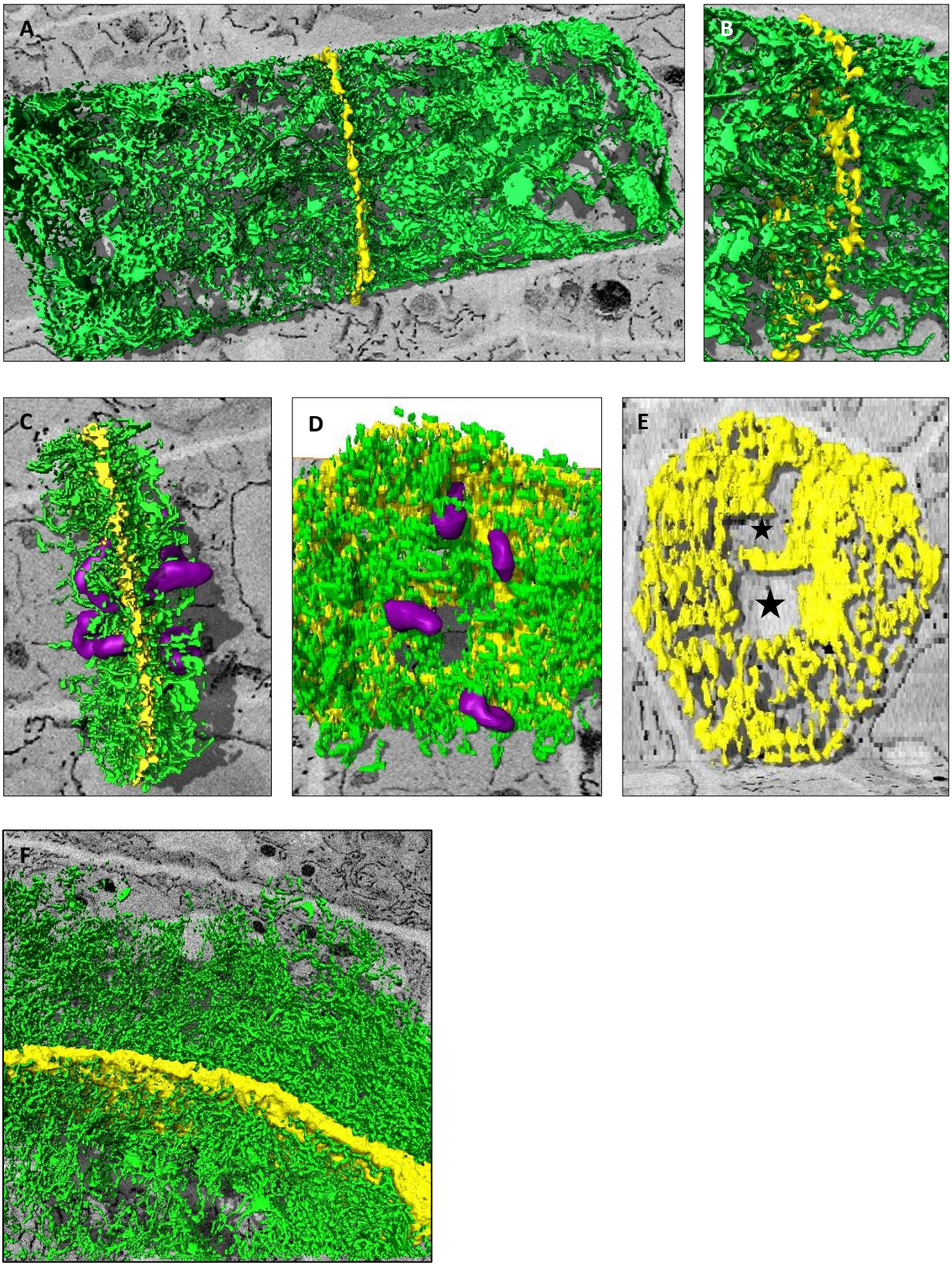


Figure 6.3.7

Figure 6.3.8: SBFSEM data and images of 3D reconstructions from the datasets, showing cross walls, developing cell plates and ER in *Arabidopsis thaliana* root tip celsl over-expressing full length RTNLB3-YFP (cell plate material – yellow, ER – green, organelles - purple).

A) A montage of SEM images of SBF sections through a cell undergoing cell plate formation. The developing cell plate region is highlighted by surrounding ZIO stained ER membrane. Arrows indicate the location of the plate within each section. The cell plate is most developed in the central region of the cell, where it extends across the cell to the existing cell walls on either side (scale bars - 2000 nm).

B) A reconstruction of the whole cell shown in figure A, with the ER, nuclear envelopes and ZIO stained organelles modelled. The cell contains a high density of ER membrane that consists of a mix of tubules and cisternae.

C) A higher magnification image of the model of the cellular ER and nuclear envelope membranes shown in figure B, focusing on the cell plate region within the centre of the cell. There is a high density of ER membrane throughout the cell and in association with the cell plate, which consists of a mix of tubular and small cisternae; however large cisternal sheets are absent.

D) A reconstructed cross wall separating two adjacent cells, with the ER membrane either side of the cross wall, consisting of densely packed tubules and small cisternae.

E) A reconstruction of the ER on either side of a cross wall (not modelled) within two adjacent interphase cells, including a section from the SBFSEM dataset of the area beneath this region. The ER membranes are composed primarily of small, fenestrated cisternae (arrows).

F) A reconstruction of peripheral ER within an interphase cell, with a slice from the SBFSEM dataset of the area beneath this region. There is a high density of ER membrane present, which is composed primarily of small, densely packed tubules and some small cisternae.

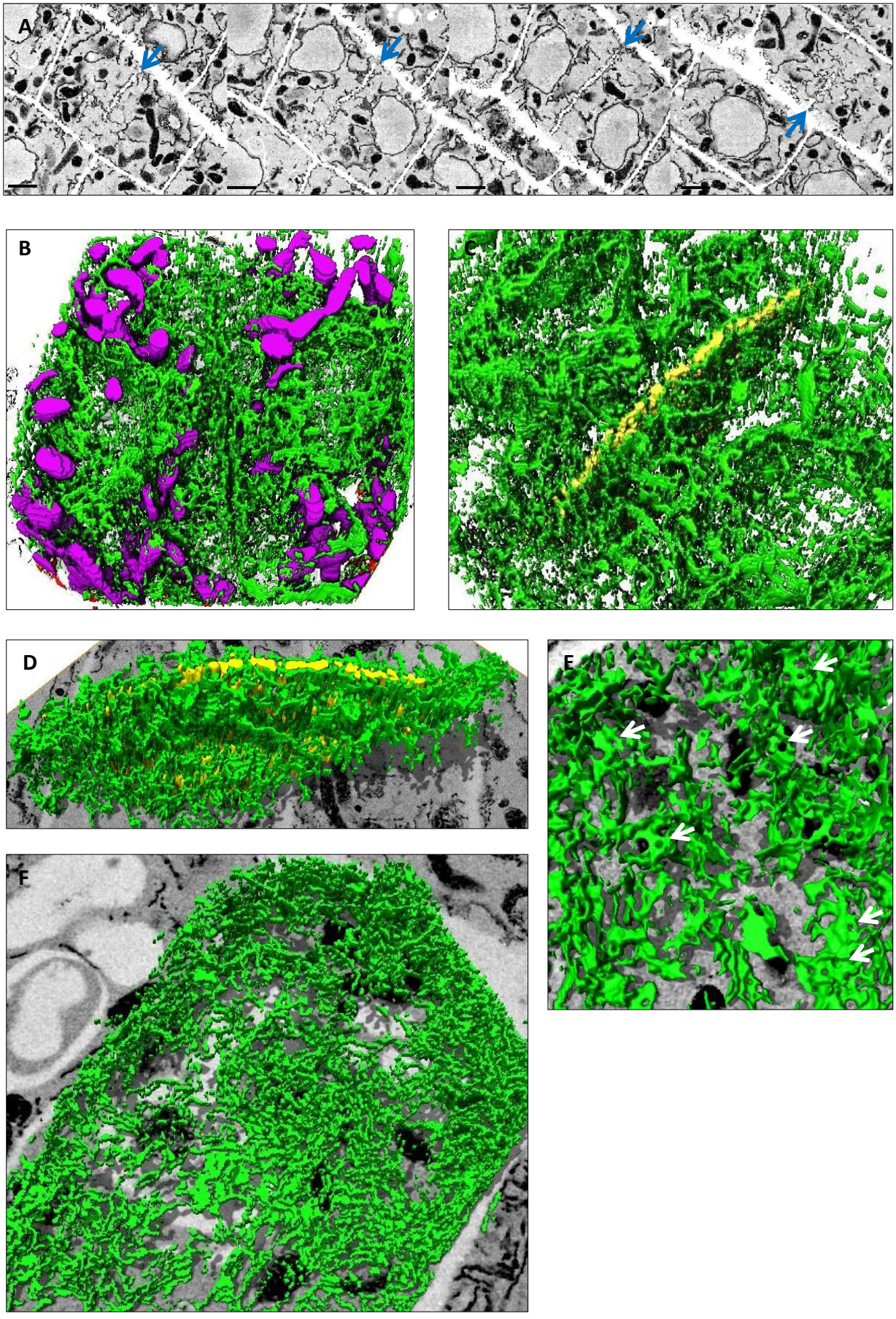


Figure 6.3.8

6.4 Discussion

Analysis of the ER, nuclear envelope membranes, cell walls and cell plates was conducted in wild-type, induced truncated and full length RNTLB3-YFP over-expressing *A. thaliana* root tip cells. In interphase cells large quantities of ER membrane was present in the peripheral regions of cells and over the surfaces of cross walls within all sample types. This is as expected for wild-type cells, as the majority of ER in plant cells is known to reside in the cell periphery, and the plant ER network (excluding the nuclear envelope) is often referred to as "cortical ER" for this reason (Ward & Brandizzi, 2004; Nakano, 2004). A similar ER distribution observed in cells over-expressing the RTNLB3 constructs indicates that expression of these constructs does not alter the localisation of the ER during interphase, which remained primarily localised to the cell periphery in all cells.

In wild-type cells, the ER morphology was a mixture of tubules and cisternae, with large cisternal ER sheets being the predominant form. This is in agreement with confocal microscopy based findings that ER cisternae are more common than tubules in meristematic cells (Ridge *et al*. 1999). Similar observations were made regarding the control samples, which was expected, as the plants were stably transformed with the inducible truncated RTNLB3-YFP construct and incubated in the components of the induction solutions except dexamethasone, the compound that triggers induction. Therefore, this confirmed that the cells remain as wild-type cells, and that the other components in the solution used for induction of the construct, do not result in phenotypic changes to the cells in isolation.

The ER structure within interphase cells of root samples in which the truncated RTNLB3-YFP construct had been induced often appeared similar to wild-type cells with regards to ER structure. Although over-expression of the construct is known to induce the formation of a predominantly cisternal structure, as wild-type meristematic *A. thaliana* root cells also possess a similar phenotype regarding ER morphology, this may account for the similarity. The non-curvature inducing mutant protein is likely incorporated into the existing cisternal ER membranes when expressed, as the network in these cells already exhibits a low degree of curvature. As the construct is induced for only a day prior to fixation of the material, the amount of over-expressed protein will be less than if over-expression had been induced for a longer period and therefore at this level the construct

likely distributes throughout the existing ER cisternae and nuclear envelope membranes, without inducing dramatic structural changes to the network in interphase cells. Some cells that were observed in these samples did contain a very high density of ER that was tightly packed together in comparison to wild-type, which could be a result of over-expression of the construct.

ER structure was found to vary in RTNLB3-YFP over-expressing interphase cells. Within most cells analysed the ER consisted of a densely packed network of tubules and small cisternae, with an absence of large sheets. However, in some cells the ER structure was found to primarily consist of small highly fenestrated sheets, without many tubules. Over-expression of the RTNLB3-YFP construct has been shown to result in a primarily tubular ER phenotype with an absence of cisternae in the leaves of *Arabidopsis thaliana* (chapter 4), *Nicotiana tabacum* (Sparkes *et al.* 2010) and in BY-2 monoculture cells (chapter 3). The phenotype observed in these samples of meristematic root tissue contained small cisternae within the cells, which may be due to differences between cell types and the wild-type ER structure. As cells in the rapidly growing region of root tips have particularly highly cisternalised ER networks, when the curvature inducing protein is over-expressed in these cells the ER may not become entirely transformed into a tubular network, instead resulting in networks of tubules and smaller cisternae than in wild-type cells. This may also account for the highly fenestrated cisternal ER phenotype observed. Within these cells the amount of over-expression may be lower due to variation between the cells, or the amount of cisternae may be even greater than average in these cell types. Therefore only fenestrations within the cisternal sheets form, as opposed to the sheets being transformed into tubules. RTNLB3 has been documented to localise to the curved edges of cisternae, as well as ER tubules (Sparkes *et al.* 2010). Therefore the over-expressed proteins could preferentially localise to the curved edges of fenestrations that form, or may already be present within the network. Lipid composition has also been shown to play a role in membrane morphology, and may be a regulating factor in addition to protein components. For example, the blocking of cyclopropynlsterol maturation in *A. porrum* seedlings induces fenestration of the Golgi membranes and that small variations in lipid constituents of membranes at a given time can have dramatic effects on membrane structure (Moreau, P. 2007).

Sites of plasmodesmata in the cross walls of all the SBFSEM data samples analysed consisted of ER that has been constricted into desmotubules, with their appearance

corresponding to that observed previously in this study using transmission electron microscopy and tomography (chapter 5) and what has been documented in the literature (Hawes *et al.* 1981; Hepler, 1982). In the 3D reconstructions of the ER in neighbouring cells surrounding the cross walls, no ER in a non-constricted tubular or cisternal form was found to pass through cell walls between cells. This would be expected in wild-type and full length RTNLB3 over-expressing samples, as no factor is present that would interfere with the constriction of the ER to form the desmotubule during cell plate formation. Within the roots where over-expression of the truncated RTNLB3-YFP construct had been induced, most of the existing cross walls would also be expected to contain fully formed desmotubules. This is because during the majority of growth of the root tissues expression of construct had not yet been induced.

The phenotype previously observed in 2D micrographs where ER appeared to pass between cells across some fully formed cell walls in all sample types was also further investigated. In wild-type cell samples, although similar observations were made within the original SBFSEM datasets, once the ER and cross walls had been reconstructed regions were found corresponding to the location of the cell wall where no ER was continuous in this form. It was concluded that the observations from the TEM and SBFSEM data were due to the appearance of the ER in relation to cell wall material within the 2D sections, and when the 3D volumes were reconstructed this revealed that defined boundaries devoid of visible ER membrane were consistently present. Therefore the suspected phenotype was not further investigated in the other samples.

Another observation made during 2D transmission electron microscopy analysis, regarding the nuclear envelopes of some cells appearing in very close proximity to, and almost embedded into cell walls, was also investigated further. Although the phenotype was observed within the mutant data set in the TEM study, as the number of cells and volume of material that can be observed was much smaller, the wild-type SBFSEM datasets were first analysed in relation to nuclear envelope localisation to see if it was present in these samples. The same phenotype was observed in WT samples, revealing that the phenotype is not a result of over-expression of the truncated RTNLB3-YFP construct, and is a characteristic of some cells within wild-type *A. thaliana* roots. Unlike in the limited 2D electron microscopy data, whole cell volumes could be viewed. Many nuclear envelopes that were closely associated with cell walls were found in cells that were very small or narrow in one orientation. Cell division and growth are occurring at a

relatively rapid rate within meristematic tissue, and therefore the nuclear envelopes may reform in close association with the cell walls for this reason.

The observations made of wild-type cell plates and those in the control samples were as expected based on the prior observations made in this study and the literature regarding cell plate structure and formation (Porter & Machado, 1960; Hawes *et al.* 1981; Samuels *et al*. 1995; Seguí-Simarro *et al.* 2004). The developing plates were situated within the central regions of the cells, forming centrifugally outward towards the existing cell walls. The cell plate material was present as vesicles in a range of sizes and as sheet like areas, forming fenestrated plates, depending on the degree of fusion that had occurred up to that point of maturation. A large quantity of ER membrane surrounded the developing cell plates in a lattice like structure, traversing through the plate and becoming incorporated into the structure as it develops. The ER within this region was composed of tubules and small cisternae, without large sheets in association with the plate. Sites of constricted ER that had formed desmotubules were observed in the SBFSEM micrographs although not included in the 3D reconstructions due to the reasons outlined in the results section (6.3.1).

Analysis of the dataset obtained of a RTNLB3-YFP over-expressing cell undergoing cell plate formation yielded similar observations as those for wild-type and control cells regarding cell plate structure and association of the surrounding ER, with no distinct phenotypic differences identified.

A cell was identified within one of the SBFSEM root datasets of a plant induced to over-express truncation 2 of RTNLB3-YFP that contained two fully formed nuclear envelopes where no distinct cross wall or developing cell plate was present. The ER within the cells was primarily cisternal in form, with some large masses of ER membrane that did not resemble wild-type or control cisternal ER. This is indicative of a high level of over-expression of the truncated RTNLB3-YFP construct, which has been shown to cause the formation of cisternal ER networks devoid of tubules in the confocal microscopy analysis conducted in this study (section 3.3.2) and that by Sparkes *et al.* (2010). Aggregates of the fluorescent construct that did not correspond to tubular or cisternal ER morphologies for which the structure could not be resolved using confocal microscopy, have also been observed previously in this work (section 4.4.2). These may account for the membranes that did not correspond to a tubular or cisternal ER phenotype.

Some cell wall or cell plate material did appear to be diffusely present within the central region of the cell; however, this lacked a surrounding lattice like framework of ER reminiscent of a cell plate, or any observable boundaries between the material and the cytoplasm, as are present for mature cell walls in the samples.

If an irregularly formed cell wall is present, despite it not being distinguishable as a clearly defined boundary, the ER spanning this region has not been constricted into desmotubules. As both nuclear envelopes are fully formed the cell is not in such an early stage of cell plate formation that a cell plate, if present, may not be clearly identifiable. Therefore, the cell is either at a late stage of division or has completed the cell cycle and is in interphase. This leads to the conclusion that material that will form the cell wall has not become localised in the region of the cell plate and properly fused during maturation, as it does during normal cell plate development.

The ER membranes that traverse this region also show no signs of constriction into narrow tubules or sites of plasmodesmata. This disruption to formation of a new cell wall could be due to the incapacity of ER membranes in which the mutant construct is highly expressed to form highly curved constricted structures. This could prevent fusion of the cell plate material into a solid structure, as well as preventing the formation of desmotubules within plasmodesmata. Some cell plate material would still be expected to be present in a high density in the region if cell plate formation was occurring, in a vesicular form as observed in wild-type, control and full length RTNLB3-YFP over-expressing cells. However, if the cell has completed the cell cycle and the plate has failed to assemble correctly, it is possible that these aggregates could diffuse into the cytoplasm if the correct molecular mechanisms are no longer in place to facilitate cell wall development. Another possibility is that RTNLB3-YFP plays some other role in the formation of the cell plate, and over-expression of the non-functional mutant form is interfering with this currently unknown function.

Another cell within the datasets obtained from the root tip samples induced to over-express truncated RTNLB3-YFP undergoing division and containing a cell plate in development was identified. The plate periphery spanned the circumference of the cell in the expected disc-like morphology observed in wild-type and control samples, which suggests a late stage of growth as cell plates form centrifugally outward from a central area of the cell towards the edges. However, unlike any of the other cell plates observed

in those samples or over-expressing full length RTNLB3-YFP, the cell plate had a large area devoid of any fused cell plate material in the central region. Some of the surrounding exterior areas of the cell plate had undergone a large degree of fusion, also indicative of a late stage of maturation.

Additionally, unlike anything observed in the other samples or the documented cellular organisation during cell plate formation, mitochondria and plastids were present that resided within the structure and spanned across it. During cell division and cytokinesis in wild-type plant cells, mitochondria and plastids have been shown to localise to distinct cytoplasmic regions away from the cell plate. Nebenführ, *et al.* (2000) demonstrated that, unlike the Golgi (which redistribute in a relatively high concentration around the cell plate and provide material for the structure), the mitochondria and plastids do not appear to be directly involved in this process. Nebenführ, *et al.* (2000) documented how, in BY-2 tobacco suspension culture cells, these organelles localise primarily to regions outside of the two forming nuclei in the cell periphery. Although some smaller plastids may be found closer to the cell plate, they remained excluded from within this region.

Therefore, over-expression of the truncated RTNLB3-YFP construct has dramatically altered cellular organisation and cell plate development within the cell. This has resulted in both an abnormal cell plate structure that is the reverse of wild-type cell plates, but also an unusual organisation of other organelles within the region. Due to the effect of the mutant construct cell plate formation may be delayed and temporal regulation of organisation of organelles within the cell during mitosis could be affected. Another possibility is that the construct interferes with the process of establishing the correct intracellular organisation and the cascade of signals to facilitate cytokinesis at an earlier stage.

The organelles may have either resided in this region and obstructed cell plate fusion, or have become situated there after an incomplete cell wall had formed but the cell otherwise progressed to interphase. Aside from this, the regions devoid of any cell plate material within the plate, that present as large open gaps, are not filled with other organelles, although there is a vacuole present that spans a portion of this region. Therefore another mechanism is likely responsible for this unusual phenotype as a result of over-expression of the truncated RTNLB3 construct.

As approximately half of the protein including two transmembrane domains and the C terminal end are deleted, it is possible that in addition to disrupting the ER membrane shaping properties that have been identified for RTNLB3, other functions of the protein may have been disrupted. As the protein becomes highly concentrated throughout the cell plate region during formation (as observed in the confocal microscopy carried out in chapters 3 and 4 of this study), it is possible that the protein in addition to curving the ER membranes plays another unknown role in the process of coordinating the formation of the cell plate structure as a whole. For example, if incorporated into the desmotubules of plasmodesmata with the conformation of RTNLB3-YFP as has been established within ER membranes (Sparkes *et al*. 2010), with the N- and C- termini extending into the cytoplasmic sleeve, either terminus could interact with surrounding proteins within the structure (Kriechbaumer *et al.* 2015). Therefore if the C- terminal region of the protein was involved in another interaction related to the structural integrity of the plate or signalling coordinating its formation, deletion of this region could result in an abnormal cell plate phenotype on a wider scale than at plasmodesmatal sites. The protein may also play other unknown roles within the cell, as there are 21 *Arabidopsis thaliana* isoforms of reticulon proteins. These have been hypothesised to possess membrane shaping properties based on possessing the RHD transmembrane regions suspected to induce curvature, which has been demonstrated in five of the plant reticulons thus far (Sparkes *et al.* 2010). This implies that the N- and C- termini, which exhibit far greater sequence variation than the conserved RHD domain, may have a variety of different roles within the cell. Such specific roles for each, alongside shared membrane shaping properties, would account for the evolution and existing presence of so many different isoforms of the protein within the same species. Recently, a study to identify RTNLB3 and RTNLB6 interacting proteins yielded a vast number of different potential interacting partners with a wide variety of functions (Kriechbaumer *et al.* 2015).

Kriechbaumer *et al* (2015) state that it is likely that the two proteins, both identified previously in a plasmodesmata proteomic screen (Fernandez-Calvino *et al*. 2011) and further indicated by their results to be plasmodesmatal components, interact in plasmodesmata and are involved in the formation of desmotubules (Kreichbaumer *et al.* 2015; Knox *et al.* 2015).

They identified known plasma membrane specific proteins that interact with RTNLB3, and a protein found at ER-plasma membrane contact sites known as Vesicle-associated

Membrane Protein-associated Protein27 (VAP27; Wang *et al.* 2014). VAP27 is known to bind to microtubules and interact with a protein known as NETWORKED3C (NET3C; Wang *et al.* 2014), which is a linker between the ER and cytoskeleton (Kreichbaumer *et al.* 2015). Kreichbaumer *et al.* state that this protein complex could facilitate anchoring and signalling between the plasma membrane and ER (Wang *et al*. 2014), and hypothesise that this same protein complex may be responsible for anchoring the desmotubule to the plasma membrane at the neck of or within plasmodesmata. Another interacting protein they identified is the $Ca2^{+}$-sensitive contractile protein synaptotagmin (SYTA; Yamazaki *et al.* 2010), which functions to regulate the distance between adjacent lipid bilayers up to approximately 5 nm (Lin *et al.* 2014). As the control of the degree of plasmodesmatal closure is very sensitive to $Ca2^{+}$ levels (Tucker and Boss, 1996), they propose that SYTA may be a candidate for facilitating close contact between the desmotubule and plasma membrane when there is an influx of $Ca2^{+}$ to the region. To support this hypothesis, they note that SYTA also appears at plasmodesmatal sites during cell plate development and hence forth remains localised to the entry points of the mature plasmodesmata (Schapire *et al.* 2008). Therefore the truncation of RTNLB3-YFP over-expressed here could lack the domain of the protein required for interactions with these proteins to occur, resulting in abnormalities in organisation and structure of the ER and cell plate formation, as found in this study. Overall, this data indicates that the correct organisation of the ER is required for successful cell plate formation and cytokinesis. The impact of over-expression of the truncated RTNLB3 construct altering ER morphology may be sufficient to disrupt this process to the degree that it cannot occur. Alternatively, the influx of a mutant form of the protein could prevent the function of endogenous RTNLB3 in facilitating the formation of the cell plate and/or desmotubules within it. A combination of these factors, or other unknown roles the protein plays in cell plate formation and in maintaining the integrity of cell wall structures, could account for the phenotypes presented here.

Chapter 7. Final discussion and conclusions

7.1 Overview of research undertaken

This study has investigated the function, localisation & dynamics of the RTNLB3 protein in both interphase and dividing plant cells, expanding on the existing limited data. This reticulon was chosen as one of three found in a plasmodesmatal database and thus may be implicated in the formation of desmotubules (Fernandez-Calvino *et al*. 2011). The role of RTNLB3 in shaping the endoplasmic reticulum, and the involvement of the protein and the ER in the process of cell plate and plasmodesmata formation was assessed. As set out in the aims of this work, methodology was developed that facilitated high resolution three-dimensional modelling of the ER network in large cellular volumes, and analysis was carried out looking at interphase cells and those undergoing cell plate formation.

The localisation of full length and truncated RTNLB3 and the effect of over-expression of the constructs on the structure of the ER network in comparison to wild-type, were first investigated in a *N. tabacum* BY-2 monoculture cell model (chapter 3). Both interphase and dividing BY-2 cells were analysed using confocal fluorescence microscopy. Preliminary electron microscopy work and optimisation of methods was also subsequently carried out with the wild-type and full length RTNLB3-YFP over-expressing cell lines.

7.2 The truncated RTNLB3 mutant construct in BY-2 *N. tabacum* cells

Following numerous attempts and changes to the methodology, it was concluded that over-expression of the truncated construct in the BY2 cell system is usually lethal in the long-term following transformation. This was based on the fact that a stably transformed BY-2 cell line over-expressing truncated RTNLB3-YFP could not be generated for cell cycle analysis and that a plasmolysed, damaged phenotype was observed in some cells that had been over-expressing the construct for extended periods. Due to the further questions this posed regarding the effect of mutant RTNLB3 over-expression on cells during cell division, and within a whole plant system, as well as some impracticalities found in using BY-2 suspension cultures for TEM preparation when screening a high number of samples for cells undergoing cell plate formation, it was decided that another model organism would best be employed for further study.

7.3 Use of the *Arabidopsis thaliana* whole plant system

It was decided that a whole plant model organism, *Arabidopsis thaliana*, would be the most appropriate choice for further addressing the research questions of this work, due to its suitability for TEM sample preparation, cell division study, ease of generation of stably transformed plant lines in a relatively short time frame (using the well-established floral dip method; Bent. 2006), and because the RTNLB3 sequence used for the constructs is the endogenous *A. thaliana* sequence. *Arabidopsis thaliana* is also one of the most widely used models in plant genetic, molecular and cell biology research. Therefore work conducted in this system can be analysed in the context of other findings within the plant, as well as research conducted in other different species and cell lines.

RTNLB3 had not been previously analysed in a stably expressing whole plant system and no studies had investigated reticulon proteins in relation to cell plate formation and cell division in this type of model. Therefore, this work provides novel insights into the phenotype of the stable over-expression of RTNLB3 and a non-functional mutant of the protein in a variety of cell types; *A. thaliana* interphase cotyledonary leaf cells, interphase root tip cells, and cells undergoing cytokinesis. As the phenotypes observed for ER localisation and dynamics of RTNLB 1-4 and 13 have been found to be similar in *N. tabacum* leaf cells (transiently over-expressing full length and truncated constructs; Sparkes *et al.* 2010), the findings here may be indicative of what can be expected for other RTNLB constructs within stably over-expressing Arabidopsis plants.

7.4 Conclusions regarding RTNLB3, truncated RTNLB3 and the cell cycle from light microscopy

Upon this work being undertaken no cell cycle related work with RTNLB proteins had been carried out in plant cell system; during the course of this study however, fluorescence microscopy work was published (Knox *et al.* 2015). This had focused on the over-expression of reticulon constructs, including those of RTNLB3, in relation to plasmodesmatal formation in BY-2 cells. The constructs used by Knox *et al.* (2015) for full length and truncated RTNLB3 were the same sequences as those employed in this study as a result of collaboration between research groups. The results obtained in this study are in agreement with their findings regarding RTNLB3's suspected involvement in desmotubule formation. Their data supports the hypothesis presented here that the protein is implicated in the formation of the cell plate and ER structure during cytokinesis. They

did not take their investigation further into high resolution electron microscopy based imaging, and therefore to date no other electron microscopy based work has been carried out investigating the expression of these constructs and the phenotypes that have been observed using light microscopy as in the early stages of this study and numerous others (Sparkes *et al.* 2010; Tolley *et al*. 2010; Knox *et al.* 2015).

7.5 Lethal *Arabidopsis thaliana* phenotype of truncated RTNLB3-YFP construct

As with the BY-2 cell model, stable over-expression of the truncated RTNLB3 construct proved to be lethal in whole plants following gametophytic transformation. Due to this plant lines could not be established in parallel to those over-expressing full length RTNLB3. Based on this result it can be concluded that over-expression of the truncated RTNLB3 construct is sufficiently disruptive to cell survival and completion of the cell cycle to result in lethality in both a monoculture cell system and whole plants when stably over-expressed. It was expected that this would be the case in Arabidopsis, due to the lethality discovered in BY-2 cells if this was a result of the presence of the construct interfering with cell function. Therefore, the lethality found following floral dipping of Arabidopsis plants provides confirmation that this is indeed the case, and is not due to the truncated construct being over-expressed in a monoculture cell model of a different species than the full length sequence originated from. The over-expression of the non-functional mutant out competing the native full-length RTNLB3 protein could be resulting in this lethal phenotype due to several mechanisms. The protein may be involved in a specific role relating to desmotubule or cell plate formation, and over-expression of the truncated construct therefore interferes directly with this process. Alternatively, the over-expression of the mutant protein could be out competing the function of all of the endogenous RTNLB proteins in relation to ER membrane shape and the resulting increasingly cisternalised ER phenotype may be too disruptive to cell function, cell plate formation and division within meristematic cells, for the cells to function and/or cell division to occur properly. Therefore regulation of the morphology of the ER network may be critical for the successful orchestration and completion of cytokinesis within meristematic plant cells.

In whole plants the construct can be concluded to be lethal at an early stage of plant development and growth. When the seeds are grown on selection it is not clear which seedlings die off shortly after germinating due to lacking the construct and the selection

media, and which may have died at a similar stage due to construct over-expression. However, seeds obtained from the floral dips were also grown without selection and screened for expression following several days of growth and no fluorescent seedlings were identified in any of these samples. As the parallel transformations carried out with the full-length construct yielded many positive transformants, with 10 plants for establishing stably expressing lines obtained from a single plate, it is likely that over-expression of the truncated construct is lethal at an embryonic stage and these seeds do not germinate. Due to the lethal phenotype of the mutant, to enable comparison with the full-length RTNLB3 construct phenotype in further work, an inducible construct was employed.

The lethality is most likely specific to cell division, as BY-2 (chapter 3), Arabidopsis cotyledonary and root (chapter 4), and *N. tabacum* leaf cells (Sparkes *et al*. 2010), transiently transformed with the construct or expression is induced in did not die as a result of over-expression over the course of the experiments. Nor showed signs of cell death or damage. This is indicative of the fact that the presence of the mutant as opposed to the full length RTNLB3 construct disrupts the process of cell division. In combination with the subsequent findings of the abnormal phenotypes of cell plates identified in the electron microscopy within this study, in root cells where an inducible form of the construct had been expressed, this is likely due to disruption of ER structure and formation of the cell plate during cell division and cytokinesis. In addition to this, the existence of ER Arabidopsis mutants within which the network is highly or entirely cisternalised that germinate and grow into whole plants (Eastmond *et al.* 2011), is indicative that the stable over-expression of a mutant ER shaping protein that results in cisternalisation of the ER network is not in isolation sufficient to result in lethality of plants. However, the mutants do exhibit a deformed phenotype with poor growth and health, and therefore the cisternalisation of the ER does have a significant impact on plant growth. Therefore if another factor was present that also disrupted cell function and division, the combined impact could be lethal.

7.6 Over-expression using the 35S promoter as opposed to native

The 35S promoter employed in this study for over-expression of the constructs enabled observation of ER phenotypes for high levels of full length and truncated RTNLB3 within

a variety of plant cells. If a native promoter was used for the fluorescent mutant construct, the high number of remaining, functional plant reticulon family members, would likely compensate for the non-functional mutant protein. Likewise, if the full length protein was expressed under a native promoter, although the localisation of the protein could be observed, the constriction phenotype observed in this study and those by Sparkes *et al.* (2010) and Tolley *et al.* (2010) would not be apparent as the protein would be present at levels corresponding to wild-type ER structure. However, it would be interesting to assess the localisation of full length and truncated RTNLB3-YFP in more detail using super-resolution laser scanning microscopy and TEM immunogold labelling, expressed under a native promoter. This would reveal the native distribution of the protein throughout the cell cycle, how much is recruited to the cell plate as it forms, and could facilitate imaging of the protein localised specifically at plasmodesmatal sites at natural levels.

7.7 Conclusions, considerations, and suggestions for future work

As other RTN proteins are known to play similar ER membrane curvature inducing roles in cells (Sparkes *et al.* 2010; Tolley *et al.* 2010; Knox *et al.* 2015), if an RTN protein is knocked out or silenced in a mutant, there may not be an ER phenotype evident in these plants. Much work has focused on shared characteristics of the protein family rather than unique functions of individual RTN protein family members. Therefore, a deletion of RTNLB3 rather than over-expression may yield a similar phenotype to that found in this study if it is unique in its function involved in cell plate formation. It would be interesting to investigate whether any phenotype is observed in mutants generated using different methodology than over-expression of a truncation, such as RNAi or knock out. As RTNLB6 has also been identified in the plasmodesmatal proteome and shown to localise to cell plates and plasmodesmata, it could play a similar or complementary role through interactions. Therefore if no phenotype was observed in a deletion mutant of RTNLB3, if both RTNLB3 and RTNLB6 were deleted and they play complementary roles within plasmodesmata and cell plate formation, a similar phenotype as evidenced here would be expected to become apparent. If RTNLB6 plays a different role and functions in synergy with RTNLB3, than a phenotype distinct from that observed for mutant RTNLB3 in isolation may be evident in such a double mutant. A study investigating both of these proteins could decipher whether or not they each serve unique functions in this process

and reveal a more refined picture of the involvement of ER membrane shaping proteins in plant cell division, cell plate and plasmodesmatal formation. Using CRISPR to knock down the proteins would be a highly specific approach that could be employed for such a study.

In addition to the role of RTNLB3 in cell plate formation, the importance of the ER and its structure in this process is revealed in the findings of this work. Other research on cell plate mutants thus far has not focussed on the ER network and has primarily elucidated the source of cell wall material to the cell plate as it undergoes development (Scheible & Pauly, 2004; Fendrych *et al.* 2010), the composition of this material (Chen & Kim, 2009), the signalling pathways, and proteins that are involved in orchestrating cell plate formation and cytokinesis (Nishihama *et al.* 2001), and the arrangement of the cell wall itself (Smith *et al.* 1996). Therefore, further research is required to elucidate what roles the ER plays in the organisation and formation of the cell plate as it develops, as the proper orchestration of this is evidently of crucial importance to the process.

The SBFSEM technique employed in this study, although enabling a large quantity of tissue to be screen efficiently to identify cells undergoing cell plate formation, did not allow for as fine analysis of structural detail of forming plasmodesmata within cell plates as can be achieved with TEM tomography. However, even with a TEM tomographic approach it would be difficult to analyse the effect of over-expression of the mutant construct on desmotubule structure. The lethality of the construct and lack of stably transformed plant lines presents a challenge in doing so, as does the subsequent solution employed here of using a construct that was induced for a short period of a day. The plasmodesmata within fully formed cross walls would be expected to be as wild-type in induced plants, and the abnormal phenotypes of cell plates observed varied so widely and were structurally so different from those in wild type and full-length over-expressing samples, that the usual fine structures of plasmodesmata would not be accurately identifiable if present within the cell plate. Consistent induction of the construct with dexamethasone over a longer time course of plant development, prior to TEM tomographic analysis, may be a viable method for conducting such resarch in future, which may reveal more abnormal cell plates or incorrectly formed cross walls due to the longer over-expression time, and perhaps contain unusual plasmodesmatal structures that could then be subject for analysis.

Another aim of this thesis was to analyse the ER in cells including wild-type and those over-expressing RTNLB3 constructs at high resolution using 3D imaging techniques and to develop a method of doing this efficiently and accurately. The ZIO technique was employed to selectively stain membranous cellular components including the ER network, so that these membranes could be reconstructed in 3D. In combination with SBFSEM this proved to be an incredibly powerful combination of methods as a tool for research analysing ER morphology.

Although there have been some recent publications describing this combination of techniques for plant ultrastructural analysis by our research group (Hughes *et al.* 2014; Kittelmann *et al.* 2016), this is the first time that the ZIO staining technique has been employed with SBFSEM for an in-depth study to investigate the organisation and morphology of the ER in plant cells.

The SBFSEM data collection of ZIO fixed samples yielded a vast quantity of high resolution raw data for further analysis, from several root samples of each data-set. During this study the number of cells, volume of material modelled, and research questions investigated, were limited by the time available to carry out this work. Much further analysis could therefore be carried out on the SBFSEM data obtained in this research, both building on the results of this study and with a focus on novel research questions. With more time to further this research measurements of volumes of the ER and the surface area to volume ratio in many whole cells could be collected and the morphological changes that occur to the ER during the plant cell cycle could be documented. The same analysis could also be carried out for different cell types within the plant tissues and be related to cell function to provide further insights into the fundamental structural characteristics of plant cells and organelles on an ultrastructural level.

This is also applicable to other organelles that are stained within the samples, such as the Golgi bodies, nuclear envelopes and plastids, and therefore these samples could be used to answer other research questions relating to these organelles, as well as for further ER analysis. For example, the Golgi bodies within dividing cells could be modelled at various stages of the cell cycle. Cell plate formation and their involvement in the process could be analysed in greater detail than has ever been previously carried out. The preparation can also be optimised for different plant material and be utilised to research a

wider range of cell types and plant species. Therefore, this work provides a demonstration of the viability of a very valuable technique that is currently in its infancy, for plant ultrastructural analysis on a subcellular level within large volumes of data, and from a large numbers of cells within tissues.

Using semi-automated thresholding techniques to isolate highly stained organelles increases accuracy in comparison to using conventionally fixed TEM samples, which possess a lower degree of contrast between cellular components. Additionally it facilitates more rapid modelling of these structures and thus enables far larger quantities of data to be processed in three dimensions than previously has been possible with ssTEM and tomography with the same hours of labour. Therefore, higher numbers of individual organelles, larger volumes, and numbers of cells can be compared. This has been one of the primary limiting factors conventional 3D electron microscopy techniques.

Within this study, sample size in relation to the number of individual root tips examined remained a limiting factor. Another was the number of cells undergoing cell plate formation within each sample. This is due to time constraints regarding the number of whole roots that were prepared and could be analysed, as well as the cost of each run on the SBFSEM system. However, the amount of data collected of whole plant roots with this technique, and the speed at which it can be modelled with regards to cell volume, is unprecedented in comparison to that which has can collected in a similar time-span by an individual using ssTEM and TEM tomography for a similar study of ultrastructural ER analysis.

In addition to the findings relating to RTNLB3 protein function within plant cells, the three- dimensional modelling of the wild-type ER in interphase cells, in relation to cross walls, surrounding cell plates, and throughout whole cells carried out in this work, comprises a far greater volume of high resolution detail for ER morphology and cellular localisation than has previously been documented. Therefore, the analysis in this research contributes a more complete picture of ER structure and distribution in three dimensions within whole plant cells than had been detailed prior to this work.

Chapter 8 - References

Alberts, B., Johnson, A., Lewis, J., Morgan, D., Raff, M., Roberts, K. & Walter, P. (2014) *Molecular Biology of the Cell*. 6th Edition. New York: Garland Science

Anderson, D. J. & Hetzer, M. W. (2008) Shaping the endoplasmic reticulum into the nuclear envelope. *Journal of Cell Science* 121, 137 - 141

Anderson, D. J., Hsiao, J. P. & Hetzer, M. W. (2009) Recruitment of functionally distinct membrane proteins to chromatin mediates nuclear envelope formation in vivo. *The Journal of Cell Biology* 186, 183 – 191

Antonin, W. (2009) Nuclear envelope: Membrane bending for pore formation? *Current Biology* 19, 410 - 412

Araki, K., & Nagata, K. (2012). Protein folding and quality control in the ER. *Cold Spring Harbor Perspectives in Biology* 3, 1 – 25

Bang, B. H. & Bang, F. B. (1957) Graphic reconstruction of the third dimension from serial electron microphotographs. *Journal of Ultrastructure Research* 1, 138 – 139

Baron-Epel, O., Hernandez, D., Jiang, L., Meiners, S. & Schindler, M. (1988) Dynamic continuity of cytoplasmic and membrane compartments between plant cells. *The Journal of Cell Biology* 106, 715 - 721

Baumann, O. & Walz, B. (2001) Endoplasmic reticulum of animal cells and its organization into structural and functional domains. *International Review of Cytology* 205, 149 – 214

Bayer, E. M., Mongrand, S. & Tilsner, J. (2014) Specialized membrane domains of plasmodesmata, plant intercellular nanopores. *Frontiers in Plant Science* Editorial Article, 1 -3

Beemster, G. T. S. & Baskin, T. I. (1998) Analysis of cell division and elongation underlying the developmental acceleration of root growth in *Arabidopsis thaliana. Plant Physiology* 116, 1515 – 1526

Benfey, P. N. & Chua, N. H. (1990) The Cauliflower Mosaic Virus 35S Promoter: Combinatorial Regulation of Transcription in Plants. *Science* 250, 4983, 959 - 966

Benning, C. (2009) Mechanisms of lipid transport involved in organelle biogenesis in plant cells. *Annual Review of Cell and Developmental Biology* 25, 71 – 91

Bent, A. F. (2006) Arabidopsis thaliana floral dip transformation method. In: Wang, K. (ed.) *Agrobacterium protocols* New Jersey: Humana Press 87 - 103

Benyamini, P., Webster, P. & Meyer, D. I. (2009) Knockdown of p180 eliminates the terminal differentiation of a secretory cell line. *Molecular Biology of the Cell* 20, 732 – 744

Bernales, S., McDonald, K. L. & Walter, P. (2006) Autophagy counterbalances endoplasmic reticulum expansion during the unfolded protein response. *PLOS Biology* 4, e423

Blackman, L. M. & Overall, R. L. (1998) Immunolocalisation of the cytoskeleton to plasmodesmata of *Chara coralline*. *The Plant Journal*, 14, 733 – 741

Bock, D.D., Lee, W.C., Kerlin, A.M., Andermann, M. L., Hood, G., Wetzel, A. W., Yurgenson, S., Soucy, E. R., Kim, H. S. & Reid, R.C. (2011) Network anatomy and in vivo physiology of visual cortical neurons. *Nature* 471, 177 – 182

Boevink, P., Martin, B., Oparka, K., Santa Cruz, S. & Hawes, C. (1999) Transport of virally expressed green fluorescent protein through the secretory pathway in tobacco leaves is inhibited by cold shock and brefeldin A *Planta* 208, 392 - 400

Borgese, N., Francolini, M. & Snapp, E. (2006) Endoplasmic reticulum architecture: structures in flux. *Current Opinion in Cell Biology* 18, 358 – 364

Borrett, S. & Hughes, L. (2016) Reporting methods for processing and analysis of data from serial block face scanning electron microscopy. *Journal of Microscopy* 263, 3 - 9

Brandizzi, F., Hanton, S., DaSilva, P., Boevink, P., Evans, D., Oparka, K., Denecke, J. & Hawes, C. (2003) ER quality control can lead to retrograde transport from the ER lumen to the cytoplasm and the nucleoplasm in plants. *Plant Journal* 34, 269 - 281

Brandizzi, F., Irons, S. L., Johansen, J., Kotzer, A. & Neumann, U. (2004) GFP is the way to glow: Bioimaging of the plant endomembrane system. *Journal of Microscopy* 214, 138 - 158

Brecknock, S., Dibbayawan, T. P., Vesk., M., Vesk, P. A., Faulkner, C., Barton., D. & Overall, R. L. (2011) High resolution scanning electron microscopy of plasmodesmata. *Planta* 234, 749 – 758

Breeze, E., Dzimitrowicz, N., Kriechbaumer, V., Brooks, R., Botchway, S.W., Brady, J.P., Hawes, C., Dixon, A.M., Schnell, J.R., Fricker, M.D. and Frigerio, L. (2016) A C-terminal amphipathic helix is necessary for the in vivo tubule-shaping function of a plant reticulon. *Proceedings of the National Academy of Sciences* 113, 10902 - 10907

Burch-Smith, T. M., Stonebloom, S., Xu, M. & Zambryski, P. C. (2011) Plasmodesmata during development: re-examination of the importance of primary, secondary and branched plasmodesmata structure versus function. *Protoplasma* 248, 61 – 74

Buschmann, H., Green, P., Sambade, A., Doonan, J. H. & Lloyd, C. W. (2011) Cytoskeletal dynamics in interphase, mitosis and cytokinesis analysed through *Agrobacterium*-mediated transient transformation of tobacco BY-2 cells. *New Phytologist* 190, 258 - 267

Cantrill, L. C., Overall, R. L. & Goodwin, P. B. (1999) Cell-to-cell communication via plant endomembranes. *Cell Biology International* 23, 653 - 661

Caroni, P. & Schwab, M. E. (1988) Two membrane protein fractions from rat central myelin with inhibitory properties for neurite growth and fibroblast spreading. *The Journal of Cell Biology* 106, 1281 - 288

Carr, D. J. (1976) Historical perspectives on plasmodesmata. In: B.E.S. Gunning & A.W. Robards (ed.) *Intercellular Communication in Plants: Studies on Plasmodesmata* 291 - 295 Berlin, Germany; Springer-Verlag

Chatterjee, S., Roy, A., Laskar, A. & Snehasikta, S. (2012) Electron microscopy in the perspective of modern biology: Ultravision and ultradimension. In: A. Mendez-Vilas (ed.) *Current microscopy contributions to advances in science and technology* Spain; Formatex Research Center 891 - 902

Chen, Y. F., Randlett, M. D., Findell, J. L. & Schaller, G, E. (2002) Localization of the ethylene receptor ETR1 to the endoplasmic reticulum of Arabidopsis. *Journal of Biological Chemistry* 277, 19861 – 19866

Chen, Y. N., Slabaugh, E. & Brandizzi, F. (2008) Membrane-tethered transcription factors in *Arabidopsis thaliana*: novel regulators in stress response and development. *Current Opinion in Plant Biology* 11, 695 – 701

Chen, X. & Kim, J. (2009) Callose synthesis in higher plants. *Plant Signaling & Behavior* 4, 489 – 492

Chen, J., Stefano, G., Brandizzi, F. & Zheng, H. (2011) *Arabidopsis* RHD3 mediates the generation of the tubular ER network and is required for Golgi distribution and motility in plant cells. *Journal of Cell Science* 124, 2241 - 2252

Chen, S., Novick, P. & Ferro-Novick S. (2012) ER network formation requires a balance of the dynamin-like GTPase Sey1p and the Lunapark family member Lnp1p. *Nature Cell Biology* 14, 707 – 716

Clough, S. J. & Bent, F. A. (1998) Floral dip: a simplified method for Agrobacterium-mediated transformation of *Arabidopsis thaliana. The Plant Journal* 16, 735 – 743

Cooper, G. M. (2000) The Cell; A Molecular Approach. 2nd Edition. Sunderland (MA): Sinauer Associates

Dağdeviren, A., Alp, H. & Ors, U. (1994) New applications for the zinc iodide-osmium tetroxide technique. *Journal of Anatomy* 184, 83 – 91

Dauwalder, M. & Whaley, G. (1973) Staining of cells of *Zea mays* root apices with the osmium-zinc iodide and osmium impregnation techniques. *Journal of Ultrastructural Research* 45, 279 - 296

David, K. M. & Perrot-Rechenmann, C. (2001) Characterization of a tobacco Bright Yellow 2 cell line expressing the tetracycline repressor at a high level for strict regulation of transgene expression. *Plant Physiology* 125, 1548 – 1553

Dawson, T. R., Lazarus, M. D., Hetzer. M. W. & Wente, S. R. (2009) ER membrane-bending proteins are necessary for de novo nuclear pore formation. *Journal of Cell Biology* 184, 659 – 675

Denk, W. & Horstmann, H. (2004) Serial block-face scanning electron microscopy to reconstruct three-dimensional tissue nanostructure. *PLoS Biology* 2: e329

Deom, C. M., Lapidot, M. & Beachy, R. N. (1992) Plant virus movement proteins. *Cell* 69, 221 – 224

Diaz, A., Wang, X. & Ahlquist, P. (2010) Membrane-shaping host reticulon proteins play crucial roles in viral RNA replication compartment formation and function. *Proceedings of the National Academy of Sciences* 107, 16291 – 16296

Ding, B., Turgeon, R. & Parthasarathy, M. V. (1992) Substructure of freeze substituted plasmodesmata. *Protoplasma* 169, 28 – 41

Ding, B., Kwon, M. O. & Warnberg, L. (1996) Evidence that actin filaments are involved in controlling the permeability of plasmodesmata in tobacco mesophyll. *Plant Journal* 10, 157 – 164

Donohoe, B. E., Mogelsvang, S., Staehelin, L. A. (2006) Electron tomography of ER, Golgi and related membrane systems. *Methods* 39, 154–162

Eastmond, P. J., Quettier, A., L., Kroon, J. T., Craddock, C., Adams, N. & Slabas, A. R. (2011) A phosphatidate phosphatase double mutant provides a new insight into plant membrane lipid homeostasis. *Plant Signalling and Behaviour* 6, 526 – 527

English, A. R., Zurek, N. & Voeltz, G. K. (2009) Peripheral ER structure and function. *Current Opinion in Cell Biology* 21, 596 – 602

English, A. R., & Voeltz, G. K. (2013a) Endoplasmic reticulum structure and interconnections with other organelles. *Cold Spring Harbor Perspectives in Biology* 5, a013227

English, A. R. & Voeltz, G. K. (2013b). Rab10 GTPase regulates ER dynamics and morphology. *Nature Cell Biology* 15, 169 – 178

Estrada, P., Kim, J., Coleman, J., Walker, L., Dunn, B., Takizawa, P., Novick, P. & Ferro-Novick, S. (2003) Myo4p and She3p are required for cortical ER inheritance in *Saccharomyces cerevisiae*. *Journal of Cell Biology* 163, 1255 – 1266

Estrada de Martin, P., Du, Y., Novick, P. & Ferro-Novick, S. (2005) Ice2p is important for the distribution and structure of the cortical ER network in *Saccharomyces cerevisiae. Journal of Cell Science* 118, 65 – 77

Faulkner, C., Akman, O. E., Bell, K., Jeffree, C. & Oparka, K. (2008) Peeking into pit fields: a multiple twinning model of secondary plasmodesmata formation in tobacco. *Plant Cell* 20, 1504 – 1518

Favard, P. & Carasso, N. (1973) The preparation and observation of thick biological sections in the high voltage electron microscope. *Journal of Microscopy* 97, 59 – 81

Fendrych, M., Synek, L., Pecenková, T., Toupalová, H., Cole, R., Drdová, E., Nebesárová, J., Sedinová, M., Hála, M., Fowler, J. E. & Zársky, V. (2010) The Arabidopsis exocyst complex is involved in cytokinesis and cell plate maturation. *Plant Cell* 22, 3053 – 3065

Fernandez - Calvino, L., Faulkner, C., Walshaw, J., Saalbach. G., Bayer, E., Benitez-Alfonso, Y. & Maule, A. (2011) Arabidopsis plasmodesmal proteome. *PloS ONE* 6, 1 - 13

Filner, P. (1965) Semi-conservative replication of DNA in a higher plant cell. *Experimental Cell Research* 39, 33 - 39

Fitzgibbon, J., Bell, K., King, E. & Oparka, K. (2010) Super-resolution imaging of plasmodesmata using three-dimensional structured illumination microscopy. *Plant Physiology* 153, 1453–1463

Friedman, J. R. & Voeltz, G. K. (2011) The ER in 3D: a multifunctional dynamic membrane network. *Trends in Cell Biology* 21, 709 – 17

Friml, J. & Jones, A. R. (2010) Endoplasmic Reticulum: The rising compartment in auxin biology. *Plant Physiology* 154, 458 - 462

Furuta, K. M., Yadav, S. R., Lehesranta, S., Belevich, I., Miyashima, S., Heo, J., Vatén, A., Lindgren, O., Rybel, B. D., Isterdael, G. V., Somervuo, P., Lichtenberger, R., Rocha, R., Thitamadee, S., Tähtiharju, S., Auvinen, P., Beeckman, T., Jokitalo, E. & Helariutta, Y. (2014) Arabidopsis NAC45/86 direct sieve element morphogenesis culminating in enucleation. *Science AAAS Report* Published Online DOI: 10.1126/science.1253736

Galili, G. (2004) ER-derived compartments are formed by highly regulated processes and have special functions in plants. *Plant Physiology* 136, 3411 – 3413

Geelen, D. N. V. & Inzé, D. G. (2001) A bright future for the bright yellow-2 cell culture. *Plant Physiology* 127, 135 - 1379

Gerondopoulos, A., Bastos, R. N., Yoshimura, S., Anderson, R., Carpanini, S., Aligianis, I., Handley, M. T. & Barr, F. A. (2014). Rab18 and a Rab18 GEF complex are required for normal ER structure. *Journal of Cell Biology* 205, 707 – 20

Gilloteaux, J. & Naud, J. (1979) The zinc iodide-osmium tetroxide staining-fixative of Maillet. Nature of the precipitate studied by x-ray microanalysis and detection of Ca2+-affinity subcellular sites in a tonic smooth muscle. *Histochemistry* 63, 227-243

Goodwin, P.B. (1983) Molecular size limit for movement in the symplast of Elodea leaf. *Planta* 157, 124-13

Goyal, U. & Blackstone, C. (2013) Untangling the web: Mechanisms underlying ER network formation. *Biochimica Et Biophysica Acta* 1833, 2492 – 2498

Grabski, S., De Feijter, A. W. & Schindler, M. (1993) Endoplasmic reticulum forms a dynamic continuum for lipid diffusion between contiguous soybean root cells. *Plant Cell* 5, 25 – 38

Graham, L. E., Cook, M. E. & Busse, J. S. (2000) The origin of plants: Body plan changes contributing to a major evolutionary radiation. *Proceedings of the National Academy of Sciences* 97, 4535 – 4540

GrandPré, T., Nakamura, F., Vartanian, T. & Strittmatter, S. M. (2000) Identification of the Nogo inhibitor of axon regeneration as a Reticulon protein. *Letters to Nature* 403, 439 - 444

Griffing, L. R., Lin, C., Perico, C., White, R. & Sparkes, I. (2016) Plant ER geometry and dynamics: biophysical and cytoskeletal control during growth and biotic response. *Protoplasma* Epub, 1 – 14

Grison, M. S., Brocard, L., Fouillen, L. Nicolas, W., Wewer, V., Dörmann, P., Nacir, H., Benitez-Alfonso, Y., Claverol, Y., Germain, V., Boutté, Y., Mongrand, S., & Bayer, E. M. (2015) Specific membrane lipid composition is important for plasmodesmata function in arabidopsis. *The Plant Cell Online* 29, 8, 1-23

Gu, X. & Verma, D. P. (1997) Dynamics of phragmoplastin in living cells during cell plate formation and uncoupling of cell elongation from the plane of cell division. *Plant Cell* 9, 157 - 169

Hall & Hawes (1991) *Electron Microscopy of Plant Cells*. 1st Edition. London: Academic Press Limited

Hamada, T., Tominaga, M., Fukaya, T., Nakamura, M., Nakano, A., Watanabe, Y., Hashimoto, T. & Baskin, T. I. (2012) RNA processing bodies, mitochondria and endoplasmic reticulum tubule junctions. *Plant Cell Physiology* 53, 699 - 708

Harris, N. (1979) Endoplasmic reticulum in developing seeds of Vicia faba – A high voltage electron microscopy study. *Planta* 146, 63 - 69

Hawes, C. R. Juniper, B. E. & Horne, J. C. (1981) Low and high voltage electron microscopy of mitosis and cytokinesis in maize roots. *Planta* 152, 297 – 407

Hawes, C. & Hummel, E. (2015) Three-dimensional SEM – the future of cell imaging. *Journal of Microscopy* 259, 79

Hawes, C., Kiviniemi, P. & Kreichbaumer, V. (2015) The endoplasmic reticulum: A dynamic and well connected organelle. *Journal of Integrative Biology* 57, 50 – 62

Hayashi, K., Hasegawa, J. & Matsunaga, S. (2013) The boundary of the meristematic and elongation zones in roots: endoreduplication precedes rapid cell expansion. *Nature Scientific Reports* 3, 2723

Heidstra, R. & Sabatini, S. (2014) Plant and animal stem cells: Similar yet different. *Nature Reviews: Molecular Cell Biology* 15, 301 - 312

Heiland, I. & Erdmann, R. (2005) Biogenesis of peroxisomes. Topogenesis of the peroxisomal membrane and matrix proteins. *Federation of European Biochemical Studies Journal* 272, 2362 – 2372

Hepler, P.K. (1982) Endoplasmic reticulum in the formation of the cell plate and plasmodesmata. *Protoplasma* 111, 121 - 133

Herman, E. M. (2008) Endoplasmic reticulum bodies: Solving the insoluble. *Current Opinion in Plant Biology* 11, 672 – 679

Hong, B., Ichida, A., Wang, Y., Gens, J. S., Pickard, B. G. & Harper, J. F. (1999) Identification of a calmodulin-regulated Ca^{2+}-ATPase in the endoplasmic reticulum. *Plant Physiology* 1165 – 1176

Hu, J., Shibata, Y., Zhu, P., Voss, C., Rismanchi, N., Prinz, W. A., Rapoport, T. A. & Blackstone, C. (2009) A class of dynamin-like GTPases involved in the generation of the tubular ER network. *Cell* 138, 549 – 561

Huang, A. H. C. (1996) Olesins and oil bodies in seeds and other organs. *Plant Physiology* 110, 1055 – 1061

Hughes, L., Towers, K., Starbourg, T., Gull, K. & Vaughan, S. (2013) A cell body groove housing the new flagellum tip suggests an adaptation of cellular morphogeneisis for parasitism in bloodstream from of *Trypanosoma brucei*. *Journal of Cell Science* 26, 5748 - 5757

Hughes, L., Hawes, C., Monteith, S. & Vaughan, S. (2014) Serial block face scanning electron microscopy – the future of cell ultrastructure imaging. *Protoplasma* 251, 395 - 401

Hwang, H. & Gelvin, S. B. (2004) Plant proteins that interact with VirB2, the *Agrobacterium tumefaciens* pilin protein, mediate plant transformation. *The Plant Cell* 16, 3148 - 3167

Ibl, V. & Stoger, E. (2012) The formation, function and fate of protein storage compartments in seeds. *Protoplasma* 249, 379 – 392

Iwahashi, J., Kawasaki, I., Kohara, Y., Gengyo-Ando, K., Mitani, S., Oshima, Y., Hamada, N., Hara, K., Kashiwagi, T. & Toyoda, T. (2002) *Caenorhabditis elegans* reticulon interacts with RME-1 during embryogenesis. *Biochemical and Biophysical Research Communications* 293, 698 - 704

Joachim, F. (2006) Introduction: Principles of electron tomography In: Joachim, J (ed.) *Electron tomography - Methods for three-dimensional visualization of structures in the cell* New York: Springer 1 - 15

Jokic, N., Gonzalez de Aguilr, J., Dimou, L., Lin, S., Fergani, A., Ruegg, M. A., Schwab, M. E., Dupuis, L. & Loeffler, J. (2006) The neurite outgrowth inhibitor Nogo-A promotes denervation in an amyotrohic lateral sclerosis model. *EMBO Reports* 7,1162 - 1167

Kafri, R., Springer, M. & Pilpel, Y. (2009) Genetic redundancy: New tricks for old genes. *Cell* 136, 3, 389 - 392

Kiseleva, E., Morozova, K.N., Voeltz, G.K., Allen, T.D., and Goldberg, M.W. (2007). Reticulon 4a/NogoA locates to regions of high membrane curvature and may have a role in nuclear envelope growth. *Journal of Structural Biology* 160, 224 – 235

Kittelmann, M., Hawes, C. & Hughes, L. (2016) Serial block-face scanning electron microscopy and the reconstruction of plant cell membrane systems. *Journal of Microscopy* 263, 200 - 211

Klopfenstein, D. R., Klumperman, J., Lustig, A., Kammerer, R. A., Oorschot, V. & Hauri, H.P. (2001) Subdomain specific localization of CLIMP-63 (p63) in the endoplasmic reticulum is mediated by its luminalα-helical segment. *Journal of Cell Biology* 153, 1287 – 30084

Knox, J. P. & Benitez-Alfonso, Y. (2014) Roles and regulation of plant cell walls surrounding plasmodesmata. *Current Opinion in Plant Biology* 22, 93 - 100

Knox, K., Wang, P., Kriechbaumer, V., Tilsner, J., Frigerio, L., Sparkes, I., Hawes, C., & Oparka, K. (2015) Putting the squeeze on plasmodesmata: A role for reticulons in primary plasmodesmata formation. *Plant Physiology* 168, 1563 – 1572

Koncz, C. & Schell, J. (1986) The promoter of T_L-DNA gene *5* controls the tissue-specific expression of chimaeric genes carried by a novel type of *Agrobacterium* binary vector. *Molecular and General Genetics* 204, 383 – 396

Kremer, A., Lippens, S., Bartunkova, S., Asselbergh, B., Blanpain, C., Fendrych, M., Goossens, A., Holt, M., Janssens, S., Krols, M., Larsimont, J. C., Mc Guire, C., Nowack, M. K., Saelens, X., Schertel, A., Schepens, B., Slezak, M., Timmerman, V., Theunis, C., Van Brempt, R., Visser, Y. & Guérin, C. J. (2015) Developing 3D SEM in a broad biological context. *Journal of Microscopy* 259, 80 – 96

Kriechbaumer, V., Botchway, S. W., Slade, S. E., Knox, K., Frigerio, L., Oparka, K. & Hawes, C. (2015) Reticulomics: Protein-protein interaction studies with two plasmodesmata-localized reticulon family proteins identify binding partners enriched at plasmodesmata, endoplasmic reticulum, and the plasma membrane. *Plant physiology* 169, 1933 – 1945

Kumagai-Sano, F., Hayashi, T., Sano, T. & Hasezawa, S. (2006) Cell cycle synchronization of tobacco BY-2 cells. *Nature Protocols* 1, 2621 – 2627

Latijnhouwers, M., Gillespie, T., Boevink, P. Kriechbaumer, V., Hawes, C., & Carvalho, C. (2007) Localization and domain characterization of Arabidopsis golgin candidates. *Journal of Experimental Botany* 58, 4373 – 4386

Lee, J., Kim., J., Sivula, M. & Strittmatter, S. M. (2004) Nogo receptor antagonism promotes stroke recovery by enhancing axonal plasticity. *The Journal of Neuroscience* 24, 6209 – 6217

Lee, H., Sparkes, I., Gattolin, S., Dzimitrowicz1, N., Roberts, L. M., Hawes, C. & Frigerio, L. (2013) An Arabidopsis reticulon and the atlastin homologue RHD3-like2 act together in shaping the tubular endoplasmic reticulum. *New Phytologist* 197, 481 – 489

Liebe, S. & Menzel, D. (1995) Actomyosin-based motility of endoplasmic reticulum and chloroplasts in *Vallisneria* mesophyll cells. *Biology of the Cell* 85, 207 – 222

Lin, C., Seikowski, J., Pérez-Lara, A., Jahn, R., Höbartner, C., Walla, P. J. (2014) Control of membrane gaps by synaptotagmin-Ca2+ measured with a novel membrane distance ruler. *Nature Communications* 5: 5859

Linberg, K.A. & Fisher, S.K. (1986) An ultrastructural study of interplexiform cell synapses in the human retina. *Journal of Comparative Neurology* 243, 561 – 576

Liu, T. J., Bian, X., Sun, S., Hu, X., Klemm, R. W., Prinz, W. A. & Rapoport, T. A. (2012) Lipid interaction of the C-terminus and association of the transmembrane segments facilitate atlastin-mediated homotypic endoplasmic reticulum fusion. *Proceedings of the National Academy of Sciences* 109, 2146 - 2154

Lu, L., Ladinsky, M. S. & Kirchhausen, T. (2009) Cisternal organization of the endoplasmic reticulum during mitosis. *Molecular Biology of the Cell* 20, 3471 – 3480

Lu, L., Ladinsky, M. S. & Kirchausen, T. (2011) Formation of the postmitotic nuclear envelope from extended ER cisternae precedes nuclear pore assembly. *The Journal of Cell Biology* 194, 425 - 440

Lucas, W. J., Ham, B. & Kim, J. (2009) Plasmodesmata – bridging the gap between neighboring plant cells. *Trends in Cell Biology* 19, 495 - 503

Lučič, V., Rigort, A. & Baumeister, W. (2013) Cryo-electron tomography: the challenge of doing structural biology in situ. *Journal of Cell Biology* 202, 407 – 419

Ma, Y. & Hendershot, L. M. (2004) ER chaperone functions during normal and stress conditions. *Journal of Chemical Neuroanatomy* 28, 51 - 65

Ma, Y., Cai, S., Lv, Q., Jiang, Q., Zhang, Q., Zhai, Z. & Zhang, C. (2007) Lamin B receptor plays a role in stimulating nuclear envelope production and targeting membrane vesicles to chromatin during nuclear envelope assembly through direct interaction with importin ß. *Journal of Cell Science* 120, 520 - 530

Margreth, A. (2002) Our debt toward Emilio Veratti. *Rendiconti Lincei* 13, 249 - 255

Marin, E. P., Moeckel, G., Lamki-Al, R., Bradley, J., Yan, Q., Wang, T., Wright, P. L., Yu, J. & Sessa, W. S. (2010) Identification and regulation of reticulon 4B (Nogo-B) in renal tubular epithelial cells. *The American Journal of Pathology* 177, 2765 – 2773

Marsh, B. J. (2007) Reconstructing mammalian membrane architecture by large area cellular tomography. In: McIntosh, J. R. (ed.) *Cellular electron microscopy.* Maryland Heights, U.S.A: Academic Press 193 – 220

Martens, H. J., Roberts, A. G., Oparka, K. J. & Schulz, A. (2006) Quantification of plasmodesmatal endoplasmic reticulum coupling between sieve elements and companion cells using fluorescence redistribution after photobleaching. *Plant Physiology* 142, 471 – 480

Matheson, L. A., Hanton, S. L. & Brandizzi, F. (2006) Traffic between the plant endoplasmic reticulum and Golgi apparatus: To the Golgi and beyond. *Current Opinion in Plant Biology* 9, 601 – 609

Maule, A. J. (2008) Plasmodesmata: structure, function and biogenesis. *Current Opinion in Plant Biology* 11, 680 - 686

McEwen, B. F. & Marko, M. (2001) The emergence of electron tomography as an important tool for investigating cellular ultrastructure. *Journal of Histological Cytochemistry* 49, 553 – 564

McGee, A. W. & Strittmatter, S. M. (2003) The Nogo-66 receptor: focusing myelin inhibition of axon regeneration. *Trends in Neurosciences* 26, 193 – 198

Mielańczyk, L., Matysiak, N., Klymenko, O. & Wojnicz, R. (2015) Transmission electron microscopy of biological samples. In: Maaz, K (ed.) *The transmission electron microscope - Theory and applications.* InTech, DOI: 10.5772/60680. Available from: https://www.intechopen.com/books/the-transmission-electron-microscope-theory-and-applications/transmission-electron-microscopy-of-biological-samples

Mishchenko, Y. (2009) Automation of 3D reconstruction of neural tissue from large volume of conventional serial section transmission electron micrographs. *Journal of Neuroscience Methods* 176, 276 – 289.

Molnár, G., Fendrych, M. & Friml, J. (2016) Plasma membrane: Negative attraction. *Nature Plants* 16102

Moore, I. Samalova, M. & Kurup, S. (2006) Transactivated and chemically inducible gene expression in plants. *The Plant Journal* 45, 651 – 683

Müller, B. & Grossniklaus, U. (2010) Model organisms – A historical perspective. *Journal of Proteomics* 73, 2054 – 2063

Nagata, T., Nemoto, Y. & Hasezawa, S. (1992) Tobacco BY-2 cell line as the “HeLa” cell in the cell biology of higher plants. *International Review of Cytology* 132, 1 – 30

Nagata, T. & Kumagai, F. (1999) Plant cell biology through the window of the highly synchronized tobacco BY-2 cell line. *Methods in Cell Science* 21, 123 – 127

Nakajimaa, K. & Benfey, P. N. (2002) Signaling in and out: Control of cell division and differentiation in the shoot and root. *The Plant Cell* S265 – S276

Nakano, A. (2004) Yeast Golgi apparatus--dynamics and sorting. *Cellular and Molecular Life Sciences* 61, 186 – 191

Nakamura, Y., Koizumi, R., Shui, G., Shimojima, M., Wenk, M.R., Ito, T. and Ohta, H. (2009) Arabidopsis lipins mediate eukaryotic pathway of lipid metabolism and cope critically with phosphate starvation. *Proceedings of the National Academy of Sciences* 106, 20978 – 20983

Nebenführ, A., Frohlick, J. A. & Staehelin, A. L. (2000) Redistribution of Golgi stacks and other organelles during mitosis and cytokinesis in plant cells. *Plant Physiology* 124, 1, 135 – 152

Nicastro, D., Schwartz, C., Pierson, J., Gaudette, R., Porter, M. E. & McIntosh, J. R. (2006) The molecular architecture of axonemes revealed by cryoelectron tomography. *Science* 313, 944 – 948

Nicolas, W. J., Grison, M. S., Trépout, S., Gaston, A., Fouché, M., Cordelières, F. P., Oparka, K., Tilsner, J., Brocard, L. & Bayer, E. M. (2017) Architecture and permeability of post-cytokinesis plasmodesmata lacking cytoplasmic sleeves. *Nature Plants* 3, 17082, 1 - 23

Nishihama, R., Ishikawa, M., Araki, S., Soyano, T., Asada, T. Machida, Y. (2001) The NPK1 mitogen-activated protein kinase kinase kinase is a regulator of cell-plate formation in plant cytokinesis. *Genes & Development* 15, 352 - 363

Nziengui, H., Bouhidel, K., Pillon, D., Der, C., Marty, F., and Schoefs, B. (2007). Reticulon-like proteins in *Arabidopsis thaliana*: Structural organization and ER localisation. *FEBS Letters* 581, 3356 – 3362

Nziengui, H., and Schoefs, B. (2009). Functions of reticulons in plants: What we can learn from animals and yeasts. *Cellular and Molecular Life Sciences* 66, 584 - 595

Oertle, T., Klinger, M., Stuermer, C.A.O., and Schwab, M.E. (2003) A reticular rhapsody: phylogenic evolution and nomenclature of the RTN/Nogo gene family. *FASEB Journal* 17, 1238 – 1247

Oparka, K. J., Prior, D. A. M. & Crawford, J. W. (1994) Behaviour of plasma membrane, cortical ER and plasmodesmata during plasmolysis of onion epidermal cells. *Plant Cell Environment* 17, 163 – 171

Oparka, K. J., Roberts, A. G., Boevink, P., Santa Cruz, S., Roberts, I., Pradel, K. S., Imlau, A., Kotlizky, G., Sauer, N. & Epel, B. (1999) Simple, but not branched, plasmodesmata allow the nonspecific trafficking of proteins in developing tobacco leaves. *Cell* 97, 743 – 754

Orso, G., Pendin, D., Liu, S., Tosetto, J., Moss, T. J., Faust, J. E., Micaroni, M., Egorova, A., Martinuzzi, A., McNew, J. A. & Daga, A. (2009) Homotypic fusion of ER membranes requires the dynamin-like GTPase atlastin. *Nature* 460, 978 – 983

Overall, R. L. & Blackman, L. M. (1996) A model of the macro-molecular structure of plasmodesmata. *Trends in Plant Science* 1, 307 – 311

Palade, G. E. & Porter, K. R. (1954) Studies on the endoplasmic reticulum. I. Its identification in cells in situ. *The Journal of Experimental Medicine* 100, 641 – 656

Palade, G. E. (1955) Studies on the endoplasmic reticulum. II. Simple dispositions in cells in situ. *The Journal of Biophysical and Biochemical Cytology* 1, 7 – 82

Park, S. H. & Blackstone, C. (2010) Further assembly required: construction and dynamics of the endoplasmic reticulum. *EMBO reports* 11, 515 – 521

Parry, G. (2014) Components of the *Arabidopsis* nuclear pore complex play multiple diverse roles in control of plant growth. *Journal of Experimental Botany* 65, 6057 – 6067

Peña, E.J. & Heinlein, M. (2013) Cortical microtubule-associated ER sites: Organisation centres of cell polarity and communication. *Current Opinion in Plant Biology* 16, 1 – 10

Phillips, M. J. & Voeltz, G. K. (2016) Structure and function of ER membrane contact sites with other organelles. *Nature Reviews Molecular Cell Biology* 17, 2, 69 - 82

Popper, Z. A., Michel, G., Herve, C., Domozych, D. S., Willats, G. T. W., Tuohy, M. G., Kloareg, B. & Stengel, D. B. (2011) Evolution and diversity of plant cell walls: From algae to flowering plants. *The Annual Review of Plant Biology* 62, 567 – 590

Porter, K. R. & Palade, G. E. (1957) Studies on the endoplasmic reticulum. III. Its form and distribution in striated muscle cells. *The Journal of Biophysical and Biochemical Cytology* 3, 269 – 300

Porter, K. R. & Machado, R. D. (1960) Studies on the endoplasmic reticulum: Its form and distribution during mitosis in cells of onion root tip. *The Journal of Biophysical and Biochemical Cytology* 7, 167 - 180

Prinz, W.A., Grzyb, L., Veenhuis, M., Kahana, J.A., Silver, P.A. & Rapoport, T.A. (2000) Mutants affecting the structure of the cortical endoplasmic reticulum in Saccharomyces cerevisiae. *Journal of Cell Biology* 150, 461 - 471

Puhka, M., Vihinen, H., Joensuu, M. & Jokitalo, E. (2007) Endoplasmic reticulum remains continuous and undergoes sheet-to-tubule transformation during cell division in mammalian cells. *Journal of Cell Biology* 179, 895 – 909

Quader, H., Hofmann, A., and Schepf, E. (1987). Shape and movement of the endoplasmic reticulum in onion bulb epidermis cells: possible involvement of actin. *European Journal of Cell Biology* 44, 17 – 26

Quader, H., Hofmann, A. & Schnepf, E. (1989) Reorganization of the endoplasmic reticulum in epidermal cells of onion bulb scales after cold stress: Involvement of cytoskeletal elements. *Planta* 177, 273 – 280

Radford, J. E. & White, R. G. (1998) Localisation of a myosin-like protein to plasmodesmata. *The Plant Journal* 14, 743 – 750

Rahier, A., Darnet, S., Bouvier, F., Camara, B. & Bard, M. (2006) Molecular and enzymatic characterization of novel bifunctional 3ß-hydroxysteroid dehydrogenases/C-4 decarboxylases from *Arabidopsis thaliana*. *The Journal of Biological Chemistry* 281, 27264 – 27277

Reicheld, J., Chaubet, N., Shen, W. H., Renaudin, J. & Gigot, C. (1996) Multiple A-type cyclins express sequentially during the cell cycle in *Nicotiana tabacum* BY2 cells. *Proceedings of the National Academy of Sciences* 93, 13819 – 13824

Reichelt, S., Knight, A. E., Hodge, T. P., Baluska, F., Samaj, J., Volkmann, D. & Kendrick-Jones, J. (1999) Characterization of the unconventional myosin VIII in plant cells and its localisation at the post-cytokinetic cell wall. *The Plant Journal* 19, 555 - 567

Reindl, M., Khantane, S., Ehling, R., Schanda, K., Lutterotti, A., Brinkhoff, C., Oertle, T., Schwab, M. E., Deisenhammer, F., Berger, T. & Bandtlow, C. E. (2003) Serum and cerebrospinal fluid antibodies to Nogo-A in patients with multiple sclerosis and acute neurological disorders. *Journal of Neuroimmunology* 145, 139 – 147

Reinecke, M. (1981) The zinc iodide-osmium tetroxide (ZIO) method. In: C. H. Heym & W. G. Forssmann (ed.) *Techniques in Neuroanatomical Research* Berlin: Springer 293 - 300

Rensink, W. A. & Buell, C. R. (2004) Arabidopsis to rice. Applying knowledge from a weed to enhance our understanding of a crop species. *Plant Physiology* 135, 622 – 629

Ridge, R. W., Uozumi, Y., Plazinski, J., Hurley, U. A. & Williamson, R. E. (1999) Developmental transitions and dynamics of the cortical ER of Arabidopsis cells seen with green fluorescent protein. *Plant Cell Physiology* 40, 1253 - 1261

Rismanchi, N., Soderblom, C., Stadler, J., Zhu, P. P. & Blackstone, C. (2008) Atlastin GTPases are required for Golgi apparatus and ER morphogenesis. *Human Molecular Genetics* 17, 1591 - 1604

Robards, A. W. (1971) The ultrastructure of plasmodesmata. *Protoplasma* 72, 315 – 323

Roberts, A. G. & Oparka, K. J. (2003) Plasmodesmata and the control of symplastic transport. *Plant, Cell & Environment* 26, 103 – 124

Robinson-Beers, K. & Evert, R, F. (1991) Fine structure of plasmodesmata in mature leaves of sugarcane. *Planta* 184, 307–318

Rolls, M. M., Hall, D. H., Victor, M., Stelzer, E. H. & Rapoport, T. A. (2002) Targeting of rough endoplasmic reticulum membrane proteins and ribosomes in invertebrate neurons. *Molecular Biology of the Cell* 13, 1778 - 1791

Runions, J., Brach, T., Kühner, S. & Hawes, C. (2006) Photoactivation of GFP reveals protein dynamics within the endoplasmic reticulum membrane. *Journal of Experimental Botany* 57, 43 - 50

Saini, S. G., Liu, C., Zhang, P. & Lee, T. H. (2014) Membrane tethering by the atlastin GTPase depends on GTP hydrolysis but not on forming the cross-over configuration. *Molecular Biology of the Cell* 25, 3942 - 3953

Saint-Jore C, M., Evins, J., Batoko, H., Brandizzi, F., Moore, I. & Hawes, C. (2002) Redistribution of membrane proteins between the Golgi apparatus and endoplasmic reticulum in plants is reversible and not dependent on cytoskeletal networks. *Plant Journal* 29, 661 – 678

Samuels, A. L., Giddings, Jr. T. H. & Staehelin, L. A. (1995) Cytokinesis in tobacco BY-2 and root tip cells: A new model of cell plate formation in higher plants. *The Journal of Cell Biology* 130, 1345 - 1357

Sano, F. D., Fazi, B., Tufi, R., Nardacci, R. & Piacentini, M. (2007) Reticulon-1C acts as a molecular switch between endoplasmic reticulum stress and genotoxic cell death pathway in human neuroblastoma cells. *Journal of Neurochemistry* 102, 345 – 353

Santos, R. B., Abranches, R., Fischer, R., Sack, M. Holland, T. (2016) Putting the spotlight back on plant suspension cultures. *Frontiers in Plant Science* 7, 1 - 12

Schapire, A. L., Voigt, B., Jasik, J., Rosado, A., Lopez-Cobollo, R., Menzel, D., Salinas, J., Mancuso, S., Valpuesta, V., Baluska, F. & Botella, M. A. (2008) Arabidopsis synaptotagmin 1 is required for the maintenance of plasma membrane integrity and cell viability. *Plant Cell* 20, 3374 - 3388

Scheible, W. R. & Pauly, M. (2004) Glycosyltransferases and cell wall biosynthesis: novel players and insights. *Current Opinion in Plant Biology* 7, 285 – 295

Scheuring, D., Löfke, C., Krüger, F., Kittelmann, M., Eisa, A., Hughes, L., Smith, R., S., Hawes, C., Schumacher, K. & Kleine-Vehn, J. (2016) Actin-dependent vacuolar occupancy of the cell determines auxin-induced growth repression. *Proceedings of the National Academy of Sciences* 113, 452 – 457

Schweizer, A., Ericsson, M., Bachi, T., Griffiths, G. & Hauri, H. P. (1993) Characterization of a novel 63 kDa membrane protein. Implications for the organization of the ER-to-Golgi pathway. *Journal of Cell Science* 104, 671 – 83

Schweizer, A., Rohrer, J., Slot, J. W., Geuze, H. J. & Kornfeld, S. (1995) Reassessment of the subcellular localization of p63. *Journal of Cell Science* 108, 2477 – 85

Seguí-Simarro, J. m., Austin II, J. R., White, E. A. & Staehelin, L. A. (2004) Electron tomographic analysis of somatic cell plate formation in meristematic cells of Arabidopsis preserved by high-pressure freezing. *The Plant Cell* 16, 836 – 856

Setiady, Y. Y., Sekine, M., Hariguchi, N., Yamamoto, T., Koichi, H. & Shinmyo, A. (1995) Tobacco mitotic cyclins: cloning, characterization, gene expression and functional assay. *The Plant Journal* 8, 949 - 957

Shibata, Y., Voeltz, G. K. & Rapoport, T. A. (2006) Rough sheets and smooth tubules. *Cell* 126, 435 – 39

Shibata, Y., Voss, C., Rist., J. M., Hu, J., Rapoport, T. A., Prinz, W. A. & Voeltz, G. K. (2008) The reticulon and Dp1/Yop1p proteins form immobile oligomers in the tubular endoplasmic reticulum. *The Journal of Biological Chemistry* 283, 18892 - 18904

Shibata, Y., Hu, J., Kozlov, M. M. & Rapoport, T. A. (2009) Mechanisms shaping the membranes of cellular organelles. *The Annual Review of Cell and Developmental Biology* 25, 329 - 354

Shibata, Y., Shemesh, T., Prinz, W. A., Palazzo, A. F., Kozlov, M. M. & Rapoport, T. A. (2010) Mechanisms determining the morphology of the peripheral ER. *Cell* 143, 774 – 788

Shin-Ru, S., Stollar, V. & Li, M. (2011) Host Factors in Enterovirus 71 Replication. *Journal of Virology* 85, 9658 – 9666

Smith, L. G., Hake, S. & Sylvester, A. W. (1996) The tangled-1 mutation alters cell division orientations throughout maize leaf development without altering leaf shape. *Development* 122, 481 - 489

Soto, G. E., Young, S. J., Martone, M. E., Deerinck, T. J., Lamont, S., Carragher, B.O., Hama, K. & Ellisman, M. H. (1994) Serial section electron tomography: a method for three-dimensional reconstruction of large structures. *Neuroimage* 1, 230 – 243

Sparkes, I. A., Frigerio, L., Tolley, N. & Hawes, C. (2009a) The plant endoplasmic reticulum: a cell-wide web. *Biochemical Journal* 423, 145 - 155

Sparkes, I., Runions, J., Hawes, C. & Griffing, L. (2009b) Movement and remodelling of the endoplasmic reticulum in nondividng cells of tobacco leaves. *The Plant Cell* 21, 3937 - 3949

Sparkes, I.A., Ketelaar, T., de Ruijter, N. C. & Hawes, C. (2009c) Grab a Golgi: Laser trapping of Golgi bodies reveals in vivo interactions with the endoplasmic reticulum. *Traffic* 10, 567 – 571

Sparkes, I., Tolley, N., Aller, I., Svozil, J., Osterrieder, A., Botchway, S., Mueller, C., Frigerio, L., and Hawes, C. (2010). Five Arabidopsis reticulon isoforms share endoplasmic reticulum location, topology, and membrane-shaping properties. *The Plant Cell* 22, 1333 - 1343

Spurr, A. R. (1969) A low-viscosity epoxy resin embedding medium for electron microscopy. *Journal of Ultrastructure Research* 26, 31 – 43

Staehelin, A. (1997) The plant ER: a dynamic organelle composed of a large number of discrete functional domains. *The Plant Journal* 11, 6, 1151 – 1165

Stefano, G., Hawes, C. & Brandizzi, F. (2014) ER – the key to the highway. *Current Opinion in Plant Biology* 22, 30 – 38

Takemura, S. Y., Bharioke, A., Lu, Z., Nern, A., Vitaladevuni, S., Rivlin, P. K., Katz, W. T., Olbris, D. J., Plaza, S. M., Winston, P., Zhao, T., Horne, J. A., Fetter, R. D., Takemura, S., Blazek, K., Chang, L. A., Ogundeyi, O., Saunders, M. A., Shapiro, V., Sigmund, C., Rubin, G. M., Scheffer, L. K., Meinertzhagen, I. A. & Chklovskii, D. B. (2013) A visual motion detection circuit suggested by Drosophila connectomics. *Nature* 500, 175 – 181

Terasaki, M., Chen, L.B. & Fujiwara, K. (1986) Microtubules and the endoplasmic reticulum are highly interdependent structures. *Journal of Cell Biology* 103, 1557 – 1568

Terasaki, M., Shemesh, T., Kasthuri, N., Klemm, R. W., Schalek, R., Hayworth, K. J., Hand, A. R., Yankova, M., Huber, G., Lichtman, J. W., Rapoport, T. A. & Kozloc, M. M. (2013) Stacked endoplasmic reticulum sheets are connected by helicoidal membrane motifs. *Cell* 154, 285 – 296

Terry, B. R. & Robards, A. W. (1987) Hydrodynamic radius alone governs the mobility of molecules through plasmodesmata. *Planta* 171, 145 - 157

Tilney, L. G., Cooke, T. J., Connelly, P. S. & Tilney, M. S. (1991) The structure of plasmodesmata as revealed by plasmolysis, detergent extraction, and protease digestion. *Journal of Cell Biology* 112, 739 – 747

Tolley, N., Sparkes, I.A., Hunter, P.R., Craddock, C.P., Nuttall, J., Roberts, L.M., Hawes, C., Pedrazzini, E., and Frigerio, L. (2008). Overexpression of a plant reticulon remodels the lumen of the cortical endoplasmic reticulum but does not perturb protein transport. *Traffic* 9, 94 - 102

Tolley, N., Sparkes, I., Craddock, C.P., Eastmond, P.J., Runions, J., Hawes, C., and Frigerio, L. (2010). Transmembrane domain length is responsible for the ability of a plant reticulon to shape endoplasmic reticulum tubules in vivo. *The Plant Journal* 63, 411 – 418

Tsai, S., Markus, T. M., Andrews, E. M., Cheatwood J. L., Emerick, A. J., Mir, A. K., Schwab. M. E. & Kartje, G. L. (2007) Intrathecal treatment with anti-Nogo-A antibody improves functional recovery in adult rats after stroke. *Experimental Brain Research* 182, 261 - 266

Tucker, E.B. (1982) Translocation in the staminal hairs of Setcreasea purpurea. A study of cell ultrastructure and cell-to cell passage of molecular probes. *Protoplasma* 113, 193 – 201

Tucker, E. B. & Boss, W. F. (1996) Mastoparan-induced intracellular Ca2+ fluxes may regulate cell-to-cell communication in plants. *Plant Physiology* 111, 459 – 467

Turner, A., Wells, B. & Roberts, K. (1994) Plasmodesmata of maize root tips: structure and composition. *Journal of Cell Science* 107, 3351 - 3361

Van Damme, D., Vanstraelen, M. & Geelen, D. (2007) Cortical division zone establishment in plant cells. *Trends in Plant Science* 12, 458 - 464

Van de Velde, H. J. K., Roebroek, A. J. M., Senden, N. H. M., Ramaekers, F. C. S & Van de Ven, W. J. M. (1994) NSP-encoded reticulons, neuroendocrine proteins of a novel gene family associated with membranes of the endoplasmic reticulum. *The Journal of Cell Science* 107, 2403 - 2416

Veratti, E. (1961) Investigations on the fine structure of striated muscle fiber read before the Reale Istituto Lombardo, 13 March 1902. *The Journal of Biophysical and Biochemical Cytology* 10, 1 – 59

Viotti, C., Krüger, F., Krebs, M., Neubert, C., Fink, F., Lupanga, U., Scheuring, D., Boutté, Y., Frescatada-Rosa, M., Wolfenstetter, S., Sauer, N., Hillmer, S., Grebe, M. & Schumacher, K. (2013) The endoplasmic reticulum is the main membrane source for biogenesis of the lytic vacuole in *Arabidopsis. The Plant Cell* 25, 3434 - 3449

Vitale, A. & Denecke, J. (1999) The endoplasmic reticulum-gateway of the secretory pathway. *The Plant Cell* 11, 615 - 628

Voeltz, G. K., Rolls, M. M. & Rapoport, T. A. (2002) Structural organization of the endoplasmic reticulum. *EMBO Report* 3, 944 - 950

Voeltz, G. K., Prinz, W. A., Shibata, Y., Rist, J. M. & Rapoprt, T. A. (2006) A class of membrane proteins shaping the tubular endoplasmic reticulum. *Cell* 124, 573 - 586

Voeltz, G. K. & Prinz, W. A. (2007) Sheets, ribbons and tubules – how organelles get their shape. *Nature reviews: Molecular cell biology* 8, 258 - 264

Wakefield, S. & Tear, G. (2006) The Drosophila reticulon RTN-1, has multiple differentially expressed isoforms that are associated with a sub-compartment of the endoplasmic reticulum. *Cellular and Molecular Life Sciences* 63, 2027 – 2038

Wallis, J. G. & Browse, J. (2010) Lipid biochemists salute the genome. *The Plant Journal* 61, 1092 - 1106

Wan, Q., Kuang, E., Dong, W., Zhou, S., Xu, H., Qi, Y. & Liu, Y. (2007) Reticulon 3 mediates Bcl-2 accumulation in mitochondria in response to endoplasmic reticulum stress. *Apoptosis* 12, 319 - 328

Wang, K. (2006) *Methods in Molecular Biology: Agrobacterium protocols.* Second edition. Volume 1. Humana Press: New Jersey

Wang, P., Hawkins, T. J., Richardson, C., Cummins, I., Deeks, M. J., Sparkes, I., Hawes, C. & Hussey, P. J. (2014) The plant cytoskeleton, NET3C, and VAP27 mediate the link between the plasma membrane and endoplasmic reticulum. *Current Biology* 24, 1397 – 1405

Wang, S., Tukachinsky, H., Romano, F. B. & Rapoport, T. A. (2016) Cooperation of the ER-shaping proteins atlastin, Lunapark, and reticulons to generate a tubular membrane network. *eLife* 5:e18605, 1 – 29

Ward, T. H. & Brandizzi, F. (2004) Dynamics of proteins in Golgi membranes: comparisons between mammalian and plant cells highlighted by photobleaching techniques. *Cellular and Molecular Life Sciences* 61, 172 – 185

Waterman-Storer, C.M. & Salmon, E.D. (1998) Endoplasmic reticulum membrane tubules are distributed by microtubules in living cells using three distinct mechanisms. *Current Biology* 8, 798 – 807

West, M., Zurek, N., Hoenger, A. & Vieltz, G. K. (2011) A 3D analysis of yeast ER structure reveals how ER domains are organized by membrane curvature. *Journal of Cell Biology* 193, 333 - 346

Westrate, L. M., Lee, J. E., Prinz, W. A. & Voeltz, G. K. (2015) Form follows function: The importance of endoplasmic reticulum shape. *Annual Review of Biochemistry* 84, 10.1 - 10.21

Weyland, M. & Midgley, P. A. (2004) Electron Tomography. *Materials Today* 7, 32 - 40

White, R. G., Badelt, K., Overall,R. L. & Vesk, M. (1994) Actin associated with plasmodesmata. *Protoplasma* 180, 169 – 184

Wiessner, C., Bareyre, F. M., Allegrini, P. R., Mir, A. K., Frentzel, S., Zurini, M., Schnell, L., Oertle, T. & Schwab, M. E. (2003) Anti-Nogo-A antibody infusion 24 hours after experimental stroke improved behavioural outcome and corticospinal plasticity in normotensive and spontaneously hypertensive rats. *Journal of Cerebral Blood Flow and Metabolism* 23, 154 - 165

Yang, Y. S. & Strittmatter, S. M. (2007) The reticulons: a family of proteins with diverse functions. *Genome Biology* 8, 234

Yamada, K., Hara-Nishimura, I. & Nishimura, M. (2011) Unique defense strategy by the endoplasmic reticulum body in plants. *Plant Cell Physiology* 52, 2039 – 2049

Yamazaki, T., Takata, N., Uemura, M. & Kawamura, Y. (2010) Arabidopsis synaptotagmin SYT1, a type I signal-anchor protein, requires tandem C2 domains for delivery to the plasma membrane. *Journal of Biological Chemistry* 285, 23165 - 23176

Zavaliev, R. & Epel, B. L. (2015) Imaging callose at plasmodesmata using aniline blue: quantitative confocal microscopy *Methods in molecular biology* 1217, 105-19

Zhang, X., Henriques, R., Lin, S., Niu, Q. & Chua, N. (2006) *Agrobacterium*-mediated transformation of *Arabidopsis thaliana* using the floral dip method. *Nature Protocols* 1, 641 - 646

Zhang, D., Utsumi, T., Huang, H., Gao, L., Sangwung, P., Chung, C., Shibao, K., Okamoto, K., Yamahuchi, K., Groszmann, R. J., Jozsef, L., Hao, Z., Sessa, W. & Iwakiri, Y. (2011) Reticulon 4B (Nogo-B) is a novel regulator of hepatic fibrosis. *Hepatology* 53, 1306 – 1315

Zhang, M., Wu, F., Shi, J., Zhu, Y., Zhu, Z., Gong, Q. & Hu, J. (2013) ROOT HAIR DEFECTIVE3 family of dynamin-like GTPases mediates homotypic endoplasmic reticulum fusion and is essential for Arabidopsis development. *Plant Physiology* 163, 2713 – 2720

Zhang, H. & Hu, J. (2016) Shaping the endoplasmic reticulum into a social network. *Trends in Cell Biology* 26, 934 – 943

Zhang, Y., Iakovidis, M. & Costa, S. (2016) Control of patterns of symmetric cell division in the epidermal and cortical tissues of the *Arabidopsis* root. *Development* 143, 978 – 982

Zurek, N., Sparks, L. & Voeltz, G. (2011) Reticulon short hairpin transmembrane domains are used to shape ER tubules. *Traffic* 12, 28 – 41